Assessment of climate change mitigation options

Yann Gaucher

université PARIS-SACLAY

Assessment of climate change mitigation options

Evaluation d'options d'atténuation du changement climatique

Thèse de doctorat de l'Université Paris-Saclay

École doctorale n°129, Sciences de l'Environnement d'Ile de France (SEIF)
Spécialité de doctorat: Géosciences
Graduate School : Géosciences, climat, environnement et planètes.
Référent : Université de Versailles Saint-Quentin-en-Yvelines

Thèse préparée dans l'unité de recherche **LSCE** (Université Paris-Saclay, CNRS, CEA, UVSQ), sous la direction de **Philippe CIAIS**, directeur de recherche CEA au LSCE, la co-direction de **Katsumasa TANAKA**, senior researcher LSCE and NIES

Thèse soutenue à Paris-Saclay, le 25 janvier 2024, par

Yann GAUCHER

Composition du jury

Membres du jury avec voix délibérative

Philippe BOUSQUET Professeur des Universités, UVSQ	Président
Sabine FUSS Professorin, Humboldt-Universität zu Berlin	Rapporteur & Examinatrice
Jean-Charles HOURCADE Directeur de recherche émérite, CIRED	Rapporteur & Examinateur
Nico BAUER Senior Scientist, Potsdam-Institut für Klimafolgenforschung	Examinateur
Nadia MAÏZI Professeure des universités, Mines Paris - Université PSL	Examinatrice
Sandrine SELOSSE Directrice de recherche, Mines Paris - Université PSL	Examinatrice

THESE DE DOCTORAT
NNT : 2024UPASJ004

université PARIS-SACLAY
ÉCOLE DOCTORALE
Sciences de l'Environnement d'Île-de-France (SEIF)

Titre: Evaluation d'options d'atténuation du changement climatique
Mots clés: Réduction d'émissions, Elimination du carbone, Elimination du méthane, Accords de Paris, Scénarios d'émissions, Coûts et analyse des coûts

Résumé: Cette thèse présente une analyse de différentes options d'atténuation du changement climatique, évaluées à l'aide de modèles numériques qui intègrent les déterminants socio-économiques des émissions de gaz à effet de serre dans une approche multidisciplinaire. La première option est une option de politique économique consistant à stimuler les économies affectées par la pandémie de COVID-19, tout en favorisant la transition énergétique en orientant les plans de relance vers des technologies bas-carbone. Nous avons proposé un calcul des effets des plans de relance sur les émissions mondiales de CO2 à l'horizon 2030, en nous appuyant sur des résultats de modèles d'évaluation intégrée antérieurs à la pandémie, que nous avons croisé avec des bases de données recensant les montants dédiés aux investissements bas-carbone liés aux plans de relance. Cette estimation simple, ainsi que deux autres approches auxquelles elle est comparée (les projections de l'agence internationale de l'énergie et des travaux de modélisation entrée-sortie), suggèrent que les plans de relance bas-carbone auront une influence limitée sur les émissions futures. Nous avons ensuite couplé un modèle du système énergétique (GET) avec un modèle simple du climat, du cycle du carbone et de la chimie atmosphérique (ACC2) pour étudier deux techniques d'éliminations des gaz à effet de serre. La première, appelée altération forcée du basalte (EW pour « enhanced weathering »), est une technique d'élimination du carbone (EDC) consistant à appliquer des poudres de basalte sur des champs cultivés ou les forêts, afin de minéraliser le carbone atmosphérique d'une part et d'augmenter la production biologique d'autre part. La minéralisation du carbone atmosphérique est due à la libération de cations basiques. L'augmentation de la production biologique est due à l'apport en nutriments, notamment en phosphore. Les deux processus sont intégrés au modèle GET-ACC2, le second via une représentation agrégée du cycle du phosphore calibrée sur le modèle de surfaces continentales ORCHIDEE-CNP. Les aspects énergétiques des processus de production, de transport et d'épandage des poudres de basalte sont quant à eux intégrés au modèle du système énergétique. Le modèle suggère que l'application de basalte sur les sols forestiers peut séquestrer jusqu'à deux fois plus de carbone qu'une application uniquement agricole, et réduire considérablement les coûts pour atteindre les objectifs de température de l'accord de Paris. Nous montrons également comment la compétition entre l'EW et la bioénergie avec capture et stockage du carbone (BECCS) dépend de la formulation des objectifs climatiques. Enfin, nous étudions l'élimination du méthane atmosphérique, un ensemble de méthodes encore embryonnaires qui a reçu moins d'intérêt que l'EDC. Nous supposons que le rôle de l'EDC dans une trajectoire d'atténuation donnée peut être quantifié par les émissions brutes cumulées de CO2 et les coûts économiques associés à cette trajectoire. A l'aide du modèle GET-ACC2, nous établissons le cahier des charges, concernant le coût unitaire et de potentiel d'élimination, qu'une technique d'élimination du méthane devrait respecter afin de jouer le même rôle que la BECCS dans l'atteinte de différents objectifs climatiques. Nous comparons les scénarios associés à un déploiement à grande échelle de l'une ou l'autre de ces technologies. Nous observons également que tenir compte de l'augmentation future des émissions naturelles de méthane due au réchauffement global n'a pas pour effet de rendre l'élimination du méthane plus nécessaire que celle du carbone.

Title: Assessment of climate change mitigation options
Keywords: Emission reductions, Carbone dioxide removal, Methane removal, Paris Agreement, Emission pathways, Costs and costs analysis

Abstract: This thesis presents an analysis of different climate change mitigation options, assessed using numerical models that integrate the socio-economic drivers of greenhouse gas emissions in a multidisciplinary approach. The first option is an economic policy option consisting of stimulating economies affected by the COVID-19 pandemic, while promoting the energy transition by directing recovery packages towards low-carbon technologies. We have estimated the reduction of global CO2 emissions until 2030 resulting from recovery packages, by combining integrated assessment models results from a set of pre-COVID-19 simulations with an analysis of low-carbon investments within recovery packages. This simple estimate, and two other approaches against which it is compared (the International Energy Agency scenarios, and input-output modelling work), suggest that low-carbon stimulus packages will have a limited influence on future emissions. I then coupled an energy system model (GET) with an aggregated carbon cycle, atmospheric chemistry and climate model (ACC2) to study two greenhouse gas removal techniques. The first, called enhanced weathering (EW), is a carbon dioxide removal (CDR) solution that consists of applying basalt dust to cultivated fields or forests, in order to mineralize atmospheric carbon on the one hand and increase biological production on the other. The mineralization of atmospheric carbon is due to the release of basic cations. The increase in biological production is due to the supply of nutrients, particularly phosphorus. Both processes are integrated into the GET-ACC2 model, the second via an aggregated representation of the phosphorus cycle calibrated on the ORCHIDEE-CNP land-surface model. The energy aspects of the basalt dust production, transport and spreading processes are integrated into the energy system model. The model suggests that the application of basalt on forest soils can sequester up to twice as much carbon as a purely agricultural application, and considerably reduce the costs of meeting the temperature targets of the Paris Agreement. It also shows how competition between EW and bioenergy with carbon capture and storage (BECCS) depends on the formulation of climate targets. Finally, I study atmospheric methane removal, a set of methods that is still in its infancy and has received less attention than CDR. I assume that the role of CDR in a given mitigation trajectory can be quantified by the cumulative gross CO2 emissions and economic costs associated with that trajectory. Using the GET-ACC2 model, I establish the unit cost and removal potential specifications that a methane removal technology would need to meet in order to play the same role as BECCS in achieving different climate goals. I compare the scenarios associated with large-scale deployment of one or other of these technologies. I also observe that considering the future increase in natural methane emissions due to global warming require stronger mitigation efforts of all greenhouse gases, but that it does not make methane mitigation comparatively more important than CDR in cost-effective pathways.

Résumé en Français

La première option évaluée est une option de politique économique consistant à stimuler les économies affectées par la pandémie de COVID-19, tout en favorisant la transition énergétique en orientant les plans de relance vers des technologies bas-carbone. Nous avons proposé un calcul des effets des plans de relance sur les émissions mondiales de CO2 à l'horizon 2030, en nous appuyant sur des résultats de modèles d'évaluation intégrée(integrated assessment models) antérieurs à la pandémie, que nous avons croisés avec des bases de données recensant les montants dédiés aux investissements bas-carbone liés aux plans de relance, à l'aide de régression linéaires à l'échelle régionale entre émissions par unité de produit intérieur brut et investissement cumulé dans les technologies bas-carbone. Cette estimation simple, ainsi que deux autres approches auxquelles elle est comparée (les projections de l'agence internationale de l'énergie et des travaux de modélisation entrée-sortie), suggèrent que les plans de relance bas-carbone auront une influence limitée sur les émissions futures. Ce travail constitue le deuxième chapitre de cette thèse, et a été publié dans la revue Environmental Research Communications. Nous avons ensuite couplé un modèle du système énergétique (GET) avec un modèle simple du climat, du cycle du carbone et de la chimie atmosphérique (ACC2) pour étudier deux techniques d'éliminations des gaz à effet de serre. La première, appelée altération forcée du basalte (EW pour « enhanced weathering »), est une technique d'élimination du carbone (EDC) consistant à appliquer des poudres de basalte sur des champs cultivés ou les forêts, afin de minéraliser le carbone atmosphérique d'une part et d'augmenter la production biologique d'autre part. La minéralisation du carbone atmosphérique est due à la libération de silicates qui augmentent l'alcalinité des eaux de surface et par conséquent la quantité de carbone inorganique dissous, sous forme d'ions bicarbonates. L'augmentation de la production biologique est due à l'apport en nutriments, notamment en phosphore, ce qui conduit à une séquestration accrue de carbone organique dans la biomasse. Les deux processus sont intégrés au modèle GET-ACC2, le second via une représentation agrégée du cycle du phosphore calibrée sur le modèle de surfaces continentales ORCHIDEE-CNP. Les aspects énergétiques des processus de production, de transport et d'épandage des poudres de basalte sont quant à eux intégrés au modèle du système énergétique. Le modèle suggère que l'application de basalte sur les sols forestiers peut séquestrer jusqu'à deux fois plus de carbone qu'une application uniquement agricole, et réduire considérablement les coûts pour atteindre les objectifs de température de l'accord de Paris, tout en étant plus économe en basalte par tonne de co2 capturée. Nous montrons également comment la compétition entre l'EW et la bioénergie avec capture et stockage du carbone (BECCS)

dépend de la formulation des objectifs climatiques. Ce travail constitue le troisième chapitre de cette thèse, et a donné lieu à un article en cours de relecture par la revue Nature Communications. Enfin, nous étudions l'élimination du méthane atmosphérique, un ensemble de méthodes encore embryonnaires qui a reçu moins d'attentio que l'élimination du carbone pour des raisons liées aux différences entre les propriétés physico-chimiques du dioxyde de carbone et du méthane, et à des concentrations atmosphériques très différentes, mais également aux modèles utilisés pour produire les scénarios d'atténuation du changement climatique. Nous supposons que le rôle de l'EDC dans une trajectoire d'atténuation donnée peut être quantifié par les émissions brutes cumulées de CO2 et les coûts économiques associés à cette trajectoire. A l'aide du modèle GET-ACC2, nous établissons le cahier des charges, concernant le coût unitaire et de potentiel d'élimination, qu'une technique d'élimination du méthane devrait respecter afin de jouer le même rôle que la BECCS dans l'atteinte de différents objectifs climatiques. Nous comparons les scénarios associés à un déploiement à grande échelle de l'une ou l'autre de ces technologies. Nous observons également que tenir compte de l'augmentation future des émissions naturelles de méthane due au réchauffement global n'a pas pour effet de rendre l'élimination du méthane plus nécessaire que celle du carbone. Ce travail constitue le 4e chapitre de cette thèse.

Publications

Tanaka, K., Azar, C., Boucher, O., Ciais, P., **Gaucher, Y.** and Johansson, D.J.A. (2022) *Paris Agreement requires substantial, broad, and sustained policy efforts beyond COVID-19 public stimulus packages*, Climatic Change, 172(1), p. 1. Available at: https://doi.org/10.1007/s10584-022-03355-6.

Gaucher, Y., Tanaka, K., Ciais, P. and Boucher, O. (2022) *Limited impact of COVID-19 recovery packages on near-term CO2 emissions pathways*, Environmental Research Communications, 4(10), p. 101006. Available at: https://doi.org/10.1088/2515-7620/ac9aa6.

Gaucher, Y., Tanaka, K., Johansson, D., Goll, D. and Ciais, P. (2023) *Leveraging ecosystems responses to enhanced rock weathering in mitigation scenarios*. preprint. In Review.

Gaucher, Y., Tanaka, K., Johansson, D., Boucher, O. and Ciais, P. (2023) *Comparing Methane and Carbon Dioxide Removal for Climate Change Mitigation: Specifications and Impacts*.To be submitted.

Remerciements

Mes remerciements vont tout d'abord à mes directeurs de thèse, Philippe Ciais et Katsumasa Tanaka, qui ont initié le projet, puis m'ont encadré avec assiduité pendant ces trois années et 4 mois de thèse et m'ont donné à voir des approches complémentaires de la recherche. Je souhaite également remercier Olivier Boucher qui a suivi de près (quoiqu'à distance, COVID oblige) mes débuts dans ce projet, Daniel Johansson qui m'a initié aux subtilités de la modélisation énergétique, ainsi que Daniel Goll et son enthousiasme pour l'altération des basaltes.

Cette thèse conclut un parcours scolaire puis étudiant que j'ai eu la chance d'effectuer dans des conditions privilégiées, bénéficiant d'un système éducatif excellent et gratuit dans un contexte familial très favorable. Je remercie donc les professeurs qui m'ont formé, ainsi que mes parents, leurs parents, leurs frères et sœurs et les miens pour leur soutien et leurs conseils. Parce qu'ils ont permis cette thèse, je souhaite également remercier les personnels administratifs du CEA, du LSCE, de l'université Paris Saclay et de l'ED SEIF.

Tributaire des vicissitudes de la pandémie, j'ai fait mes premiers pas de doctorant à différents endroits, de Lanleff à Bad Kohlgrub, en passant par Bures sur Yvette et Bezornay, avec différents amis et collègues de circonstance que je remercie pour avoir égayé ces journées de télétravail. J'adresse également ces remerciements à mes collègues et amis du LSCE, en particulier Léna, Isma, Martin et Thomas, ainsi que les joueurs de tarot et autres amateurs de mots croisés et de promenades à Saint-Aubin : leur camaraderie et leur agréable compagnie justifiaient largement de subir les caprices de la RATP. Enfin, je dois plus que des remerciements à Charlotte pour l'appui qu'elle m'a apporté, la confiance qu'elle m'a témoignée et la patience dont elle a fait preuve depuis le début.

CONTENTS

CHAPTER I

INTRODUCTION

1 About Climate Change

The Summary for Policymakers of the Sixth Assessment Report of the Intergovernmental Panel on Climate Change (IPCC) states that the global temperatures have already risen by 1.1 degrees in the period 2011-2020 compared to 1850-1900 level (IPCC, 2023). It also states that anthropogenic emissions of greenhouse gases (GHG), which have been rising steadily since the beginning of the Industrial Revolution in the 19th century, are responsible for this temperature increase. The greenhouse gases are the gases that have the property to absorb and reemit the longwave radiation that are emitted by the Earth surface (Matthews et al., 2021), but are almost transparent to incident solar radiation. They are responsible for the greenhouse effect by trapping the heat radiative from the Earth surface. GHG are naturally present in the atmosphere, but an increase of the GHG concentration shifts the earth's energy balance towards an increase of global surface temperature. The resulting climate change is not limited to global warming: precipitation patterns are affected, sea levels are rising, and climate extremes such as droughts and heat waves are becoming more frequent and intense (IPCC, 2023). In addition to these gradual changes, global warming could also trigger irreversible abrupt changes in the Earth system, known as "tipping points", such as the dieback of the amazon rainforest, the collapse of the Atlantic meridional overturning circulation, which is responsible for the temperate climate in our latitudes, or the collapses of the west Antarctic and Greenland ice sheets, which could result in a rapid rise in sea-levels (Lenton et al., 2008). Climate change already has adverse effects on ecosystems and human societies, and they are projected to worsen with increasing temperatures (IPCC, 2022b).

Recognizing the threat posed by climate change, a growing number of countries have committed to reducing their greenhouse gas emissions, or even offsetting their residual emissions by eliminating atmospheric carbon to achieve "carbon neutrality". In spite of this, since the creation of the United Nations Framework Convention on Climate Change in 1994, successive agreements have so far failed to curb the trajectory of global warming. The current framework for global climate negotiations and action is the Paris Agreement. It was adopted by 196 Parties at the twenty first United Nations Climate Change Conference, the 12th December 2015, in Paris. Its goal is to limit “the increase of the global temperature well below 2°C above pre-industrial warming” and pursue efforts to “limit the temperature increase to 1.5°C above pre-industrial levels” (Article 2). Parties to the Paris Agreement also agreed to undertake rapid emission reductions, “so as to achieve a balance between anthropogenic emissions by sources and removals by sinks of greenhouse gases in the second half of this century” (Article 4). The present work forms part of the assessment of global strategies for the 21st century that aim at mitigating climate change in order to achieve the objectives of the Paris Agreement.

2 Climate change mitigation

2.1 A Multidisciplinary Issue

Climate change is primarily caused by the increase of atmospheric carbon dioxide concentration, where about half of anthropogenic carbon dioxide emissions accumulate (Archer et al., 2009; Joos et al., 2013). The combustion of fossil fuels, and to a lesser extent land-use change are the main sources of carbon dioxide emissions. Land-use change emissions are caused by the extension of croplands and pasture to meet the increasing food demand per capita of a growing world population (J. IPCC, 2019). The consumption of fossil fuels, such as coal and later oil and natural gas, has grown continuously since the industrial revolution in the 19th century. Initially used as a substitute for firewood, coal played a crucial role in powering the machinery and engines that drove the Industrial Revolution, providing an abundant source of energy for industrial processes, transportation, and electricity generation, which transformed economies and societies by enabling mass production and urbanisation. The consumption of fossil fuels has shaped not only the economic development of industrial countries, but also their social and political structures (Mitchell, 2011). Four-fifths of the global primary energy use in 2023 is fossil fuel (IEA, 2022). Developed societies and our material prosperity are based on energy-intensive lifestyles, to which our conception of individual freedom is also linked: in a sense, atmospheric greenhouse gases are also the “ashes of industrial freedom piling up

over our heads" (Charbonnier, 2020). Due to their central place in our economies, fossil fuel companies are among the world's most powerful organisations. Fossil fuels exports are a major economic development lever and a powerful geopolitical tool for producer states. Cutting down the use of fossil fuels and reducing GHG emissions would therefore not only require a profound technological transformation of all sectors of the economy. It could also reconfigure the social organisation including economic and political power relations, spatial planning, diets and leisure activities (IPCC, 2022a). This non-exhaustive list illustrates that climate change mitigation is a cross-cutting issue and as such, it is a multidisciplinary field of study, involving social sciences and natural sciences as well as engineering.

2.2 Modelling Mitigation strategies

The development of climate change mitigation strategies has to cope with the complexity of the global system of anthropic GHG emissions, whose components include land use, industry, energy, construction, extraction and transport, all of which interact with each other. Besides this complexity, mitigation strategies also face "deep uncertainty" (Guivarch et al., 2017), when there is no agreement on how to model the interactions among the system's variables, nor on the probability distribution of the uncertainty, nor on how to value the alternatives (**lempertShapingNextOne2003**). Scenarios based on contrasted storylines of possible futures are developed to explore this fundamental uncertainty, and to integrate the knowledge of the different scientific communities working on climate change. The most widely used scenarios in the latest IPCC report are the shared socio-economic pathways (SSP) (O'Neill et al., 2017). SSPs are classified depending on socio-economic challenges to climate change mitigation and climate change adaptation, yielding 5 SPPs including a middle-of-the-road pathway. The variables used to contrast the SSPs are both quantitative (population, education, urbanisation, technological change and economic growth pathways) and qualitative (e.g. lifestyle, policies and institutions...). SSPs do not integrate climate policies nor the effects of climate change.

Scenarios are quantitatively analysed with large numerical models called Integrated Assessment Models (IAMs). IAMs provide a "simplified representation of physical and social systems, focusing on the interaction between economy, society and the environment" ("Annex III", 2023), targeting internal quantitative consistency despite the systemic complexity. Modelling efforts to address environmental problems began in the early 1970s and their history is deeply intertwined with the evolution of the scientific and political framing of the climate change issue (van Beek et al., 2020). The publication of the "Limits to Growth" report by the Club of Rome (1972), based on a system dynamics model (World 3), contributed to the emer-

gence of environmental change as a global issue. When the 1973 first oil shock made the economy's dependence on energy a tangible reality, the need for forecasts fostered the development of energy-economy models. At the same time, the first climate-economy models were used to compute the costs of climate action (W. D. Nordhaus, 1993). Since these pioneering works, the sophistication and complexity of IAMs have progressed hand-in-hand, while the number of associated publications has grown exponentially, with the last IPCC assessment of climate change mitigation pathways relying on 1200 scenarios produced with IAMs (Riahi et al., 2022). IAMs have become prominent tools at the science-policy interface, as they can provide insights on the long-term future consequences of climate policies (or the lack thereof) or conversely on the near-term actions that are needed to achieve long-term objectives, although numerical models such as IAMs have a quantitative focus per nature and cannot address all the issues at stake (Geels et al., 2016), such as the analysis of power relations and the role of interest groups, which can be important facilitators or obstacles to climate change mitigation (Kornek et al., 2020).

There are two kinds of IAMs (Weyant, 2017): detailed process IAMs, and benefit-cost IAMs, associated with different kinds of mitigation pathways. On the one hand, benefit-cost IAMs are typically very aggregated. They integrate stylized economics, comprising an endogenous growth model and emission reductions costs with a simple climate model and a representation of climate damages. They can compute the "social cost of carbon" (SCC), defined as the economic damage due to the climate change caused by one more ton of CO2 (Tol, 2011) or similarly the social cost of methane (Azar et al., 2023). Benefit-cost IAMs are also used to compute cost-optimal mitigation pathways, in which climate policies are "optimal" in the sense that the marginal cost of emission reduction is worth this SCC. On the other hand, detailed process IAMs aim at a sufficient sectoral and geographic resolution to understand the evolution of key processes driving greenhouse gas emissions. There is a large diversity of models, with different macroeconomic assumptions, levels of technological coverage, and different resolution procedures. An overview of the diversity of detailed-process IAMs can be found in the Annex III of the Third Working Group of the Sixth Assessment Report of the IPCC ("Annex III", 2023). Cost-efficient (as opposed to cost-optimal) mitigation pathways, in which the climate policies aim at achieving an exogenous climate target at the lowest cost without consideration for climate damages, can be computed by detailed process IAMs. The climate target can take several forms, and be expressed for instance as a carbon budget, a radiative forcing ceiling, a CO2 concentration target, an emission target, a temperature target or a combination of them (Johansson et al., 2020). The model GET-ACC2 that we use later (see chapters 3 and 4), does not exactly fall into one of these categories. It is not a benefit-cost IAM, as it does not consider the damages from climate change, and produces cost-effective rather than cost-benefit scenar-

ios, with a technology-rich description of the energy system. Yet, like cost-benefit IAMs, it is coupled with a simple climate model.

2.3 Climate targets and overshoots

The Paris agreement mentions two temperature targets: 2°C and 1.5°C. Limiting the global temperature increase to well below 2°C above pre-industrial levels, commonly referred to as the '2°C target', became the benchmark for international climate governance with the Copenhagen conference in 2009. It was adopted as a climate change mitigation target because it was considered to be a threshold beyond which "anthropogenic interference with the climate system " (following UNFCCC terminology (Oppenheimer & Petsonk, 2005)) would be too dangerous. This 2°C threshold was first mentioned in an 1979 article by W. Nordhaus (W. D. Nordhaus, n.d.; Oppenheimer & Petsonk, 2005; Randalls, 2010), as the upper range of normal mean temperature variations during the Holocene. The 2°C target was proposed in a similar way by the German Advisory Council on Global Change (wissenschaftlicher Beirat der Bundesregierung globale Umweltveränderungen WBGU), in 1995, by considering that the 2°C target was the upper range of a "tolerable window", defined as the range of temperatures during the Holocene, outside of which "dramatic" ecosystem changes could be expected (Aykut & Dahan, 2011). The 1.5°C target has a more recent origin, as it was initially mainly promoted during the Copenhagen Conference, by the members of the Alliance of Small Islands States (AOSIS) (Cointe & Guillemot, 2023) which are particularly endangered by sea level rise. This led to a science-based review process, the "structured expert dialogue" (SED), which was mandated by the UNFCCC to examine the implications of limiting temperature change to 1.5°C instead of 2°C, and concluded that a 2°C warming could not be considered safe (Schleussner et al., 2016). The 1.5°C level was adopted as a target for the first time in the Paris Agreement. Contrarily to the 2°C target, the 1.5°C target was not originally a scientific benchmark but a diplomatic invention. Supporters of the cost-benefit approach still argue that the warming target should be dictated by a weighting of costs against damages (AB, 2023), but this was not the reason behind the target. It is however interesting to note that, although cost-benefits analyses have traditionally advocated for optimal peak warming around 3°C to 3.5°C (W. Nordhaus, 2019), recent studies showed that it possible (Hänsel et al., 2020) to obtain 2°C as the optimal end-of-century temperature using a cost-benefit approach, and that trajectories are closer to the 1.5°C target if the discount rate is lowered.

The slow pace of emissions reductions and the lack of ambition of current climate policies make it less and less likely that the global average annual temperature will be kept below 1.5°C

of warming (van de Ven et al., 2023). Limiting warming below 1.5°C with 50% probability would require us to emit less than 380GtCO2 from 2023 onwards, less than 9 years at the current emission level (Friedlingstein et al., 2022), with recent assessment indicating even smaller numbers: 250GtCO2, 6 years of current emissions (Forster et al., 2023; Lamboll et al., 2023). As a consequence, in most scenarios achieving aiming at 1.5°C, the temperature temporarily exceeds the target. The 1.5°C target has introduced these overshoot scenarios as a "new normality". This could provide policymakers with an argument for interpreting climate targets more leniently in the future (Geden & Löschel, 2017). Furthermore, staying below the 1.5°C warming target is not the same as reaching 1.5°C by the end of the century after an overshoot of several tenths of a degree: transitory warming could have irreversible consequences (Ritchie et al., 2021), and the possibility of crossing tipping points between 1.5°C and 2°C of warming cannot be ruled out (Ditlevsen & Ditlevsen, 2023; Wunderling et al., 2023). Furthermore, overshoot pathways require a more enhanced use of carbon dioxide removal, sometimes at levels that may not be feasible or acceptable in the real-world (Tanaka et al., 2020). However, in this thesis (chapters 3 and 4) we acknowledge that the Paris Agreements text is open to interpretation, and we compare different temperature targets based on our but common interpretation of the Paris Agreement targets: 1.5°C with a small overshoot, or with an unconstrained overshoot, 2°C without overshoot, or 2°C with overshoot. This last case is used for reasons of symmetry and because stated policies still imply an end-of-century temperature higher than 2°C (van de Ven et al., 2023), even though the Paris agreements explicitly state that the temperature must be kept below 2°C, thus ruling out a temporal overshoot.

3 Contributions and structure of this thesis

This thesis explores certain economic and technological aspects of climate change mitigation pathways. I assessed the role of different policy and technology options for mitigating climate change at the global scale. In the following three chapters, I analyse three mitigation 'options', including two GHG removal technologies. We study the role of these 'options' by building scenarios in which they are deployed and scenarios in which they are not, and subsequently comparing them. The use of IAMs or similar modelling tools is a common thread running through my thesis, albeit in different ways in each of the three chapters.

3.1 Climate Effects of COVID-19 recovery packages

The first option assessed is an economic policy option: green stimulus investment to boost the economy weakened by the COVID-19 pandemic, thereby fostering a green transition. This work was motivated by the rather unexpected peculiar conditions at the start of my thesis: lockdowns, social distancing, no travel. These measures were adopted by governments, in order to contain the spread of the virus and keep healthcare systems functioning. They led to a sharp drop in activities, particularly in the transport sector, and subsequently to an unprecedented drop in CO2 emissions (Forster et al., 2020; Liu et al., 2022). Since most developed countries were committed to strongly reduce their CO2 emissions in the framework of the Paris agreement, and were taking massive plans to revive the economy by supporting companies and investing in infrastructures, there could have been an opportunity to take advantage of the disruption caused by the pandemic to rebuild the economy on a more sustainable basis (Andrijevic et al., 2020; Hepburn et al., 2020). A significant part of COVID-19 recovery packages was indeed dedicated to sectors critical to energy transition and emission reductions. **In this work, I have attempted to estimate the effects of green recovery packages on decadal emissions trajectories.** This study contrasts the results from three approaches that quantified the impact of post-COVID-19 policies on emissions pathways. I first conducted an ex-post analysis of IAMs results from a set of pre-COVID-19 simulations (McCollum et al., 2018) to derive correlation relationships between low-carbon investments and the associated reduction of the emissions per unit of GDP in 2030, at a regional level. By comparing these relationships against the announced low-carbon investments within recovery packages retrieved from an existing database (O'Callaghan et al., 2021), I then obtained the 2030 difference in emissions per unit of GDP compared to a baseline level. Multiplying this shift by the assumed 2030 GDP level returns the absolute magnitude of emission reductions associated with the recovery packages. These results were then benchmarked against the IEA scenarios (IEA, 2020, 2021): they show that green recovery packages can lead to an emission reduction of 1%-6% from 2030 baseline levels at most. A third approach (Shan et al., 2021) modelled the disruptions in supply chains following successive lockdowns and fiscal stimuli, and shows that fiscal stimuli prioritising high-technology sectors do not prevent emission rebounds. We conclude that green recovery packages targeting low-carbon technologies have a limited impact on near-term CO2 emissions. This work has been published as a letter in Environmental Research Communications (Gaucher et al., 2022) entitled Limited impact of COVID-19 recovery packages on near-term CO2 emissions pathways (Y. Gaucher, K. Tanaka, P. Ciais and O. Boucher, 2022) and constitutes the second chapter of the thesis.

3.2 Enhanced Weathering

The second option studied is a carbon dioxide removal (CDR) solution known as enhanced basalt weathering. This technique entails the application of basalt dust to soils. When basalt dissolves, released silicates can mineralize atmospheric carbon dioxide, while the phosphorus contained in basalt can enhance the ecosystem production and thereby increase the land carbon sink. This technique is usually assumed to be deployed in crop fields, but recent modelling study using the land surface model ORCHIDEE-CNP showed that applying basalt on natural phosphorus-depleted areas on top of agricultural land could bring substantial additional carbon sequestration in biomass through improved ecosystem production (Goll et al., 2021). **The objective of this research was to understand how enhanced weathering could fit into a portfolio of low-carbon and negative emission technologies and how mobilising the biological sequestration effect by applying enhanced weathering on non-agricultural areas was useful in the context of climate mitigation pathways.** We also assessed the competition with bioenergy with carbon capture and storage (BECCS) and its interactions with the energy system. For this purpose, I have developed a coupled energy-economy-climate model by linking a global model of the energy system and a simple climate model that describes the key geophysical and biogeochemical processes of the land and ocean carbon cycle and atmospheric chemistry (Tanaka et al., 2007). To study the sequestration of atmospheric carbon by enhanced weathering, I integrated into the model a set of equations describing the interactions between enhanced weathering, the energy system and the carbon cycle, in particular by developing a simplified representation of the phosphorus cycle which is calibrated on a land-surface model. By comparing the use of EW to achieve different temperature targets, the results show that enabling application of basalt dust on forest soils could triple the cost-efficient deployment of enhanced weathering, compared to agricultural application only, and significantly reduce the costs of achieving the Paris agreement temperature targets. The study indicates that the trade-off between bioenergy with carbon capture and storage and enhanced weathering depends on the definition of the climate targets. By analysing the willingness to pay for bioenergy across the different scenarios, it further shows that EW reduces the price of biomass and possibly the pressure on food prices, but that bioenergy with carbon capture and storage remains a major CDR option and is not totally replaced by enhanced weathering. I have also explored the robustness of the model's results to a wide range of assumptions by conducting a detailed sensitivity analysis. This study, entitled Leveraging ecosystems responses to enhanced rock weathering in mitigation scenarios (Y. Gaucher, K. Tanaka, D. Johansson, D. Goll, P. Ciais, 2023) is currently under review in *Nature Communications*, and constitutes the third chapter of this thesis.

3.3 Methane Removal

The third option explored is methane removal, an approach in its infancy and whose potential relevance is more controversial than that of CDR. CDR is considered "unavailable to achieve carbon neutrality" in the Summary for Policymakers of the sixth assessment report from the third working group of the IPCC (IPCC, 2022c). The prominence of carbon dioxide removal in IAMs led to CDR being seen as critical to climate change mitigation before CDR demonstrators existed (Obersteiner et al., 2001), although the current slow deployment of CDR makes future scale-up challenging (Smith et al., 2023). Here, I use the same modelling framework as in chapter 3, yet in contrast to the above, the aim is not to assess a highly uncertain methane removal technology with the model but instead to try to determine the conditions in which methane removal becomes useful. Methane is an important anthropogenic greenhouse gas, and methane mitigation recently gained attention at the international level, as 150 countries signed the "Global Methane Pledge", committing to take voluntary actions to reduce global methane emissions by at least 30% from 2020 levels by 2030. Atmospheric methane removal could therefore be used to reduce the contribution of methane to climate change in addition to conventional mitigation efforts targeting emissions from fossil fuels and waste which are currently on the political agenda, because the high emissions from agriculture are likely hard to abate. Furthermore, it has been claimed that atmospheric methane removal could be required to offset the increase of natural methane emissions due to global warming (Boucher & Folberth, 2010; Jackson et al., 2019; Jackson et al., 2021; Ming et al., 2022). **The objective of this study is to explore the conditions that a methane removal technology should meet to play the same crucial role as CDR, in particular BECCS, in mitigation pathways, and to explore whether temperature feedback on methane emissions is an argument in favour of methane removal.** Since the success of BECCS in IAMs is due to their ability to enable stringent climate targets to be met by compensating for excess emissions in hard-to-abate sectors (van Vuuren et al., 2007) at greatly reduced costs (Azar et al., 2013), I hypothesised that a MR technology would play the same role as CDR if a given temperature target was met with the same gross cumulative CO2 emissions and at the same economic costs. I modelled a generic MR technology parameterized with constant unit removal costs and a maximal removal potential, to find the set of costs and potentials for which MR is equivalent to BECCS based on gross CO2 budget and mitigation costs for several climate targets. "Equivalent" MR and CDR produce different mitigation pathways. The intertemporal effort distribution is delayed, and the temperature overshoot lasts longer with MR. Non-temperature effects are also different: using MR instead of CDR increases ocean acidification but reduces the concentration of harmful tropospheric ozone. Finally, I added a simple model for the temperature feedback on natural methane emissions (Kleinen et al., 2021). It suggests that while the higher future methane emis-

sions caused by the feedback require stronger mitigation efforts of all GHG, the feedback does not make methane mitigation comparatively more important that carbon dioxide removals in cost-effective pathways. This study has not been submitted to a peer-reviewed journal yet at the time of writing and constitutes the fourth chapter of this thesis.

References

AB, N. P. O. (2023). William D. Nordhaus – Biographical. https://www.nobelprize.org/prizes/economic-sciences/2018/nordhaus/biographical/

Andrijevic, M., Schleussner, C.-F., Gidden, M. J., McCollum, D. L., & Rogelj, J. (2020). COVID-19 recovery funds dwarf clean energy investment needs. *Science*, *370*(6514), 298–300. https://doi.org/10.1126/science.abc9697

Annex III: Scenarios and Modelling Methods. (2023, August 17). In IPCC (Ed.), *Climate Change 2022 - Mitigation of Climate Change* (1st ed., pp. 1841–1908). Cambridge University Press. https://doi.org/10.1017/9781009157926.022

Archer, D., Eby, M., Brovkin, V., Ridgwell, A., Cao, L., Mikolajewicz, U., Caldeira, K., Matsumoto, K., Munhoven, G., Montenegro, A., & Tokos, K. (2009). Atmospheric Lifetime of Fossil Fuel Carbon Dioxide. *Annual Review of Earth and Planetary Sciences*, *37*(1), 117–134. https://doi.org/10.1146/annurev.earth.031208.100206

Aykut, S. C., & Dahan, A. (2011). Le régime climatique avant et après Copenhague : sciences, politiques et l'objectif des deux degrés ». *Natures Sciences Sociétés*, *19*(2), 144–157. Retrieved October 27, 2023, from https://www.cairn.info/revue-natures-sciences-societes-2011-2-page-144.htm

Azar, C., Johansson, D. J. A., & Mattsson, N. (2013). Meeting global temperature targets—the role of bioenergy with carbon capture and storage. *Environmental Research Letters*, *8*(3), 034004. https://doi.org/10.1088/1748-9326/8/3/034004

Azar, C., Martín, J. G., Johansson, D. J., & Sterner, T. (2023). The social cost of methane. *Climatic Change*, *176*(6), 71. https://doi.org/10.1007/s10584-023-03540-1

Boucher, O., & Folberth, G. A. (2010). New Directions: Atmospheric methane removal as a way to mitigate climate change? *Atmospheric Environment*, *44*(27), 3343–3345. https://doi.org/10.1016/j.atmosenv.2010.04.032

Charbonnier, P. (2020). 1. Critique de la raison écologique. In *Abondance et liberté* (pp. 15–51). La Découverte. https://www.cairn.info/abondance-et-liberte--9782348046780-p-15.htm

Cointe, B., & Guillemot, H. (2023). A history of the 1.5°C target. *WIREs Climate Change*, *14*(3), e824. https://doi.org/10.1002/wcc.824

Ditlevsen, P., & Ditlevsen, S. (2023). Warning of a forthcoming collapse of the Atlantic meridional overturning circulation. *Nature Communications*, *14*(1), 4254. https://doi.org/10.1038/s41467-023-39810-w

Forster, P. M., Forster, H. I., Evans, M. J., Gidden, M. J., Jones, C. D., Keller, C. A., Lamboll, R. D., Quéré, C. L., Rogelj, J., Rosen, D., Schleussner, C.-F., Richardson, T. B., Smith, C. J., & Turnock, S. T. (2020). Current and future global climate impacts resulting from COVID-19. *Nature Climate Change*, *10*(10), 913–919. https://doi.org/10.1038/s41558-020-0883-0

Forster, P. M., Smith, C. J., Walsh, T., Lamb, W. F., Lamboll, R., Hauser, M., Ribes, A., Rosen, D., Gillett, N., Palmer, M. D., Rogelj, J., von Schuckmann, K., Seneviratne, S. I., Trewin, B., Zhang, X., Allen, M., Andrew, R., Birt, A., Borger, A., … Zhai, P. (2023). Indicators of Global Climate Change 2022: Annual update of large-scale indicators of the state of the climate system and human influence. *Earth System Science Data*, *15*(6), 2295–2327. https://doi.org/10.5194/essd-15-2295-2023

Friedlingstein, P., O'Sullivan, M., Jones, M. W., Andrew, R. M., Gregor, L., Hauck, J., Le Quéré, C., Luijkx, I. T., Olsen, A., Peters, G. P., Peters, W., Pongratz, J., Schwingshackl, C., Sitch, S., Canadell, J. G., Ciais, P., Jackson, R. B., Alin, S. R., Alkama, R., … Zheng, B. (2022). Global Carbon Budget 2022. *Earth System Science Data*, *14*(11), 4811–4900. https://doi.org/10.5194/essd-14-4811-2022

Gaucher, Y., Tanaka, K., Ciais, P., & Boucher, O. (2022). Limited impact of COVID-19 recovery packages on near-term CO2 emissions pathways. *Environmental Research Communications*, *4*(10), 101006. https://doi.org/10.1088/2515-7620/ac9aa6

Geden, O., & Löschel, A. (2017). Define limits for temperature overshoot targets. *Nature Geoscience*, *10*(12), 881–882. https://doi.org/10.1038/s41561-017-0026-z

Geels, F. W., Berkhout, F., & van Vuuren, D. P. (2016). Bridging analytical approaches for low-carbon transitions. *Nature Climate Change*, *6*(6), 576–583. https://doi.org/10.1038/nclimate2980

Goll, D. S., Ciais, P., Amann, T., Buermann, W., Chang, J., Eker, S., Hartmann, J., Janssens, I., Li, W., Obersteiner, M., Penuelas, J., Tanaka, K., & Vicca, S. (2021). Potential CO2 removal from enhanced weathering by ecosystem responses to powdered rock. *Nature Geoscience*, *14*(8), 545–549. https://doi.org/10.1038/s41561-021-00798-x

Guivarch, C., Lempert, R., & Trutnevyte, E. (2017). Scenario techniques for energy and environmental research: An overview of recent developments to broaden the capacity to deal with complexity and uncertainty. *Environmental Modelling & Software*, *97*, 201–210. https://doi.org/10.1016/j.envsoft.2017.07.017

Hänsel, M. C., Drupp, M. A., Johansson, D. J. A., Nesje, F., Azar, C., Freeman, M. C., Groom, B., & Sterner, T. (2020). Climate economics support for the UN climate targets. *Nature Climate Change*, *10*(8), 781–789. https://doi.org/10.1038/s41558-020-0833-x

Hepburn, C., O'Callaghan, B., Stern, N., Stiglitz, J., & Zenghelis, D. (2020). Will COVID-19 fiscal recovery packages accelerate or retard progress on climate change? *Oxford Review of Economic Policy*, *36*, S359–S381. https://doi.org/10.1093/oxrep/graa015

IEA. (2020). *World Energy Outlook 2020*. https://www.oecd-ilibrary.org/content/publication/557a761b-en

IEA. (2021). *World Energy Outlook 2021*. https://www.oecd-ilibrary.org/content/publication/14fcb638-en

IEA. (2022). *World Energy Outlook 2022*. https://www.iea.org/reports/world-energy-outlook-2022

IPCC. (2022a). *Climate Change 2022: Mitigation of Climate Change. Contribution of Working Group III to the Sixth Assessment Report of the Intergovernmental Panel on Climate Change*. IPCC.

IPCC. (2022b). Summary for Policymakers. In H.-O. Pörtner, D. Roberts, E. Poloczanska, K. Mintenbeck, M. Tignor, A. Alegría, M. Craig, S. Langsdorf, S. Löschke, V. Möller, & A. Okem (Eds.), *Climate Change 2022: Impacts, Adaptation, and Vulnerability. Contribution of Working Group II to the Sixth Assessment Report of the Intergovernmental Panel on Climate Change* (pp. 3–33). Cambridge University Press. https://doi.org/10.1017/9781009325844.001

IPCC. (2022c). Summary for Policymakers. In P. Shukla, J. Skea, R. Slade, A. A. Khourdajie, R. van Diemen, D. McCollum, M. Pathak, S. Some, P. Vyas, R. Fradera, M. Belkacemi, A. Hasija, G. Lisboa, S. Luz, & J. Malley (Eds.), *Climate Change 2022: Mitigation of Climate Change. Contribution*

of Working Group III to the Sixth Assessment Report of the Intergovernmental Panel on Climate Change. Cambridge University Press. https://doi.org/10.1017/9781009157926.001

IPCC. (2023). *Summary for Policymakers*. IPCC. Geneva, Switzerland. https://doi.org/10.59327/IPCC/AR6-9789291691647.001

IPCC, J. (2019). Summary for Policymakers. In P. R. Shukla, J. Skea, E. C. Buendia, V. Masson-Delmotte, H.-O. Pörtner, D. C. Roberts, P. Zhai, R. Slade, S. Connors, R. van Diemen, M. Ferrat, E. Haughey, S. Luz, S. Neogi, M. Pathak, J. Petzold, J. P. Pereira, P. Vyas, E. Huntley, ... M. Belkacemi (Eds.), *Climate Change and Land: An IPCC special report on climate change, desertification, land degradation, sustainable land management, food security, and greenhouse gas fluxes in terrestrial ecosystems*.

Jackson, R. B., Solomon, E. I., Canadell, J. G., Cargnello, M., & Field, C. B. (2019). Methane removal and atmospheric restoration. *Nature Sustainability*, *2*(6), 436–438. https://doi.org/10.1038/s41893-019-0299-x

Jackson, R. B., Abernethy, S., Canadell, J. G., Cargnello, M., Davis, S. J., Féron, S., Fuss, S., Heyer, A. J., Hong, C., Jones, C. D., Damon Matthews, H., O'Connor, F. M., Pisciotta, M., Rhoda, H. M., De Richter, R., Solomon, E. I., Wilcox, J. L., & Zickfeld, K. (2021). Atmospheric methane removal: A research agenda. *Philosophical Transactions of the Royal Society A: Mathematical, Physical and Engineering Sciences*, *379*(2210), 20200454. https://doi.org/10.1098/rsta.2020.0454

Johansson, D. J. A., Azar, C., Lehtveer, M., & Peters, G. P. (2020). The role of negative carbon emissions in reaching the Paris climate targets: The impact of target formulation in integrated assessment models. *Environmental Research Letters*, *15*(12), 124024. https://doi.org/10.1088/1748-9326/abc3f0

Joos, F., Roth, R., Fuglestvedt, J. S., Peters, G. P., Enting, I. G., von Bloh, W., Brovkin, V., Burke, E. J., Eby, M., Edwards, N. R., Friedrich, T., Frölicher, T. L., Halloran, P. R., Holden, P. B., Jones, C., Kleinen, T., Mackenzie, F. T., Matsumoto, K., Meinshausen, M., ... Weaver, A. J. (2013). Carbon dioxide and climate impulse response functions for the computation of greenhouse gas metrics: A multi-model analysis. *Atmospheric Chemistry and Physics*, *13*(5), 2793–2825. https://doi.org/10.5194/acp-13-2793-2013

Kleinen, T., Gromov, S., Steil, B., & Brovkin, V. (2021). Atmospheric methane underestimated in future climate projections. *Environmental Research Letters*, *16*(9), 094006. https://doi.org/10.1088/1748-9326/ac1814

Kornek, U., Flachsland, C., Kardish, C., Levi, S., & Edenhofer, O. (2020). What is important for achieving 2 °C? UNFCCC and IPCC expert perceptions on obstacles and response options for climate change mitigation. *Environmental Research Letters*, *15*(2), 024005. https://doi.org/10.1088/1748-9326/ab6394

Lamboll, R. D., Nicholls, Z. R. J., Smith, C. J., Kikstra, J. S., Byers, E., & Rogelj, J. (2023). Assessing the size and uncertainty of remaining carbon budgets. *Nature Climate Change*, 1–8. https://doi.org/10.1038/s41558-023-01848-5

Lenton, T. M., Held, H., Kriegler, E., Hall, J. W., Lucht, W., Rahmstorf, S., & Schellnhuber, H. J. (2008). Tipping elements in the Earth's climate system. *Proceedings of the National Academy of Sciences*, *105*(6), 1786–1793. https://doi.org/10.1073/pnas.0705414105

Liu, Z., Deng, Z., Davis, S. J., Giron, C., & Ciais, P. (2022). Monitoring global carbon emissions in 2021. *Nature Reviews Earth & Environment*, *3*(4), 217–219. https://doi.org/10.1038/s43017-022-00285-w

Matthews, J., Möller, V., van Diemen, R., Fuglestvedt, J., Masson-Delmotte, V., Méndez, C., Semenov, S., & Reisinger, A. (2021). Annex VII: Glossary. In V. Masson-Delmotte, P. Zhai, A. Pirani, S.

Connors, C. Péan, S. Berger, N. Caud, Y. Chen, L. Goldfarb, M. Gomis, M. Huang, K. Leitzell, E. Lonnoy, J. Matthews, T. Maycock, T. Waterfield, O. Yelekçi, R. Yu, & B. Zhou (Eds.), *Climate Change 2021: The Physical Science Basis. Contribution of Working Group I to the Sixth Assessment Report of the Intergovernmental Panel on Climate Change* (pp. 2215–2256). Cambridge University Press. https://doi.org/10.1017/9781009157896.022

McCollum, D. L., Zhou, W., Bertram, C., de Boer, H.-S., Bosetti, V., Busch, S., Després, J., Drouet, L., Emmerling, J., Fay, M., Fricko, O., Fujimori, S., Gidden, M., Harmsen, M., Huppmann, D., Iyer, G., Krey, V., Kriegler, E., Nicolas, C., … Riahi, K. (2018). Energy investment needs for fulfilling the Paris Agreement and achieving the Sustainable Development Goals. *Nature Energy*, *3*(7), 589–599. https://doi.org/10.1038/s41560-018-0179-z

Ming, T., Li, W., Yuan, Q., Davies, P., de Richter, R., Peng, C., Deng, Q., Yuan, Y., Caillol, S., & Zhou, N. (2022). Perspectives on removal of atmospheric methane. *Advances in Applied Energy*, *5*, 100085. https://doi.org/10.1016/j.adapen.2022.100085

Mitchell, T. (2011). *Carbon Democracy: Political Power in the Age of Oil*. Verso Books.

Nordhaus, W. (2019). Climate Change: The Ultimate Challenge for Economics. *American Economic Review*, *109*(6), 1991–2014. https://doi.org/10.1257/aer.109.6.1991

Nordhaus, W. D. (n.d.). Strategies for the Control of Carbon Dioxide.

Nordhaus, W. D. (1993). Rolling the 'DICE': An optimal transition path for controlling greenhouse gases. *Resource and Energy Economics*, *15*(1), 27–50. https://doi.org/10.1016/0928-7655(93)90017-O

Obersteiner, M., Azar, Ch., Kauppi, P., Möllersten, K., Moreira, J., Nilsson, S., Read, P., Riahi, K., Schlamadinger, B., Yamagata, Y., Yan, J., & van Ypersele, J.-P. (2001). Managing Climate Risk. *Science*, *294*(5543), 786–787. https://doi.org/10.1126/science.294.5543.786b

O'Callaghan, B., Yau, N., Murdock, E., Tritsch, D., Janz, A., Blackwood, A., Purroz Sanchez, L., Sadler, A., Wen, E., Kope, H., Flodell, H., Tillman-Morris, L., Ostrovsky, N., Kitsberg, A., Lee, T., Hristov, D., Didarali, Z., Chowdhry, K., Karlubik, M., … Heeney, L. (2021). *Global Recovery Observatory*. Oxford University Economic Recovery Project. Retrieved January 24, 2022, from https://recovery.smithschool.ox.ac.uk/tracking/

O'Neill, B. C., Kriegler, E., Ebi, K. L., Kemp-Benedict, E., Riahi, K., Rothman, D. S., Van Ruijven, B. J., Van Vuuren, D. P., Birkmann, J., Kok, K., Levy, M., & Solecki, W. (2017). The roads ahead: Narratives for shared socioeconomic pathways describing world futures in the 21st century. *Global Environmental Change*, *42*, 169–180. https://doi.org/10.1016/j.gloenvcha.2015.01.004

Oppenheimer, M., & Petsonk, A. (2005). Article 2 of the UNFCCC: Historical Origins, Recent Interpretations. *Climatic Change*, *73*(3), 195–226. https://doi.org/10.1007/s10584-005-0434-8

Randalls, S. (2010). History of the 2 ° C climate target. *WIREs Climate Change*, *1*(4), 598–605. https://doi.org/10.1002/wcc.62

Riahi, K., Schaeffer, R., Arango, J., Calvin, K., Guivarch, C., Hasegawa, T., Jiang, K., Kriegler, E., Matthews, R., Peters, G., Rao, A., Robertson, S., Sebbit, A., Steinberger, J., Tavoni, M., & Van Vuuren, D. (2022). Mitigation pathways compatible with long-term goals. In P. Shukla, J. Skea, R. Slade, A. A. Khourdajie, R. van Diemen, D. McCollum, M. Pathak, S. Some, P. Vyas, R. Fradera, M. Belkacemi, A. Hasija, G. Lisboa, S. Luz, & J. Malley (Eds.), *Climate Change 2022: Mitigation of Climate Change. Contribution of Working Group III to the Sixth Assessment Report of the Intergovernmental Panel on Climate Change*. Cambridge University Press. https://doi.org/10.1017/9781009157926.005

Ritchie, P. D. L., Clarke, J. J., Cox, P. M., & Huntingford, C. (2021). Overshooting tipping point thresholds in a changing climate. *Nature*, *592*(7855), 517–523. https://doi.org/10.1038/s41586-021-03263-2

Schleussner, C.-F., Rogelj, J., Schaeffer, M., Lissner, T., Licker, R., Fischer, E. M., Knutti, R., Levermann, A., Frieler, K., & Hare, W. (2016). Science and policy characteristics of the Paris Agreement temperature goal. *Nature Climate Change*, *6*(9), 827–835. https://doi.org/10.1038/nclimate3096

Shan, Y., Ou, J., Wang, D., Zeng, Z., Zhang, S., Guan, D., & Hubacek, K. (2021). Impacts of COVID-19 and fiscal stimuli on global emissions and the Paris Agreement. *Nature Climate Change*, *11*(3), 200–206. https://doi.org/10.1038/s41558-020-00977-5

Smith, S., Geden, O., Nemet, G., Gidden, M., Lamb, W., Powis, C., Bellamy, R., Callaghan, M., Cowie, A., Cox, E., Fuss, S., Gasser, T., Grassi, G., Greene, J., Lueck, S., Mohan, A., Müller-Hansen, F., Peters, G., Pratama, Y., … Minx, J. (2023). State of Carbon Dioxide Removal - 1st Edition. https://doi.org/10.17605/OSF.IO/W3B4Z

Tanaka, K., Boucher, O., Ciais, P., Daniel J. A. Johansson, Johansson, D. J., Daniel J. A. Johansson, Morfeldt, J., & Morfeldt, J. (2020). Cost-effective implementation of the Paris Agreement using flexible greenhouse gas metrics
MAG ID: 3165110065.

Tanaka, K., Kriegler, E., Bruckner, T., Hooss, G., Knorr, W., Raddatz, T., & Tol, R. (2007). Aggregated Carbon cycle, atmospheric chemistry and climate model (ACC2): Description of forward and inverse mode, 14069106. https://doi.org/10.17617/2.994422

Tol, R. S. (2011). The Social Cost of Carbon. *Annual Review of Resource Economics*, *3*(1), 419–443. https://doi.org/10.1146/annurev-resource-083110-120028

van de Ven, D.-J., Mittal, S., Gambhir, A., Lamboll, R. D., Doukas, H., Giarola, S., Hawkes, A., Koasidis, K., Köberle, A. C., McJeon, H., Perdana, S., Peters, G. P., Rogelj, J., Sognnaes, I., Vielle, M., & Nikas, A. (2023). A multimodel analysis of post-Glasgow climate targets and feasibility challenges. *Nature Climate Change*, *13*(6), 570–578. https://doi.org/10.1038/s41558-023-01661-0

van Beek, L., Hajer, M., Pelzer, P., van Vuuren, D., & Cassen, C. (2020). Anticipating futures through models: The rise of Integrated Assessment Modelling in the climate science-policy interface since 1970. *Global Environmental Change*, *65*, 102191. https://doi.org/10.1016/j.gloenvcha.2020.102191

van Vuuren, D. P., den Elzen, M. G. J., Lucas, P. L., Eickhout, B., Strengers, B. J., van Ruijven, B., Wonink, S., & van Houdt, R. (2007). Stabilizing greenhouse gas concentrations at low levels: An assessment of reduction strategies and costs. *Climatic Change*, *81*(2), 119–159. https://doi.org/10.1007/s10584-006-9172-9

Weyant, J. (2017). Some Contributions of Integrated Assessment Models of Global Climate Change. *Review of Environmental Economics and Policy*, *11*(1), 115–137. https://doi.org/10.1093/reep/rew018

Wunderling, N., Winkelmann, R., Rockström, J., Loriani, S., Armstrong McKay, D. I., Ritchie, P. D. L., Sakschewski, B., & Donges, J. F. (2023). Global warming overshoots increase risks of climate tipping cascades in a network model. *Nature Climate Change*, *13*(1), 75–82. https://doi.org/10.1038/s41558-022-01545-9

CHAPTER II

POST-COVID-19 EMISSIONS PATHWAYS

Extended abstract

Context and aims of the chapter

The COVID-19 pandemic that emerged in China at the end of 2019, spread worldwide in the beginning of 2020 and led a majority of states to implement restrictive measures to curb the pandemic. It led to one of the most severe global recessions since 1900. Lockdowns and quarantines have forced many businesses to close, the subsequent disruptions of supply chains have further caused shortages of goods and delays in production. Many industries, such as travel and hospitality, have been hit particularly hard. Containment measures led to a significant reduction in automobile traffic and air travel. As a consequence, energy use declined, and so have CO_2 emissions.

The decline in CO_2 emissions, at an unprecedented level since the second world war (Liu et al., 2020), and the impossibility of predicting the future course of the pandemic have challenged the time horizons of climate mitigation studies, typically several decades. Furthermore, a new era of state interventionism started in the wake of the pandemic, as governments announced trillions of dollars of support and recovery measures to protect jobs and businesses and stimulate the economy. As most governments were committed to reducing emissions through their participation in the Paris Agreements, a nascent literature suggested steering the recovery in a climate friendly direction (IEA, 2020; Kikstra et al., 2021). One of these studies (Andrijevic et al., 2020) claimed that "a small fraction of announced COVID-19 economic recovery

packages could provide the necessary financial basis for a decided shift toward a Paris Agreement–compatible future" (Andrijevic et al., 2020). Their assertion was based on climate change mitigation scenarios generated by IAMs. IAMs calculated the investment needs required in each type of technology to limit CO_2 emissions and the rise in global temperature. The authors compared the investments from the mitigation scenarios with the current investments in the energy sectors, and derived the required increase in low-carbon investments, as well as the decrease in fossil-fuel investments. The net increase in total investment required in the energy sector appeared relatively low (20 billion dollars per year over the coming 5 years, as low-carbon investments should increase by 300 billion dollars per year while carbon-intensive investments should decrease by 280 billion dollars) compared to the more than 12 trillion dollars of total stimulus. In a study led by K. Tanaka, which I participated in as a co-author, we discussed the statements made in this study. One of the core arguments was that scenarios produced by IAMs are driven by a carbon tax whose trajectory determines the level of emissions and therefore not suited for investment analysis. A carbon tax incentivises low carbon investments, disincentivises carbon-intensive investments, but also strongly reduces near-term energy demand as energy prices increase: energy supply and demand are both affected by a carbon price, whereas subsidies to energy investments only affect the energy supply side. This study was published in Climatic Change (Tanaka et al., 2022). I contributed to the analysis of the IAMs data.

The aforementioned study provides a context to the study presented in this chapter. The objective of this study is to assess the impact of the coronavirus pandemic on future climate change pathways. As we consider the effects up to 2030, we have restricted ourselves to analysing emissions trajectories, without looking at the (negligible) impact on temperature trajectories. The study was published in *Environmental Research Communications* as a letter entitled: Limited impact of COVID-19 recovery packages on near-term CO2 emissions pathways (Y. Gaucher, K. Tanaka, P. Ciais and O. Boucher, 2022).

Methods

To estimate post-COVID-19 emission pathways, I started from existing recovery measures to estimate their possible impact on climate change mitigation. I computed projections of CO_2 based on two elements: an economic growth scenario and a carbon intensity scenario. I used the country-level GDP forecasts from the International Monetary Fund, which accounted for the pandemic effect on the economic activity, and extrapolated them until 2030. The scenarios of carbon intensity of GDP were built at the regional level. To build regional-level scenarios for the carbon intensity of GDP, I assumed that there was a linear correlation between carbon

intensity of GDP and low-carbon investments. These correlation coefficients were derived from existing scenarios produced with six different IAMs (McCollum et al., 2018), and they represent the decrease in the carbon intensity of GDP per dollar invested in low-carbon technology.

To project the decrease of the carbon intensity of GDP, I multiplied the reduction of the carbon intensity of GDP per dollar invested in low carbon technology at the regional level with the total post-COVID-19 low-carbon investment within the recovery packages. In the meantime, the International Energy Agency had published their annual World Energy Outlook reports (IEA, 2020, 2021), accounting for the recovery packages in their emission projections, based on a bottom-up model of the energy sector. An assessment of the impact of fiscal stimuli using the ARIO model, which describes the propagation of shocks through supply chains, had been published by Y. Shan, et al (Shan et al., 2021). We compared these two studies with the simple approach based on the relationship between investment and emissions.

Results

The analysis of the correlations between low-carbon investments and the carbon intensity of GDP led us to disregard the results of two IAMs out of six to establish the projections based on low-carbon packages. The relationship between low-carbon investments and emission reductions from the IEA World Energy Model lies within the range of the IAMs results. The emission reductions estimated using the results of the four remaining IAMs vary between 1% and 6% of the stated policy scenario of the IEA. The analysis of the scenarios produced using the ARIO model showed that the distribution of the stimulus across economic sectors, targeting heavy industry or high-technologies, had a very little impact on emission rebound.

Limits

The very simple analysis described above has three main caveats. First, it focused on low-carbon investments without considering fossil fuel investments that also influence emissions, and did not account for the very important US Inflation Reduction Act, which was adopted after the publication of the paper. Second, fiscal stimuli in the real world are only approximately equivalent to investments in IAMs, and the sectoral distribution of the recovery packages is not the same as that in IAMs, in contrast to what were assumed in our calculation. Third, as discussed in the Climatic Change (Tanaka et al., 2022) study conducted simultaneously , it is not the investment but the carbon price that is the driver of emission reductions in IAMs. Besides these economic arguments, it should be noted that the relationship between investments and

the carbon intensity of GDP is not always linear (see supplements 5.1.2), but we used a linear approximation because the investment amounts involved were relatively low.

Perspectives

I started to use the GET energy system model (Azar & Lindgren, 2003; Azar et al., 2006, 2013; Johansson et al., 2020), which was shared with me by Daniel Johansson, during this work, and we evaluated ways to use GET to infer the impacts of recovery packages on emission pathways. It turned out that this intertemporal optimisation model is not well suited to assess the role of energy system investments from public stimulus packages, which are only endogenously calculated as a part of the costs to optimize, without modelling of the financial system and its possible interactions with public investments through crowding-out or crowding-in effects, for instance. Furthermore, a model including a degree of path dependency, for example through technological learning and spill-over effects, could have been used to assess the long-term effects of public investments (Grubb et al., 2021), but these features are absent from the GET model. As a consequence, we did not use the GET model in this study but extensively used it in the next two studies that assess negative emission technologies (presented in chapters 3 and 4).

Limited impact of COVID-19 recovery packages on near-term CO_2 emissions pathways

Abstract

Part of the economic recovery plans implemented by governments following COVID-19 is directed towards the energy transition. To understand the potential effects of these post-COVID green recovery packages on reductions of greenhouse gases emissions, we investigated three different approaches. Firstly, we analysed simulation results of Integrated Assessment Models (IAMs) to infer the change in CO_2 intensity of GDP that could result from post-COVID low-carbon investment plans. Secondly, we investigated the scenarios provided by the International Energy Agency (IEA) based on a bottom-up energy system model. By combining the two approaches, we found that green recovery packages implemented and planned globally can lead to an emission reduction of merely 1%-6% from 2030 baseline levels at most. Thirdly, we looked into the results of the Adaptative Regional Input-Output model, which simulates the dynamic effects of economic crisis and fiscal stimuli through supply chains following labour shortage. The third approach shows that the increase of activity driven by fiscal stimuli leads to a rebound of CO_2 emissions even if they do not target carbon-intensive sectors. We conclude that green recovery packages targeting low-carbon technologies have a limited impact on near-term CO_2 emissions and that demand-side incentives, as well as other policy efforts to disincentivise the use of fossil fuels, are also important for scaling up climate mitigation.

1 Introduction

To foster the economic recovery in the aftermath of the COVID-19 crisis, stimulus plans exceeding 18 trillion USD in March 2022 were adopted by 89 countries with 95% of the funding concerning advanced economies and China (O'Callaghan et al., 2021). These countries have also committed to strongly reducing their greenhouse gas emissions, in line with the Paris Agreement targets that require a rapid phase-out of fossil fuels and enhanced investments in low-carbon sources (Tanaka & O'Neill, 2018). Many scholars have thus advocated for a "green recovery" that would take advantage of this unprecedented amount of public spending to restart the economy on a more sustainable basis (Andrijevic et al., 2020; Li & Li, 2021). The design of recovery measures is critical to reducing CO_2 emissions (Gawel & Lehmann,

2020). At the beginning of the crisis, (Hepburn et al., 2020) provided a qualitative assessment of possible recovery measures based on three indicators: the impact on growth, the climate impact, and the speed of implementation. However, they did not provide quantitative insights on them. (Andrijevic et al., 2020) (thereafter, A20) advocated for a fraction of the fiscal stimulus to be dedicated to the energy transition, as they estimated that additional low-carbon investments amounting to 300 billion USD/year during the 2020-2024 period were needed to put the world on a pathway to limit the global warming to 1.5°C. (Tanaka et al., 2022) analysed this assessment and argued that the required total energy investments can be larger in the near term, that energy investments must be sustained over the long term, and that other measures (in particular, high carbon pricing) are also needed to accompany energy investments. Using two IAMs, Rochedo et al. (Rochedo et al., 2021) showed that recovery investments would reduce emissions only by 3%-7

The objective of our study is to further assess the impact of stimulus packages on near-term emission pathways by analysing and comparing three different approaches. The first one builds upon A20, focusing on the impacts of low-carbon investments on CO_2 emissions. Correlations between low-carbon investments and the carbon intensity of GDP (the quantity of CO_2 emitted per GDP unit) from IAM results (McCollum et al., 2018)are combined with an analysis of post-COVID recovery investments in low-carbon technologies (O'Callaghan et al., 2021) to infer resulting emissions reductions. The second approach is the World Energy Outlook (WEO) reports of IEA published in October 2020 (IEA, 2020) and 2021 (IEA, 2021), which describe how different policies enforced in the post-COVID era can shape future energy scenarios. The third approach is that of (Shan et al., 2021) (thereafter, S21) who focus on emissions rebounds following fiscal stimuli with a model simulating the propagation of disruptions along supply chains.

2 Methods

2.1 Diagnostic from IAM scenarios

The first approach exploits the relationships between the increase of investments in low-carbon technologies and the associated decrease of the carbon intensity of GDP simulated by six IAMs driven by carbon prices: AIM/CGE, IMAGE, MESSAGEix-GLOBIOM, POLES, REMIND-MAgPIE, and WITCH-GLOBIOM, as provided in (McCollum et al., 2018) (thereafter, M18). Four scenarios are considered for each model: a scenario reflecting current policies, a scenario where Nationally Determined Contributions (NDC) are implemented, and two scenarios with global

carbon budgets of 1,000 and 400 Gt CO_2 until 2100, corresponding to 2°C and 1.5°C targets, respectively. The model results are available at the regional level, with the following five aggregated regions: OECD90+EU (OECD as it was in 1990 and EU countries), REF ("Reforming economies" indicating the former Soviet Union), LAM (Latin America), MAF (Middle East and Africa), and Asia (remaining Asian countries, including China).

M18 quantified the investments in the energy system required to achieve these climate goals through carbon pricing while developing energy supply across the 21st century and minimised the total discounted cost of mitigation (intertemporal optimisation) or the step-by-step costs supported by the economy (recursive dynamics). These costs include investments, fuel costs, operation and maintenance costs, and welfare loss due to lower consumption. Satisfying the carbon budget constraint requires high carbon prices, incentivising investments in energy efficiency and low-carbon energy sources, disincentivising carbon-intensive energy production, and reducing energy demand. This in general leads to a decrease in the CO_2 intensity of GDP. Low-carbon investments are thus negatively correlated with the CO_2 intensity of GDP in 2030 across the scenarios, both at the global and regional levels (Figure II.1).

To calculate the CO_2 emission reduction in 2030 for given low-carbon investments, we follow two successive steps. First, for each model and region, we linearly regress the carbon intensity of GDP in 2030 (in kg CO_2 per USD2020) against the cumulative low-carbon investment over 2021-2030 across all scenarios. Second, for each model, we apply these relationships on a region-by-region basis to calculate the reduction of the carbon intensity of GDP for given low-carbon investments and deduce the emission reduction by using the GDP growth forecast of the International Monetary Fund (IMF). Considering CO_2 intensity per GDP unit enables us to account separately for the effects of i) low-carbon investments on carbon intensity and ii) COVID-19 and fiscal stimuli on economic activity, which are already included in the IMF analysis. Low-carbon investments over 2021-2030 should decrease CO_2 emissions after 2030 as well, but we focus on emission reductions until 2030. The emission reductions before 2030 were linearly interpolated. The method discussed here is useful for our purpose, but one should bear in mind that it carries certain limitations arising from the use of IAM simulations driven by carbon prices, among others (see Section 4).

More technically, the regression slope $c_{r,\,m}$ represents the change in CO_2 intensity of GDP in 2030 (in kg CO_2/USD) in region r estimated from model m, accompanied by cumulative low-carbon investments of 1 billion USD between 2021 and 2030. Thus, increasing low-carbon investments by δI_r over this period yields a change in the regional carbon intensity of GDP, $\delta\, e_{r,m}$.

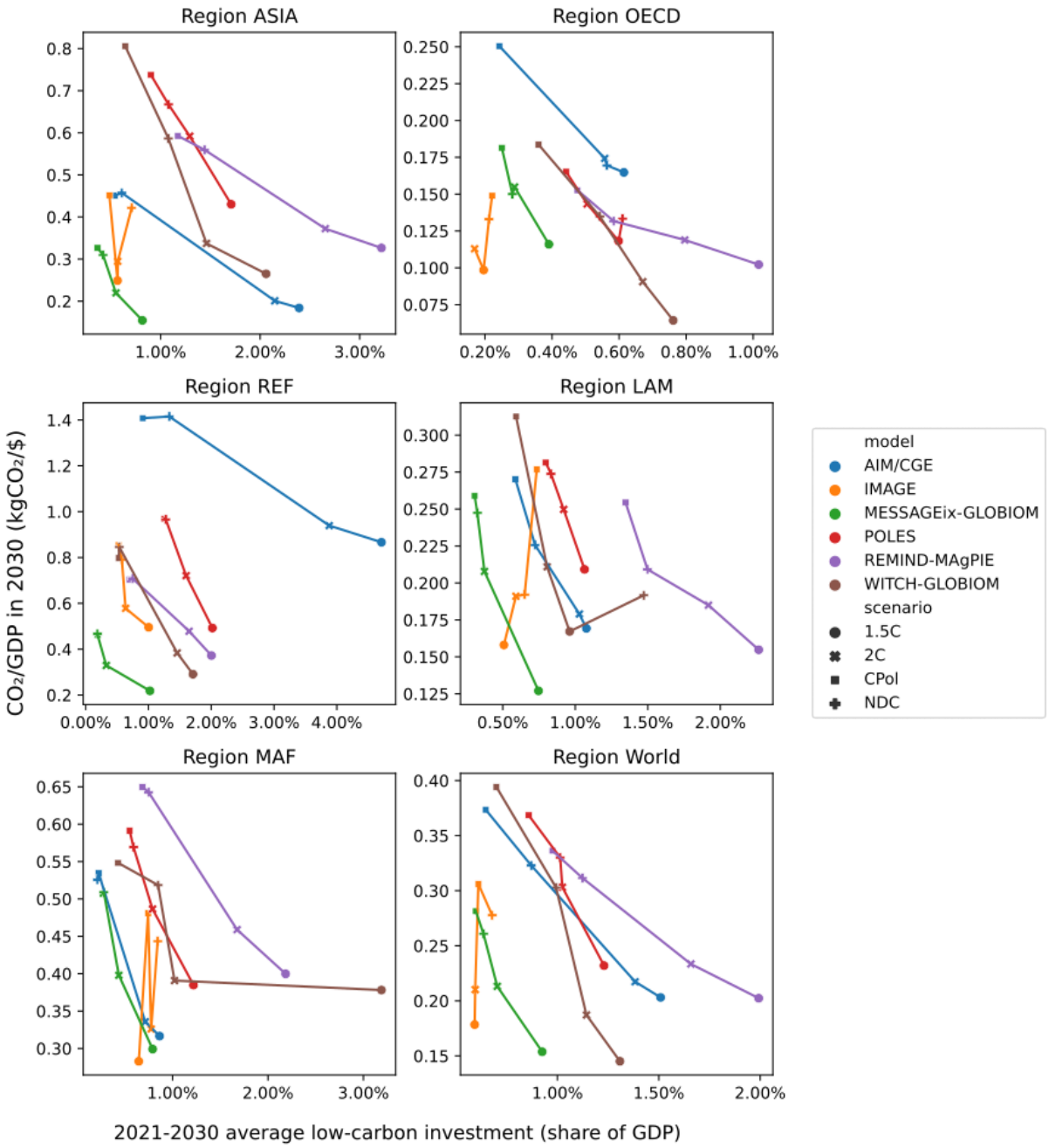

Figure II.1: Relationship between the CO_2 intensity of the GDP in 2030 and the 10-year (2021-2030) cumulative low-carbon investment in billion USD obtained from IAMs in M18. The monetary unit is USD2020. Each curve is composed of four points, one for each scenario, each panel is for a different region: Asia, LAM: Latin America, MAF: the Middle East and Africa, OECD: OECD as it was in 1990 and EU countries, REF: former Soviet Union, and the whole world.

$$\delta e_{r,m}(2030) = c_{r,m} \cdot \delta I_r$$

As a result, the regional emission changes by $\delta\, E_{r,m}(2030) = \delta\, e_{r,m}(2030) \cdot GDP_r(2030)$.

Regional GDP values in 2030 are based on IMF growth projections of October 2021 for 2021-2026 (IMF, 2021), extrapolated until 2030. The sum of $\delta\, E_{r,m}$ across regions gives the change in

global emissions.

To estimate the increase in low-carbon investments until 2030, we use the classification of the Oxford Recovery Project (United Nations Environment Programme, 2021). In M18, low-carbon investments cover "investments into renewable electricity and hydrogen production, bioenergy extraction and conversion, uranium mining and nuclear power, fossil energy equipped with CCS, and the portion of electricity T&D and storage investments that can be attributed to low-carbon electricity generation". For consistency with IAMs, we consider investments only in the categories of "clean transport infrastructure, clean energy sector, building upgrades and energy efficiency as low-carbon investments within the recovery packages." The other categories of green public investments are not considered as low-carbon investments: namely, "clean research and development investment and natural infrastructure and green spaces investments", which are not modelled in IAMs analysed by M18. Recovery packages inventoried by the Oxford Recovery Project are just partly dedicated to low-carbon technologies: low-carbon investments amount to 511 billion USD, 20% of total recovery investments (Table II.1).

The CO_2 emissions pathway is obtained by subtracting the emission reduction from a baseline pathway that does not account for recovery packages. The IEA 'Stated Policies Scenario' from WEO (IEA, 2020) (thereafter STEPS2020) is used as a baseline because it includes only a small fraction of recovery packages: low-carbon investments packages announced before mid-2020 amounted to 63 billion USD (O'Callaghan et al., 2021) when STEPS2020 was developed.

Table II.1: Total recovery investments by category. Data were obtained from the Oxford Recovery Project report, which reflected data available in the Oxford Recovery Observatory up to February 2022. In the Oxford Recovery Observatory, the total COVID-related fiscal spendings amount to 14.6 trillion USD and fall into three categories: recovery spending, rescue spending, and unclear spending. Investments in "recovery spending" (total amount: 2.6 trillion USD) are shown in Table II.2.

Type	Billion USD	Share
Low-carbon investments:	511.2	19.7%
Buildings upgrades and energy efficiency infrastructure investment	52.8	2.0%
Clean energy infrastructure investment	153.2	5.9%
Clean transport infrastructure investment	303.2	11.7%
Clean new housing investment	2.0	0.1%
Other investments:	2080.5	80.3%
Clean research and development investment	59.7	2.3%
General research and development investment	366.1	14.1%
Local (project-based) infrastructure investment	206.9	8.0%
Natural infrastructure and green spaces investment	169.7	6.5%
Other large-scale infrastructure investments	438.4	16.9%
Traditional energy infrastructure investments	40.5	1.6%
Traditional transport infrastructure investments	604.0	23.3%
Disaster preparedness and capacity building	177.0	6.8%
Military investments	18.2	0.7%
Total	2591.7	

Table II.2: Low-carbon recovery investments by region. Data were obtained from the Oxford Recovery Project report. See the caption of Table II.1.

Region	δIr (Billion USD)
ASIA	46.1
LAM	3.6
MAF	0.7
OECD	460.8
REF	0
Total	511.2

2.2 WEO scenarios of IEA

The second approach is based on the WEO reports from 2020 and 2021 (IEA, 2020, 2021). We consider the following three scenarios proposed by the IEA: STEPS2020, its update in 2021 (STEPS2021), and the Sustainable Development Scenario (SDS2020). STEPS are scenarios "which reflects current policy settings based on a sector-by-sector assessment of the specific policies that are in place, as well as those that have been announced by governments around the world." STEPS2020 and STEPS2021 incorporate NDCs and recovery measures adopted

before mid-2020 and mid-2021, respectively. SDS2020 has the same assumptions as those in STEPS2020 regarding economic growth, except that stringent climate and sustainable development policies are implemented in SDS2020: "a surge in clean energy policies and investment puts the energy system on track to achieve sustainable energy objectives in full, including the Paris Agreement, energy access and air quality goals".

These storylines describe the evolution of the energy system until 2050, from the extraction of fossil fuels to final energy use, energy markets, and investments required to satisfy the energy demand. The storylines are implemented to the World Energy Model (WEM), a technology-rich and data-intensive model. WEM computes how the energy system evolves to meet exogenous energy demand without feedback on the economy. STEPS2020 and SDS2020 have the same GDP growth.

SDS2020 incorporates a plan (sustainable recovery plan) designed to foster economic recovery while mitigating climate change. This plan is a set of various climate policies, from regulatory frameworks to market design and fiscal incentives, modelled with high granularity. For instance, the lifetimes of nuclear plants are extended, stronger standards are applied to domestic appliance energy efficiency, coal-fired powerplants are retired early or retrofitted to capture and store carbon, and motorway speed is reduced. Decarbonisation is not primarily driven by public investment: governments create appropriate policy frameworks including carbon pricing, but 70% of these investments are realised by private companies and are thus assumed to come from private finance.

2.3 Adaptative Regional Input-Output model

The third approach developed by S21 analyses the impact of the pandemic and fiscal stimuli on global emissions. The description of the economic impact of the pandemic focuses on the propagation of shocks through supply chains, including the interdependencies across different sectors and regions. They applied to this case study an Adaptative Regional Input-Output model (ARIO) (Hallegatte, 2008), which is designed to study the economic consequences of disasters.

It describes the economy as a set of households and producers belonging to different sectors and regions. Households create the final demand, and the supply from producers creates an intermediate demand. The production by a sector Δ of a good α requires three production factors: exogenous capital, exogenous labour, and other intermediate goods. Initially, production meets demand. Then comes the pandemic and associated restrictions: a temporary labour shortage

in sector Δ leads the production of good α to decrease. Substitution between factors is assumed to be impossible as actors cannot make the necessary adjustments on time. The demand of Δ for intermediate goods shrinks (backward propagation), as well as the downstream production that requires α (forward propagation). Firms can overproduce to rebuild their inventories to overcome the disruption, as labour and capital are not fully employed at pre-crisis production levels. Intermediate demand increases and then returns to the pre-crisis level. Furthermore, fiscal stimuli increase final demand: a 1 billion USD fiscal stimulus targeting sector Δ is modelled as an increase of 1 billion USD of final demand for α. CO_2 emissions are computed as the sum over all sectors of their activities multiplied by their exogenous emissions factor. The global carbon intensity of GDP is therefore susceptible to vary as the weight of different sectors and regions in the global economy changes and as emissions factors evolve exogenously.

S21 analysed several emissions pathways, termed fiscal stimuli (FS) scenarios, which differ by the severity of the pandemic and the fiscal measures taken until 2024 to mitigate economic damages. They differ in three regards: (i) the size of stimuli ("current FS" as of mid-2020 and "FS+" where fiscal stimuli amount to 10% of 2019 GDP in major economies, both distributed until 2024), (ii) the distribution across sectors (either targeting high-technology sectors or heavy industry, or keeping the current distribution), and (iii) the evolution of the emissions factor of each sector, to account for climate policies beyond fiscal stimuli. Furthermore, three cases are considered for emissions factors: in one case, they remain at the current level (Carbon Intensive Scenario (CIS)). The other cases were derived from the WEO of 2019: emissions factors either evolve consistently with the SDS scenario (SDS emissions factors) or the Stated Policy scenario (SPS emissions factors).

The main difference between ARIO and the other model approaches considered here is that ARIO explicitly models dynamic changes in activity levels. This enables a realistic account of the economic decline and rebound following the pandemic, whereas partial or general equilibrium models like the IAMs in M18 might overestimate short-term flexibility and substitution possibility (Hallegatte, 2008). But, contrarily to these IAMs, there is no 'investment' in ARIO that could increase means of low-carbon production because capital is exogenous. Mitigation measures appear only through sectoral carbon intensities.

3 Results

3.1 Linear regressions between low-carbon investments and carbon intensity

While the goodness of fit is very high in a majority of IAMs, IMAGE displays poor correlations (Table II.4). The regional regression slopes are highly model-dependent but negative throughout, except those of a few regions in IMAGE. Low-carbon investments are positively related to the carbon intensity of GDP in those regions of IMAGE because energy demands in IMAGE are so sensitive to the carbon price driving the simulations that energy demands shrink in response to high carbon prices, unlike those in most other IAMs (Tanaka et al., 2022). Poor correlations can also be seen in the results of WITCH-GLOBIOM, in which some regions are affected by the same phenomenon. Thus, the relationship between low-carbon investments and the carbon intensity of GDP holds only in a subset of IAM simulations we examine. For the sake of the analysis, we disregard these two models and apply the correlations estimated from other four models in the rest of this study.

Table II.3: Estimates of $c_{r,m}$ (in ($kgCO_2$/USD) / (billion USD)) of each model and region. $c_{r,m}$ represents the change in CO_2 intensity of GDP in 2030 (in $kgCO_2$/USD) associated with an increase of 1 billion USD in low-carbon investments during the period 2021 to 2030.

$c_{r,m}$	Model					
Region	AIM/CGE	IMAGE	MESSAGEix-GLOBIOM	POLES	REMIND-MAgPIE	WITCH-GLOBIOM
ASIA	-5.9×10^{-5}	-1.2×10^{-5}	-8.8×10^{-5}	-1.4×10^{-4}	-4.7×10^{-5}	-1.6×10^{-4}
LAM	-2.9×10^{-4}	6.1×10^{-4}	-3.1×10^{-4}	-3.8×10^{-4}	-1.2×10^{-4}	-1.5×10^{-4}
MAF	-5.1×10^{-4}	1.1×10^{-3}	-4.5×10^{-4}	-4.0×10^{-4}	-2.3×10^{-4}	-8.6×10^{-5}
OECD90+EU	-4.2×10^{-5}	1.1×10^{-4}	-7.1×10^{-5}	-3.5×10^{-5}	-1.3×10^{-5}	-4.6×10^{-5}
REF	-6.4×10^{-4}	-2.2×10^{-3}	-5.2×10^{-4}	-3.7×10^{-3}	-1.2×10^{-3}	-1.2×10^{-3}

Table II.4: $R^2_{r,m}$, the determination coefficient of the regression of the carbon intensity of GDP in 2030 against the cumulative low-carbon investment over 2021-2030.

$R^2_{r,m}$	Model					
	AIM/CGE	IMAGE	MESSAGEix-GLOBIOM	POLES	REMIND-MAgPIE	WITCH-GLOBIOM
ASIA	0.995	0.001	0.946	0.999	0.992	0.914
LAM	0.971	0.851	0.944	0.999	0.907	0.387
MAF	0.985	0.339	0.953	0.979	0.992	0.551
OECD	0.994	0.463	0.920	0.851	0.948	0.998
REF	0.985	0.705	0.849	0.995	0.995	0.996

3.2 Emissions pathways

The emission reduction obtained from the first approach using our estimate of green recovery packages (Table II.2) is 0.5-2.2 $GtCO_2$/year in 2030, which represents merely a 1%-6% emission reduction from the baseline level (Figure II.2 and Table II.5). This reduction is small: for comparison, the 2030 emissions level in SDS2020 is 8.98 $GtCO_2$/year lower than in STEPS2020. This 2030 emissions reduction in SDS2020 of 25% from 2019 levels is within the range of emission pathways towards the 1.5°C target with a high overshoot (IPCC, 2022).

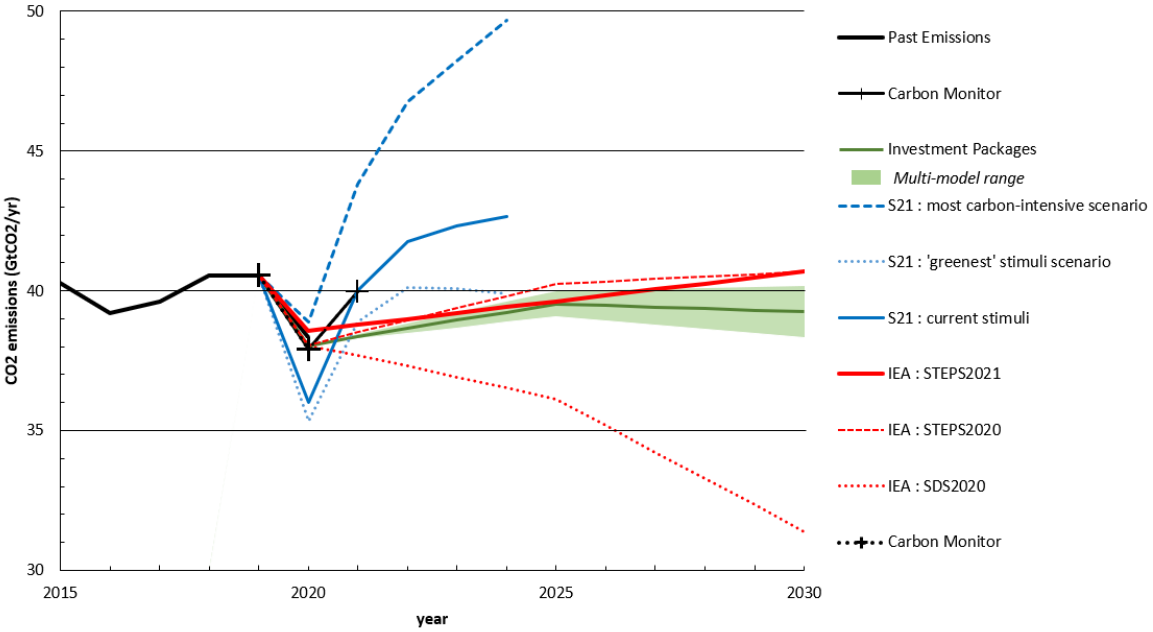

Figure II.2: Global total anthropogenic CO_2 emissions pathways (in $GtCO_2$/year) until 2030. The black curve represents historical emissions until 2020 from the Global Carbon Project (GCP) (**friedlingsteinGlobalCarbonBudget2022**). The black cross represents the estimate by the Carbon Monitor (Liu et al., 2020). The red curves are based on IEA WEO scenarios. The green curve represents the multi-model mean of emissions pathways obtained by subtracting the emission reduction based on the correlation with low-carbon investments from the STEPS2020 baseline. The green area represents the multi-model range of such emissions pathways. Blue curves are obtained from S21: The most carbon-intensive scenario has CIS emission factors, FS+ targeting heavy industries. The current stimuli scenario has current FS and SPS emissions factors. The 'greenest' stimuli scenario has current FS targeting high-technology sectors and SDS emission factors. All emissions pathways are adjusted to match the GCP estimates for 2019 (see supplements 5.3 for scenario corrections).

3.3 Low-carbon investments and emission reductions

Investment and emission reductions in IAMs The slopes of the linear regression (Figure II.1, Table II.3) can be used to infer the amount of low-carbon investment in each region between 2021 and 2030 required to reduce emissions by 1 tCO_2/year in 2030 [USD/ (tCO_2/year)], which is given as $\frac{-1000}{c_{r,m} \times GDP_r(2030)}$ (where $GDP_r(2030)$ is in billion USD). At the global scale, low-

carbon investments per t CO_2 of emission reduction in 2030 are obtained by dividing the global post-COVID low-carbon investments (Table II.2) by the amount of resulting emissions reduction in 2030 (Table II.5). This quantity was estimated to have a range from 230 to 1,120 USD/ (t CO_2/year) across the IAMs, with a multi-model mean of 540 USD/ (t CO_2/year). The comparison between STEPS2020 and SDS2020 returns similar results: low-carbon investments during the 2021-2030 period in SDS2020 are higher by 570 billion USD/year than in STEPS2020. This corresponds to an additional cumulative investment of 5,690 billion USD. The emissions differ by 8.98 $GtCO_2$ in 2030, resulting in a low-carbon investment per tCO_2 reduction of 633 USD/ (tCO_2/year).

By using the same IAM results as in our study (i.e. data from M18), A20 estimated that additional low-carbon investments of 300 billion USD/year until 2024 (hence, 1,500 billion USD until 2024) were required to put the energy system on track to achieve the 1.5°C target. Our corresponding estimate is 410-1,220 billion USD/year (see SM4). The A20 estimate is slightly below our range, which can be explained by the following methodological differences between the two studies. Firstly, when deriving the relationship between low-carbon investments and emission reductions from IAMs, A20 considered only 1.5°C and current policies scenarios till 2024 at global level, whereas our study considered four scenarios (including NDC and 2°C scenarios) till 2030 at regional level. Secondly, while A20 used the results from all available IAMs, our study excluded a subset of IAMs that exhibits energy demand being very sensitive to carbon prices. Thirdly, we incorporated the effect of GDP growth in estimating emission reductions, which was not considered in A20. Fourthly, the scope of low-carbon investments considered in A20 is wider than that in our study (and therefore that in M18).

We further note that, whereas A20 and our study reached similar estimates of required low-carbon investments, the two studies provide different yet complementary perspectives. A20 emphasized how little the required low-carbon investment is, compared to the massive COVID-related fiscal spendings, calling primarily for more green recovery investments. In contrast, our study focuses on the estimate of current green recovery packages and argues that current green recovery packages are inadequate for achieving the 1.5°C target of the Paris Agreement and highlights the need for other measures to support climate mitigation efforts, as discussed in the rest of this paper.

Fiscal stimuli and emissions in ARIO We have a few remarks regarding the role of fiscal stimuli in S21. In the third approach, an analysis of the results shows that the main driver of emission levels is the assumed emissions intensity of each sector In 2024, the emission levels in scenarios with SDS and CIS sectoral carbon intensities are about 8% lower and 20% higher than in the reference scenario (based on SPS carbon intensities, “current fiscal stimulus size”, “current fiscal stimulus structure”). In contrast, the emission levels change by just less than

0.3% across different structures and sizes of fiscal stimulus for a given set of carbon intensities. Hence, varying the size and structure of fiscal stimuli has a minor impact compared to the choice of sectoral carbon intensities.

In the third approach, neither the size nor the structure of fiscal stimuli plays a decisive role: prioritising high-tech industries over heavy industries is insufficient to reduce emissions. This approach provides useful insights into the short-term emission decline and rebound following the pandemic through supply chains across different sectors and regions. However, such an approach is of lesser use to assess the role of fiscal stimuli on emission pathways involving the longer-term decarbonization of energy system because emission levels are essentially the direct outcome of the choice of sectoral carbon intensities, which are not driven by the fiscal stimuli.

4 Discussion and conclusions

This study provides insight into the claim that low-carbon investments included in the recovery packages will not induce a sufficient change in the energy system to achieve the Paris agreement targets (Rochedo et al., 2021; Tanaka et al., 2022; United Nations Environment Programme, 2021). It should however be noted that the use of the investment-emission relationships has three caveats. Firstly, it focuses on low-carbon investments, only a very small fraction of fiscal stimuli, leaving fossil fuel investments that also influence emissions. Secondly, fiscal stimuli in the real world can be only coarsely related to low-carbon investments in IAMs. Thirdly, low-carbon investments are just partially related to CO_2 emissions reductions in the results of IAMs that are driven by carbon prices. These imply that the use of the investment-emission relationships may lead to an overestimation of CO_2 emission reductions per unit investment. Each of the three caveats are discussed below.

Firstly, the investment-emission relationships only reflect a tiny part of the total fiscal stimuli (i.e. 511 billion USD of low-carbon investments for the total fiscal stimulus of more than 18 trillion USD). Although the recovery of economic activity through fiscal stimulus measures is factored into the estimates of GDP levels in 2030, this approach assumes that only low-carbon investments affect the emissions intensity of GDP. Measures supporting carbon-intensive industry within fiscal stimuli are neglected, as well as recovery investments dedicated to carbon-intensive sectors (40 billion USD for traditional energy infrastructure and 600 billion USD for traditional transportation infrastructures), but could increase the carbon intensity of GDP. Hence, the focus on low-carbon investments may lead to an overestimation of subsequent emission reductions.

Secondly, low-carbon investments in recovery packages cannot be related unambiguously

to low-carbon investments in IAMs for two reasons: i) investments are not categorised in the same way between the Oxford Recovery Project database and IAMs, and ii) the allocation of investments across sectors and regions is different. Low-carbon investments modelled by IAMs are mainly supply-side investments (70% of low-carbon investments (IEA, 2020)). In contrast, the supply side represents only 30% of current low-carbon recovery packages through clean energy infrastructure investment (Table 1). The current regional allocation of the low-carbon investment package is different from the allocation in cost-effective mitigation pathways in IAMs. 90% of the low-carbon investments from recovery packages are deployed in OECD90+EU countries. 9% are deployed in Asia, less than 2% in Latin America, the Middle East and Africa, and 0% in the former Soviet Union. These mismatches of regional allocations will limit the global efficiency of the investments, as also pointed out in the latest version of the WEO (IEA, 2021) and the associated Sustainable Recovery Tracker updated in February 2022 (IEA, 2022). The use of the suboptimal investment allocation in the optimal IAM results implies that the amount of emission reductions for given low-carbon investments may be overestimated.

Thirdly, in the IAM results we analysed, low-carbon investments do not fully explain CO_2 emissions reductions because these IAMs are driven by carbon pricing that can induce changes in CO_2 emissions also through other pathways. In IAMs, an increase in carbon prices incentivises investments in energy efficiency and low-carbon energy sources, disincentivises carbon-intensive energy production, and reduces energy demand to satisfy the carbon budget constraint (Tanaka et al., 2022). The impact of low-carbon investments alone is limited: Rochedo et al. (Rochedo et al., 2021) used IAMs that directly simulated low-carbon investments (i.e. without driven by carbon pricing) and has shown that, even if the recovery investments represent a significant part (17-35%) of the investments in low-carbon technologies until 2030, they reduce emissions by only a small fraction (3-7%) of what is needed to achieve the 1.5°C target. Low-carbon investment is only one of the levers mobilised in the models to achieve a given climate policy target. This also suggests that the use of the investment-emission relationships may lead to an overestimation of emission reductions.

Our numerical analysis based on the investment-emission relationship suggested that near-term CO_2 emission reductions to be realized through current green recovery packages would be insufficient for climate mitigation toward the 1.5°C target. The final discussion here further suggests that such emission reductions may even be an overestimate due to the methodological limitations. Counterbalancing the rebound of emissions stimulated by fiscal stimuli and ensuring emission reductions on a long-term basis requires broader measures to disincentivize the use of fossil fuels, incentivise demand-side requirements, and make the most of low-carbon investments deployed by governments.

Table II.5: Emissions reduction in 2030 (in $GtCO_2$/year) calculated from its correlation with low-carbon investments found in the Oxford Recovery Project database.

Model	Emission reduction in 2030 ($GtCO_2$/year)	As a percentage of baseline emissions level in 2030
AIM/CGE	1.30	3.7%
MESSAGEix-GLOBIOM	2.22	6.2%
POLES	1.26	3.5%
REMIND-MAgPIE	0.46	1.3%

Acknowledgements We are grateful to Dabo Guan and Yuli Shan for sharing with us the GDP data of the ARIO simulations and providing useful insights on their model to us. We also thank Christian Azar and Daniel Johansson for their useful comments during the development of this study.

Funding Y.G. acknowledges financial support from the Carbon Circular Economy (FOCUS) programme at the Commissariat à l'énergie atomique et aux énergies alternatives (CEA), France. K.T. benefited from State assistance managed by the National Research Agency in France under the Programme d'Investissements d'Avenir under the reference ANR-19-MPGA-0008.

Conflict of Interest The authors declare no conflict of interest.

Data availability Data supporting the conclusions, Excel files and Python code used to generate the figures in the paper are available on Zenodo with https://doi.org/10.5281/zenodo.6554030

References

Andrijevic, M., Schleussner, C.-F., Gidden, M. J., McCollum, D. L., & Rogelj, J. (2020). COVID-19 recovery funds dwarf clean energy investment needs. *Science*, *370*(6514), 298–300. https://doi.org/10.1126/science.abc9697

Azar, C., Johansson, D. J. A., & Mattsson, N. (2013). Meeting global temperature targets—the role of bioenergy with carbon capture and storage. *Environmental Research Letters*, *8*(3), 034004. https://doi.org/10.1088/1748-9326/8/3/034004

Azar, C., & Lindgren, K. (2003). Global energy scenarios meeting stringent CO2 constraints— cost-effective fuel choices in the transportation sector. *Energy Policy*, 16.

Azar, C., Lindgren, K., Larson, E., & Möllersten, K. (2006). Carbon Capture and Storage From Fossil Fuels and Biomass – Costs and Potential Role in Stabilizing the Atmosphere. *Climatic Change*, *74*(1-3), 47–79. https://doi.org/10.1007/s10584-005-3484-7

Gawel, E., & Lehmann, P. (2020). Killing Two Birds with One Stone? Green Dead Ends and Ways Out of the COVID-19 Crisis. *Environmental & Resource Economics*, 1–5. https://doi.org/10.1007/s10640-020-00443-y

Grubb, M., Wieners, C., & Yang, P. (2021). Modeling myths: On DICE and dynamic realism in integrated assessment models of climate change mitigation. *WIREs Climate Change*, *12*(3), e698. https://doi.org/10.1002/wcc.698

Hallegatte, S. (2008). An Adaptive Regional Input-Output Model and its Application to the Assessment of the Economic Cost of Katrina. *Risk Analysis*, *28*(3), 779–799. https://doi.org/10.1111/j.1539-6924.2008.01046.x

Hepburn, C., O'Callaghan, B., Stern, N., Stiglitz, J., & Zenghelis, D. (2020). Will COVID-19 fiscal recovery packages accelerate or retard progress on climate change? *Oxford Review of Economic Policy*, *36*, S359–S381. https://doi.org/10.1093/oxrep/graa015

IEA. (2020). *World Energy Outlook 2020*. https://www.oecd-ilibrary.org/content/publication/557a761b-en

IEA. (2021). *World Energy Outlook 2021*. https://www.oecd-ilibrary.org/content/publication/14fcb638-en

IEA. (2022). *Sustainable Recovery Tracker – Analysis*. IEA. Retrieved March 4, 2022, from https://www.iea.org/reports/sustainable-recovery-tracker

IMF. (2021, October). *World Economic Outlook*.

IPCC. (2022). *Climate Change 2022: Mitigation of Climate Change. Contribution of Working Group III to the Sixth Assessment Report of the Intergovernmental Panel on Climate Change*. IPCC.

Johansson, D. J. A., Azar, C., Lehtveer, M., & Peters, G. P. (2020). The role of negative carbon emissions in reaching the Paris climate targets: The impact of target formulation in integrated assessment models. *Environmental Research Letters*, *15*(12), 124024. https://doi.org/10.1088/1748-9326/abc3f0

Kikstra, J. S., Vinca, A., Lovat, F., Boza-Kiss, B., van Ruijven, B., Wilson, C., Rogelj, J., Zakeri, B., Fricko, O., & Riahi, K. (2021). Climate mitigation scenarios with persistent COVID-19-related energy demand changes. *Nature Energy*, *6*(12), 1114–1123. https://doi.org/10.1038/s41560-021-00904-8

Li, R., & Li, S. (2021). Carbon emission post-coronavirus: Continual decline or rebound? *Structural Change and Economic Dynamics*, *57*, 57–67. https://doi.org/10.1016/j.strueco.2021.01.008

Liu, Z., Ciais, P., Deng, Z., Lei, R., Davis, S. J., Feng, S., Zheng, B., Cui, D., Dou, X., Zhu, B., Guo, R., Ke, P., Sun, T., Lu, C., He, P., Wang, Y., Yue, X., Wang, Y., Lei, Y., … Schellnhuber, H. J. (2020). Near-real-time monitoring of global CO2 emissions reveals the effects of the COVID-19 pandemic. *Nature Communications*, *11*(1), 5172. https://doi.org/10.1038/s41467-020-18922-7

McCollum, D. L., Zhou, W., Bertram, C., de Boer, H.-S., Bosetti, V., Busch, S., Després, J., Drouet, L., Emmerling, J., Fay, M., Fricko, O., Fujimori, S., Gidden, M., Harmsen, M., Huppmann, D., Iyer, G., Krey, V., Kriegler, E., Nicolas, C., … Riahi, K. (2018). Energy investment needs for fulfilling the Paris Agreement and achieving the Sustainable Development Goals. *Nature Energy*, *3*(7), 589–599. https://doi.org/10.1038/s41560-018-0179-z

O'Callaghan, B., Yau, N., Murdock, E., Tritsch, D., Janz, A., Blackwood, A., Purroz Sanchez, L., Sadler, A., Wen, E., Kope, H., Flodell, H., Tillman-Morris, L., Ostrovsky, N., Kitsberg, A., Lee, T., Hristov, D., Didarali, Z., Chowdhry, K., Karlubik, M., … Heeney, L. (2021). *Global Recovery Observatory*. Oxford University Economic Recovery Project. Retrieved January 24, 2022, from https://recovery.smithschool.ox.ac.uk/tracking/

Rochedo, P. R. R., Fragkos, P., Garaffa, R., Couto, L. C., Baptista, L. B., Cunha, B. S. L., Schaeffer, R., & Szklo, A. (2021). Is Green Recovery Enough? Analysing the Impacts of Post-COVID-19 Economic Packages. *Energies*, *14*(17), 5567. https://doi.org/10.3390/en14175567

Shan, Y., Ou, J., Wang, D., Zeng, Z., Zhang, S., Guan, D., & Hubacek, K. (2021). Impacts of COVID-19 and fiscal stimuli on global emissions and the Paris Agreement. *Nature Climate Change*, *11*(3), 200–206. https://doi.org/10.1038/s41558-020-00977-5

Tanaka, K., Azar, C., Boucher, O., Ciais, P., Gaucher, Y., & Johansson, D. J. A. (2022). Paris Agreement requires substantial, broad, and sustained policy efforts beyond COVID-19 public stimulus packages. *Climatic Change*, *172*(1), 1. https://doi.org/10.1007/s10584-022-03355-6

Tanaka, K., & O'Neill, B. C. (2018). The Paris Agreement zero-emissions goal is not always consistent with the 1.5 °C and 2 °C temperature targets. *Nature Climate Change*, *8*(4), 319–324. https://doi.org/10.1038/s41558-018-0097-x

United Nations Environment Programme. (2021). Are We Building Back Better? Evidence from 2020 and Pathways to Inclusive Green Recovery Spending. https://wedocs.unep.org/20.500.11822/35281

5 Supplements

5.1 Calculations underlying investment-emissions relationships

The definition of each region can be found in M18.

5.1.1 Mathematical formulation

Following M18, we consider as low-carbon investments the investments dedicated to : 'renewable electricity and hydrogen production, bioenergy extraction and conversion, extraction and conversion of nuclear energy, fossil energy equipped with CCS, and the portion of electricity T&D and storage investments that can be attributed to low-carbon electricity generation '.

The low-carbon investments in McCollum et al. (2018) expressed as a share of GDP between 2021 and 2030 are negatively correlated with the CO_2 intensity of GDP in 2030 across the scenarios, both at the global (Figure 1) and regional levels. For each aggregated region r (including the World) and each model m, and scenario s we denote $i^s_{r,m}(t)$ the low-carbon investment at time t divided by MER GDP: the average annual low-carbon investment as a share of GDP over 2021-2030 is equal to:

$$i^s_{r,m} = \frac{1}{5} i^s_{r,m}(2020) + \frac{11}{20} i^s_{r,m}(2025) + \frac{1}{4} i^s_{r,m}(2030)$$

The emission intensity in 2030 is noted $e^s_{r,m}(2030) = \frac{E^s_{r,m}(2030)}{GDP^s_{r,m}(2030)}$. For each pair *(r,m)*, we ap-

ply a linear regression between the 'observed value' $e^s_{r,m}(2030)$ and the 'explanatory variables' $i^s_{r,m}$. The regression slope is noted $c_{r,m}$.

Increasing yearly low-carbon investments by $\delta I_r(k), k \in [2021, 2030]$ (where k is the year) yields a change in the carbon intensity of GDP of:

$\delta e_{r,m}(2030) = c_{r,m} \cdot \frac{1}{10} \sum_{2020k \leq 2030} \frac{\delta I_r(k)}{GDP_r(k)}$ (Eq 1)

$\delta I_r = \frac{P_r}{10}$, where P_r is the low-carbon investment within recovery package of region r, because investments are assumed to be evenly distributed until 2030. The following regional emission change in 2030 is $\delta E_{r,m}(2030) = \delta e_{r,m}(2030) \cdot GDP_r(2030)$, and we sum across regions to obtain the global emission reduction:

$$\delta E_m(2030) = \sum_r \delta E_{r,m}(2030)$$

The 2030 global emission level is obtained by adding $\delta E_m(2030)$ (which is negative) to the 2030 CO_2 emission level projected in STEPS2020: $E(2030) = E_{STEPS2020}(2030) + \delta E_m(2030)$. The emissions reductions between 2021 and 2030 are growing linearly from zero to $\delta E_m(2030)$:

$E(t) = E_{STEPS2020}(t) + \frac{t-2020}{10} \delta E_m(2030)$ for t between 2021 and 2030.

5.1.2 Mathematical caveat

The relation between low-carbon investments and the carbon intensity of GDP cannot be always linear, because of an aggregation issue. Assume that it is linear, and that we have one region R composed of two sub regions R1 and R2. We would have:

$\delta E = c_R \delta I_R GDP_R = c_R (\delta I_{R1} + \delta I_{R2}) (GDP_{R1} + GDP_{R2})$

$\delta E = c_{R1} \delta I_{R1} GDP_{R1} + c_{R2} \delta I_{R2} GDP_{R2}$

Which implies $c_R = c_{R1} = c_{R2} = 0$ if the relations must be true for all values of $\delta I_{R1} and\ \delta I_{R2}$. Therefore, the relation should be considered as a local linearisation and used carefully.

5.2 Cumulated investment abatement cost

For a total green recovery package of Y $ yielding an emission reduction of X tCO_2/year in 2030 compared to a reference scenario, we define the 'cumulated investment abatement cost' as Y/X. Conversely, if one uses the investment-emission relationship to compute required cumulated low-carbon investments to reduce emissions by X tCO_2/yr. in 2030 compared to a reference scenario, the necessary amount X * CIACW, where CIACW is the 'cumulated investment abatement cost' for the whole world, that is to say without using the regional disaggregation as investments should be distributed as in the model. Extension of IMF forecasts

The IMF forecasts only goes until 2026. We extended the growth rates forecasts until 2030 by linearly extrapolating regional growth rates, and the dollar inflation rates which reaches 2\% in 2030 (extrapolation starts in 2027) (Figures II.3 & II.4 .)

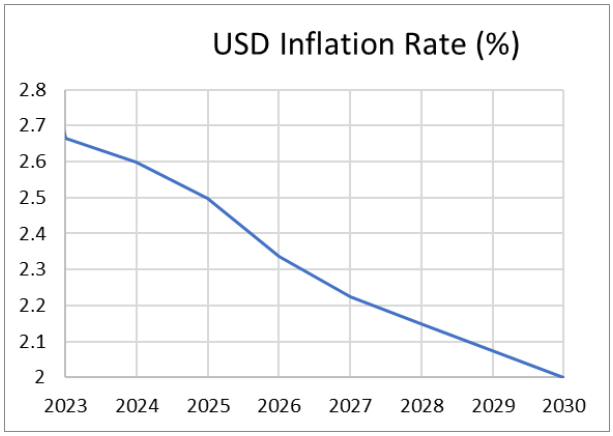

Figure II.3: Inflation rate forecast: IMF 2023-2026, extrapolation 2027-2030

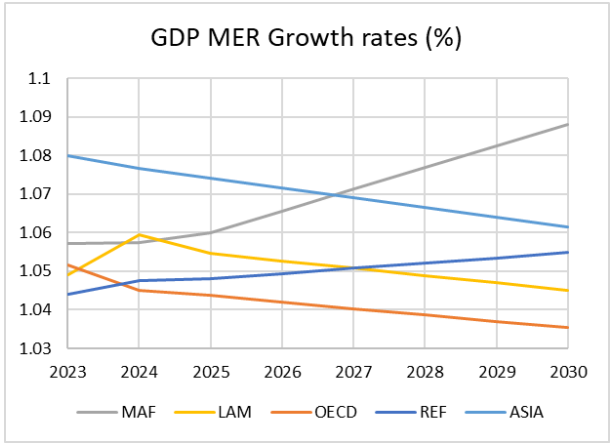

Figure II.4: Gross domestic product (market exchange rates) growth rate. Forecast: IMF 2023-2026, extrapolation 2027-2030.

5.3 Scenarios corrections

The scenarios are derived from 4 datasets, that have different estimations of the CO_2 emissions levels. Therefore, we assume that we can correct them in order to ease the comparison.

1/ The GCP was used for historical fossil CO_2 emissions and land use CO_2 emissions. We also used it as a reference to make all emissions forecasts start at the same level.

2/ The IEA emissions pathways only include energy and industry CO_2 emissions. IEA emissions pathways start in 2015. Between 2015 and 2019, the levels between IEA estimate and GCP fossil fuel estimates differ on average by 1.013 $GtCO_2/yr$. Hence, we add this difference to future IEA emission levels.

3/ The Carbon monitor estimate for 2019 is 1.384 $GtCO_2/yr$ lower than the GCP estimate. We add this difference to the 2020 and 2021 carbon monitor emission levels.

4/ The S21 emissions forecasts include 79 countries that are responsible for 90\% of 2017 global emissions. As we are interested in global emissions, we scale the S21 estimates, by multiplying the emissions levels by 100/90. The S21 emissions pathways start in 2017, and the difference with GCP between 2017 and 2019 after scaling is still 5.34 $GtCO_2/yr$. We add this difference to 2020 to 2024 S21 estimates.

Finally, the land-use emissions over the past five years (2016-2020) are 3.65 $GtCO_2/yr$ according to GCP. As land-use emissions are stable over the past five years, we assume that land-use emissions will remain constant over the next ten years, and add this average of $3.65GtCO_2/yr$ to the IEA pathways, the Carbon monitor estimate and the S21 emissions forecasts.

CHAPTER III

ENHANCED WEATHERING

Extended abstract

Context and aims of the chapter

The large-scale deployment of carbon dioxide removal techniques required to achieve ambitious mitigation targets raises sustainability questions. Mitigation scenarios produced by IAMs often rely on intensive use of BECCS and afforestation, which could have adverse effects on food security, water and nutrient resources (Fajardy et al., 2021; Fuss et al., 2018; Köberle, 2019; Li et al., 2021). For this reason, many studies have emphasized the need to explore complementary CDR methods. This chapter explores one of them: the enhanced weathering (EW) of basalt.

Geochemical weathering is a natural process that erodes rocks and mineralizes atmospheric CO_2, sequestering it for millions of years. This phenomenon affects the carbon cycle over geological timescales (Lenton & Britton, 2006). Enhanced weathering is a carbon dioxide removal solution that aims at accelerating this natural process by increasing the reactive surface of silicate or carbonate-rich rocks by grinding and applying them to conductive locations. EW is a low-tech carbon dioxide removal and can thus be scaled up rapidly, with no carbon dioxide storage infrastructures required, contrarily to direct air carbon capture and storage or bioenergy with carbon capture and storage. However, EW is energy-intensive: rocks must be extracted, grounded, transported to suitable application sites and spread over soils. To reduce the energy consumption of rock grinding, alternatives have been suggested: coastal applica-

tion taking advantage of the kinetic energy of waves to erode the rocks (Fakhraee et al., 2023; Hangx & Spiers, 2009; Renforth & Henderson, 2017), or the use of industrial waste (Bullock et al., 2021; Santos et al., 2023), including mine tailings (Bullock et al., 2022; Wilson et al., 2009) and steel slag (Reddy et al., 2019). The carbon dioxide removal potential of EW has been assessed in previous publications (Beerling et al., 2018, 2020; Fuss et al., 2018; Kantzas et al., 2022; Renforth, 2012; Renforth, 2019; Smith et al., 2016). Its role in future mitigation strategies has been explored with IAMs such as REMIND-MAgPIE (Strefler et al., 2018, 2021a) and GCAM (Fuhrman et al., 2023), which have notably considered aspects of energy and land use. These works suggest a significant potential contribution of EW to climate change mitigation.

In addition to carbon dioxide removal, EW of silicates has been advocated as a means of improving soil quality, particularly in agricultural areas, by limiting soil acidity and replacing fertilizers and lime (Barak et al., 1983; Beerling et al., 2018; Hinsinger et al., 1995; Van Straaten, 2006). Basalt in particular has attracted attention because it contains elements that are essential for plant growth, in particular phosphorus (**deoliveiragarciaImpactsEnhancedWeathering2020**), with low concentrations of harmful elements such as nickel or chromium, unlike other fast weathering rocks such as olivine (Beerling et al., 2018). The fertilizing potential of basalt could therefore be used to increase the land carbon sink. Since the fixation of carbon dioxide through photosynthesis is limited by low soil fertility in a wide range of ecosystems, it could theoretically be possible to enhance ecosystem carbon storage by spreading nutrient-rich basalt dust: this is what D. Goll called the biotic CDR pathway of EW (Goll et al., 2021), in contrast to the abiotic or geochemical mineralization of CO_2. Using ORCHIDEE-CNP, a land-surface model that resolves how phosphorus stimulates ecosystems, D. Goll and his co-authors (which include my two PhD supervisors, K. Tanaka and P. Ciais) have estimated that the biotic CDR could be larger than the geochemical CDR from EW. Since their results are based on an idealized scenario in which large quantities of basalt are applied everywhere all at once, we cannot directly deduce what the potential role of this method could be in a mitigation pathway (Tan & Aviso, 2021). Furthermore, existing IAMs studies have only considered applications of EW in agricultural areas, without accounting for the effects on vegetation productivity due to nutrient inputs. The objective of the research presented in this chapter is thus to address this gap, by assessing the potential of enhanced weathering, including the biotic effect, in cost-effective mitigation pathways. This study, entitled Leveraging ecosystems responses to enhanced rock weathering in mitigation scenarios (Y. Gaucher, K. Tanaka, D. Johansson, D. Goll, P. Ciais, 2023) is currently under review in Nature Communications.

Methods

This work is based on a coupled model that I developed during my thesis, GET-ACC2, which produces least-cost energy transition pathways while keeping endogenous climate variables, such as global-annual mean temperature, within prescribed constraints. I started from two pre-existing models: the GET model, a model of the energy system, and the ACC2 model, an aggregated model of climate, the carbon cycle and atmospheric chemistry. The GET model is a partial equilibrium model of the global energy system with a single region. GET calculates least-cost scenarios with perfect foresight, to meet the energy demand in 5 end-use sectors, and computes the CO_2, CH4 and N2O emissions of the energy system. The model was developed and maintained at Chalmers University of Technology (C. Azar & Lindgren, 2003; C. A. Azar et al., 2000), and is notably one of the first models that introduced bioenergy with carbon capture and storage, called "BECS" (C. Azar et al., 2006). A single-region version coupled with a simple carbon cycle and climate model, GET-Climate (C. Azar et al., 2013), was shared with me by Daniel Johansson. I updated the costs of energy supply technologies and of electric vehicles, which had become obsolete in view of the recent decline of the costs of wind turbines, solar photovoltaic panels and batteries, and I replaced the climate and carbon cycle module with ACC2.

Furthermore, I developed and added a module for enhanced weathering to the model. It has two main components. The first one is the representation of the supply of basalt dust from rock mining to soil amendment. This component is coupled to the energy system model, as energy is used during each step of the process. The model distinguishes application to agricultural land or forests, without further spatial disaggregation. Forests application incurs higher costs since it is assumed that not all suitable areas can be accessed via tractors. Aircrafts are thus required to spread basalt dust over forest, similar to aerial liming (Bošeľa & Šebeň, 2018). The second one is the representation of the processes associated with basalt once it has been added to soils, including the weathering and carbon dioxide removal through geochemical and biotic processes. The application to agricultural land does not increase the land carbon sink because the biomass is harvested. Therefore, biotic CDR only occurs in forests. Our weathering model is relatively simple. It has been designed to reproduce the results of the ORCHIDEE-CNP land surface model. In our weathering model, basalt amendment increases a stock of undissolved basalt in agricultural or forest soils, of which a fixed proportion dissolves each year. Dissolution of basalt is assumed to remove atmospheric CO_2 immediately via the geochemical pathway. Dissolution of basalt in forest soils also releases phosphorus, which accumulates in soils and gradually leaches into inland waters. We added a phosphorus enhancement factor to the net primary productivity (NPP) in ACC2 so that the land carbon sink in ACC2 increases

with the amount of soil phosphorus, but this effect saturates with increasing application.

Results

We assess the role of EW in least-cost mitigations pathways to four climate target cases: 1.5°C and 2°C, with or without overshoot. Since the 1.5°C without overshoot is not feasible with the model, we allow for a relatively low overshoot of 0.2°C above this limit. Three use cases are compared: no EW, EW on croplands only (the use case that is usually assessed) and EW on croplands and forests. Our results show that EW can be applied on forests as a cost-effective solution for two contrasted reasons depending on the temperature target. In the 2°C scenario, carbon prices are typically lower, and EW is applied only to a limited extent, implicitly targeting the most reactive application sites, allowing for a more cost-efficient CDR, and the total cost reductions are relatively modest. In the 1.5°C scenarios with overshoot, emission reductions are delayed and compensated by huge (and possibly unrealistic) amount of CDR, strongly reducing the net present value of policy costs. As a consequence, carbon prices reach very high levels in the end of the century, and forest application is used because it increases the surface area available for EW. In this case, most of the CDR is due to the geochemical effect because the biotic effect is saturated. We also analyze to what extent EW can replace BECCS: in no- or low-overshoot cases, EW partly substitutes for BECCS, whereas in high-overshoot cases, EW rather adds up with BECCS. This affects the willingness to pay for bioenergy calculated by the model, which may be linked to food prices through market mechanisms in the real world. We also analyzed the robustness of our results to a wide range of parameter uncertainty, following two procedures: a latin hypercube sampling procedure to quantify uncertainties, and a Morris sampling procedure to assess the sensitivity of the results to each parameter. In particular, it shows that the use of EW is strongly dependent on the assumed weathering rates.

Limits

Our model is highly aggregated, to limit modelling and numerical complexity. This leads to a lack of realism at several levels. First, we assume that the basalt dissolves following an exponential law. This is convenient, as it allows us to have only one variable to represent the undissolved basalt. However, in reality, the weathering rate of basalt decreases with time as the reduction in grain size reduces the reactive surface area. Weathering should follow complex dynamics, depending on local biological and hydrological processes, albeit with large uncertainty (Calabrese et al., 2022). Second, we did not consider any supply-side limit to basalt application, resulting in (potentially unrealistic) massive rock extraction in our scenarios. Fi-

nally, the environmental impact of the technique is not explicitly considered in our analysis. Some of the side-effects of the application of basalt dust to natural areas are analyzed in (Goll et al., 2021) and its appendix.

Leveraging ecosystems responses to enhanced rock weathering in mitigation scenarios

Abstract

Carbon dioxide removal (CDR) is deemed necessary to attain the Paris Agreement's climate objectives. While bioenergy with carbon capture and storage (BECCS) has generated substantial attention, sustainability concerns have led to increased examination of alternative strategies, including enhanced rock weathering (EW). We analyse the role of EW under cost-effective mitigation pathways, by including the CDR potential of basalt applications from silicate weathering (geochemical CDR) and enhanced ecosystem growth and carbon storage in response to phosphorus released by basalt (biotic CDR). Using an integrated carbon cycle, climate and energy system model, we show that the application of basalt to forests could triple the level of carbon sequestration induced by EW compared to an application restricted to croplands. EW also reduces the costs of achieving the Paris Agreement targets as well as the reliance on BECCS. Further understanding requires improved knowledge of weathering rates and basalt side-effects through field testing.

1 Introduction

Parties to the Paris Agreement committed to keeping global warming well below 2°C, and to continuing their efforts to aim for 1.5°C of warming relative to the preindustrial level. Meeting this goal requires reducing emissions at an unprecedented pace to reach carbon neutrality by the middle of the century. Carbon dioxide removal (CDR) is known to be required to compensate for both temporary overshoots of carbon budgets and for residual emissions that may persist after emission reductions from all sectors. The longer the delay in emission reductions, the greater the need for CDR(IPCC, 2022).

While bioenergy with carbon capture and storage (BECCS) and afforestation are so far the most widely explored carbon dioxide removal solutions(Minx et al., 2018), concerns have been raised regarding the technical feasibility and sustainability of BECCS at the scales envisaged in the mitigation scenarios assessed by the IPCC(Rogelj et al., 2018). In particular, the amounts of biomass needed to reach sufficient CDR levels could have high impacts on water, land and nutrient use(Fuss et al., 2018; Li et al., 2021; Smith et al., 2016). Sustainable deployment of

large-scale CDR thus requires the examination of alternative CDR portfolios (Chiquier et al., 2022; Rueda et al., 2021). Enhanced weathering of basalt (EW) is an emerging and promising CDR that consists in amending soils with basalt dust(Beerling et al., 2020; Hartmann et al., 2013; Moosdorf et al., 2014; Renforth, 2012). As basalt erodes, the minerals released react with CO2 and sequester carbon for at least several hundred years(Köhler, 2020), a process called 'geochemical CDR'. Unlike BECCS, EW does not disrupt existing land use and is usually assumed to be deployed on croplands (Beerling et al., 2020; Hartmann et al., 2013; IPCC, 2022; Moosdorf et al., 2014; Renforth, 2012; Strefler et al., 2018), that are accessible for transporting and spreading basalt. Furthermore, co-benefits of crop yields from amendment with basalt have been studied in previous work, including dedicated experiments, showing improvement of soils quality (Beerling et al., 2018) which could reduce fertilisers use(Kantola et al., 2017; Kantzas et al., 2022), plant health, and yields (Beerling et al., 2024; Haque et al., 2019, 2020; Kelland et al., 2020; Wang et al., 2024). Moreover, EW stimulates biomass production through nutrients released during basalt dust dissolution, thereby increasing carbon sequestration and storage in natural ecosystems. This additional CO2 removal process from EW called 'biotic CDR' has only recently been quantified. Biotic CDR could potentially double the global CDR of EW(Goll et al., 2021) (2-5 GtCO2 per year (Beerling et al., 2020; Fuss et al., 2018; Strefler et al., 2018)), yet non-agricultural application is not part of CDR portfolios in existing assessments (IPCC, 2022; Minx et al., 2018; Rueda et al., 2021). While EW presents co-benefits for soils and ocean pH(Hartmann et al., 2013), emissions associated with extracting, crushing and spreading basalt could partly offset the CDR potentials, depending on the underlying energy mix (Eufrasio et al., 2022; Goll et al., 2021). Here we explore how the application of EW on crop fields and forests could affect mitigation pathways using a new hard-linked carbon-cycle, climate and energy system model that considers geochemical and biotic CDR and associated energy requirements within a single framework. We quantified the potential CDR from EW for ambitious climate mitigation pathways and the subsequent reduction in reliance on BECCS. The addition of EW to the CDR portfolio of mitigation technologies could make ambitious climate targets achievable with lower mitigation costs(Strefler et al., 2021b). We thus examined how EW affects mitigation costs, energy consumption and temperature pathways over the 21st century in four climate target cases: 1.5°C scenarios with medium overshoot (up to 0.2°C) and high overshoot (no limit) and 2.0°C scenarios with no overshoot and with high overshoot (no limit). All three overshoot scenarios achieve the respective temperature target by 2100. In our 1.5°C medium overshoot scenario, we allow a higher overshoot than what is defined as low overshoot scenarios in IPCC AR6 (up to 0.1°C), as the latter would lead to very large unrealistic short-term demand reductions in our model (Gaucher et al., 2022; Tanaka et al., 2022). By taking advantage of our energy-climate modelling framework, we further highlight key uncertainties that influence the role of EW for climate mitigation.

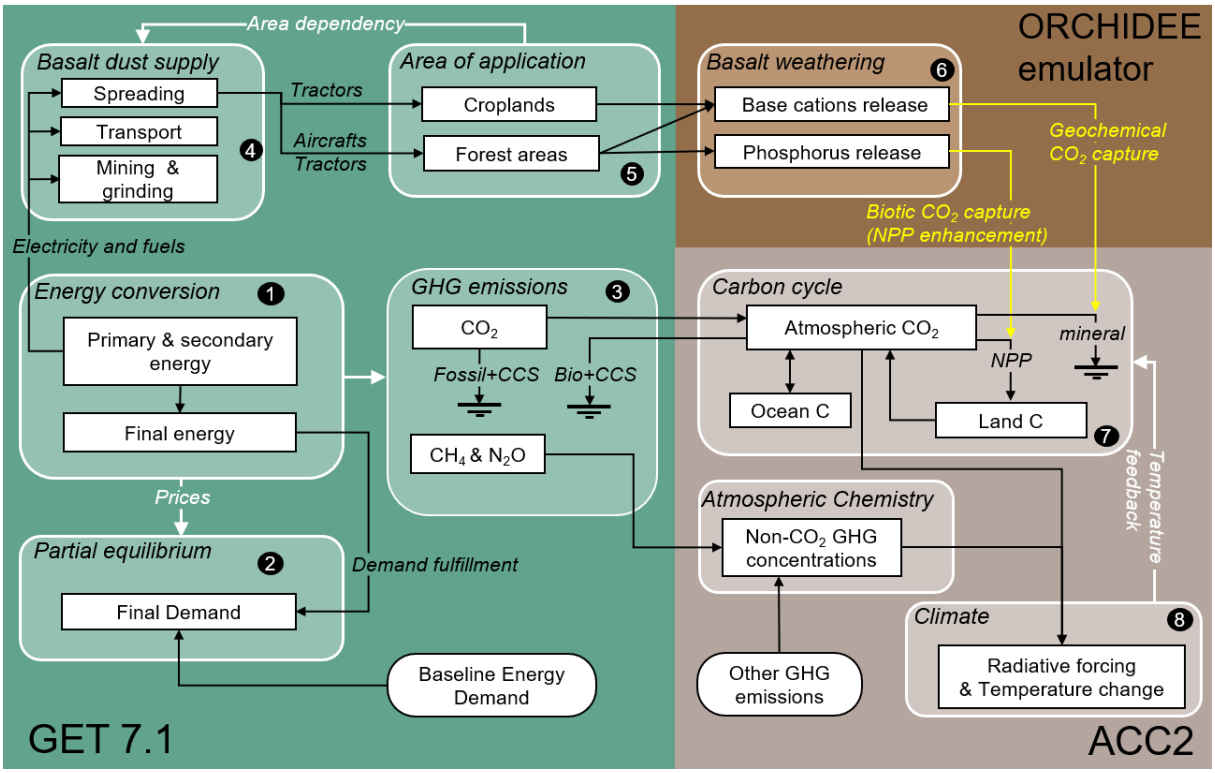

Figure III.1: Integrated model of climate, carbon, and energy economics. This diagram highlights the key processes resolved in the model related to BECCS and EW, and their interactions with the energy and climate systems. Round boxes are exogenous projections. **Key outputs are**: (1) Energy production, mix and associated costs. (2) Price-responsive energy demand (3) Resulting net GHG emissions from the energy sector, including negative emissions from BECCS. (4) Costs and energy requirements of EW. (5) Quantity of basalt applied on croplands or forest areas. (6) Geochemical CO_2 capture from basalt weathering. (7) CO_2 capture from phosphorus-driven NPP increase (the biotic effect). (8) Global temperature pathway.

We developed a new version of the partial-equilibrium energy model GET7.1 (C. Azar et al., 2013; Johansson et al., 2020) , which we integrated with the aggregated carbon cycle, atmospheric chemistry and climate model (ACC2 (Tanaka & O'Neill, 2018; Tanaka et al., 2007)). The resulting coupled model GET-ACC2 (figure III.1) quantifies least-cost pathways where low-carbon technologies, CDR, and abatement measures for CH_4 and N_2O are deployed to mitigate climate change. The net present value of the social surplus (i.e. the sum of consumers surplus minus the energy costs, discounted at a 5% rate) is maximised with perfect foresight, leading to a preference for late spending, including late abatement. We also developed an EW module and coupled it with the carbon cycle module of GET-ACC2, where the dissolution of basalt directly removes atmospheric CO2, and delivers phosphorus to the soil which stimulates the net primary production (NPP). The increase in terrestrial vegetation carbon storage is the difference between NPP and CO2 released from heterotrophic respiration, which are resolved in ACC2 on a global-annual-mean basis. We emulated the stimulation of NPP through the release of phosphorus from basalt performed by ORCHIDEE-CNP(Goll et al., 2017), a global biosphere model that resolves the phosphorus cycle, in order to quantify the geochemical (abi-

otic) and biotic CDR from basalt applied to forest ecosystems. The spatial heterogeneity of the response of ecosystems to basalt application and the local factors driving additional biological carbon sequestration have been discussed in Goll et al. (2021)(Goll et al., 2021). The biotic CDR was found to be highly variable across regions, strongly dependent on ecosystem type, and most effective where the natural background phosphorus availability was insufficient for plants to benefit from increasing atmospheric CO2 and warming, notably in tropical and boreal forests(Goll et al., 2021). It should however be noted that this spatial heterogeneity is only implicitly represented in the emulator (see Methods), and that we only accounted for the phosphorus fertilisation effect on plants, not other effects of basalt weathering on soil microbes and soil biota, or other biotic effects such as interactions with the nitrogen cycle, plant health and resistance to pathogens(Vicca et al., 2022). To address parametric uncertainty, we sampled uncertain parameters, such as equilibrium climate sensitivity (ECS), technology costs and diffusion constraints, and EW parameters (see Methods and SI.2). When ECS exceeds 3.7°C, keeping global warming below 1.7°C becomes infeasible with GET-ACC2. Consequently, we set ECS at 3°C for the 1.5°C scenario with medium overshoot, while ECS is varied between 2°C and 4.7°C(Sherwood et al., 2020) in all other scenarios. Unless otherwise noted, the reported results represent the mean of simulations performed on this set of parameter samples.

2 Results

2.1 Enhanced weathering deployment

Under each climate target case, we assessed the following three CDR portfolios: i) BECCS only (No EW), ii) BECCS with EW on croplands only (EW on CL), and iii) BECCS with EW on croplands and forest areas (EW on CL+FA). In the latter, we assumed that basalt could be spread over forest areas, yet with a significant energy and cost penalty compared to croplands. The cost-effective magnitude of CDR from EW deployment is very contrasted across climate target scenarios (figure III.2): EW is more used to achieve 1.5°C than to achieve 2°C, and it is also used more in high-overshoot than in medium and no-overshoot scenarios. EW is applied when the net present value of future carbon removals, occurring in the years following basalt application and extending over decades for biotic sequestration, outweighs application costs. Cropland application costs range from $43 to 132$ per ton basalt, increasing at higher application levels due to prioritising accessible fields first, leading to higher transport costs for more remote areas. It corresponds to $116 to 242$ per ton of CO2 removed, within the range of existing assessments (Beerling et al., 2020; Strefler et al., 2018). Possible co-benefits could increase the

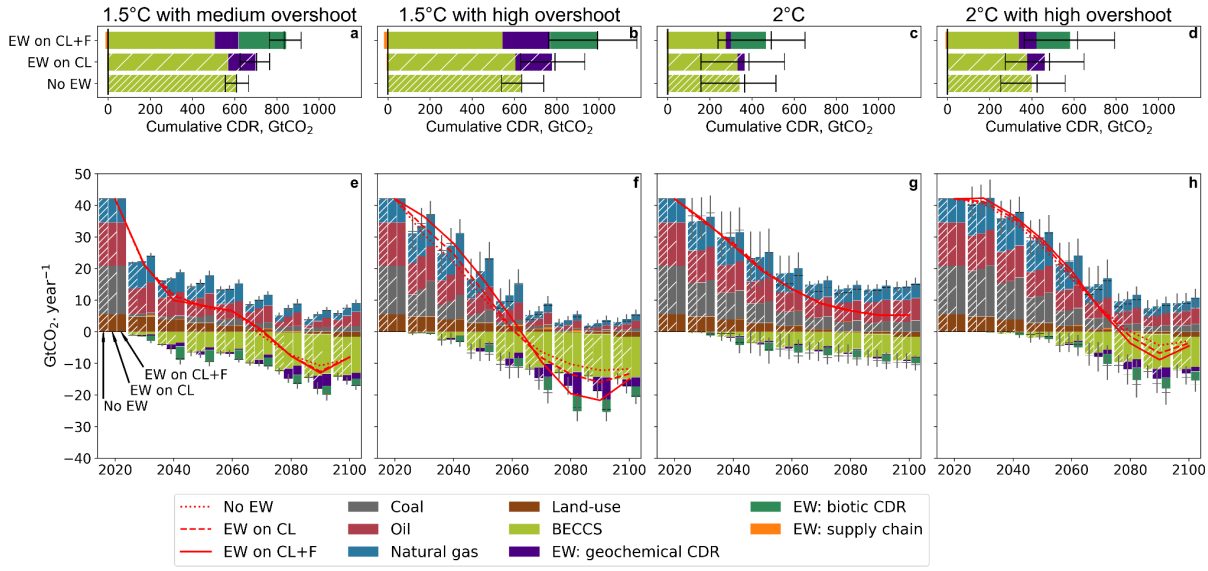

Figure III.2: Carbon dioxide emissions from three CDR portfolios for different climate targets across the 21st century. Three CDR portfolios are assessed: No EW: BECCS only. EW on CL: EW deployed on croplands only, and BECCS. EW on CL+FA: EW deployed on croplands and forest areas, and BECCS. The bars indicate the mean, the black dashes the median and the 25%-75% range. Four climate policy targets are compared (one per column): 1.5°C with low OS: The temperature change is limited to 1.5°C after 2100, with a possible overshoot of up to 0.2°C before 2100. 1.5°C with high OS: the temperature change is limited to 1.5°C after 2100. 2°C with no OS: the temperature change is limited to 2°C. 2°C with high OS: the temperature change is limited to 2°C after 2100. 'EW: supply chain' (in orange) represents the emissions from fossil fuels used to apply EW. The red lines represent the net CO_2 emissions (excluding land-use).

cost-effectiveness of EW(Lewis et al., 2021) if they can act as fertilisers, but our model does not include food systems and land use and these effects were not considered in the study.

We assume no absolute limit to the production of basalt dust although its growth rate is limited (to 10-20% per year). The maximum CDR potential by EW on croplands thus depends on the application rate of basalt (15 kg/m2), the area of suitable croplands with sufficiently warm and rainy climate, 7.9 Mkm2, i.e. a third of global croplands(Strefler et al., 2018), and the weathering rate (1% to 25% per year). The maximum cropland CDR is 4.9 GtCO2 per year, consistent with other estimates assuming unlimited basalt supply(Beerling et al., 2020; Strefler et al., 2021a). Here, the EW application only on croplands approaches its full potential in the 1.5°C with high overshoot scenario with an annual CDR peak of 4.4 GtCO2 per year and a cumulative removal of 173 GtCO2.

Forest application is more expensive, with costs varying from $146 to $364 per ton of basalt, hinging primarily on the expenses associated with airborne application, and on carbon price-sensitive energy costs, constituting 20-40% of the total. However, the phosphorus effect enhances CO2 removal efficiency, resulting in substantially reduced removal costs of $20-$166 per ton CO2, especially at low application levels (see SM for a detailed analysis of removal

costs). Allowing basalt application in forests reduces the carbon price threshold above which EW becomes cost-efficient and increases the CDR potential in two ways: by expanding the area for basalt application, increasing the geochemical CDR potential, and by enabling biotic CDR in forests. As a consequence, the EW-induced CDR is almost tripled when basalt can be applied on forests, with a peak of 12.4 GtCO2 per year and 446 GtCO2 cumulatively in the 1.5°C with high overshoot scenario. The relative contributions of geochemical and biotic removals vary depending on scenarios; for example, in the 1.5°C with high overshoot scenario, the increase in geochemical CDR due to the additional area available is more pronounced than in other scenarios because cropland application is at full potential. Furthermore, the share of the biotic CDR is proportionally lower at high application levels because the phosphorus stimulation of forest production gradually saturates, thereby limiting the biotic CDR potential. This limit explains why biotic CDR by EW varies less than geochemical CDR by EW among different scenarios.

2.2 Impact of enhanced weathering on mitigation scenarios

2.2.1 Policy costs

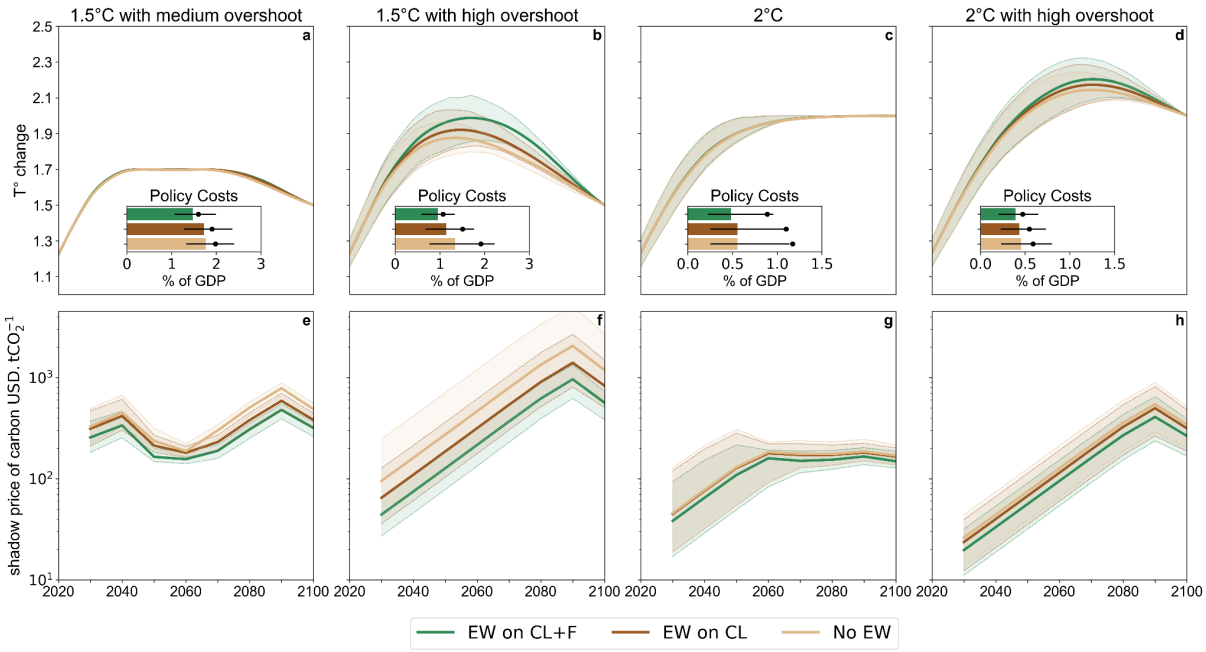

Figure III.3: Temperature, policy costs and carbon price pathways across the 21st century. (a-d) Global-mean surface temperature change relative to the preindustrial level. Policy costs are the net present values of future energy production costs and consumption losses as a percentage of GDP, compared to the no-policy scenario. The coloured bars indicate the median, the black dot the mean, and the error bars the 25%-75% range. Policy costs scale exponentially with the ECS, which can push the mean above the 25-75% range of the sample. **(e-h):** Median price of carbon across the 21st century for different climate targets (log scale). The shaded area represents the 25%-75% range. The vertical scales are different between the panels.

EW provides flexibility, not only by replacing more expensive mitigation measures but also by allowing abatement to be delayed. This reduces the costs of achieving climate objectives, here quantified as the net present value of policy cost (the energy system costs plus the loss of consumer surplus) compared to a baseline without climate policy (figure III.3, see also Fig. S4 for energy demand reduction and SI3 for annual costs). Abatement, including EW deployment (figure III.2), is delayed in overshoot scenarios: in our forward-looking optimisation model, the greater the future opportunity for negative emissions, the lower the near-term abatement and the discounted costs. Therefore, applying EW on croplands and forest areas reduces policy costs most significantly in the high overshoot scenarios, by 44% in the 1.5°C scenario with high overshoot, against 20% in the 1.5°C scenario with medium overshoot. In the latter case, the rapid reduction required over the next decade is too early for basalt to be used on a large scale, and relies largely on a severe contraction in the demand. The application of EW on croplands only has a weaker impact, in particular in the 2°C scenario without overshoot where the median cost reduction is zero and the mean reduction is 6%.

The increasing stringency of climate policies across the 21st century is reflected by the endogenous carbon price (figure III.3). EW reduces it, on average, by 67% if applied on croplands and forests in the 1.5°C with high overshoot scenario, and by 31% when applied on croplands. When aiming at 2°C, EW reduces it by 27%. But if application over croplands only is considered, the carbon price is only reduced by 10%. Thus, applying EW on crop fields helps to reduce the efforts required to achieve the most ambitious climate objectives but is not a game-changer when aiming at the 2°C target. Overall, EW pays off more when aiming at 1.5°C than when aiming at 2°C, and more with overshoot than without.

As a consequence of delaying abatement and changing the net emission pathways, EW increases the peak temperature level in high overshoot scenarios: from 1.88°C without EW to 1.98°C with EW in the 1.5°C case, and from 2.13°C to 2.20°C in the 2°C case (figure III.3). The change in peak warming depends on the assumed discount rate, and is strongly reduced with a lower discount rate of 2% (figure III.9 and III.10).

2.2.2 Reduction of BECCS

Reducing the reliance on BECCS for achieving negative emissions could limit the deployment of bioenergy crops and alleviate the threats they pose to food security, water and nutrient resources and biodiversity(Jeswani et al., 2020). Therefore, it is of interest to analyse if EW and BECCS are complementary or in competition with each other. EW does not directly compete with BECCS for resources: BECCS provides energy while EW uses energy, and EW could be

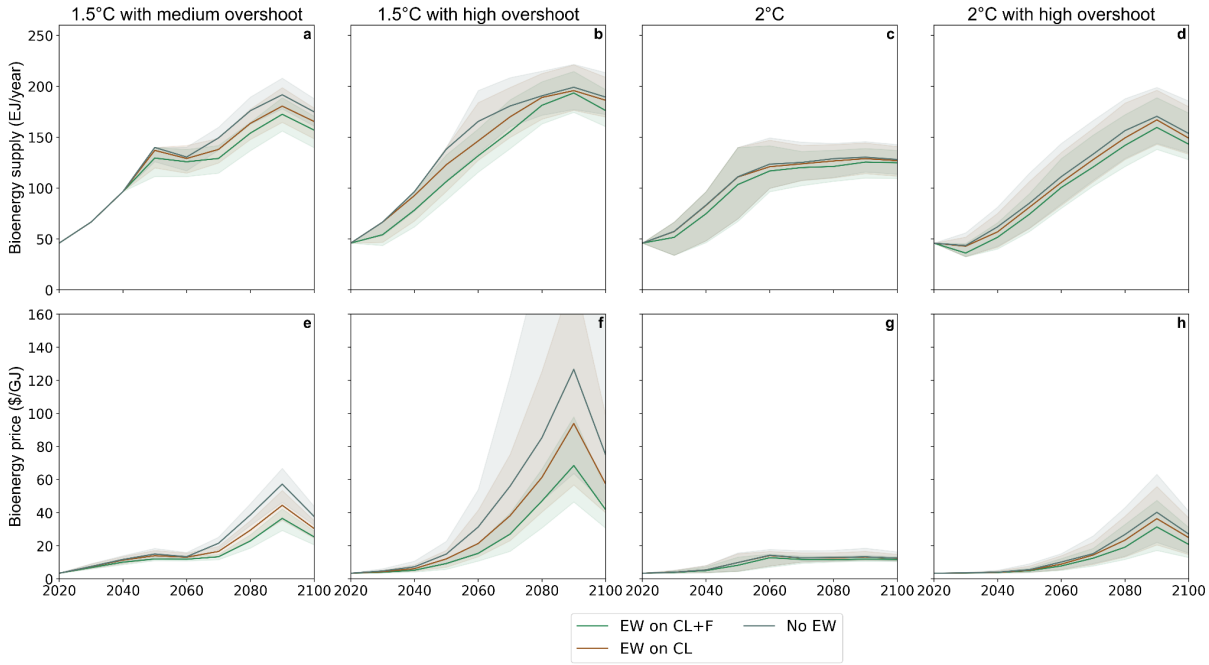

Figure III.4: Price and use of bioenergy. (a-d): Median primary bioenergy consumption**. Top, right y-axis (dotted line):** Median primary bioenergy supply in the no EW scenarios. **(e-h):** Median biomass price**. Shaded area:** 25-75% range.

applied on bioenergy crops areas. BECCS are used in all our mitigation scenarios to supply electricity and heat, but also hydrogen (for transportation, and industrial processes) when high levels of negative emissions are required. We found that adding EW to the CDR portfolio increases the total CDR level but reduces the use of BECCS which becomes partially unnecessary (figure III.2). The reduction in BECCS per tonne of EW-induced CDR is higher in medium or no overshoot scenarios than in high overshoot scenarios, where BECCS and EW rather add up. By reducing the dependence on bioenergies, the EW could also reduce the pressure on food prices and lower land rents and the market incentive to cultivate food or bioenergy crops in pristine areas. Due to the competition for land(Fajardy et al., 2021), food prices are expected to increase with biomass prices(Johansson & Azar, 2007), which reflect the willingness to pay for bioenergy and increase with carbon prices. Applying EW on croplands and forests reduces biomass prices and cuts the use of bioenergy, but limiting EW to croplands reduces these effects (figure III.4). In summary, EW only partially replaces BECCS, but reduces the demand for bioenergy.

2.2.3 Impacts on energy use

EW generally requires smaller energy input than other CDR options, such as direct air carbon capture and storage. The energy use of EW can be divided in three components: i) mining and grinding of basalt (here, a size of 20µm was assumed (Strefler et al., 2018)) which consumes fuel and electricity, ii) transport to application sites which increases the freight demand, and

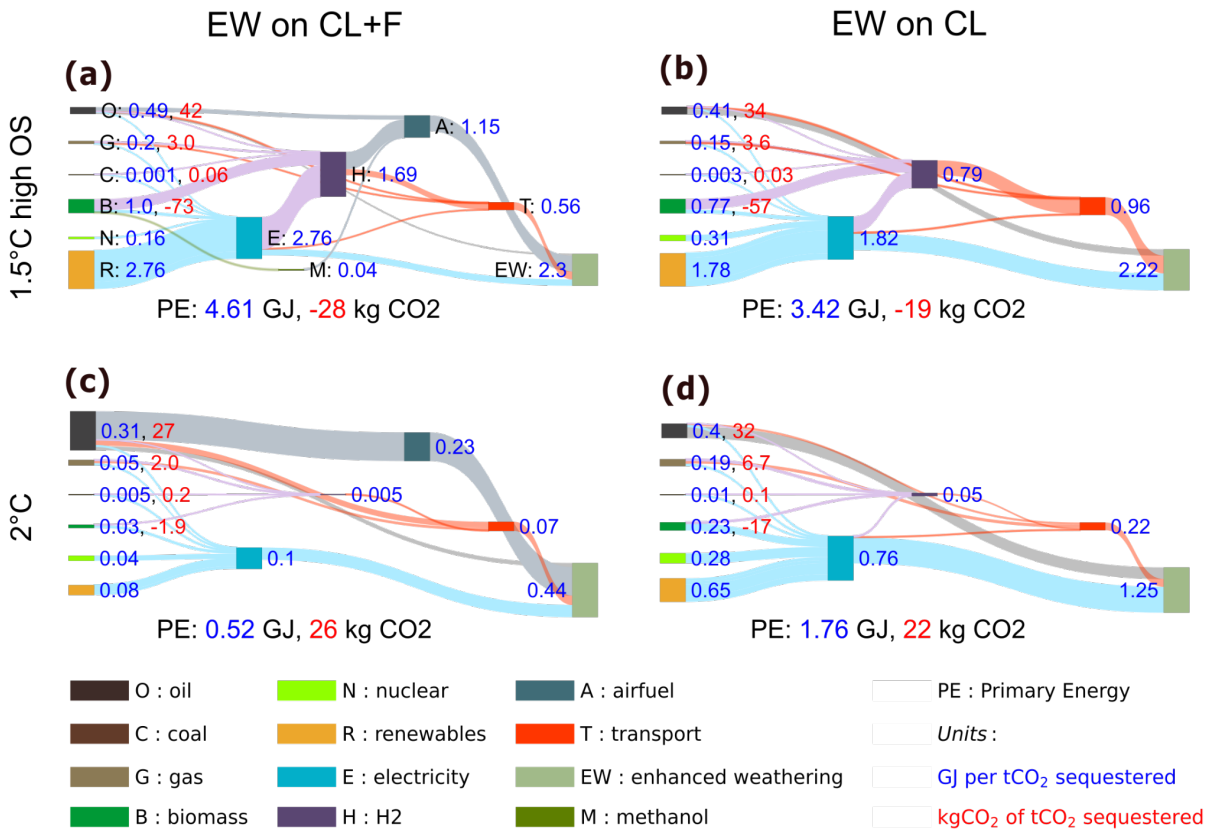

Figure III.5: Average energy use and average CO_2 emissions of enhanced weathering per tCO_2 sequestered (average across the 21st century)**. (a,c)**: enhanced weathering is applied on forest areas and croplands. **(b,d)**: enhanced weathering is applied only on croplands. **(a,b)**: 1.5°C case with high overshoot. **(c,d)**: 2°C case without overshoot. **Blue labels:** The energy used to apply EW, for each energy vector, expressed in GJ per ton of CO_2 that is sequestered through EW. **Red labels:** The emissions associated with the use of each primary energy source, expressed in kg of CO_2 emitted per ton of CO_2 captured through EW. Note that the vertical scale is different in each panel.

iii) spreading of basalt dust requiring fuel if tractors are used (for crop fields for instance) and aviation fuel if basalt is spread on forests (see **Methods**).

The average final energy intensity of EW per ton of CO_2 sequestered depends on the level of EW deployment, and thus on the scenario (figure III.5). In crop fields, the final energy input increases with basalt application as transport distance increases. Therefore, if basalt is only applied on crop fields, the final energy use per tCO_2 removed varies between 1.2 GJ/tCO_2 in the 2°C without overshoot where EW is less applied, and 2.2 GJ/tCO_2 in the 1.5°C scenario with high overshoot. In forests, CO_2 removal per ton of basalt is higher than on croplands due to the biotic effect but it decreases with increasing application, whereas energy use per ton of basalt varies little because the areas chosen first are those most stimulated by phosphorus, rather than the nearest ones. The application on forest areas therefore reduces the energy intensity in the 2°C scenario without overshoot (0.4 GJ/tCO_2), but increases it in the 1.5°C scenario with high overshoot (2.3 GJ/tCO_2) due to the saturation of the biotic effect. For comparison, direct air carbon capture and storage would typically require 4 to 12.4 GJ/tCO_2 (Creutzig et al., 2019;

Negative Emissions Technologies and Reliable Sequestration: A Research Agenda. n.d.) depending on the technology used.

Electricity and aviation fuel are the predominant energy carriers used for EW, which uses 8% of the projected total electricity production, and 23% of the projected aviation fuel until 2100 in the 1.5°C with high overshoot scenario. The emissions from EW depend on the energy sources used, and thereby on the carbon price. In the medium and no overshoot scenarios, the share of kerosene among the aviation fuel used for basalt application is higher than in the high overshoot scenarios where higher carbon prices at the time of basalt application on forests lead to a switch to hydrogen. Moreover, since a share of this hydrogen is produced from BECCS, the net basalt supply emissions are negative in the 1.5°C scenario with high overshoot. Conversely, in the 2°C scenario the carbon price is lower, kerosene continues to be used, and the EW-related emissions offset 2.6% of the CDR (figure III.5c).

2.3 Uncertainty analysis

CDR plays a critical role in mitigation pathways developed by IAMs despite low technology readiness of the majority of CDR technologies. Thus, uncertain costs and scalability(Grant et al., 2021a) calls for an analysis of the impact of related model assumptions on our results. Besides, costs of competing technologies(Grant et al., 2021b) and discount rates(Emmerling et al., 2019) have been shown to affect uncertainties in the role of CDR. To gain insight into uncertainties related to key model parameters, we use the Morris method (Campolongo et al., 2007; King & Perera, 2013). It quantifies the mean of the variations of an output variable resulting from an increase in the value of a single parameter over a representative sample of all parameter values (see Methods). A positive mean indicates that the output increases with a higher parameter value. This method is applied to analyse the sensitivity of EW and BECCS deployment to key model parameters, as shown in figure III.6 (**a-d**).

The parameters that increase the efficiency of EW tend to reduce the use of BECCS, and vice versa, so that EW and BECCS appear as competing technologies or substitutes. The use of CDR also increases with the costs of other mitigation technologies, such as wind, solar or nuclear energy: a decrease in their costs reduces the carbon price and therefore disincentivises the use of CDR(Grant et al., 2021b). Similarly, increasing the system flexibility such as the maximal rate at which the installed capacity of technologies can grow, or the price-elasticity of the demand, generally reduces the use of CDR. The use of CDR further depends on the climate uncertainty, as assessed through the ECS(Sherwood et al., 2020).

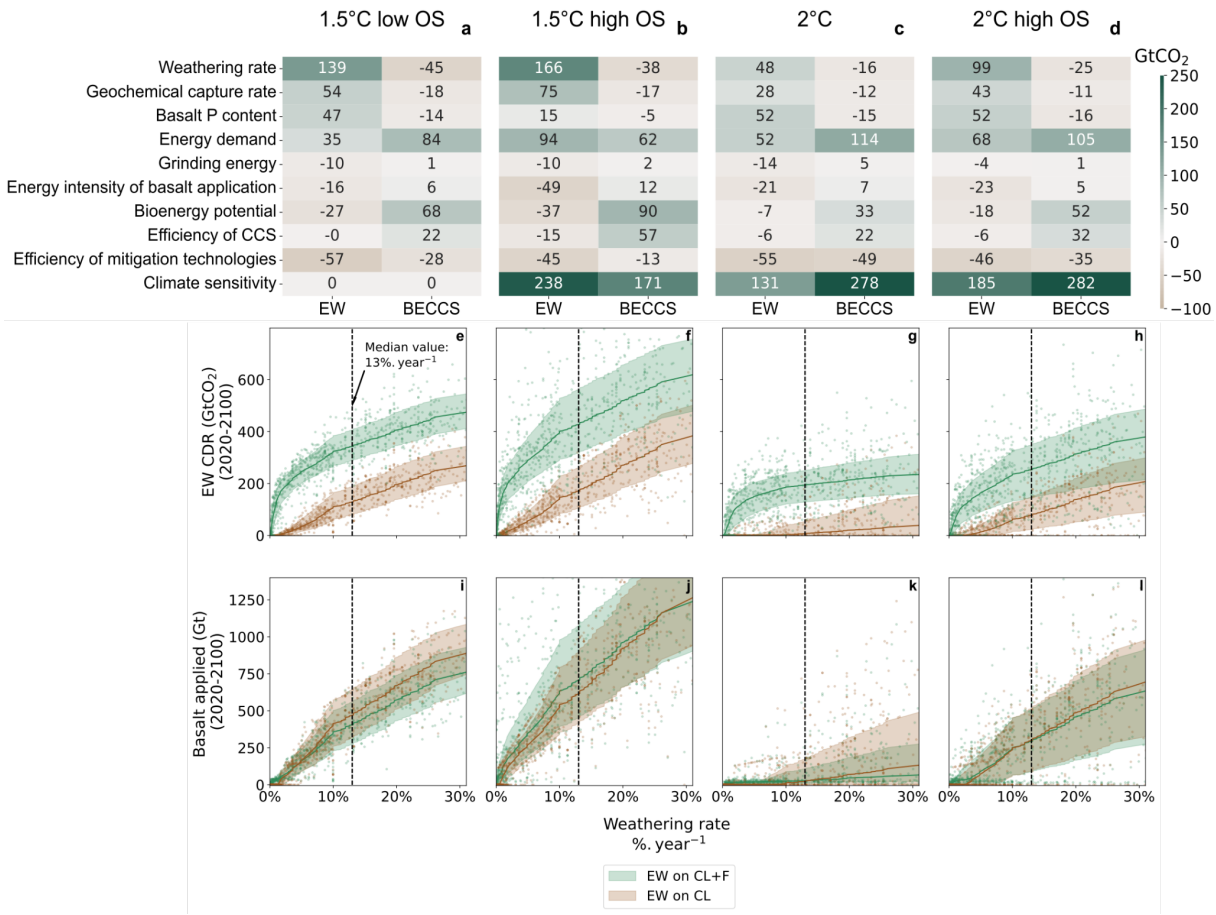

Figure III.6: Sensitivity Analysis. **(a-d): Morris screening**: mean variation of the output (**columns**), when the input (**rows**) is increased by half of its uncertainty range. The sources of uncertainty assessed are: the weathering rate, the geochemical capture rate, the phosphorus content of basalt, the baseline energy demand, the climate sensitivity, the efficiency of CCS, the energy intensity of basalt grinding, the energy intensity of basalt application, the annual bioenergy potential and the efficiency of other mitigation technologies. The outputs displayed are: 'EW', the cumulative CDR by enhanced weathering when applied on croplands and forests; 'BECCS', the cumulative CDR from BECCS when EW is applied on croplands and forests. **(e-h): Carbon dioxide removal with EW depending on weathering rate. (i-l): Application of EW depending on weathering rate**. Each dot is a simulation in the sample. Solid line: median. Shaded area: 25-75% range for a given value of the weathering rate. The vertical dotted line shows the mean weathering rate considered in the rest of the paper (13% per year). Additional runs were performed to cover a wider range of weathering rates.

We found that the uncertainty related to the physical processes of EW (weathering rate, geochemical capture rate, and the phosphorus content of basalts) strongly influence the magnitude of EW CDR, it is less sensitive to the uncertainties of parameters surrounding the energy requirements of EW, in particular the electricity use for grinding the rocks.

Weathering rates in soils remain highly uncertain (Amann et al., 2020; Cipolla et al., 2021; Rinder & von Hagke, 2021) (see methods). The weathering rates used in modelling studies are calibrated on laboratory experiments (Beerling et al., 2020; Fuhrman et al., 2023; Renforth, 2012; Rinder & von Hagke, 2021; Strefler et al., 2018). Field or pot conditions experiments generally provide lower estimates than laboratory experiments (Amann et al., 2020; Buckingham

et al., 2022; Renforth et al., 2015; Swoboda et al., 2022), because the weathering rate depends on complex interplay of soil pH, temperature, hydrological conditions, and biological activity (Swoboda et al., 2022; Vicca et al., 2022). Soil column (Renforth et al., 2015) and mesocosm (Amann et al., 2020) experiments have suggested surface-normalised weathering rates respectively two and three orders of magnitude slower than those used in Strefler et al. 2018 (Strefler et al., 2018). The latter define the high range of the weathering rates used in the present work (25% per year). However, field (Beerling et al., 2024; Kantola et al., 2023; Ryan et al., 2024; Wang et al., 2024) and forest (Taylor et al., 2021) studies have shown promising CDR rates corresponding to weathering rates exceeding this range. For instance, ref (Beerling et al., 2024) reports a 16 ± 6% loss of cations from basalt applied on agricultural crops over 4 years. This corresponds to a mean weathering rate of 3-6% per year. As they report a grain size of 267 µm, 20µm-sized grains could weather around ten times faster, because weathering speed scales with the reactive surface. The wide variations across experiments indicate that the weathering rate is a critical source of uncertainty. As shown in III.6 (**e-l**), the lower the weathering rate, the less basalt is applied and the less carbon is captured. For weathering rates below 1% per year, EW can become a viable cost-effective option only if basalt is applied on natural areas, because the supply of even very low quantities of phosphorus to phosphorus-depleted soils yields a significant biotic CDR. Thus, the efficiency of basalt application over forest is more robust to low weathering rates than cropland application (see also the reproduction of figure Ss 2 and 3 for weathering rates of 1 and 25% in SI 1.1.1).

3 Discussion

We showed that the CDR potentials of EW under cost-effective mitigation pathways can be larger than previously thought by additionally considering the potentials associated with the phosphorus fertilisation, or 'biotic' effect of EW. EW neither accelerates climate change mitigation nor reduces temperature overshoot in our cost-effectiveness analysis, yet its potential for lowering peak temperatures to mitigate near-term climate damage could be further assessed elsewhere through cost-benefit analyses. Deploying EW in addition to BECCS reduces the willingness to pay for biomass and could thereby lower the pressure on land conversion as well as on food prices, although the reliance on bioenergy remains significant.

We further demonstrated that under mitigation pathways, in particular, for the 1.5°C warming target, the use of EW reduces the total mitigation cost, lowers the peak carbon price, and replaces a larger amount of BECCS when the 'biotic' effect is included, even if we account for the high costs for EW application over forest areas by aeroplanes. These findings are robust

under a range of uncertainties considered, unless weathering rates are orders of magnitude below predictions. Such benefits of EW were found to be more pronounced under pathways with high temperature overshoot than those with medium or no overshoot. Nevertheless, in high overshoot pathways, EW is used to compensate for higher emissions for the upcoming decades, which is a risky strategy, given the increased likelihood of climate disasters at high overshoot levels, which is not considered in our analysis.

Potential impacts of EW on human health or ecosystems (Buckingham et al., 2022; Dupla et al., 2023), possible scaling constraints on basalt supply, or lower-than-expected geochemical CDR from incomplete basalt weathering are not considered in the model, which may both limit the sustainable deployment of basalt soil amendment and restrict EW efficiency. For instance, the needed basalt extraction in the 1.5°C with high overshoot case reaches 46 Gt/year (figure III.7), which is half of the current global material footprint and ten times the global cement production today, potentially having a large ecological and societal impact. The dust pollution associated with the aerial application of finely milled basalt could lead to silicosis and other respiratory diseases (Taylor et al., 2016), and must therefore be prevented, for example by mixing the dust with water to form aggregates or by pelletisation (Taylor et al., 2021). The release of metals in basalts causing toxicity for humans must also be avoided in agricultural settings by choosing carefully the right material (Cobo et al., 2023). Basalt dust potential impacts on tree canopy, possibly blocking leafs stomata and reducing tree growth (Farmer, 1993; Taylor et al., 2016) as well as potential impacts on riverine chemistry (Zhang et al., 2022) must also be anticipated. The application of basalt in forests could alter soil geochemistry for centuries, possibly disrupting natural systems and impacting the composition of plant communities (Vandeginste et al., 2024). Wisely exploited, these geochemistry side-effects could serve as an additional tool for biotic CDR in addition to phosphorus fertilisation, as observed in an acid-rain impacted forest where the release of calcium through weathering of added silicate led to a biotic CDR of 3.2-3.5 tCO_2 per ton of wollastonite applied (Taylor et al., 2021). Ultimately, biotic effects may either offset the net carbon removal in the case of soil carbon leaching to rivers (Klemme et al., 2022), or enhance it by increasing soil carbon sequestration (Buss et al., 2024; Vicca et al., 2022). More experiments are therefore required to explore the side-effects of enhanced weathering particularly as rock material cannot be removed from the soil after its application.

At face value, a life cycle analysis comparing EW with other mitigation technologies showed that EW has the advantage to use less land than BECCS or afforestation, less energy than direct air capture, and less water than for those three technologies (Eufrasio et al., 2022). The application of basalt in forests is therefore a promising method for mitigating climate change, but it requires the deployment of an appropriate regulatory framework, to ensure that EW helps ecosystems sequester more carbon without adverse side-effects. Furthermore, even if we ex-

plored uncertainties as comprehensively as possible, the true uncertainties cannot be wholly captured inherently and certain classes of uncertainties cannot be assessed via quantitative means, indicating a need for careful interpretation and dissemination of our results for stakeholders.

4 Methods

4.1 Modelling framework

We developed an energy-economy-climate model by hard-linking GET7.1 with the reduced-complexity carbon-cycle, atmospheric chemistry and climate model ACC2. GET7.0 is a bottom-up, cost-minimising energy system model, with a focus on energy supply and transformation. GET7.1 derives from GET7.0 with updated techno-economic parameters, and a price-responsive energy demand, that follows the SSP2 baseline (Hasegawa et al., 2021). The coupled model allows to assess least-cost emission pathways directly considering the temperature target (and not a carbon budget target) with a detailed representation of the energy system. Such a feature is important for an analysis under overshoot pathways involving several different greenhouse gases and EW as a CDR option, where the carbon budget approach may not necessarily work.

The coupled model produces internally consistent social-surplus maximising pathways to meet a reference energy demand in five end-use sectors (transportation, electricity, heat for industrial processes, space heat and industrial feedstocks), with perfect foresight, while respecting a given climate target as well as resource constraint for a range of primary energy source (oil, gas, coal, uranium, wind power, solar power, biomass and hydropower). **figure S1** shows the structure of the model. Primary energy is transformed into secondary and then final energy through investments and operations in order to satisfy a demand-supply equilibrium. CCS can abate emissions from fossil fuel power plants, or directly remove CO_2 from the atmosphere if combined with bioenergy (BECCS). The maximum achievable carbon capture by BECCS is limited by the deployment of carbon storage infrastructures, and bioenergy supply, as BECCS are competing with other bioenergy uses. Land-use is not explicitly modelled: the primary bioenergy supply is exogenously limited to 50 EJ in 2020 and to 260 EJ per year in 2100 following a supply curve (see SI.3). The growth rates of energy conversion technologies and CO_2 storage are limited under assumed upper bounds. There is no constraint on emission levels reduction rate as long as the energy demand is met. Since energy demand is price-responsive, stringent

climate targets are achievable in an optimization model sense. The energy module has a 10-year timestep, while ACC2 has an annual resolution.

The anthropogenic CH_4, N_2O emissions and net energy-related CO_2 emissions are calculated in GET7.1 and are transferred to ACC2 for temperature calculations. The temperature calculations also use exogenous non-energy-related CO_2 emissions and other greenhouse gas and pollutants emissions, which are assumed to follow SSP1-1.9 and SSP1-2.6 for the 1.5°C and 2°C target cases, respectively. In ACC2, a box model represents oceanic and terrestrial carbon cycles. The ocean CO_2 uptake is represented by a four-layer box model, with the uppermost representing the atmosphere and ocean mixed layer and the others the ocean's inorganic carbon storage capacity, and the land CO_2 uptake model consists of four reservoirs connected with the atmosphere. The atmospheric concentrations of multiple greenhouse gases respond dynamically to their emissions and removals e.g. chemical sinks. The resulting radiative forcing is an input to a heat diffusion model, which further calculates the global temperature. The temperature change in turn affects the carbon cycle through soil respiration and ocean-atmosphere carbon flux. ACC2 is comprehensively described in ref (Tanaka et al., 2007).

GET-ACC2 is fully coupled and optimised with perfect foresight, therefore the biotic CDR, which is the net increase of land carbon stock due to phosphorus fertilisation, the geochemical CDR, the basalt application, the energy system and the climate system are optimised simultaneously, reaching a global least-cost solution achieving the temperature target. No revenue flows are explicitly considered in the model. Carbon fluxes related to afforestation and deforestation are not optimised in the model.

4.1.1 Enhanced weathering module: Basalt supply

The enhanced weathering module has two main components: the basalt dust supply and the biogeochemical module calculating the removal rate of CO_2. The costs and energy requirements of basalt supply are integrated in GET. We followed ref. (Strefler et al., 2018) for the parameterisation of the extraction, grinding and tractor application costs. The electricity for grinding basalt is 0.2 EJ/Gt (central value) and ranges from 0.07 to 0.6 EJ/Gt in the uncertainty analysis, which is the range provided in ref (Strefler et al., 2018) for grain size of 20µm. Tractors used to spread basalt in agricultural fields and mining machinery were assumed to use petroleum products (Thrikawala et al., 1999). The energy requirements of transport from mines to application areas are based on ref. (Renforth, 2012) and increase the energy demand in each transport subsector (road, train or water freight). Transport modes are substitutable but an assumed minimum share (70-90%) must be transported on the road. The transport dis-

tance for basalt applied on croplands follows ref. (Strefler et al., 2018), the mean distance for the basalt applied on forest areas ranges from 350 to 550 km. It was estimated by comparing a map of basalt resources (Hartmann & Moosdorf, 2012), airports (Hartmann & Moosdorf, 2012) and suitable application sites (see SI.1). A share of the basalt spread on forests is assumed to be applied with aircrafts (70%-90%), since 80% of the global surface is more than 1 km away from the nearest road (Ibisch et al., 2016). This share can be expected to decline in the future, with the expansion of new roads (Ibisch et al., 2016). On the other hand, applying basalt on forests by means of land transport can be challenging, even when a road is available. This share depends on the development of roads and on the share of forests that tractors can penetrate. Aerial application is likely to be more expensive and energy intensive than land-based alternatives. If the share of aircraft use were lower, the energy consumption would also be lower, and basalt application could become higher in a cost-optimisation model. Assuming a large part of aerial spraying is therefore pessimistic as far as costs are concerned.

4.1.2 Enhanced weathering module: Airborne basalt application

Global forests are divided into five land response classes based on the net primary productivity (NPP) response to basalt addition. Basalt is applied evenly in a given class, but the cost and energy intensity of application depends on the time taken to apply 1 ton of rock, which is inversely proportional to the desired application rate of rock in kg/m2 over the fixed area of a given land response class.

We considered that small agricultural aeroplanes such as the AirTractor 802 (AT802), which can be equipped with a dust spreader, could be used to spread basalt dust. This kind of aircraft is commonly used to spread limestone (Bošeľa & Šebeň, 2018; Clair & Hindar, 2005; M. C. E. Grafton et al., 2011) although issues with rock discharge have been reported, due to the wide range of the particle size distribution (M. C. E. Grafton et al., 2011). Details of rock dust discharge are beyond the scope of this analysis, and more research would be needed on how to spread large quantities of basalt dust by air. An AT802 burns 330 litres of kerosene per hour, flies at 306 km/h, can carry 4.3t of rocks (we assume that rock dust can be spread without mixing it with water, either as flee-flowing particles or as pellets) and costs USD 1.8 million. Using an open-source map of airports, we estimate that the mean distance per flight ranges between 160 and 240 km. If one adds 10 minutes for spreading operations, the average flight should last between 41 and 57 minutes, lasting longer if the application rate (in kg/m2) is lower, and thereby increasing the application cost per ton of rock. This represents an energy use of 1.8 to 2.5GJ/t_{rock} for a spreading duration of 10 minutes, but it could virtually be infinite for infinitely low application rates. Assuming 20 minutes of ground operations per flight, 10

hours of use per day, five days out of seven, the capacity cost for spreading one ton per year is $170-210. Including ground operation and maintenance, pilot fees, insurance and housing (see SI 1.3), the non-energy cost per ton applied in forests is $110-170, and total costs (including energy costs) reach $142-355 per ton of basalt depending notably on the energy prices. We do not consider the non-CO_2 climate effect of aerial application (Fuglestvedt et al., n.d.), nor those of diesel combustion (Tanaka et al., 2018).

4.1.3 Enhanced weathering module: ORCHIDEE emulator

The biogeochemical module is an emulator of the response of NPP to phosphorus fertilisation induced by the dissolution of phosphorus-rich basalt dust, as simulated by the land surface model ORCHIDEE-CNP model. Tailored simulations in which basalt dust is applied on all ice-free non-agricultural land in the year 2018 were used for the calibration. Once applied to soils, basalt is assumed to have a constant dissolution rate, referred to in this study as the weathering rate. This simplistic approach reflects current understanding and data availability to parameterize weathering rates, and does not account for certain phenomena, such as the reduction of reactive surface over time, as well as the soils, plants and hydrological processes that can potentially influence weathering. More detailed models that account for some of these processes have been proposed (**cipollaEffectsPrecipitationSeasonality2022**; Beerling et al., 2020); however, many processes are not yet well quantified, and consequently the weathering rates (Buckingham et al., 2022).

Here, the stock of basalt in soils B [Gt] increases with the supply S_B **[Gt]**. The dissolution of basalt follows a law of decay, parameterized with the weathering rate w_r [year^{-1}] (E.1).

$$\frac{dB}{dt} = -w_r B + S_B \quad \text{(E.1)}$$

As we assume that the grain size is 20µm, a range of 1%-25% per year is assumed for w_r. The high end is the global average weathering rate used in ORCHIDEE-CNP, where the pixel-level values are based on ref (Strefler et al., 2018) and on temperatures at a given model pixel. The low end follows ref (Rinder & von Hagke, 2021), which assumes similar grain size, temperature and pH as in ref (Strefler et al., 2018), but a lower dissolution rate per unit of specific surface area, and a lower specific surface area than in ref (Strefler et al., 2018). However, this uncertainty range is small compared to the variations in the observed weathering rates from different field and lab experiments, see SI 1.2.1 for a partial review of measured and simulated weathering rates.

Geochemical CO_2 capture happens when basalt dissolves: the released base cations (calcium potassium, natrium, and magnesium) are transferred to surface waters, where they are charge-balanced by the formation of bicarbonate ions (Goll et al., 2021). The capture rate p_B depends on the assumed concentration of these elements in rock material, and ranges between 0.24 and 0.37 t_{CO2} /t_{rock}. In GET-ACC2, the geochemical capture G_{CO2} is assumed to be instantaneous and controlled by equation (E.2), but it should be noted that these values are not necessarily reached before minerals are leached to the ocean, and that the actual rate of in situ capture depends on local freshwater pH and alkalinity (Bertagni & Porporato, 2022).

$$G_{CO_2} = p_B w_r B \quad \text{(E.2)}$$

4.1.4 Land carbon cycle

The land carbon cycle component of ACC2 interacts with the enhanced weathering module. It consists of four carbon pools C_i [Gt], with different turnover rates, which exchange carbon with the atmosphere. The inflow is the net primary production of the terrestrial biosphere: its magnitude is assumed to depend on the atmospheric CO_2 concentration and (to a lesser extent) on the global temperature change ΔT. The outflow is the heterotrophic respiration (HR) (E.3b): it is proportional to the quantity of carbon in each pool and to their turnover rate $\frac{1}{\tau_i(\Delta T)}$ [year^{-1}], which increases with land surface temperature. The apparent NPP is thus the sum of the temperature-dependent NPP ($NPP^{climate}$), plus the CO_2 fertilisation effect F^{CO2} (E.3a). The net land sink is thus the difference between the NPP and the heterotrophic respiration, and is zero at equilibrium (E.3c) (i.e. a quasi-steady state assumption at preindustrial). Note that land use CO_2 emissions are treated separately and do not directly influence the land biomass as typically assumed in many simple climate and carbon cycle models.

$$\Sigma_{i \in pools} {NPP_i}^{climate}(\Delta T) + {F_i}^{CO_2} = NPP^{climate}(\Delta T) + F^{CO_2}(\Delta CO_2) \quad \text{(E.3a)}$$

$$HR_i(t) = \frac{C_i(t)}{\tau_i(\Delta T)} \quad \text{(E.3b)}$$

$$\frac{dC_i}{dt} = NPP_i(t) - HR_i(t) \quad \text{(E.3c)}$$

4.1.5 Increase of the land carbon sink

The dissolution of basalt releases phosphorus which is available for plant uptake, leading to an increase in the NPP by a fraction $\delta NPP(t)$. In the extreme case where 50 kg/m^2 of basalt dust are applied on all forests worldwide, global NPP over the next 40 years is 4.4 GtC/year higher on average than without basalt application, based on the results of ORCHIDEE-CNP (Daniel Goll, unpublished). The assumed phosphorus content in basalt is 0.161%-weight (with an uncertainty range of 0.036-0.28%), thus 50 kg/m^2 on 41Mkm^2 would supply 70 times the current global use of phosphorus as a fertiliser.

Global NPP is higher in ACC2 than in ORCHIDEE. Therefore, in order to replicate the absolute magnitude of its increase in ORCHIDEE, we scale its increase by the ratio of its respective initial values in the two models (E.4). The CO_2 fertilisation term F^{CO2} is not affected by phosphorus from basalt as it was calibrated based on predictions of models which omit nutrient constraints on the CO_2 fertilisation effect (Tanaka et al., 2007) and thus reflects an upper boundary of the stimulation of NPP by increasing CO_2 (Fleischer et al., 2019) which cannot be further enhanced by phosphorus additions.

We limit basalt application to forest ecosystems, where the stimulation of NPP results in substantially more carbon sequestered for multiple decades compared to grasslands in simulations by ORCHIDEE-CNP.

$$NPP_i(t) = NPP_i^{climate}(\Delta T)(1 + \frac{NPP^{ORCHIDEE-CNP}(2018)}{\Sigma_{i \in pools} NPP_i^{climate}} \delta NPP(t)) + F_i{}^{CO_2}(t) \quad \text{(E.4)}$$

The increase in the NPP is followed by the increase of heterotrophic respiration, which releases a part of the sequestered carbon following the decay rate constant (E.3b). Our phosphorus cycle emulator quantifies δNPP, the fractional increase of NPP following basalt application: $\delta NPP = \frac{NPP_{EW}}{NPP_{Baseline}} - 1$.

In the spatially explicit land surface model ORCHIDEE-CNP, the increase of NPP due to phosphorus release depends on the soil, biome and climate and saturates with increasing basalt additions.

Application pixels are ranked according to their NPP stimulation from high to low, and grouped in M land response classes of areas a_i. In the current setting, M=5 (more details on classes in the SM). A function of the rock application rate $c_{B,i}$ [Gt.Mkm^{-2}] is used to fit the mean NPP response in each class i during the forty years that follow basalt application, $\delta \bar{NPP}_i$ (E.5). These classes are an implicit representation of the spatial heterogeneity of the response of forest

ecosystems to phosphorus addition.

$$\delta \bar{NPP}_i = \delta \bar{NPP}_{i,\max} \left(1 - e^{-\alpha_i c_{B,i}}\right) \text{ (E.5)}$$

The emulator is based on the following assumptions: the increase in NPP in class i responds to the increase $\delta c_{P,i}$ in soil phosphorus concentration [Gt.Mkm^{-2}], which is proportional to the application rate of basalt, and decreases over time (E.6).

$$\delta NPP_i(t) = \delta NPP_{i,\max} \left(1 - e^{-\alpha_i \delta c_{P,i}(t)}\right) \text{ (E.6)}$$

The dynamic evolution of the soil phosphorus concentration $\delta c_{P,i}$ is designed to reproduce the results of ORCHIDEE-CNP. It is modelled with an auxiliary pool of phosphorus which is unavailable to plants, exchanges phosphorus with the soil concentration with exchange times $\tau_{p,i}$ and $\tau_{u,i}$, and is leached to inland waters with a time $\tau_{l,i}$. Noting B_i the undissolved basalt in class i, and $\delta u_{P,i}$ the concentration of unavailable phosphorus, we calibrate the exchange times on the ORCHIDEE-CNP outputs using the following system of equations (see SM for more details on the calibration procedure).

$$\frac{d\delta c_{P,i}}{dt} = \frac{\lambda w_r B_i}{a_{B,i}} - \frac{\delta c_{P,i}}{\tau_{p,i}} + \frac{\delta u_{P,i}}{\tau_{u,i}} \text{ (E.7a)}$$

$$\frac{du_{P,i}}{dt} = \frac{\delta c_{P,i}}{\tau_{p,i}} - \frac{\delta u_{P,i}}{\tau_{u,i}} - \frac{\delta u_{P,i}}{\tau_{l,i}} \text{ (E.7b)}$$

Figure IV.6 shows the comparison of the emulator with ORCHIDEE-CNP data. Finally, the total NPP increase is the sum of the increase over all land response classes (E.8)

$$\delta NPP(t) = \sum_i \delta NPP_i(t) \text{ (E.8)}$$

4.2 Uncertainty analysis

To assess the sensitivity of our results to the uncertainty of parameters, we apply a double uncertainty analysis.

4.2.1 Quasi Monte-Carlo

First, we use a quasi-Monte Carlo sampling method to derive the distribution of outputs from the distributions of parameters. A Quasi Monte Carlo method is similar to a Monte Carlo method but uses quasi-random sampling instead of random sampling to minimise errors. The

Latin Hypercube Sampling method is used. On the supply side, we vary the costs and efficiency of new technologies, as well as their maximum diffusion speed and rates. The climate model uncertainty is also quantified by varying the equilibrium climate sensitivity (Sherwood et al., 2020). More details about the parameters assessed, as well as their distribution, are described in SI.2.

4.2.2 Morris method

Second, we apply the Morris screening method (Campolongo et al., 2007; King & Perera, 2013; Morris, 1991) to quantify the influence of each parameter on the outputs Let $X = x_1,\ldots,x_m$ be a vector of parameters which are normalised to [0,1], $Y = f(X)$ the output. A *trajectory* T is initiated by choosing an initial point $X_0^t \in \left[\frac{1}{2*N-1}, \frac{2}{2*N-1}, \ldots, \frac{2N-1}{2(2N-1)}\right]^m$, and then iteratively increasing each parameter i by $\frac{N}{(2N-1)}$ in a random order $P^t(i)_{i\in[1,p]}$ where P^t is a permutation, to obtain $T = X_0^t, X_1^t \ldots X_m^t$. Computing the output along this trajectory yields the elementary effects for each parameter i: $d_i^t = f\ (X_{\sigma(i)}^t) - f(X_{\sigma(i)-1}^t) = f(x_1,\ldots x_i + \Delta\ \ldots x_m) - f(x_1,\ldots x_m)$. We produce $N = 20$ trajectories. The means μ_i of the elementary effects, their standard deviation σ_i and the mean of their absolute values $\mu_i^\star$ give useful information about the influence of these parameters.

Initial points are sampled following a Latin Hypercube method, and trajectories are chosen to maximise their dispersion and thus their coverage of the parameters space, following (Campolongo et al., 2007), but we improve the sampling strategy by changing the dispersion measure: we maximise the sum over all parameters of the Euclidean pairwise distances of all the points used to compute elementary effects of this parameter. Additionally, we use a simulated-annealing algorithm instead of their brute force approach, which greatly reduces the computational burden (more details in SI.2).

5 Supplementary figures

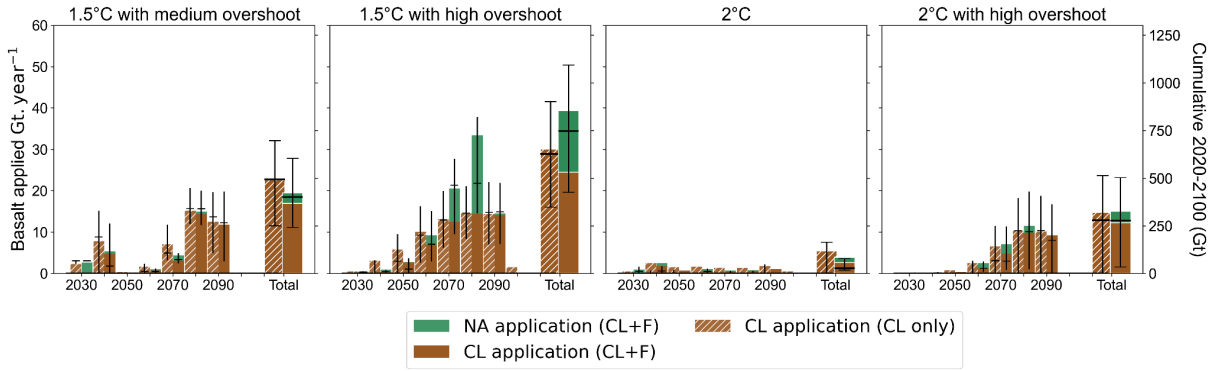

Figure III.7: Basalt applied on crop fields and forest areas. Left y-axis: predicted annual application rate (Gt/year). **Right y-axis:** cumulative application across the 21st century (Gt). The coloured bars indicate the mean, the black horizontal dashes the median and the error bars the 25%-75% range.

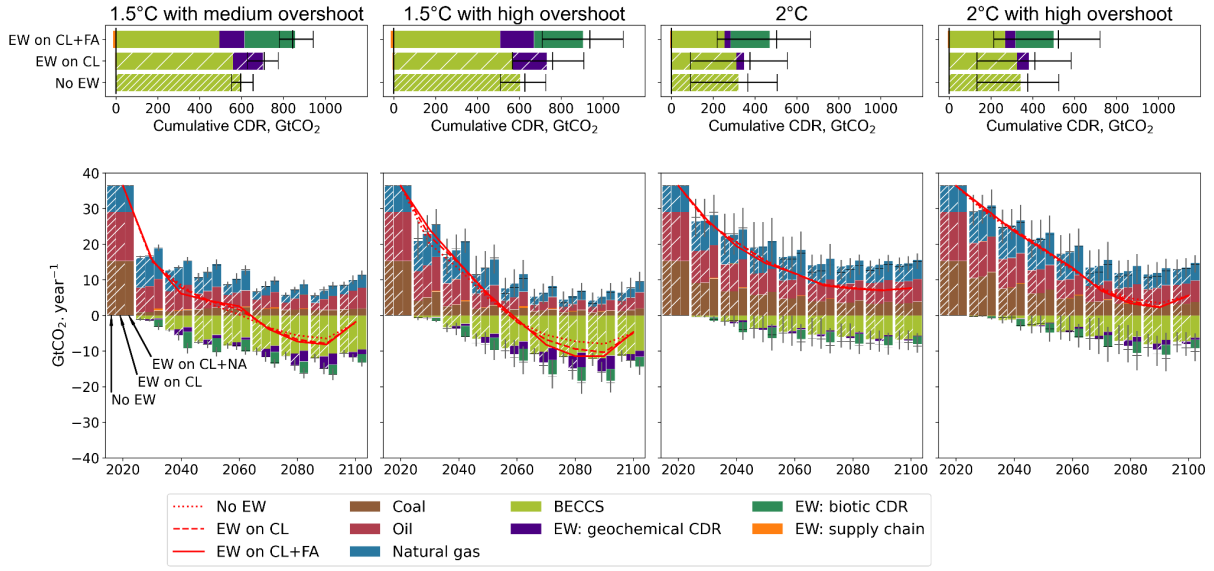

Figure III.8: Carbon dioxide emissions across the 21st century for different climate targets, with a discount rate of 2% per year. The red lines represent the net CO_2 emissions from the energy system. Four climate policy targets are compared (one per column): 1.5°C with low OS: The temperature change is limited to 1.5°C after 2100, with a possible overshoot of up to 0.2°C before 2100. 1.5°C with high OS: the temperature change is limited to 1.5°C after 2100. 2°C with no OS: the temperature change is limited to 2°C. 2°C with high OS: the temperature change is limited to 2°C after 2100. Three NET portfolios are assessed: No EW: BECCS only. EW on CL: EW deployed on croplands only, and BECCS. EW on CL+FA: EW deployed on croplands and forest areas, and BECCS. The bars indicate the mean, the black dashes the median and the 25%-75% range.

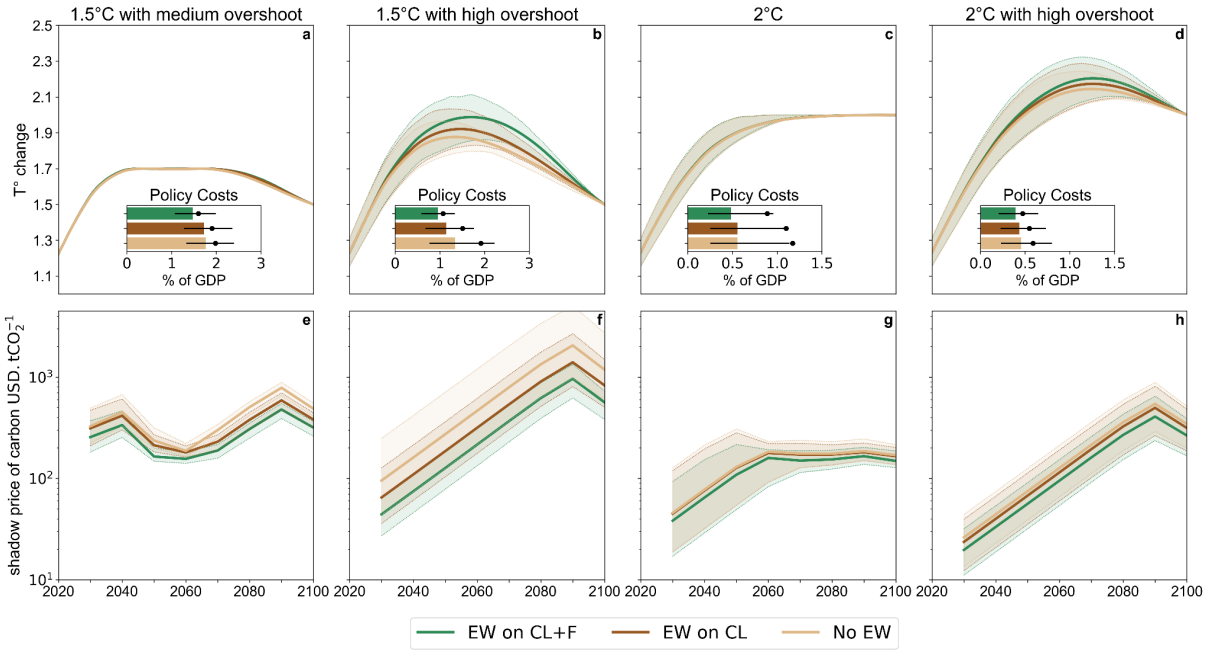

Figure III.9: Discount rate of 2% per year. Top: Mean surface temperature change compared to preindustrial period. **Bottom:** Shadow price of carbon across the 21st century for different climate targets. The shaded area represents the 25%-75% range. The scale changes between the panels. Policy costs are the net present values of future energy production costs and consumption losses as a percentage of GDP, compared to the no-policy scenario.

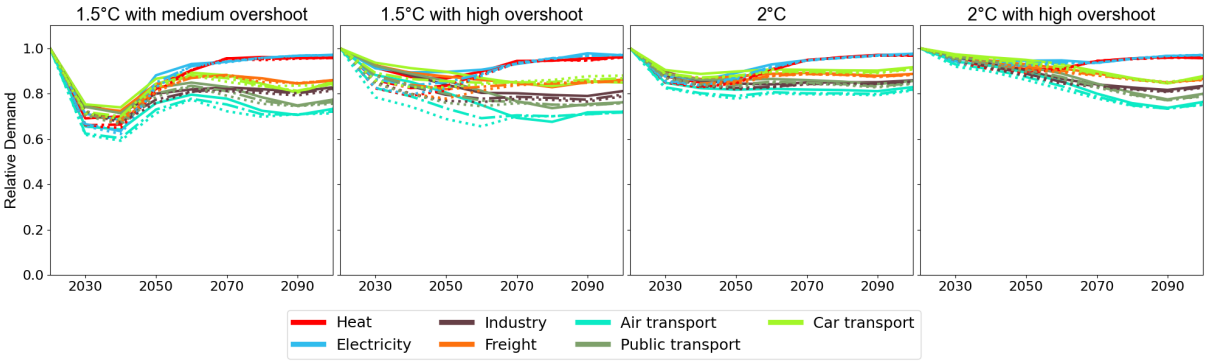

Figure III.10: Top: Relative energy demand in mitigation scenarios compared to the baseline. **Bottom:** Relative biomass price compared to the no-EW scenarios. Solid line: EW on CL+FA. **Dash-dotted line:** EW on CL only. **Dotted line :** No EW.

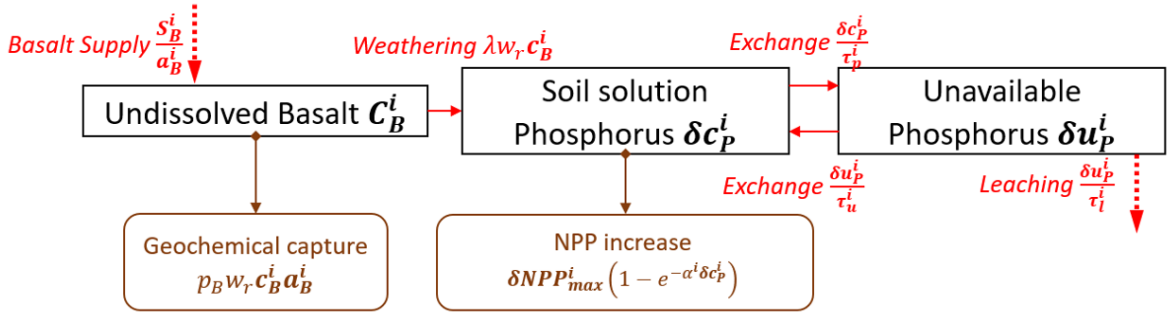

Figure III.11: Phosphorus cycle emulation. Rectangles: pools. Red arrows: flows. Brown arrows: effects on the carbon cycle.

References

Amann, T., Hartmann, J., Struyf, E., de Oliveira Garcia, W., Fischer, E. K., Janssens, I., Meire, P., & Schoelynck, J. (2020). Enhanced Weathering and related element fluxes – a cropland mesocosm approach. *Biogeosciences*, *17*(1), 103–119. https://doi.org/10.5194/bg-17-103-2020

Azar, C., Johansson, D. J. A., & Mattsson, N. (2013). Meeting global temperature targets—the role of bioenergy with carbon capture and storage. *Environmental Research Letters*, *8*(3), 034004. https://doi.org/10.1088/1748-9326/8/3/034004

Azar, C., & Lindgren, K. (2003). Global energy scenarios meeting stringent CO2 constraints— cost-effective fuel choices in the transportation sector. *Energy Policy*, 16.

Azar, C., Lindgren, K., Larson, E., & Möllersten, K. (2006). Carbon Capture and Storage From Fossil Fuels and Biomass – Costs and Potential Role in Stabilizing the Atmosphere. *Climatic Change*, *74*(1-3), 47–79. https://doi.org/10.1007/s10584-005-3484-7

Azar, C. A., Lindgren, K., & Andersson, B. (2000). Hydrogen Or Methanol in the Transportation Sector?

Barak, P., Chen, Y., & Singer, A. (1983). Ground basalt and tuff as iron fertilizers for calcareous soils. *Plant and Soil*, *73*(1), 155–158. https://doi.org/10.1007/BF02197765

Beerling, D. J., Epihov, D. Z., Kantola, I. B., Masters, M. D., Reershemius, T., Planavsky, N. J., Reinhard, C. T., Jordan, J. S., Thorne, S. J., Weber, J., Val Martin, M., Freckleton, R. P., Hartley, S. E., James, R. H., Pearce, C. R., DeLucia, E. H., & Banwart, S. A. (2024). Enhanced weathering in the US Corn Belt delivers carbon removal with agronomic benefits. *Proceedings of the National Academy of Sciences*, *121*(9), e2319436121. https://doi.org/10.1073/pnas.2319436121

Beerling, D. J., Kantzas, E. P., Lomas, M. R., Wade, P., Eufrasio, R. M., Renforth, P., Sarkar, B., Andrews, M. G., James, R. H., Pearce, C. R., Mercure, J.-F., Pollitt, H., Holden, P. B., Edwards, N. R., Khanna, M., Koh, L., Quegan, S., Pidgeon, N. F., Janssens, I. A., … Banwart, S. A. (2020). Potential for large-scale CO2 removal via enhanced rock weathering with croplands. *Nature*, *583*(7815), 242–248. https://doi.org/10.1038/s41586-020-2448-9

Beerling, D. J., Leake, J. R., Long, S. P., Scholes, J. D., Ton, J., Nelson, P. N., Bird, M., Kantzas, E., Taylor, L. L., Sarkar, B., Kelland, M., DeLucia, E., Kantola, I., Müller, C., Rau, G., & Hansen, J. (2018). Farming with crops and rocks to address global climate, food and soil security. *Nature Plants*, *4*(3), 138–147. https://doi.org/10.1038/s41477-018-0108-y

Bertagni, M. B., & Porporato, A. (2022). The Carbon-Capture Efficiency of Natural Water Alkalinization: Implications For Enhanced weathering. *Science of The Total Environment*, *838*, 156524. https://doi.org/10.1016/j.scitotenv.2022.156524

Bošeľa, M., & Šebeň, V. (2018). Analysis of the aerial application of fertilizer and dolomitic limestone. *Journal of Forest Science*, *56*, 47–57. https://doi.org/10.17221/29/2009-JFS

Buckingham, F. L., Henderson, G. M., Holdship, P., & Renforth, P. (2022). Soil core study indicates limited CO2 removal by enhanced weathering in dry croplands in the UK. *Applied Geochemistry*, *147*, 105482. https://doi.org/10.1016/j.apgeochem.2022.105482

Bullock, L. A., James, R. H., Matter, J., Renforth, P., & Teagle, D. A. H. (2021). Global Carbon Dioxide Removal Potential of Waste Materials From Metal and Diamond Mining. *Frontiers in Climate*, *3*, 694175. https://doi.org/10.3389/fclim.2021.694175

Bullock, L. A., Yang, A., & Darton, R. C. (2022). Kinetics-informed global assessment of mine tailings for CO2 removal. *Science of The Total Environment*, *808*, 152111. https://doi.org/10.1016/j.scitotenv.2021.152111

Buss, W., Hasemer, H., Ferguson, S., & Borevitz, J. (2024). Stabilisation of soil organic matter with rock dust partially counteracted by plants. *Global Change Biology*, *30*(1), e17052. https://doi.org/10.1111/gcb.17052

Calabrese, S., Wild, B., Bertagni, M. B., Bourg, I. C., White, C., Aburto, F., Cipolla, G., Noto, L. V., & Porporato, A. (2022). Nano- to Global-Scale Uncertainties in Terrestrial Enhanced Weathering. *Environmental Science & Technology*, *56*(22), 15261–15272. https://doi.org/10.1021/acs.est.2c03163

Campolongo, F., Cariboni, J., & Saltelli, A. (2007). An effective screening design for sensitivity analysis of large models. *Environmental Modelling & Software*, *22*(10), 1509–1518. https://doi.org/10.1016/j.envsoft.2006.10.004

Chiquier, S., Fajardy, M., & Dowell, N. M. (2022). CO2 removal and 1.5 °C: What, when, where, and how? *Energy Advances*. https://doi.org/10.1039/D2YA00108J

Cipolla, G., Calabrese, S., Noto, L. V., & Porporato, A. (2021). The role of hydrology on enhanced weathering for carbon sequestration I. Modeling rock-dissolution reactions coupled to plant, soil moisture, and carbon dynamics. *Advances in Water Resources*, *154*, 103934. https://doi.org/10.1016/j.advwatres.2021.103934

Clair, T. A., & Hindar, A. (2005). Liming for the mitigation of acid rain effects in freshwaters: A review of recent results. *Environmental Reviews*, *13*(3), 91–128. https://doi.org/10.1139/a05-009

Cobo, S., Negri, V., Valente, A., Reiner, D. M., Hamelin, L., Dowell, N. M., & Guillén-Gosálbez, G. (2023). Sustainable scale-up of negative emissions technologies and practices: Where to focus. *Environmental Research Letters*, *18*(2), 023001. https://doi.org/10.1088/1748-9326/acacb3

Creutzig, F., Breyer, C., Hilaire, J., Minx, J., Peters, G. P., & Socolow, R. (2019). The mutual dependence of negative emission technologies and energy systems. *Energy & Environmental Science*, *12*(6), 1805–1817. https://doi.org/10.1039/C8EE03682A

Dupla, X., Möller, B., Baveye, P. C., & Grand, S. (2023). Potential accumulation of toxic trace elements in soils during enhanced rock weathering. *European Journal of Soil Science*, *74*(1), e13343. https://doi.org/10.1111/ejss.13343

Emmerling, J., Drouet, L., Wijst, K.-I. van der, Vuuren, D. van, Bosetti, V., & Tavoni, M. (2019). The role of the discount rate for emission pathways and negative emissions. *Environmental Research Letters*, *14*(10), 104008. https://doi.org/10.1088/1748-9326/ab3cc9

Eufrasio, R. M., Kantzas, E. P., Edwards, N. R., Holden, P. B., Pollitt, H., Mercure, J.-F., Koh, S. C. L., & Beerling, D. J. (2022). Environmental and health impacts of atmospheric CO2 removal by enhanced rock weathering depend on nations' energy mix. *Communications Earth & Environment*, *3*(1), 106. https://doi.org/10.1038/s43247-022-00436-3

Fajardy, M., Morris, J., Gurgel, A., Herzog, H., Mac Dowell, N., & Paltsev, S. (2021). The economics of bioenergy with carbon capture and storage (BECCS) deployment in a 1.5 °C or 2 °C world. *Global Environmental Change*, *68*, 102262. https://doi.org/10.1016/j.gloenvcha.2021.102262

Fakhraee, M., Li, Z., Planavsky, N. J., & Reinhard, C. T. (2023). A biogeochemical model of mineral-based ocean alkalinity enhancement: Impacts on the biological pump and ocean carbon uptake. *Environmental Research Letters*, *18*(4), 044047. https://doi.org/10.1088/1748-9326/acc9d4

Farmer, A. M. (1993). The effects of dust on vegetation—a review. *Environmental Pollution*, *79*(1), 63–75. https://doi.org/10.1016/0269-7491(93)90179-R

Fleischer, K., Rammig, A., De Kauwe, M. G., Walker, A. P., Domingues, T. F., Fuchslueger, L., Garcia, S., Goll, D. S., Grandis, A., Jiang, M., Haverd, V., Hofhansl, F., Holm, J. A., Kruijt, B., Leung, F., Medlyn, B. E., Mercado, L. M., Norby, R. J., Pak, B., … Lapola, D. M. (2019). Amazon forest

response to CO2 fertilization dependent on plant phosphorus acquisition. *Nature Geoscience*, *12*(9), 736–741. https://doi.org/10.1038/s41561-019-0404-9

Fuglestvedt, J., Lund, M. T., Kallbekken, S., Samset, B. H., & Lee, D. S. (n.d.). A "greenhouse gas balance" for aviation in line with the Paris Agreement. *WIREs Climate Change*, *n/a*(n/a), e839. https://doi.org/10.1002/wcc.839

Fuhrman, J., Bergero, C., Weber, M., Monteith, S., Wang, F. M., Clarens, A. F., Doney, S. C., Shobe, W., & McJeon, H. (2023). Diverse carbon dioxide removal approaches could reduce impacts on the energy–water–land system. *Nature Climate Change*, *13*(4), 341–350. https://doi.org/10.1038/s41558-023-01604-9

Fuss, S., Lamb, W. F., Callaghan, M. W., Hilaire, J., Creutzig, F., Amann, T., Beringer, T., Garcia, W. d. O., Hartmann, J., Khanna, T., Luderer, G., Nemet, G. F., Rogelj, J., Smith, P., Vicente, J. L. V., Wilcox, J., Dominguez, M. d. M. Z., & Minx, J. C. (2018). Negative emissions—Part 2: Costs, potentials and side effects. *Environmental Research Letters*, *13*(6), 063002. https://doi.org/10.1088/1748-9326/aabf9f

Gaucher, Y., Tanaka, K., Ciais, P., & Boucher, O. (2022). Limited impact of COVID-19 recovery packages on near-term CO2 emissions pathways. *Environmental Research Communications*, *4*(10), 101006. https://doi.org/10.1088/2515-7620/ac9aa6

Goll, D. S., Ciais, P., Amann, T., Buermann, W., Chang, J., Eker, S., Hartmann, J., Janssens, I., Li, W., Obersteiner, M., Penuelas, J., Tanaka, K., & Vicca, S. (2021). Potential CO2 removal from enhanced weathering by ecosystem responses to powdered rock. *Nature Geoscience*, *14*(8), 545–549. https://doi.org/10.1038/s41561-021-00798-x

Goll, D. S., Vuichard, N., Maignan, F., Jornet-Puig, A., Sardans, J., Violette, A., Peng, S., Sun, Y., Kvakic, M., Guimberteau, M., Guenet, B., Zaehle, S., Penuelas, J., Janssens, I., & Ciais, P. (2017). A representation of the phosphorus cycle for ORCHIDEE (revision 4520). *Geoscientific Model Development*, *10*(10), 3745–3770. https://doi.org/10.5194/gmd-10-3745-2017

Grant, N., Hawkes, A., Mittal, S., & Gambhir, A. (2021a). The policy implications of an uncertain carbon dioxide removal potential. *Joule*, *5*(10), 2593–2605. https://doi.org/10.1016/j.joule.2021.09.004

Grant, N., Hawkes, A., Napp, T., & Gambhir, A. (2021b). Cost reductions in renewables can substantially erode the value of carbon capture and storage in mitigation pathways. *One Earth*, *4*(11), 1588–1601. https://doi.org/10.1016/j.oneear.2021.10.024

Hangx, S. J., & Spiers, C. J. (2009). Coastal spreading of olivine to control atmospheric CO2 concentrations: A critical analysis of viability. *International Journal of Greenhouse Gas Control*, *3*(6), 757–767. https://doi.org/10.1016/j.ijggc.2009.07.001

Haque, F., Santos, R. M., & Chiang, Y. W. (2020). CO2 sequestration by wollastonite-amended agricultural soils – An Ontario field study. *International Journal of Greenhouse Gas Control*, *97*, 103017. https://doi.org/10.1016/j.ijggc.2020.103017

Haque, F., Santos, R. M., Dutta, A., Thimmanagari, M., & Chiang, Y. W. (2019). Co-Benefits of Wollastonite Weathering in Agriculture: CO2 Sequestration and Promoted Plant Growth. *ACS Omega*, *4*(1), 1425–1433. https://doi.org/10.1021/acsomega.8b02477

Hartmann, J., & Moosdorf, N. (2012). The new global lithological map database GLiM: A representation of rock properties at the Earth surface. *Geochemistry, Geophysics, Geosystems*, *13*(12). https://doi.org/10.1029/2012GC004370

Hartmann, J., West, A. J., Renforth, P., Köhler, P., De La Rocha, C. L., Wolf-Gladrow, D. A., Dürr, H. H., & Scheffran, J. (2013). Enhanced chemical weathering as a geoengineering strategy to reduce

atmospheric carbon dioxide, supply nutrients, and mitigate ocean acidification. *Reviews of Geophysics*, *51*(2), 113–149. https://doi.org/10.1002/rog.20004

Hasegawa, T., Fujimori, S., Frank, S., Humpenöder, F., Bertram, C., Després, J., Drouet, L., Emmerling, J., Gusti, M., Harmsen, M., Keramidas, K., Ochi, Y., Oshiro, K., Rochedo, P., van Ruijven, B., Cabardos, A.-M., Deppermann, A., Fosse, F., Havlik, P., … Riahi, K. (2021). Land-based implications of early climate actions without global net-negative emissions. *Nature Sustainability*, *4*(12), 1052–1059. https://doi.org/10.1038/s41893-021-00772-w

Hinsinger, P., Bolland, M. D. A., & Gilkes, R. J. (1995). Silicate rock powder: Effect on selected chemical properties of a range of soils from Western Australia and on plant growth as assessed in a glasshouse experiment. *Fertilizer Research*, *45*(1), 69–79. https://doi.org/10.1007/BF00749883

Ibisch, P. L., Hoffmann, M. T., Kreft, S., Pe'er, G., Kati, V., Biber-Freudenberger, L., DellaSala, D. A., Vale, M. M., Hobson, P. R., & Selva, N. (2016). A global map of roadless areas and their conservation status. *Science*, *354*(6318), 1423–1427. https://doi.org/10.1126/science.aaf7166

IPCC. (2022). *Climate Change 2022: Mitigation of Climate Change. Contribution of Working Group III to the Sixth Assessment Report of the Intergovernmental Panel on Climate Change*. IPCC.

Jeswani, H. K., Chilvers, A., & Azapagic, A. (2020). Environmental sustainability of biofuels: A review. *Proceedings of the Royal Society A: Mathematical, Physical and Engineering Sciences*, *476*(2243), 20200351. https://doi.org/10.1098/rspa.2020.0351

Johansson, D. J. A., & Azar, C. (2007). A scenario based analysis of land competition between food and bioenergy production in the US. *Climatic Change*, *82*(3), 267–291. https://doi.org/10.1007/s10584-006-9208-1

Johansson, D. J. A., Azar, C., Lehtveer, M., & Peters, G. P. (2020). The role of negative carbon emissions in reaching the Paris climate targets: The impact of target formulation in integrated assessment models. *Environmental Research Letters*, *15*(12), 124024. https://doi.org/10.1088/1748-9326/abc3f0

Kantola, I. B., Blanc-Betes, E., Masters, M. D., Chang, E., Marklein, A., Moore, C. E., von Haden, A., Bernacchi, C. J., Wolf, A., Epihov, D. Z., Beerling, D. J., & DeLucia, E. H. (2023). Improved net carbon budgets in the US Midwest through direct measured impacts of enhanced weathering. *Global Change Biology*, *29*(24), 7012–7028. https://doi.org/10.1111/gcb.16903

Kantola, I. B., Masters, M. D., Beerling, D. J., Long, S. P., & DeLucia, E. H. (2017). Potential of global croplands and bioenergy crops for climate change mitigation through deployment for enhanced weathering. *Biology Letters*, *13*(4), 20160714. https://doi.org/10.1098/rsbl.2016.0714

Kantzas, E. P., Val Martin, M., Lomas, M. R., Eufrasio, R. M., Renforth, P., Lewis, A. L., Taylor, L. L., Mecure, J.-F., Pollitt, H., Vercoulen, P. V., Vakilifard, N., Holden, P. B., Edwards, N. R., Koh, L., Pidgeon, N. F., Banwart, S. A., & Beerling, D. J. (2022). Substantial carbon drawdown potential from enhanced rock weathering in the United Kingdom. *Nature Geoscience*, *15*(5), 382–389. https://doi.org/10.1038/s41561-022-00925-2

Kelland, M. E., Wade, P. W., Lewis, A. L., Taylor, L. L., Sarkar, B., Andrews, M. G., Lomas, M. R., Cotton, T. E. A., Kemp, S. J., James, R. H., Pearce, C. R., Hartley, S. E., Hodson, M. E., Leake, J. R., Banwart, S. A., & Beerling, D. J. (2020). Increased yield and CO_2 sequestration potential with the C_4 cereal *Sorghum bicolor* cultivated in basaltic rock dust-amended agricultural soil. *Global Change Biology*, *26*(6), 3658–3676. https://doi.org/10.1111/gcb.15089

King, D. M., & Perera, B. J. C. (2013). Morris method of sensitivity analysis applied to assess the importance of input variables on urban water supply yield – A case study. *Journal of Hydrology*, *477*, 17–32. https://doi.org/10.1016/j.jhydrol.2012.10.017

Klemme, A., Rixen, T., Müller, M., Notholt, J., & Warneke, T. (2022). Destabilization of carbon in tropical peatlands by enhanced weathering. *Communications Earth & Environment*, *3*(1), 1–9. https://doi.org/10.1038/s43247-022-00544-0

Köberle, A. C. (2019). The Value of BECCS in IAMs: A Review. *Current Sustainable/Renewable Energy Reports*, *6*(4), 107–115. https://doi.org/10.1007/s40518-019-00142-3

Köhler, P. (2020). Anthropogenic CO2 of High Emission Scenario Compensated After 3500 Years of Ocean Alkalinization With an Annually Constant Dissolution of 5 Pg of Olivine. *Frontiers in Climate*, *2*. Retrieved February 14, 2023, from https://www.frontiersin.org/articles/10.3389/fclim.2020.575744

Lenton, T. M., & Britton, C. (2006). Enhanced carbonate and silicate weathering accelerates recovery from fossil fuel CO2 perturbations. *Global Biogeochemical Cycles*, *20*(3). https://doi.org/10.1029/2005GB002678

Lewis, A. L., Sarkar, B., Wade, P., Kemp, S. J., Hodson, M. E., Taylor, L. L., Yeong, K. L., Davies, K., Nelson, P. N., Bird, M. I., Kantola, I. B., Masters, M. D., DeLucia, E., Leake, J. R., Banwart, S. A., & Beerling, D. J. (2021). Effects of mineralogy, chemistry and physical properties of basalts on carbon capture potential and plant-nutrient element release via enhanced weathering. *Applied Geochemistry*, *132*, 105023. https://doi.org/10.1016/j.apgeochem.2021.105023

Li, W., Ciais, P., Han, M., Zhao, Q., Chang, J., Goll, D. S., Zhu, L., & Wang, J. (2021). Bioenergy Crops for Low Warming Targets Require Half of the Present Agricultural Fertilizer Use. *Environmental Science & Technology*, *55*(15), 10654–10661. https://doi.org/10.1021/acs.est.1c02238

M. C. E. Grafton, I. J. Yule, C. E. Davies, R. B. Stewart, & J. R. Jones. (2011). Resolving the Agricultural Crushed Limestone Flow Problem from Fixed-Wing Aircraft. *Transactions of the ASABE*, *54*(3), 769–775. https://doi.org/10.13031/2013.37092

Minx, J. C., Lamb, W. F., Callaghan, M. W., Fuss, S., Hilaire, J., Creutzig, F., Amann, T., Beringer, T., Garcia, W. d. O., Hartmann, J., Khanna, T., Lenzi, D., Luderer, G., Nemet, G. F., Rogelj, J., Smith, P., Vicente, J. L. V., Wilcox, J., & Dominguez, M. d. M. Z. (2018). Negative emissions—Part 1: Research landscape and synthesis. *Environmental Research Letters*, *13*(6), 063001. https://doi.org/10.1088/1748-9326/aabf9b

Moosdorf, N., Renforth, P., & Hartmann, J. (2014). Carbon Dioxide Efficiency of Terrestrial Enhanced Weathering. *Environmental Science & Technology*, *48*(9), 4809–4816. https://doi.org/10.1021/es405202z

Morris, M. D. (1991). Factorial Sampling Plans for Preliminary Computational Experiments. *Technometrics*, *33*(2), 161–174. https://doi.org/10.2307/1269043

Negative Emissions Technologies and Reliable Sequestration: A Research Agenda. (n.d.). https://doi.org/10.17226/25259.%20National%20Academies%20of%20Sciences,%20Engineering,%20and%20Medicine.%202019.%20Negative%20Emissions%20Technologies%20and%20Reliable%20Sequestration:%20A%20Research%20Agenda.%20Washington,%20DC:%20The%20National%20Academies%20Press.%20https://doi.org/10.17226/25259.

Reddy, K. R., Gopakumar, A., & Chetri, J. K. (2019). Critical review of applications of iron and steel slags for carbon sequestration and environmental remediation. *Reviews in Environmental Science and Bio/Technology*, *18*(1), 127–152. https://doi.org/10.1007/s11157-018-09490-w

Renforth, P. (2012). The potential of enhanced weathering in the UK. *International Journal of Greenhouse Gas Control*, *10*, 229–243. https://doi.org/10.1016/j.ijggc.2012.06.011

Renforth, P., Pogge von Strandmann, P. A. E., & Henderson, G. M. (2015). The dissolution of olivine added to soil: Implications for enhanced weathering. *Applied Geochemistry*, *61*, 109–118. https://doi.org/10.1016/j.apgeochem.2015.05.016

Renforth, P. (2019). The negative emission potential of alkaline materials. *Nature Communications*, *10*(1), 1401. https://doi.org/10.1038/s41467-019-09475-5

Renforth, P., & Henderson, G. (2017). Assessing ocean alkalinity for carbon sequestration. *Reviews of Geophysics*, *55*(3), 636–674. https://doi.org/10.1002/2016RG000533

Rinder, T., & von Hagke, C. (2021). The influence of particle size on the potential of enhanced basalt weathering for carbon dioxide removal - Insights from a regional assessment. *Journal of Cleaner Production*, *315*, 128178. https://doi.org/10.1016/j.jclepro.2021.128178

Rogelj, J., Shindell, D., Jiang, K., Fifita, S., Forster, P., Ginzburg, V., Handa, C., Kheshgi, H., Kobayashi, S., Kriegler, E., Mundaca, L., Seferian, R., Vilarino, M. V., Calvin, K., Edelenbosch, O., Emmerling, J., Fuss, S., Gasser, T., Gillet, N., … Zhou, W. (2018, September). Chapter 2: Mitigation pathways compatible with 1.5oC in the context of sustainable development. In *Global Warming of 1.5 oC an IPCC special report on the impacts of global warming of 1.5 oC above pre-industrial levels and related global greenhouse gas emission pathways, in the context of strengthening the global response to the threat of climate change*. Intergovernmental Panel on Climate Change. https://www.ipcc.ch/report/sr15/

Rueda, O., Mogollón, J. M., Tukker, A., & Scherer, L. (2021). Negative-emissions technology portfolios to meet the 1.5 °C target. *Global Environmental Change*, *67*, 102238. https://doi.org/10.1016/j.gloenvcha.2021.102238

Ryan, P. C., Santis, A., Vanderkloot, E., Bhatti, M., Caddle, S., Ellis, M., Grimes, A., Silverman, S., Soderstrom, E., Stone, C., Takoudes, A., Tulay, P., & Wright, S. (2024). The potential for carbon dioxide removal by enhanced rock weathering in the tropics: An evaluation of Costa Rica. *Science of The Total Environment*, *927*, 172053. https://doi.org/10.1016/j.scitotenv.2024.172053

Santos, R. M., Zhang, N., & Bakhshoodeh, R. (2023). Multiscale Process Intensification of Waste Valorization Reactions. *Accounts of Chemical Research*, *56*(19), 2606–2619. https://doi.org/10.1021/acs.accounts.3c00364

Sherwood, S. C., Webb, M. J., Annan, J. D., Armour, K. C., Forster, P. M., Hargreaves, J. C., Hegerl, G., Klein, S. A., Marvel, K. D., Rohling, E. J., Watanabe, M., Andrews, T., Braconnot, P., Bretherton, C. S., Foster, G. L., Hausfather, Z., Heydt, A. S., Knutti, R., Mauritsen, T., … Zelinka, M. D. (2020). An Assessment of Earth's Climate Sensitivity Using Multiple Lines of Evidence. *Reviews of Geophysics*, *58*(4). https://doi.org/10.1029/2019RG000678

Smith, P., Davis, S. J., Creutzig, F., Fuss, S., Minx, J., Gabrielle, B., Kato, E., Jackson, R. B., Cowie, A., Kriegler, E., van Vuuren, D. P., Rogelj, J., Ciais, P., Milne, J., Canadell, J. G., McCollum, D., Peters, G., Andrew, R., Krey, V., … Yongsung, C. (2016). Biophysical and economic limits to negative CO2 emissions. *Nature Climate Change*, *6*(1), 42–50. https://doi.org/10.1038/nclimate2870

Strefler, J., Amann, T., Bauer, N., Kriegler, E., & Hartmann, J. (2018). Potential and costs of carbon dioxide removal by enhanced weathering of rocks. *Environmental Research Letters*, *13*(3), 034010. https://doi.org/10.1088/1748-9326/aaa9c4

Strefler, J., Bauer, N., Humpenöder, F., Klein, D., Popp, A., & Kriegler, E. (2021a). Carbon dioxide removal technologies are not born equal. *Environmental Research Letters*, *16*(7), 074021. https://doi.org/10.1088/1748-9326/ac0a11

Strefler, J., Kriegler, E., Bauer, N., Luderer, G., Pietzcker, R. C., Giannousakis, A., & Edenhofer, O. (2021b). Alternative carbon price trajectories can avoid excessive carbon removal. *Nature Communications*, *12*(1), 2264. https://doi.org/10.1038/s41467-021-22211-2

Swoboda, P., Döring, T. F., & Hamer, M. (2022). Remineralizing soils? The agricultural usage of silicate rock powders: A review. *Science of The Total Environment*, *807*, 150976. https://doi.org/10.1016/j.scitotenv.2021.150976

Tan, R. R., & Aviso, K. B. (2021). On life-cycle sustainability optimization of enhanced weathering systems. *Journal of Cleaner Production*, *289*, 125836. https://doi.org/10.1016/j.jclepro.2021.125836

Tanaka, K., Azar, C., Boucher, O., Ciais, P., Gaucher, Y., & Johansson, D. J. A. (2022). Paris Agreement requires substantial, broad, and sustained policy efforts beyond COVID-19 public stimulus packages. *Climatic Change*, *172*(1), 1. https://doi.org/10.1007/s10584-022-03355-6

Tanaka, K., Kriegler, E., Bruckner, T., Hooss, G., Knorr, W., Raddatz, T., & Tol, R. (2007). Aggregated Carbon cycle, atmospheric chemistry and climate model (ACC2): Description of forward and inverse mode, 14069106. https://doi.org/10.17617/2.994422

Tanaka, K., Lund, M. T., Aamaas, B., & Berntsen, T. (2018). Climate effects of non-compliant Volkswagen diesel cars. *Environmental Research Letters*, *13*(4), 044020. https://doi.org/10.1088/1748-9326/aab18c

Tanaka, K., & O'Neill, B. C. (2018). The Paris Agreement zero-emissions goal is not always consistent with the 1.5 °C and 2 °C temperature targets. *Nature Climate Change*, *8*(4), 319–324. https://doi.org/10.1038/s41558-018-0097-x

Taylor, L. L., Driscoll, C. T., Groffman, P. M., Rau, G. H., Blum, J. D., & Beerling, D. J. (2021). Increased carbon capture by a silicate-treated forested watershed affected by acid deposition. *Biogeosciences*, *18*(1), 169–188. https://doi.org/10.5194/bg-18-169-2021

Taylor, L. L., Quirk, J., Thorley, R. M. S., Kharecha, P. A., Hansen, J., Ridgwell, A., Lomas, M. R., Banwart, S. A., & Beerling, D. J. (2016). Enhanced weathering strategies for stabilizing climate and averting ocean acidification. *Nature Climate Change*, *6*(4), 402–406. https://doi.org/10.1038/nclimate2882

Thrikawala, S., Weersink, A., Fox, G., & Kachanoski, G. (1999). Economic Feasibility of Variable-Rate Technology for Nitrogen on Corn. *American Journal of Agricultural Economics*, *81*(4), 914–927. https://doi.org/10.2307/1244334

Van Straaten, P. (2006). Farming with rocks and minerals: Challenges and opportunities. *Anais da Academia Brasileira de Ciências*, *78*(4), 731–747. https://doi.org/10.1590/S0001-37652006000400009

Vandeginste, V., Lim, C., & Ji, Y. (2024). Exploratory Review on Environmental Aspects of Enhanced Weathering as a Carbon Dioxide Removal Method. *Minerals*, *14*(1), 75. https://doi.org/10.3390/min14010075

Vicca, S., Goll, D. S., Hagens, M., Hartmann, J., Janssens, I. A., Neubeck, A., Peñuelas, J., Poblador, S., Rijnders, J., Sardans, J., Struyf, E., Swoboda, P., van Groenigen, J. W., Vienne, A., & Verbruggen, E. (2022). Is the climate change mitigation effect of enhanced silicate weathering governed by biological processes? *Global Change Biology*, *28*(3), 711–726. https://doi.org/10.1111/gcb.15993

Wang, F., Zhu, F., Liu, D., Qu, Y., Liu, D., Xie, J., Wang, A., Kang, R., Quan, Z., Li, Y., Chen, X., Li, G., Hobbie, E. A., & Fang, Y. (2024). Wollastonite powder application increases rice yield and CO2 sequestration in a paddy field in Northeast China. *Plant and Soil*. https://doi.org/10.1007/s11104-024-06570-5

Wilson, S. A., Dipple, G. M., Power, I. M., Thom, J. M., Anderson, R. G., Raudsepp, M., Gabites, J. E., & Southam, G. (2009). Carbon Dioxide Fixation within Mine Wastes of Ultramafic-Hosted Ore

Deposits: Examples from the Clinton Creek and Cassiar Chrysotile Deposits, Canada. *Economic Geology*, *104*(1), 95–112. https://doi.org/10.2113/gsecongeo.104.1.95

Zhang, S., Planavsky, N. J., Katchinoff, J., Raymond, P. A., Kanzaki, Y., Reershemius, T., & Reinhard, C. T. (2022). River chemistry constraints on the carbon capture potential of surficial enhanced rock weathering. *Limnology and Oceanography*, *67*(S2), S148–S157. https://doi.org/10.1002/lno.12244

6 Supplementary Information

6.1 Enhanced weathering module

6.1.1 Carbon dioxide removal

We considered two distinct processes that lead to carbon dioxide removal from enhanced weathering: the geochemical capture and the biotic capture. Here, we first describe the release of these elements as modelled in GET-ACC2, and then each of the capture processes.

1.1.1 Weathering rates In the main text, we assume that the grain size is 20µm. The range of weathering rate used in this study is 1% to 26% per year. The low end is reported in Rinder and von Hagke (2021) (Rinder & von Hagke, 2021). The high end is the mean weathering rate in ORCHIDEE, where the values are based on Strefler et al. (2018) (Strefler et al., 2018) and on local temperatures. For a temperature of 25°C and a pH of 5.85, Rinder and von Hagke report a weathering rate of 2.63 10^{-12} mol.g^{-1}.s^{-1}, which is 12.7 times lower than what one obtains with equation G-2 in Strefler et al. (2018), with the same temperature and pH, notably because of a lower reactive surface. Given these diverse estimates of weathering rate, we assume that the uncertainty range of weathering rate is uniformly distributed between 1% and 26% per year. This uncertainty range is small compared to the 5-95% uncertainty range in Strefler et al. (2018) (Strefler et al., 2018), which varies by a factor of a thousand. However, due to the critical role of weathering rate, we investigate the impacts of very low values separately. We also assume that all minerals contained in basalt are weathered simultaneously.

The weathering rates are strongly influenced by the rock types, the in situ physicochemical and hydrological conditions as well as by biological processes, which leads to a large dispersion of the experiments results. Furthermore, robust and standardised methods for measuring CDR and rock weathering are still lacking, which may also explain the dispersion of the observed

weathering rates. In the following table, we reviewed the recent literature (Amann et al., 2020; Beerling et al., 2024; Berge et al., 2012; Buckingham et al., 2022; Dietzen et al., 2018; Haque et al., 2020; Kelland et al., 2020; Larkin et al., 2022; Lewis et al., 2021; Reershemius et al., 2023; Rinder & von Hagke, 2021; Ryan et al., 2024; Strefler et al., 2018; Vanderkloot & Ryan, 2023; F. Wang et al., 2024) on enhanced weathering experiments. The reported weathering rates were scaled to a value that would correspond to a grain size of 20µm. More precisely, if $w_r\ (d_1)$ is the weathering rate of a feedstock of grain size d_1, we have $\frac{w_r\ (d_1)}{w_r\ (d_2)} = (\frac{d_2}{d_1})^{\alpha}$. It is important to note that the relationship between weathering rate and grain size is uncertain, and that the existing literature reports both sublinear (α 1, e.g. ref (Vanderkloot & Ryan, 2023)) and superlinear (α 1, e.g. ref (Rinder & von Hagke, 2021; Strefler et al., 2018)) relationships between weathering rates and the inverse of grain sizes. For simplicity, we assumed that weathering rates are proportionate to the inverse of grain sizes $(\alpha = 1)$, as would be the case for perfect spheres, whose weathering rates depend on the reactive surface. For each mineral, we assume an exponential law of dissolution like in the main text, where the share of dissolved basalt x_t follows: $1 - x_t = \exp(-w_r\ t)$. For experiments during less than one year, we thus to obtain the share dissolved after 1 year as follows: $1 - x_T = \exp(\frac{T}{D}\ln(1 - x_D))$ where D is the duration of the equation and T is one year.

Study type	Grain size and reported weathering rate (% per year)	Linearly scaled weathering rate for 20µm-grains	Rock type	Ref
Reactor simulating humid tropical soil.	size: 300µm rate: 12-19 %/year	173-283 %/year	Basaltic flow (“Arenal”)	Ryan et al 2024
Reactor simulating humid tropical soil.	size: 47.2 µm rate: 30-42 %/year	70-100 %/year	Basaltic flow (“Barva”)	Ryan et al 2024
Reactor simulating humid tropical soil.	size: 14.1 µm rate: 20-78 %/year	14-55 %/year	Basalt flow (“BHVO-1”)	Ryan et al 2024
Reactor simulating humid tropical soil.	size < 45µm rate: 3-27 %/year	7-63 %/year	Basalt (BR-fine)	Vanderkloot et al 2023
Reactor simulating humid tropical soil.	size <45µm rate: 6-41 %/year	14-96 %/year	Basalt (PV-fine)	Vanderkloot et al 2023
Planted Mesocosm	size ~ 100µm rate: 30 %/year (1.6 t/ha)	120 %/year	Olivine	ten Berge et al. 2012

Planted Mesocosm	size ~ 100µm rate: 2 %/year (204 t/ha)	10 %/year	Olivine	ten Berge et al. 2012
Planted Mesocosm	size: 43 µm rate: 0.03%/year	0.06 %/year	Dunite	Amann et al. 2018
Planted Mesocosm	size: 1020µm rate: 0.01%/year	0.5 %/year	Dunite	Amann et al. 2018
Planted Mesocosm	size: 20µm rate: 91%/year (10t/ha)	91%/year	Olivine	Dietzen et al. 2018
Planted Mesocosm	size: 20µm rate: 40 %/year (50t/ha)	40 %/year	Olivine	Dietzen et al. 2018
Planted Mesocosm	size: 25 µm rate: 94 %/year	117 %/year	Wollastonite	Haque et al. 2019
Planted Mesocosm	size: 1250µm rate: 17 %/year	600 %/year	Basalt	Kelland et al 2020
Planted Mesocosm	size: 128µm rate: 21.7 %/year	139 %/year	Basalt	Kelland et al 2020
Planted Mesocosm	size: 35µm rate: 23 %/year	40 %/year	Basalt	Reershemius et al 2023
Field Trial (oil palm plantation)	No weathering measured	No weathering measured	Basalt	Larkin et al 2022
Field trial (Potato field)	size ~ 10µm rate: 93%/year	41 %/year	Wollastonite	Haque et al 2020
Field trial (Soybean field)	size ~ 10µm rate: 43%/year	21 %/year	Wollastonite	Haque et al 2020
Field Trial (Corn plantation)	size: 367µm rate: 3-6 %/year	48-110 %/year	Basalt	Beerling et al 2024
Field Trial (Rice paddy)	size < 75 µm rate: 91%/year	341%/year	Wollastonite	Wang et al 2024
Soil core study	size: 125-250µm rate: 0.04-0.05 %/year	0.5-0.8 %/year	Basalt	Buckingham et al 2022
Modelling (reactive transport model)	size: 714µm rate: 5.7 %/year	205 %/year	Basalt (Oregon)	Lewis et al 2021
Modelling (reactive transport model)	size: 1128µm rate: 5.5 %/year	308 %/year	Basalt (Craigmill)	Lewis et al 2021
Modelling (reactive transport model)	size: 1531 µm rate: 4.7 %/year	362 %/year	Basalt (Tichum)	Lewis et al 2021
Modelling (reactive transport model)	size: 267µm rate: 0.8 %/year	11 %/year	Basalt (Blue ridge)	Lewis et al 2021
Modelling (reactive transport model)	size: 1767µm rate: 3.8 %/year	336 %/year	Basalt (Tawau)	Lewis et al 2021
Modelling	size: 20µm rate: 1.03 %/year	1.03 %/year	Basalt	Rinder et von Hagke 2021

Modelling	size: 20µm rate: 19.6 %/year	19.6%/year	Basalt	Strefler et al 2018

Ryan et al, 2024: The share of minerals present in the rocks that were leached after 14 days are given in their table 4b. For each rock type, we report the range of weathering rates of Ca and Mg scaled by the grain size.

Vanderkloot et al 2023 reports a similar experimental design as Ryan et al, 2024. We do the same calculation to extrapolate annual weathering rates, considering only the cases with fine grain size (<45µm) to limit the errors when scaling to 20µm grains.

Kelland et al 2020 reports that 17% and 21.7% of the maximal CO_2 removal were obtained after 1 year, for relatively large grains (p80 = 1350µm, p50 $\approx$ 700µm). The weathering rates for ten Berge et al. 2012, Amann et al 2018, Dietzen et al 2018 and Haque et al 2019 were obtained from the table 3 of Kelland et al 2020

Reershemius et al 2023 reports that 15.7% of the maximum CO_2 removal was obtained after 235 days for grain size close to 20µm (p80 = 35µm, p50 $\approx$ 20µm).

Larkin et al 2022 reports no difference of CO_2 drawdown through alkalinity export between basalt-amended and reference fields.

Beerling et al 2024 reports a 16 ± 6% loss of cations from basalt applied on crop fields over 4 years. This corresponds to a mean weathering rate of around 4 ± 2% per year. Since the reported grain size in this study is 267 µm, and the weathering speed is proportional to the reactive surface of the grains, we can extrapolate that 20µm-sized grains should weather more than ten times faster.

Haque et al 2020 reports that in one field, the application of wollastonite at the rate of 1.24t/ha resulted in a CDR of 0.32tCO_2/ha after 5 months, which means that around 70% of the rocks have been weathered in 5 months assuming a stoichiometric rate of 1 mole of CO_2 sequestered per mole of wollastonite weathered after full precipitation of carbonates. The same calculation for another field, where coarser wollastonite was applied, indicates that around 20% of the initial input was weathered after 20 weeks.

Buckingham et al 2022 report the release rates (in mol.cm^{-2}.s^{-1}) of calcium and magnesium ions from basalt grains of size 150-250 µm. As they also report the mass composition of their basalt feedstock and its reactive surface, it is straightforward to derive the correspond-

ing weathering rate in %/year. These results they report have been contested (ref (West et al., 2023), with a response in ref (Buckingham et al., 2023)).

Lewis et al 2021 simulate the weathering of different basalt feedstocks depending on their mineralogy using a reactive transport model. They report the share of maximum CDR after 15 years, which we assume to be equal to the share of rock weathered.

Rinder et von Hagke 2021 simulate the weathering of 20-µm sized grains and obtain lower weathering rates than Strefler et al 2018, due to a lower reactive surface.

Due to the importance of weathering rates, we reproduced figure Ss 2 and 3 for weathering rates equal to 1%/year and 25%/year, which are the bounds of the assumed uncertainty range.These figure Ss show that although the biotic and geochemical CDR are higher at high weathering rates, the biotic effect is, relative to the geochemical effect, more efficient at low weathering rates.

1.1.1.1 Weathering rate = 1% per year

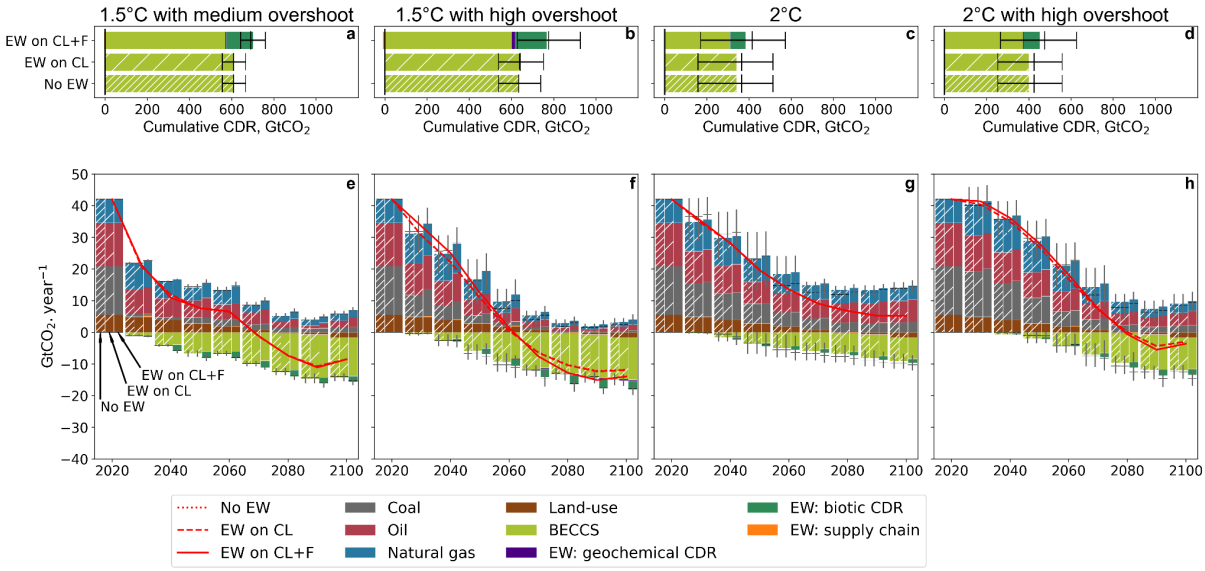

Figure III.12: Carbon dioxide emissions from three CDR portfolios for different climate targets across the 21st century. Discount rate = 5%. Weathering rate= 1% per year.

1.1.1.2 Weathering rate = 25% per year

1.1.2 Calibration of the model The response of the net primary production (NPP) to basalt amendment in GET-ACC2 is calibrated using simulations from the ORCHIDEE-CNP land-surface model. Previous publications have described the phosphorus cycle in ORCHIDEE-CNP and the model validation (D. S. Goll et al., 2017, 2021).

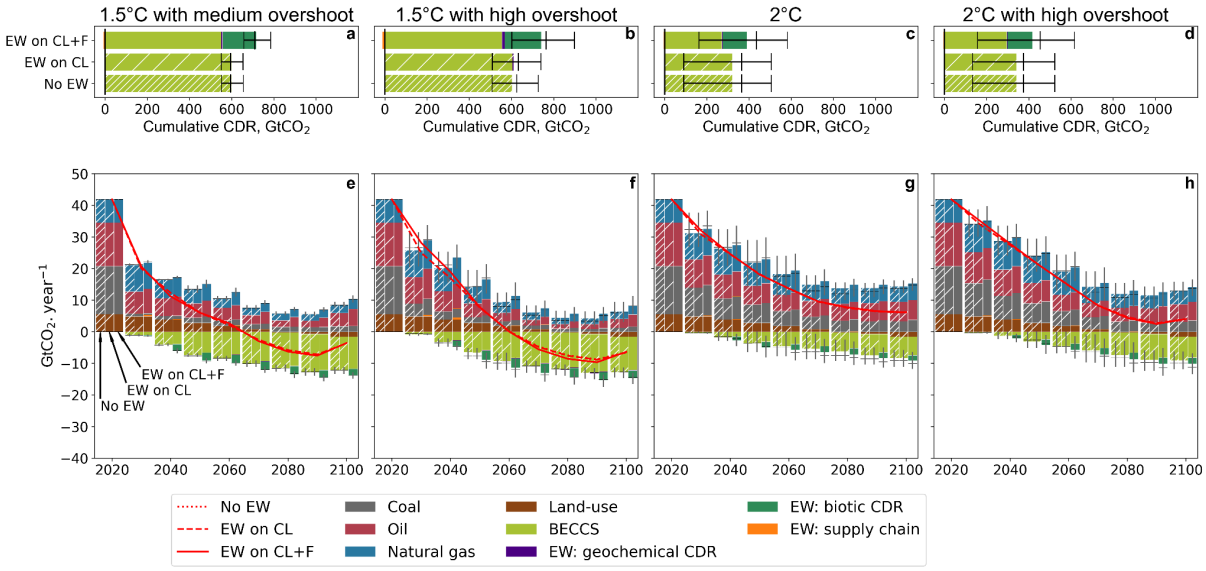

Figure III.13: Carbon dioxide emissions from three CDR portfolios for different climate targets across the 21st century. Discount rate = 2%. Weathering rate= 1% per year

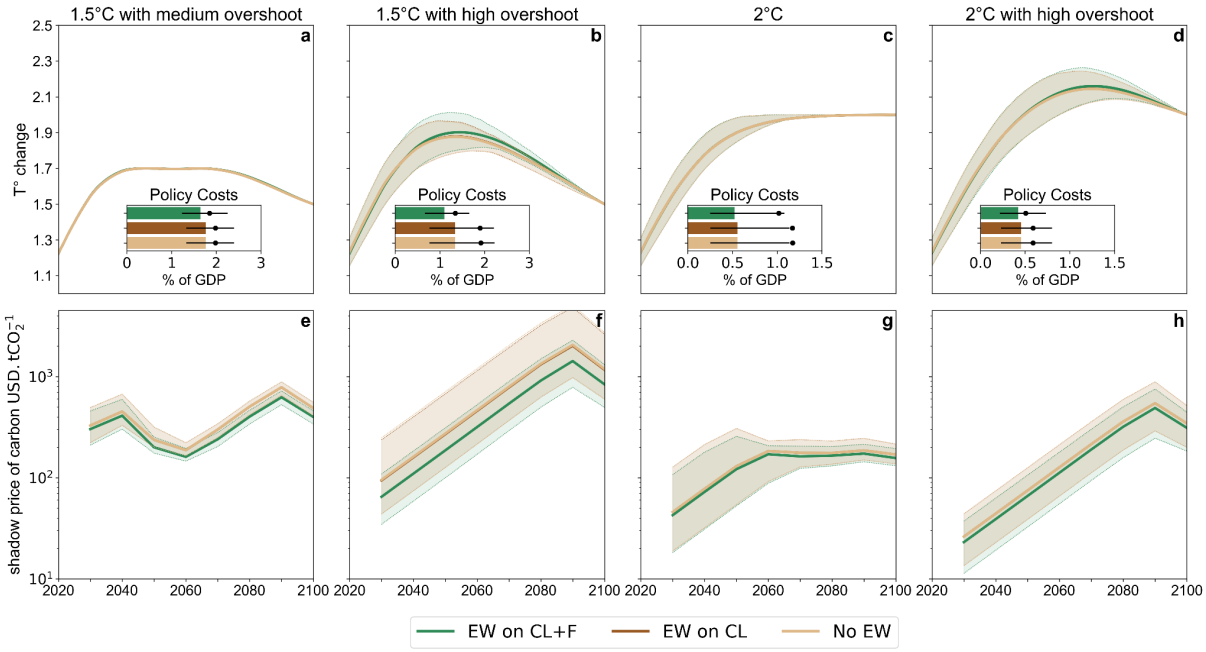

Figure III.14: Temperature, policy costs and carbon price pathways across the 21st century. Discount rate = 5%. Weathering rate= 1% per year.

The ORCHIDEE-CNP scenarios assume a uniform application of basalt dust over all land surfaces at the beginning of 2018, with different application rates: 0, 0.5, 1, 2, 3, 4, 5 kg.m^{-2}. The simulation runs until the end of 2200. The temperature, climate and atmospheric composition are unchanged from current levels until the end of 2200 in the simulation. The weathering rate only depends on temperature in these simulations. We use two kinds of output data for calibration: the net primary production, which is resolved over a 0.5° grid, at the plant functional type level, with a one-year timestep, and the geochemical CO_2 capture, at the same spatial and temporal resolution. The geochemical CO_2 capture follows an exponential decay, which is used

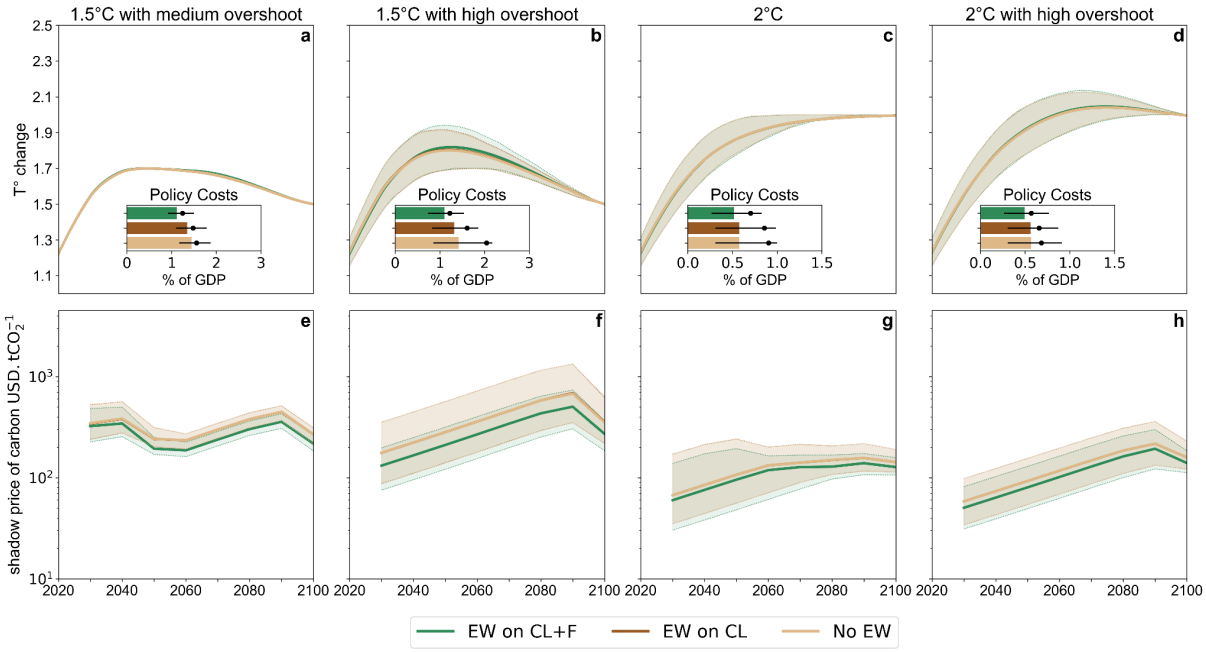

Figure III.15: Temperature, policy costs and carbon price pathways across the 21st century. Discount rate = 2%. Weathering rate= 1% per year.

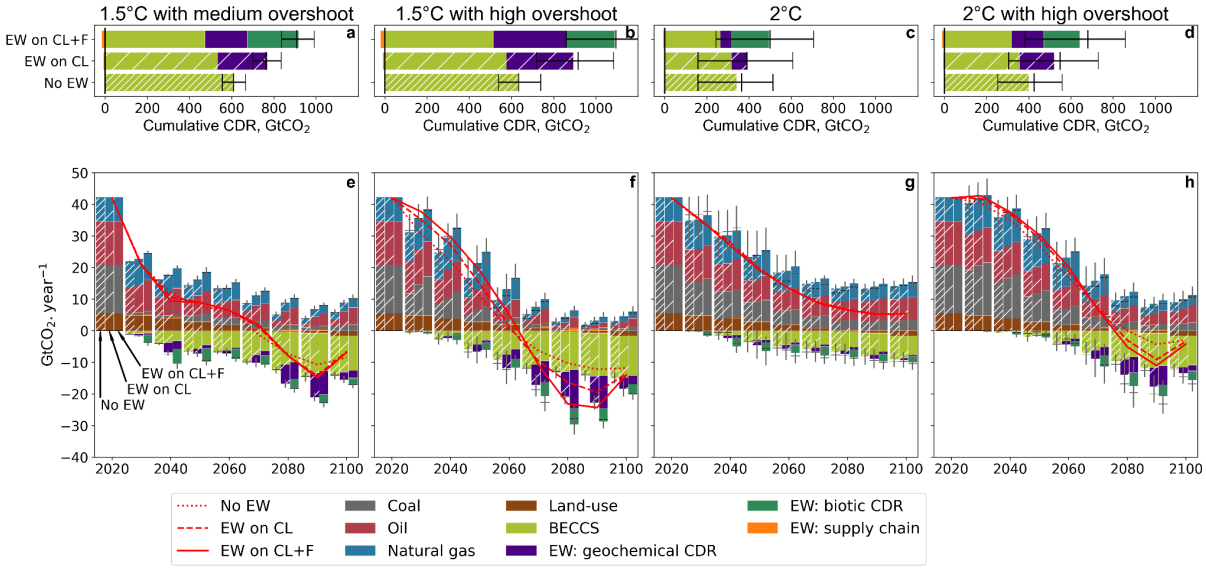

Figure III.16: Carbon dioxide emissions from three CDR portfolios for different climate targets across the 21st century. Discount rate = 5%. Weathering rate= 25% per year.

to obtain the assumed weathering rate.

The NPP increase in forests following basalt application depends on local conditions (D. S. Goll et al., 2021). It is stronger in tropical forests and in boreal forests. To make the most of the biotic carbon storage, it is more efficient to start applying basalt to the most "responsive" areas, that is to say the areas where the NPP increases the most after basalt application (figure S1.1.2.a). Therefore, the land surface pixels from ORCHIDEE-CNP are sorted from the most responsive to the least responsive to basalt application, and are grouped into M land response

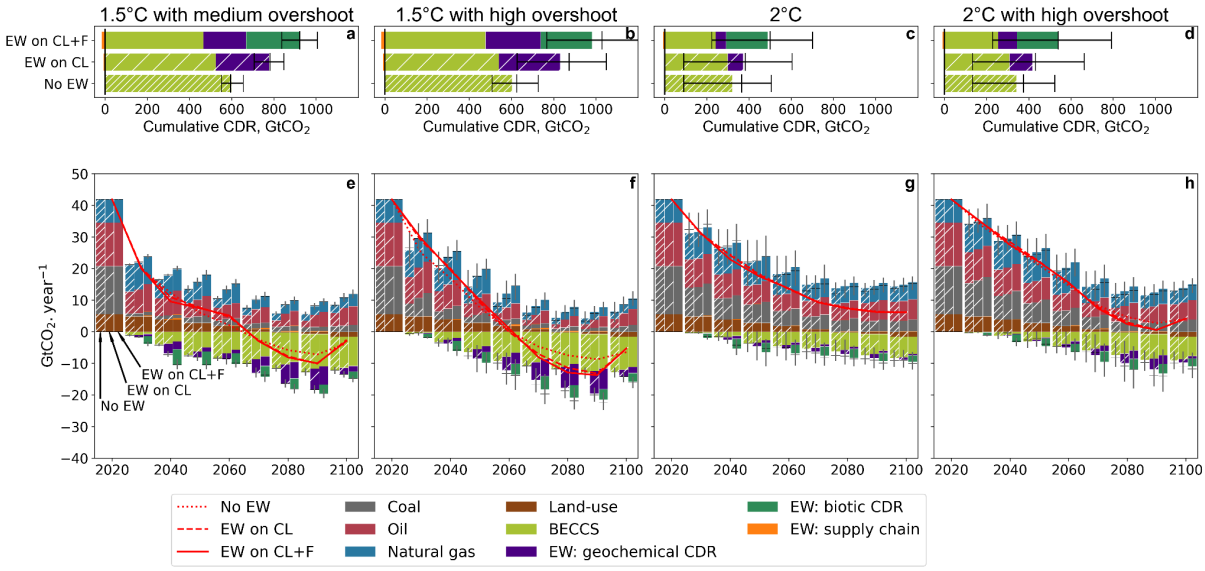

Figure III.17: Carbon dioxide emissions from three CDR portfolios for different climate targets across the 21st century. Discount rate = 2%. Weathering rate= 25% per year

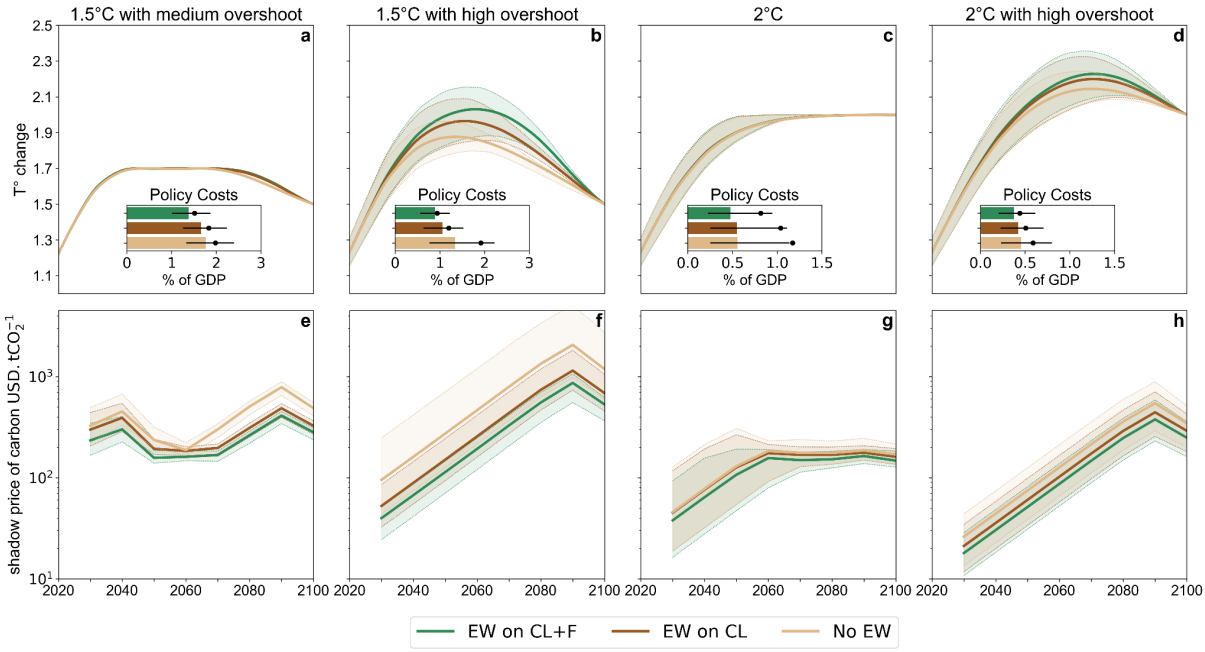

Figure III.18: Temperature, policy costs and carbon price pathways across the 21st century. Discount rate = 5%. Weathering rate= 25% per year.

classes$_1$, c_2,...c_M. c_1 gathers the most responsive application sites, and c_M the areas where the NPP increase following basalt application is the lowest. The classes are made to contribute equally to the total NPP increase (in GtC/year). Therefore, the surfaces of the classes c_i increase with i, as a larger area is required to obtain a given NPP increase when basalt is applied on less responsive areas. It should be noted that the classes are not composed of contiguous pixels.

In GET-ACC2, at each given timestep, the basalt application is distributed across classes, and the application rate is uniform within each class. The costs of application in $\$/t_{rock}$ does not

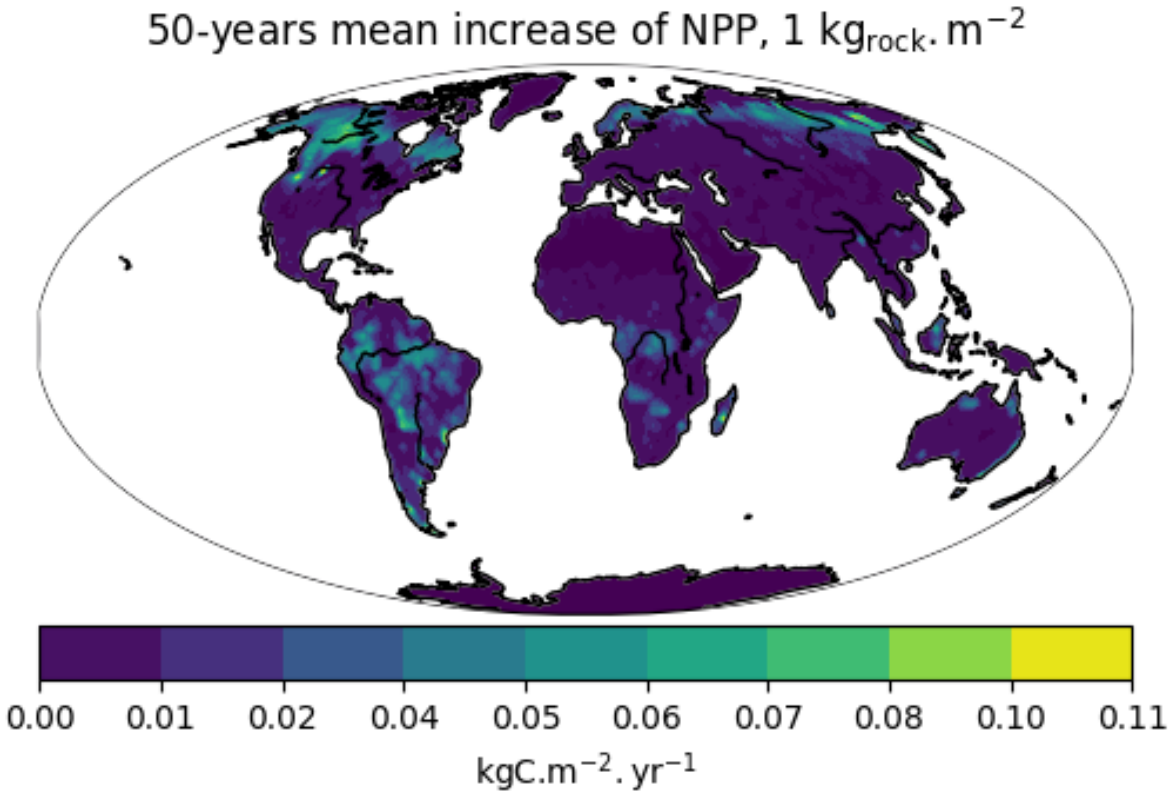

Figure III.19: Increase of the NPP, averaged over 50 years after the application of 1kg of basalt per m^2

depend on the class, but is lower for higher mean application rates (in kg/m^2) across classes, incentivising higher basalt application rates in a lower number of classes. The more land response classes there are, the higher the possibility for efficient application of basalt is, but the more complex to solve the model is. We took a number of classes M=5 in the following, to limit the complexity of the model due to the large number of simulations (figure III.17).

The phosphorus cycle emulator is built based on the following three assumptions: first, that the increase of net primary productivity is a function of the increase of soil phosphorus concentration. Second, the rate of increase of the soil phosphorus concentration is proportionate to the weathering of basalt. Third, we assume that the cycle of added phosphorus is open, with two phosphorus pools, the first one that is available to plants and which is fed by basalt weathering, the second one that is unavailable to plants and which exchanges phosphorus with the first one, but from which phosphorus also leaches away. The exchange rates follow classical diffusion dynamics.

The increase of NPP in the land response class i, δNPP_{i} (in GtC/year), increases as basalt weathers and releases phosphorus, and then decreases with time. The quantity of phosphorus released is proportionate to the amount of basalt applied. The increase of NPP increases with the quantity of added phosphorus $\delta c_{P,i}$, up to a maximum that depends on the class, following

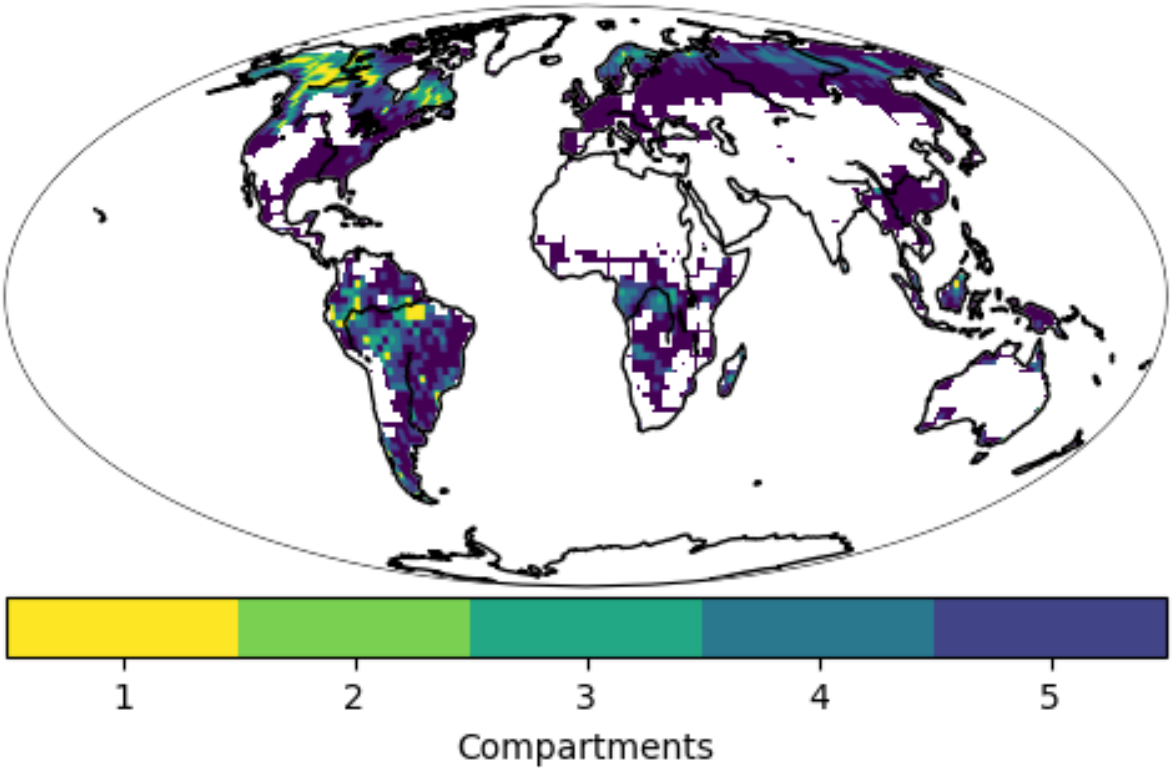

Figure III.20: Forest classes used in the current setting.

an exponential saturation pattern (E.5).

$$\delta NPP_i = \delta NPP_{i,\,\max}\left(1 - e^{-\alpha_i \delta c_{P,i}}\right) \quad \text{(E.5)}$$

The dynamic evolution of the soil phosphorus concentration δc_P is designed to reproduce the results of ORCHIDEE. It is modelled with an auxiliary pool of phosphorus which is unavailable to plants. It exchanges phosphorus with the soil concentration with exchange rates $1/\tau_{p,i}$ (from the soil solution phosphorus to the unavailable phosphorus pool) and $1/\tau_{u,i}$ (from the unavailable phosphorus pool to the soil solution), and leaches with a decay time $\tau_{l,i}$ (figure III.21)

$$\frac{d\delta c_P}{dt} = \frac{\lambda w_r B}{a_B} - \frac{\delta c_P}{\tau_p} + \frac{\delta u_P}{\tau_u} \quad \text{(E.6a)}$$

$$\frac{du_P}{dt} = \frac{\delta c_P}{\tau_p} - \frac{\delta u_P}{\tau_u} - \frac{\delta u_P}{\tau_l} \quad \text{(E.6b)}$$

For each land response class i, the parameters α_i, $\delta NPP_{i,\,\max}$, $\tau_{p,i}$, $\tau_{u,i}$ and $\tau_{l,i}$ are calibrated on the ORCHIDEE-CNP simulations using a gradient descent procedure. For each box, two methods are used: a step by step calibration, and a direct calibration.

In the step by step procedure, the temporal signal is filtered to remove the noise. Then, α_i

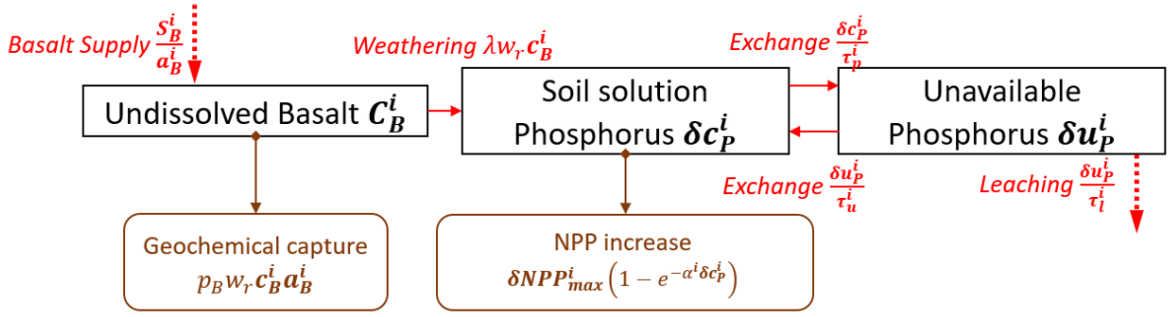

Figure III.21: Phosphorus cycle emulation in forest class *i*. Rectangles: phosphorus pools. Red arrows: phosphorus flows. Brown arrows: effects of enhanced weathering on the carbon cycle.

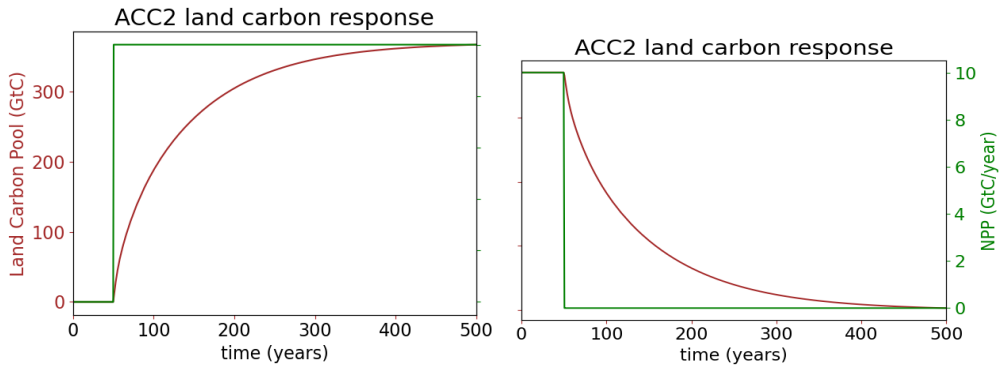

Figure III.22: Response of the land carbon pool to a NPP change from equilibrium (CO_2 and temperature conditions of the year 2000).

and $\delta NPP_{i,\,\max}$ are determined by comparing the maximum NPP increase for different basalt application levels. $\delta NPP_i = \delta NPP_{i,\,\max}\left(1 - e^{-\alpha_i \delta c_{P,i}}\right)$. To calibrated the remaining parameters $\tau_{p,i}$, $\tau_{u,i}$ and $\tau_{l,i}$, we follow a simple gradient descent procedure, using the python method scipy.optimize.minimize (Virtanen et al., 2020). To compute the error function to minimise over a set of possible values of parameters, we solve the set of equations E6a, E6b with current parameters values, then compute the resulting NPP increase (E5) with the known values of α_i, $\delta NPP_{i,\,\max}$, and finally compute the quadratic difference with the filtered signal. In the direct calibration procedure, we directly calibrate α_i, $\delta NPP_{i,\,\max}$, $\tau_{p,i}$, $\tau_{u,i}$ and $\tau_{l,i}$ on the filtered signal using the gradient descent. For each land response class, we export the set of parameters that yield the smallest quadratic error with the unfiltered ORCHIDEE-CNP output.

1.1.3 Long-term dynamics of the model When the phosphorus addition has stopped, δNPP^i gradually turns to zero, with a characteristic timescale of ${\tau_l}^i$. As a consequence, the additional carbon stored progressively returns to the atmosphere. (figure Ss III.22 III.23)

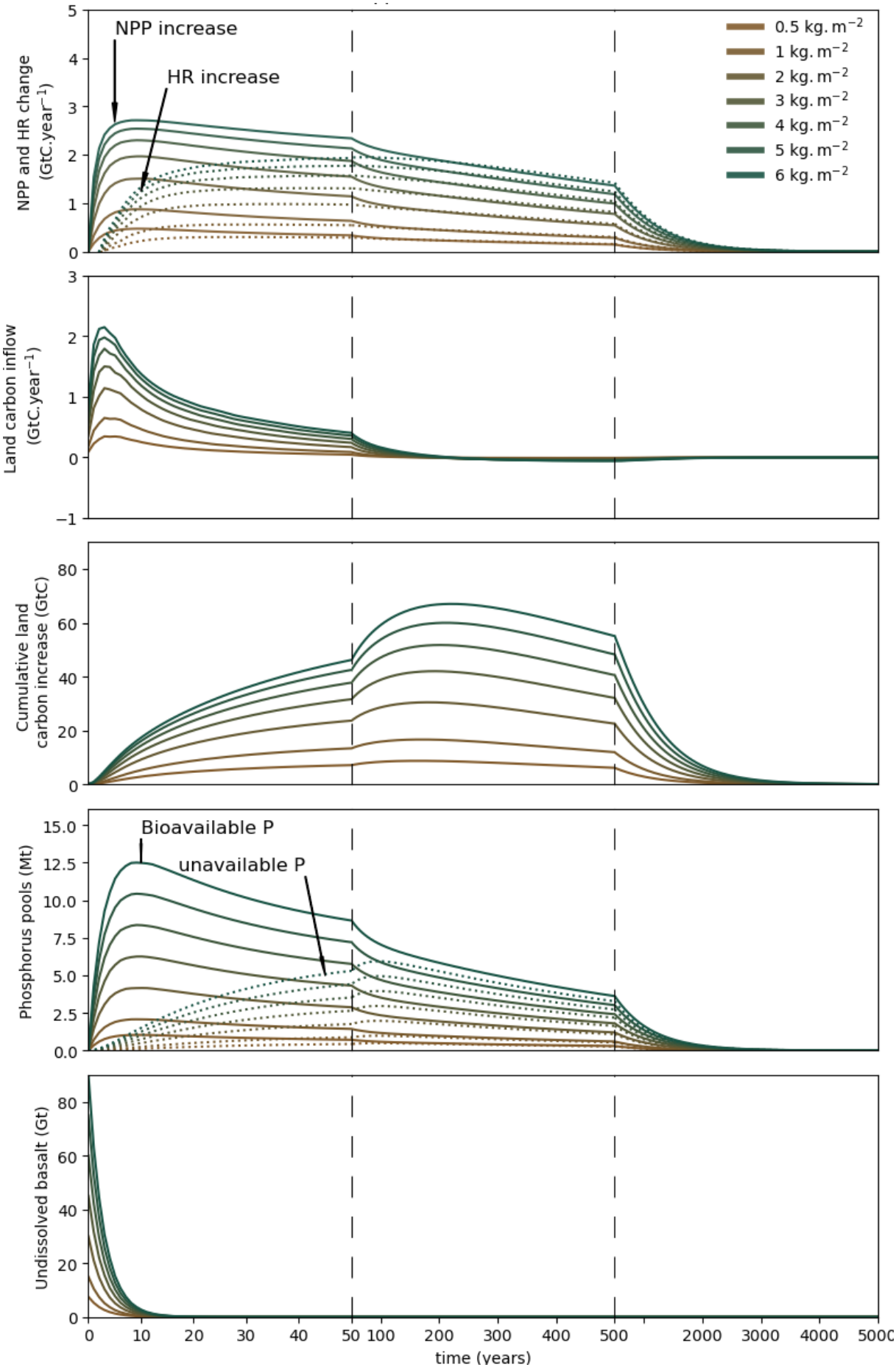

Figure III.23: Response of the land carbon stocks, land carbon flows and phosphorus pools to a basalt addition at year 0. (weathering rate = 26%), CO_2 and temperature conditions of the year 2000. **First panel:** dotted lines represent the increase of heterotrophic respiration (HR), solid line the increase of net primary production (NPP). **Second panel:** Net flow from atmosphere to land carbon (NPP-HR). **Third panel:** Cumulative land carbon increase.**Fourth panel:** dotted lines represent the unavailable phosphorus pool, solid line the soil phosphorus pool.

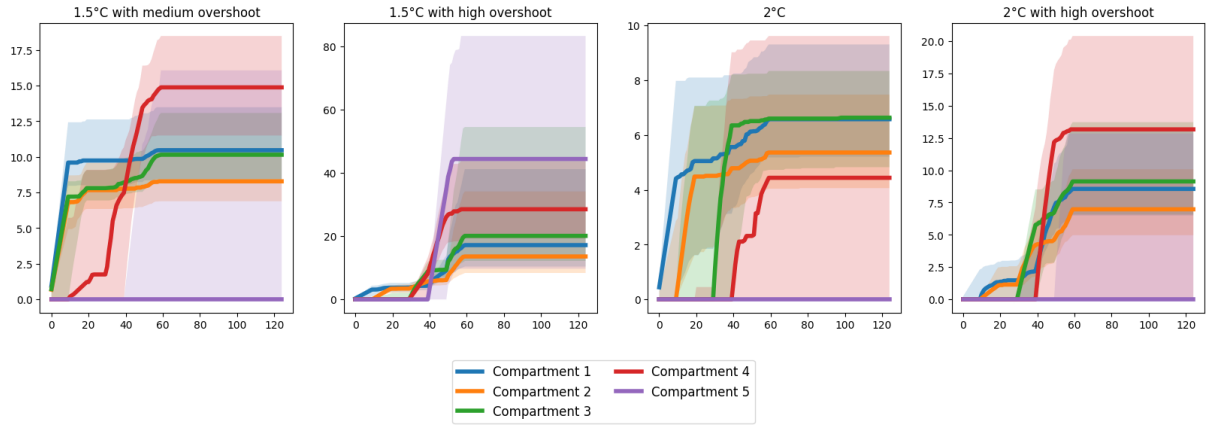

Figure III.24: Cumulative basalt application in the different forest classes across the 21st century. The solid line is the median, the shaded area is the 25-75% range.

1.1.4 Spatial distribution of basalt application Land response classes are built as follows: first, pixels are sorted out depending on their local increase in NPP after basalt application, from the most responsive to the least. Then they are grouped in N classes so that each class represents an equal share of the total NPP increase: the first class is therefore much smaller than the last one. Basalt is generally applied successively in the different classes, because it is cheaper to apply large concentrations of rocks and because carbon is sequestered during a long period after basalt application. The smallest class is therefore used first, then the second, etc. The fifth class is used only in the largest application case, the 1.5°C case with high OS (figure III.24).

6.1.2 Basalt supply

The basalt dust supply is integrated in GET7.1 with a 10 year timestep: costs and energy requirements of basalt supply are fed back into GET. Basalt must be mined, crushed and ground, and transported. Each of these steps requires energy. We assume that diesel or gasoline are used for mining and crop-fields spreading. Basalt could be transported by trains, trucks or ships. Here we assume that a minimum share of 70-90% must be transported by trucks. The energy requirements of transport increase the demand in each transport subsector (road, train or water freight). Transport modes are substitutable but a minimum share (70-90%) must be transported on the road.

Process	Energy Intensity	Financial cost	Energy type	Demand in GET-ACC2
Mining (Atima & Suthirat, 2016)	0.02 EJ/Gt	-	Diesel	Diesel or gasoline

Mining and Crushing (Strefler et al., 2018)	0.02 EJ/Gt	27.3$/t	Electricity	Electricity
Grinding (Strefler et al., 2018)	mean: 0.2, range 0.07-0.6 EJ/Gt	included in crushing costs	Electricity	Electricity
Road Transport (Renforth, 2012)	0.0013 EJ/Gt/km	0.08$/t/km	Endogenous	Road freight
Sea and rail transport (Renforth, 2012)	0.0002 EJ/Gt/km	0.05$/t/km	Endogenous	Sea or rail freight
Spreading (tractors) (Thrikawala et al., 1999)	0.078 EJ/Gt	10.9$/t (ref. (Strefler et al., 2018))	Diesel	Diesel or gasoline
Spreading (aeroplanes)	1.8-2.5 EJ/Gt	capacity cost : 170-214$/t/year O&M costs: 70-110$/t	Endogenous (kerosene, hydrogen or methanol)	Aviation fuel

1.2.1 Transport distances There are 3 cases : basalt is either spread on croplands with tractors, or basalt is spread on forest areas with tractors, or basalt is spread on forest areas with aircrafts.

Application on croplands: the transport distance for cropland application is derived from Strefler, et al (2018) (Strefler et al., 2018). The transport distance is generally lower than 200km. It starts from zero and increases (up to a maximum of 490 km) as long as the unweathered quantity of basalt applied on croplands increases, as we follow their assumption that the application rate is 15kg/m^2 which can be easily incorporated into soils.

Application on forests: we assume that the share of roadless forests (i.e. forest areas inaccessible by roads) is approximately the same as the share of global roadless areas, that is to say 80% (Ibisch et al., 2016). This share can be expected to decline in the future, despite the threats roads pose to ecosystems (Ibisch et al., 2016). On the other hand, applying basalt on forests by means of land transport can be challenging, even when a road is available. We therefore assume that between 70% to 90% of basalt application on forests must be spread with aircrafts until 2100. This share depends on the development of roads and on the share of forests that tractors can penetrate. Aerial application is likely to be more expensive and energy intensive

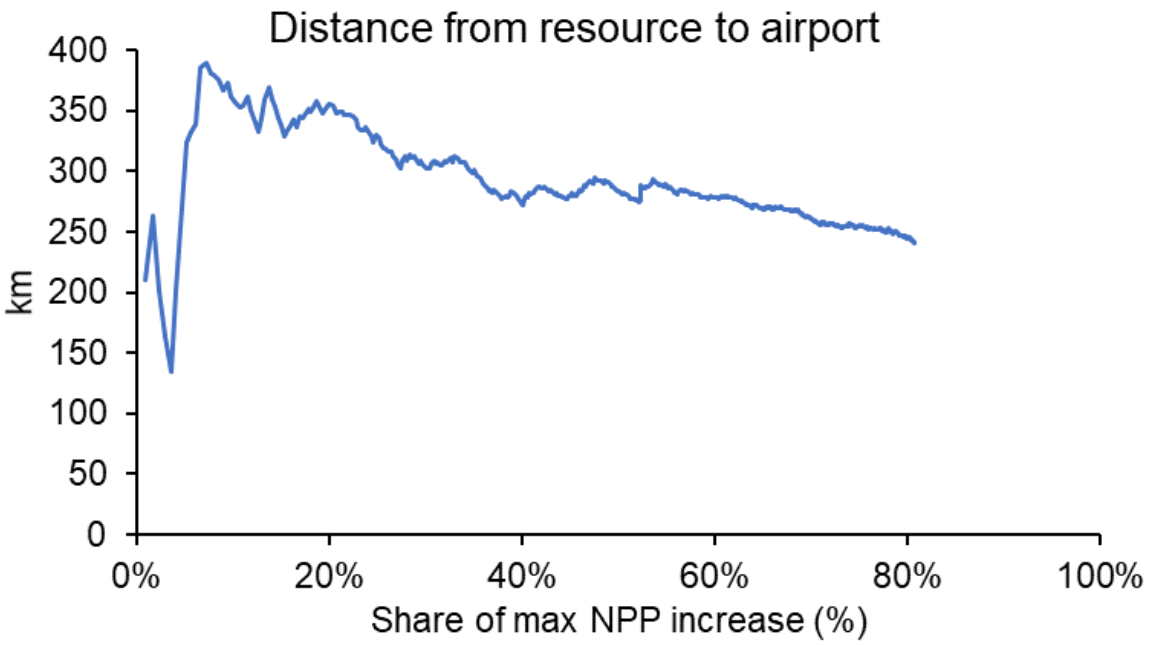

Figure III.25: Straight line distance from basalt resource to the nearest airport from an application site. The x-axis is the cumulative contribution from the application sites, ranked from the most reactive to the least reactive to basalt amendment, to the total NPP increase. The y-axis is the mean distance corresponding to these cumulative contributions.

than land-based alternatives. If the share of aircraft use were lower, the energy consumption would also be lower, and basalt application could become higher in a cost-optimisation model. Assuming a large part of aerial spraying is therefore pessimistic as far as costs are concerned.

We assume that the rock is ground at a location proximate to the mine. The mean straight-line distance between the airport and the closest area where basalt is available is 250 to 400 km (figure III.25). We estimate the average road distance to be around 350 to 560 km by assuming that the actual travel distance on the road is on average larger than the straight-line distance by a factor of the square root of 2 (i.e., a simple analogy from geometry). If basalt is applied with tractors, the distance between basalt source and application site is generally lower than 250 km (figure III.26), thus the road distance is estimated to be around 350 km under the assumption of the square root of 2. We therefore consider a range of 350 to 550 km for basalt transport distance.

The distances are computed using the software QGIS. The database for basalt resources is the one used in Strefler, et al. (2018), GLiM (Hartmann & Moosdorf, 2012). The database for airports is the one used by Goll, et al. (2021) (D. S. Goll et al., 2021) openflights.org.

1.2.2 Cost of aircraft application Our analysis aims to identify a range of energy require-

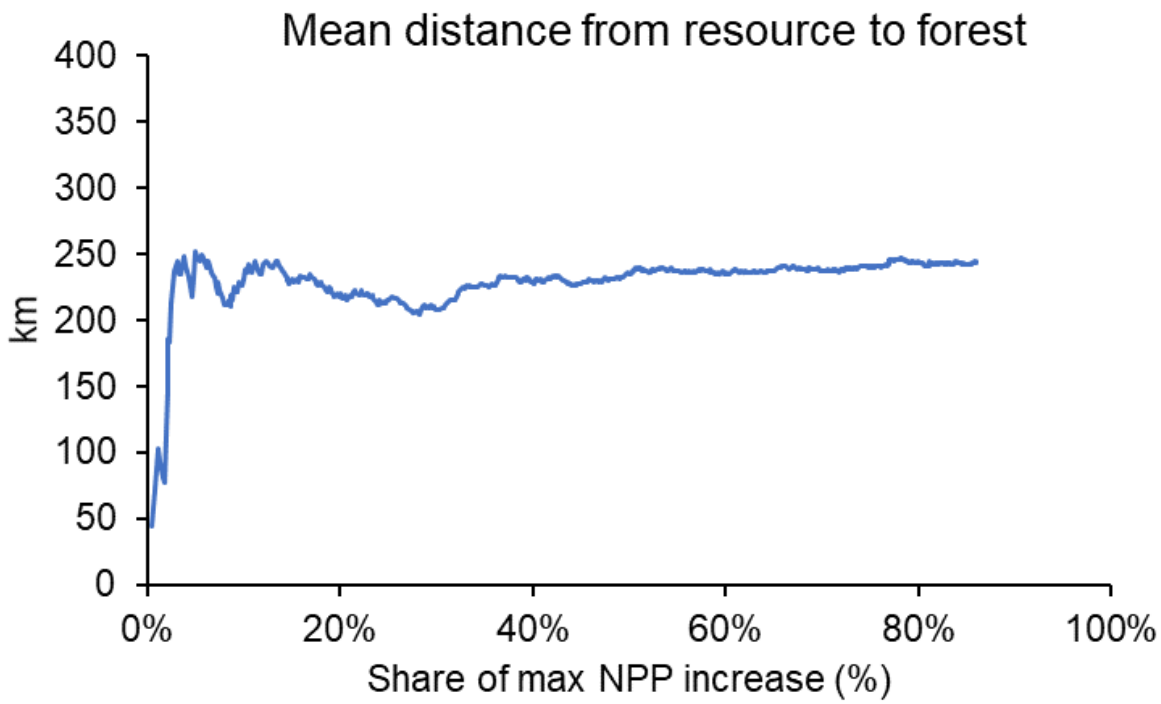

Figure III.26: Distance from basalt resource to application site (straight line).The x-axis is the cumulative contribution from the application sites, ranked from the most reactive to the least reactive to basalt amendment, to the total NPP increase. The y-axis is the mean distance corresponding to these cumulative contributions.

ments and financial costs for airborne spreading of basalt. A small agricultural aircraft like the AirTractor 802, which can be equipped with a dust spreader, could be used to spread basalt dust. This kind of aircraft is commonly used to spread limestone (Bošeľa & Šebeň, 2018; Clair & Hindar, 2005; M. C. E. Grafton et al., 2011) although issues with rock discharge have been reported, due to the large particle size distribution (M. C. E. Grafton et al., 2011). The details of rock dust discharge are beyond the scope of this analysis, and more research would be needed on how to spread large quantities of basalt dust by air.

The following table summarises the key values used for our cost estimate:

Feature	Source
Useful load : 4.3t	Guide to Air Tractor Aircraft
Cost: USD 1.8 million	https://air.one/
Fuel consumption: up to 330 l/h	Guide to Air Tractor Aircraft
ground O&M costs: 120-210$/hour	Ref. (Moraes et al., 2021)
Housing & Insurance: 5% of purchase cost each year	Ref. (Moraes et al., 2021)
Pilot labour cost: 300$/hour	Ref. (Moraes et al., 2021)
Speed: 306 km/h	AIR TRACTOR AT-802/802A Pilot Training Program

The distance between the centre of spreading sites and the nearest airport ranges between

80 and 120 km (figure III.25). We therefore assume a flying distance ranges between 160 and 240 km. It represents a flight duration of 31-47 minutes. Adding 10 minutes for spreading, the average flight duration would reach 41-57 minutes. This represents 226-314 litres of kerosene per mission, or 7.6-10.6 GJ per mission, or 1.8 to 2.5 GJ/t of basalt applied. Assuming that 20 minutes are required to refuel and refill with basalt between each flight, and that the aircraft operates 10 hours per day, and that it is used 5 days out of 7, an aircraft can realise between 2030 and 2550 missions per year. Therefore, the capacity cost per ton/year is 170-214$/t/year (it depends on the average distance flown). We assume a lifetime of 30 years.

The hourly costs, including ground operations & maintenance costs, and labour, amount to 420-510 $/hour. With the previous assumptions, it takes 9 to 13 minutes of flight to spread 1 ton of rocks. Therefore, the total O&M costs per ton, including pilot's labour cost is 70-120$ per ton, or 56-102$ if the discharge takes 1 minute instead of 10. Finally, maintaining the landing trail, housing the plane and insuring it costs around 5% of the aircraft purchase cost each year. We are considering only existing landing trails.

The cost depends on the number of hours flown. A very low application rate (in kg per m^2) would result in a longer application duration, and therefore in higher costs per ton applied. We assume that the energy and financial costs of aerial application are proportionate to the duration of each flight. The flight duration is equal to: $D_{tot} = D_{travel} + \frac{m}{vLr}$ where D_{travel} is the time required to access (and return from) the spreading site (31-47 minutes), m is the load of basalt carried (4 tons), v is the velocity (306 km/h), L is the spreading width (assumed to be 10 m), and r is the application rate (in kg/m^2). If the discharge takes 10 minutes, the application rate equals to 0.008 kg $/m^2$. If the discharge takes 1 minute, the resulting application rate is 0.08kg/m².

The use of electric drones could also be considered and be cheaper. However, considering their current performances, they cannot carry large amounts of rocks up to the most remote areas, and the application over forests with drones could therefore require developing more roads. Therefore, we consider the application by aircrafts only.

6.1.3 Break-even CO_2 price of basalt application

Basalt is applied when the net present value of costs becomes lower than that of benefits, which are defined as the discounted sum of future CDR multiplied by future carbon prices. Intertemporal effects, especially biotic CDR, are crucial due to CDR continuing for decades after basalt dust application. It is important to note that although we analyse the costs and benefits of basalt

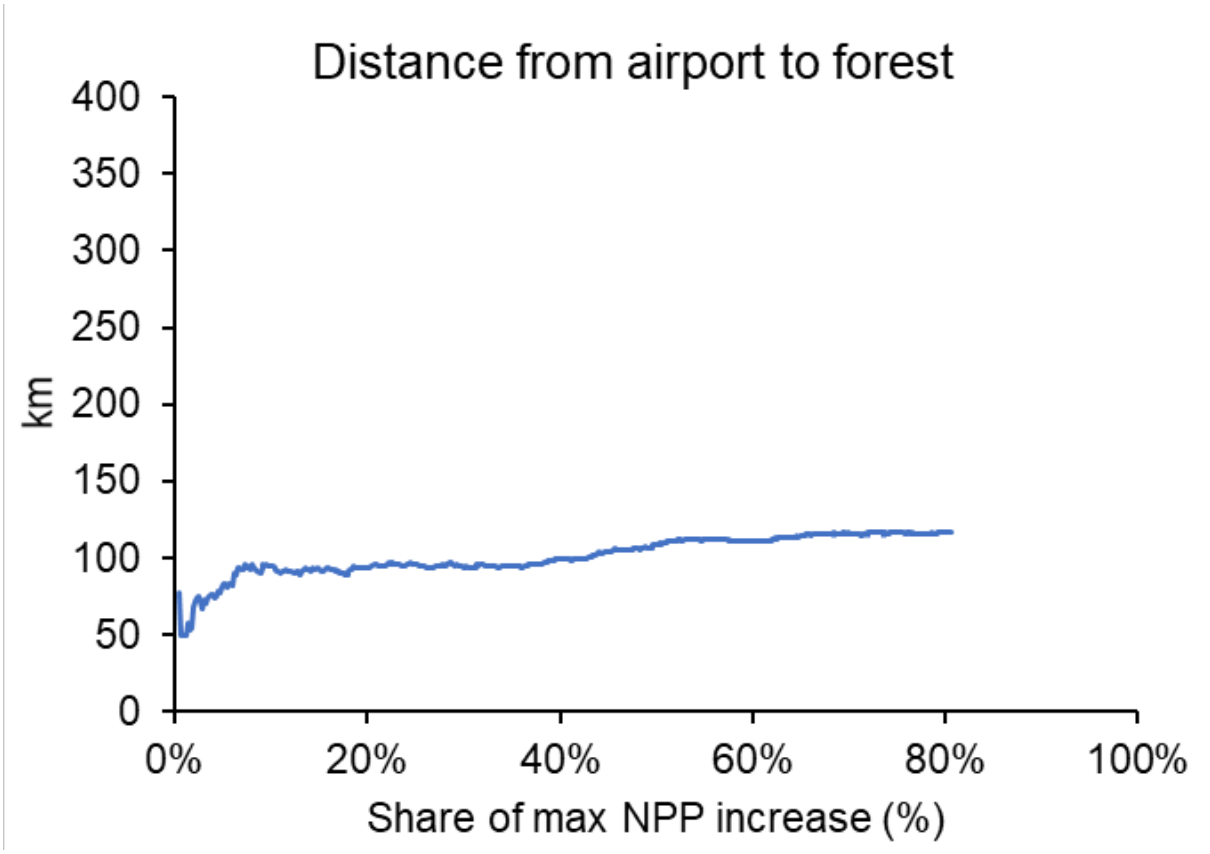

Figure III.27: Distance between application site and nearest airport. The x-axis is the cumulative contribution from the application sites, ranked from the most reactive to the least reactive to basalt amendment, to the total NPP increase. The y-axis is the mean distance corresponding to these cumulative contributions.

application, GET-ACC2 optimises the deployment of enhanced weathering without resorting to intermediate prices and benefits computations. The dual solution of the optimization offers a means to retrospectively determine the marginal energy, non-energy costs and the benefits of basalt application on both croplands and forests (figure III.28).

1.3.1 Costs The cost of basalt application can be broken down into two categories: non-energy cost and energy cost. The non-energy cost has a constant part and a variable part which depends on the quantity of basalt applied. The energy cost is determined by aggregating the quantity of all energy carriers used, each multiplied by their respective energy prices which vary depending on the scenario.

Non-energy costs *Production:* the production cost of basalt dust is $27 per ton.

Transportation: when applied on croplands, transportation costs rise as more distant fields are accessed for increased basalt application, reaching a maximum of $34 per ton. An additional

$11 per ton is incurred for spreading. Hence, non-energy costs escalate from $38 to $72 per ton applied as (endogenous) application rates increase. If basalt is applied in forests, transportation costs range from $25 to $37 per ton, depending on the proportion applied with tractors (10-30%) and the distance between the mine and airport (350-550 km).

Application: aerial spreading operation costs (excluding energy expenses) vary based on ground operation and maintenance costs, as well as the endogenous application rate (costs approach infinity as application rates decrease towards zero kg per m^2), ranging from $56 to $102 per ton for rapid discharges, depending on flight duration to the nearest airport. Pilot fees constitute approximately 60% of this cost. With an aircraft lifespan of 30 years and a 5% discount rate, the annual cost for spreading capacity priced at $170-210 per ton per year is $11-13.7 per ton, to which we add 5% of the purchase cost for housing and insurance costs, $8.5-10.5 per ton. Thus, non-energy costs for aerial spreading range between $84 and $123 per ton. Considering the proportion of basalt applied with tractors, direct forest spreading costs range from $55 to $104 per ton. Incorporating basalt extraction, grinding, and transport, the total non-energy cost per ton applied per aircraft in forests is $136-191. This cost escalates with increased (exogenous) aerial application share, (exogenous) average distance between airports and application sites, and (exogenous) ground operation and maintenance expenses. Including the 10-30% applied with tractors, the total range of non-energy cost of forest application is $114-179 per ton.

Energy costs *Production:* the energy cost for basalt dust production is minimal, primarily utilising electricity at an average rate of 0.2 GJ/ton (ranging from 0.07-0.6 GJ/t). In the GET-ACC2 model, electricity prices remain relatively stable over time in the business-as-usual scenario (around $14/GJ or $50/MWh). Prices increase in climate mitigation scenarios, particularly in the first half of the century but rarely surpass $28/GJ or $100/MWh, except in the 1.5°C case with medium overshoot, necessitating rapid decarbonization of the electric system. Thus, electricity costs typically range from $2.8 to $5.6 per ton, with uncertainty on basalt grinding electricity intensity leading to a range of $1-17 per ton.

Transport: the energy cost per ton-km for basalt transport varies from $0.02/t/km in the business-as-usual scenario (where no basalt is applied) to approximately $0.06-0.1/t/km in climate mitigation scenarios. This cost correlates positively with the carbon price and depends on the proportion of basalt transported by roads. Consequently, transporting basalt incurs an energy cost of up to $40 per ton for cropland application and $20-55 per ton for forest application.

Application: the energy consumption for airborne spreading ranges from 1.8-2.5 GJ/t, whereas for terrestrial spreading, it is 0.078 GJ/t. Since kerosene and diesel are priced equally in the model, the energy cost for airborne spreading is 23 to 32 times higher than that for terrestrial spreading. The cost of kerosene and diesel follows an affine function of the carbon price. When carbon prices exceed approximately \$300/tCO2, the cost of kerosene surpasses that of hydrogen (around \$40/GJ), leading to its substitution by hydrogen as aviation fuel, limiting further increases in aviation fuel prices. Consequently, aviation fuel prices range from \$8 to \$50 per GJ primarily depending on the carbon price, resulting in energy costs for basalt airborne spreading between \$15 and \$125 per ton. However, if carbon prices are very high in the near-term, technological diffusion constraints hinder the quick substitution of kerosene by hydrogen, and energy costs can exceed \$125 per ton. This is the case in low-overshoot cases if the climate sensitivity is high. The energy cost of terrestrial spreading remains below \$4 per ton. Overall, energy costs for cropland application range from \$5 to \$60 per ton. These costs primarily hinge on the quantity of basalt applied, endogenous carbon prices, and the exogenous energy intensity of basalt comminution. In contrast, energy costs for airborne forest application are significantly higher, spanning from \$36 to \$200 per ton, with a strong sensitivity to carbon prices. Since 10-30% share of basalt is applied with tractors, the mean energy costs of forest amendment with basalt dust range from \$32 to \$185 per ton.

Adding the energy and non-energy costs, the total costs of enhanced weathering on croplands range from \$43 to \$132 per ton, and the cost of the first ton applied ranges from \$43 to \$58. The total costs of enhanced weathering on forests range from \$146 to \$364 per ton, in line with a precedent assessment (162-325\$/t, see ref (Taylor et al., 2016)), and the share of energy costs within total costs is primarily driven by the carbon price (figure III.28), besides exogenous parameters variation.

1.3.2 Benefits The benefits per ton basalt application depend on future carbon prices:

$$R_N(t) = \Sigma_{k \geq t} P(k) \rho^{-k} \cdot \left[r_{CO_2} w_r \left(1 - w_r\right)^{(k-t)} + CDR_{bio}(k) \right]$$

Where $CDR_{bio}(k)$ is the marginal biotic capture at time k, P(k) is the price of carbon at time k, ρ is the discount factor, r_{CO2} is the geochemical removal rate (the mass of CO_2 removed per ton of rock applied) and w_r is the weathering rate. The quantity $(1 - w_r)^{(k-t)}$ is the unweathered proportion at time k of the initial basalt applied at time t. The revenue of basalt application increases with future carbon prices. On the other hand, the cost of basalt application also increases with the carbon price, which affects the energy cost of basalt application. Therefore, a

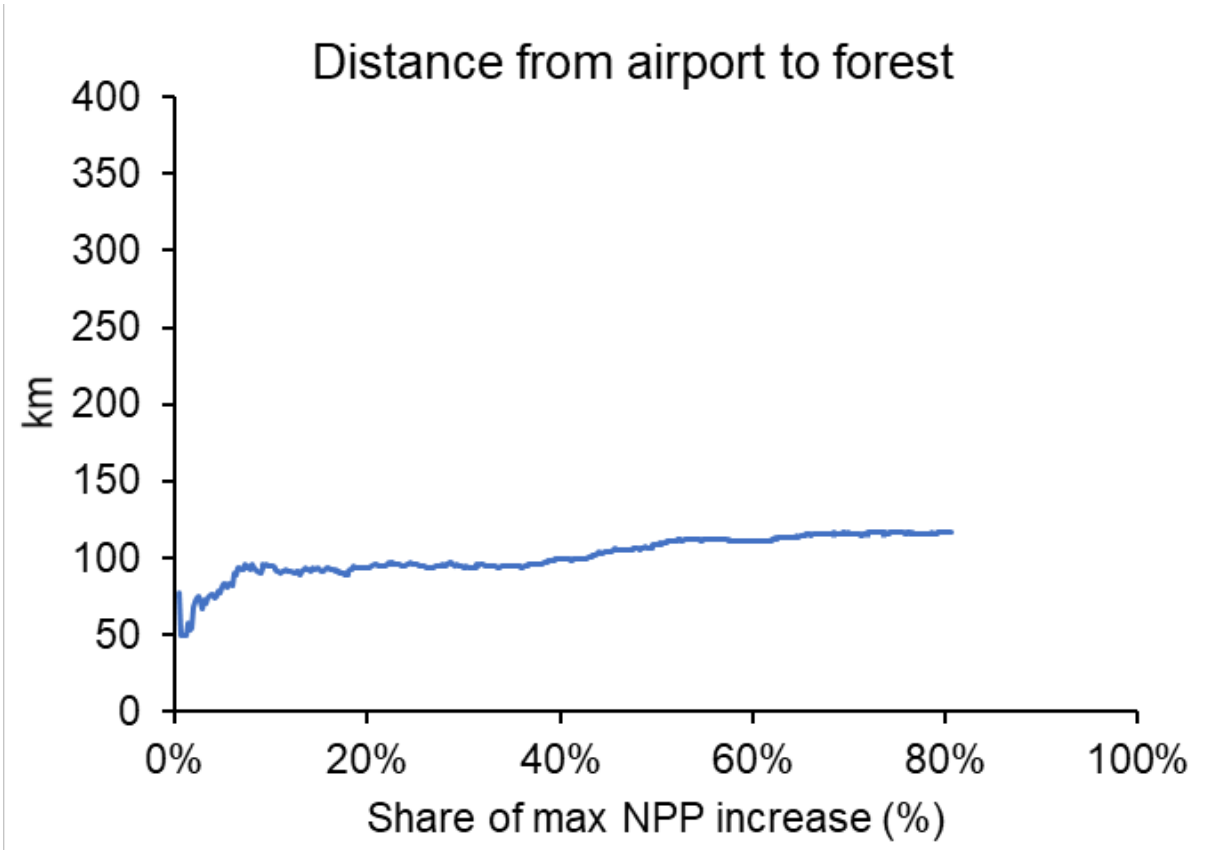

Figure III.28: Marginal revenues and costs of basalt application in the different climate policy scenarios. Line: median. Shaded areas: 5-95% (light) and 25-75% ranges (dark). The marginal revenue of basalt application is defined as the nominal benefit associated with the CDR resulting from the application of one ton of rock, if no financial or energy expenditure is required. The marginal cost of basalt application is the nominal cost of applying one ton of rock without any resulting CDR. The energy cost is the nominal price of the energy that would be used to apply one ton of basalt. **The dotted lines** represent the ratio of energy cost over total basalt application cost (**right y-axis**).

path of increasing carbon prices is more opportune to enhanced weathering deployment than stable or declining prices. This explains how the marginal revenue can exceed the product of the removal rate by the current carbon price, as well as the decrease of the marginal revenue of basalt application in 2100 (figure III.28).

1.3.3 Hotelling rule and beyond Due to its non linear behaviour and intrication with the carbon cycle, the term $CDR_{bio}(k)$ is hardly analytically tractable. Let us consider a case where there is no biotic effect ($CDR_{bio} = 0$) and the carbon price increases with the discount rate: $P(t) = \rho^t P_0$ (Hotelling rule), and we thus obtain the very simple expression: $R_N(t) = \rho^t \, P_0 \Sigma_{k \geq 0} r_{CO_2} w_r \, (1 - w_r)^k = P(t) r_{CO_2}$, that is to say, the benefit is the product of the CO_2 removed per ton of rock by the price of CO_2. Since the first ton of rocks applied on croplands costs between \$43 and \$58, and the removal rate is 0.24 to 0.37, the break-even CO_2 price ranges from \$116 to \$242 per ton CO_2. This is in the range of existing assessments of CO_2 removal costs: 80-180\$/tCO_2 in ref (Beerling et al., 2020), 200\$/tCO_2 in ref (Strefler et al., 2018).

The same analysis where basalt is applied on forests would yield break-even CO_2 prices between \$400 and \$1450 per ton CO_2 if the biotic effect is not included. Break-even CO_2 prices when the biotic effect is included are hard to derive analytically, as the CDR associated with basalt application depends on how much basalt is applied and on previous basalt application. However, one can use the mean removal rate in forests, which is obtained by dividing the total CDR due to enhanced weathering in forests by the cumulative mass of basalt applied over forests over the century. Since the removal rate decreases with increasing basalt application, the scenario where the lowest quantity of basalt is applied displays the highest removal rate. The mean removal rate ranges from 2.2 t_{CO2}/t_{rock} in the 1.5°C with high OS case to 7.2 t_{CO2}/t_{rock} in the 2°C case (figure III.29). This corresponds to average break-even CO_2 prices between \$20 and \$166 per tCO_2 depending on the scenario.

The break-even CO_2 price is higher if the carbon prices grows slower than the Hotelling rule, as it decreases the benefits of the future removals from current basalt application, and vice-versa. In high OS cases, the CO_2 prices increase faster than the discount rate until 2090, and decline afterwards. In medium or no-OS cases, the CO_2 prices stabilise when temperature stabilises.

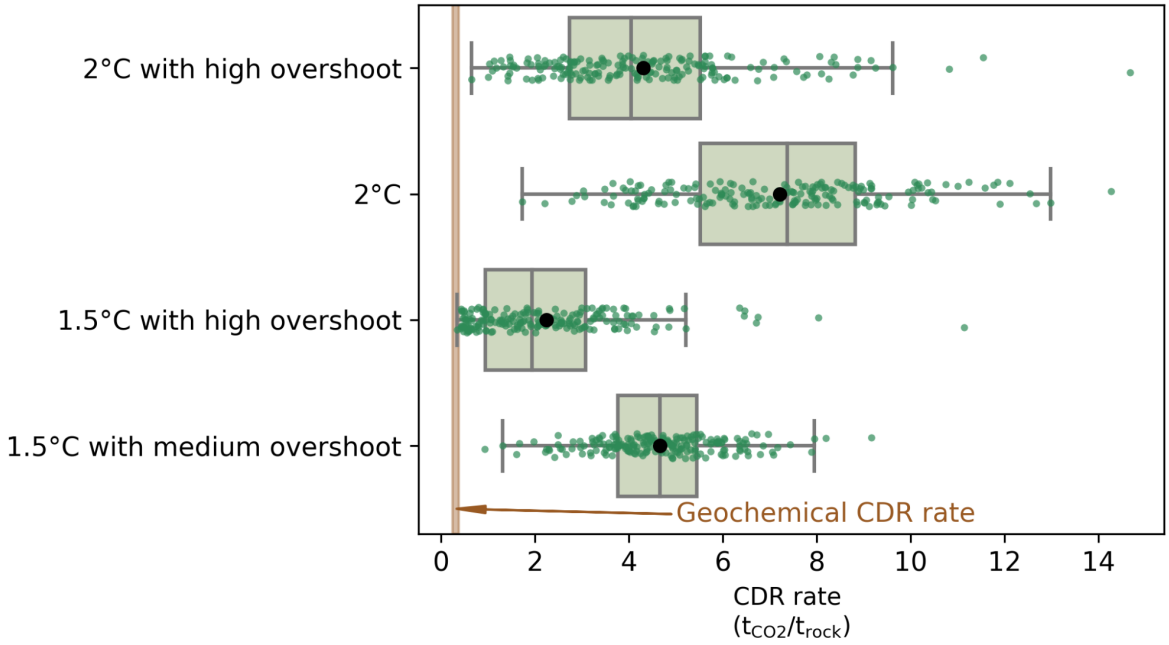

Figure III.29: Mean CDR rate over forests in the different climate policy scenarios.The boxes represent the 25-75% range, while the vertical bars and black dots inside the boxes represent the median and mean, respectively. The error bars indicate the 5-95% range. Each green dot represents a simulation of the parameters sample. The brown shaded area represents the range of geochemical CDR rate: 0.24-0.37 t_{CO2}/t_{rock}.

6.2 Sensitivity Analysis

6.2.1 Parameters distributions

The following table lists the uncertain parameters that are varied in the sensitivity analysis. As many of these parameters have the same kind of influence on the output (e.g. the costs of competing conventional mitigation technologies such as batteries, nuclear power plants & renewables have the same influence), we vary them simultaneously in order to reduce the number of required simulations while covering the full uncertainty space. Parameters are therefore gathered into 10 groups, and are varied together although not in the same direction. For instance, to increase the efficiency of mitigation technology, the costs of low-carbon technologies are decreased while their load factors and maximum penetration levels are increased. The sign of the variation of each parameter relative to the variation of the group is indicated in the table by a (+) or a (-). We have isolated the parameters directly related to enhanced weathering to track their effects independently.

Parameter	**Range**	**distribution**	**Justification**	**Group & variation**
Energy demand	multiplied by 0.75-1.25	Uniform	Source: SSP database. The standard deviation of the final energy use in 2100 (across SSP2 scenarios) is assumed to be 25% of its mean value.	Energy demand (+)
Electric share of PHEV use	0.2-0.69	Uniform	0.69 : NEDC, 20% real-world	Efficiency of mitigation technologies (+)
Maximum diffusion of technologies (e.g.: maximum share of cogeneration in urban heating systems).	constraints multiplied by 0.9-1.1	Uniform		Efficiency of mitigation technologies (+)

H2 vehicle costs	Incremental cost (compared to internal combustion engine vehicle): 3,000$/car, 25,020$ for bus and trucks, multiplied by 0.3-2.7	Uniform	Multiplier range from Cox, et al 2021 (Cox et al., 2020).	Efficiency of mitigation technologies (-)
EV costs (PHEV & BEV)	Incremental cost (compared to internal combustion engine vehicle): 7,200$/car, 62,200$ for bus and trucks, multiplied by 0.9-1.9	Uniform	Multiplier range from Cox, et al. (Cox et al., 2020)	Efficiency of mitigation technologies (-)
CCS costs	The extra cost of adding CCS to an energy conversion plant (1,340$/kW for gas to electricity, 1,920$/kW for coal to electricity and biomass to electricity, 1,050$/kW for biomass to H2, 1,580$ for biomass to MeOH) is multiplied by 0.8-1.2.	Uniform	The technology readiness level (TRL) is quite low: 6 to 7 (biomass), and 8 to 9 (coal & gas).	Efficiency of CCS (-)
Variable renewable energy costs	1,100$/kW (onshore wind), 895$/kW (solar), multiplied by 0.9-1.1	Uniform	TRL[1] is high : 9-10	Efficiency of mitigation technologies (-)
Nuclear costs	5,240$/kW, multiplied by 0.95-1.05	Uniform	TRL is high : 10 to 11	Efficiency of mitigation technologies (-)

[1]Source for all TRLs : IEA (2022), ETP Clean Energy Technology Guide, IEA, Paris https://www.iea.org/data-and-statistics/data-tools/etp-clean-energy-technology-guide

Biomass to H2 or Methanol costs	6,000$/kW and 3000$/kW for MeOH and H2 (without CCS), respectively, multiplied by 0.7-1.3	Uniform	Low TRL (5 to 6)	Efficiency of mitigation technologies (-)
Electrolysers costs	1,500$/kW (400$/kW in 2050) multiplied by 0.9-1.1	Uniform	TRL is quite high (9)	Efficiency of mitigation technologies (-)
Storage costs	2,500$/kW multiplied by 0.85-1.15	Uniform	TRL 8-9	Efficiency of mitigation technologies (-)
capacity factor of wind and solar	0.36 for wind, 0.16 solar. multiplied by 0.8-1.00	Uniform	Coupling of power system model with MESSAGE: slight overestimation of VRE capacity factor in IAMs (Brinkerink, et al. 2022)	Efficiency of mitigation technologies (+)
carbon storage cost	37 $/tC for fossil carbon, 73$/tC for bio carbon, multiplied by 0.85-1.15	Uniform	Base: GET7.0 parameters, range due to medium TRL (7-8).	Efficiency of CCS (-)
Bioenergy crops potential	160-260 EJ/year, that added to 50EJ of other bioenergy sources (residuals, waste) amount to the range 210-310 EJ/year presented in the text.	Uniform	Global Energy Assessment (Rogner et al., 2012), range from Li, et al (2021) (Li et al., 2021)	Bioenergy potential (+)
Max. capital growth	10-20%	Uniform	Base 15% per year (GET7.0 parameter).	Efficiency of mitigation technologies (+)

max CCS per year	10-20 GtCO2/year	Uniform	Range of maximal annual CCS from ENGAGE IAMs in the EN_NPI700 and EN_NPI1000 scenarios (AIM/CGE, MESSAGEix-GLOBIOM, REMIND-MAGPIE): the mean of IAMs maximum annual CCS is 15GtCO_2, the standard deviation of these maximums is 5GtCO_2.	Efficiency of CCS (+)
Max growth of fuel supply (transport)	15% per year, multiplied by 0.5-2	Uniform	Central value : GET7.0 parameter	Efficiency of mitigation technologies (+)
Max intermittent power share	Maximum penetration of wind and solar energy without storage =30%, multiplied by 0.8-1.25	Uniform	The power system representation is not very detailed in GET7.0 : we assume 30% of VRE penetration without storage or curtailment, and we test the sensitivity of our results to this parameter.	Efficiency of mitigation technologies (+)
Mean basalt transport distance	350-550 km	Uniform	see *supra 1.1*	Energy intensity of basalt application (+)
Minimum share of basalt road transport	70-90%	Uniform	Most application sites are in countries where alternative freight modes are not widely available.	Energy intensity of basalt application (+)

Weathering rate	1-26% per year	Uniform	low range: rinder et al. 2021. 3.55 10^{-12} mol/m2/s (corresponding to pH=5.84 T=25°C), SSA_{BET} =0.74 m2/g => 1% dissolved after 1 year for a grain size of 20µm. high range: ORCHIDEE calibration (based on ref (Strefler et al., 2018) for a grain size of 20µm)	Weathering rate (+)
CO2 abiotic capture per ton of rock	0.24 -0.37 tCO_2/t_{rock}	Uniform	T. Amann personal communication.	Geochemical capture rate (+)
Basalt Phosphorus content	0.036%-0.28%	Uniform	Goll et al 2021	Basalt Phosphorus content (+)
Share of basalt applied on natural areas with aircrafts	70-90%	Uniform	see *supra*	Energy intensity of basalt application (+)
Energy use of aircraft application	1.8-2.5 EJ/Gt	Uniform	see *supra*	Energy intensity of basalt application (+)
Electricity required for rock comminution	0.07-0.6EJ/Gt	quadratic (max= 0.2 EJ/Gt)	Streffler 2018 : for 20µm, 0.2 EJ/Gt is the central estimate, 0.07 low and 0.61 high: we take a quadratic distribution such that the median is 0.2, the max is 0.6 and the min 0.07.	Grinding energy (+)
Equilibrium climate sensitivity	lognormal distribution : sigma=0.22,µ=1.12	lognormal	Sherwood et al., 2020 Assessment of earth's climate sensitivity using multiple lines of evidence.	Climate sensitivity (+)

For several parameters, we base the cost uncertainty range on the "Technological Readiness Level" (TRL). The Technological Readiness Level (TRL) describes the maturity of a technology or innovation. It provides a scale to evaluate the progress of a technology from its conception to its deployment in real-world application (Mankins, 1995). Although TRL does

not explicitly address the cost uncertainty, it reflects the overall progress of a technology, which can influence the accuracy of future costs projections. An exhaustive assessment of cost uncertainty would consider the additional factors such as economies of scale, learning effects, supply chains, labour costs and regulatory requirements that may affect cost estimates.

Source for all TRLs : IEA (2022), ETP Clean Energy Technology Guide, IEA, Paris https://www.iea.org/data-and-statistics/data-tools/etp-clean-energy-technology-guide

6.2.2 Latin hypercube sampling

In the main text, the values are the means of the model simulations performed over a large sample of parameters values. We sample these parameters using a quasi random sampling method, the 'Latin hypercube sampling' method. The idea is as follows: the set of values accessible for each parameter is divided into N (=620) contiguous segments of equal probability. By taking the weighted mean of each segment, we obtain a set of N values $\{v_1{}^p, v^p{}_2, \ldots v^p{}_N\}$ for each parameter p. For each simulation, each parameter takes a single new value from this set, in a random order. This ensures that the k-dimensional space of parameters is properly covered.

The equilibrium climate sensitivity (ECS) is sampled over 20 values, in order to limit the computational burden: the climate model ACC2 must be re-calibrated (the process called inverse simulation in the model documentation (Tanaka et al., 2007)) each time we change the assumption on ECS because a different ECS value implies different optimal values of other parameters to best explain the historical observations given prior information on all parameters (Tanaka et al., 2009). We also run a set of simulations without considering the uncertainty in climate sensitivity: the mean net emission pathways tend to be slightly lower without ECS sampling than with ECS sampling. It is because the relationship between carbon budget for a given temperature target and ECS is not linear, but rather slightly convex.

6.2.3 Morris sampling

We apply the Morris screening method (Campolongo et al., 2007; King & Perera, 2013; Morris, 1991) to quantify the influence of each parameter on the outputs. Let $X = \{x_1, \ldots, x_k\}$ be a vector of parameters which are normalised to [0,1], $Y = f(X)$ the output. The idea is to assess the sensitivity of f to each parameter x_i by sampling its 'elementary effects' $EE_i = f(x_1, \ldots x_i + \Delta \ldots x_k) - f(x_1, \ldots x_k)$ over a sufficiently large set of values of all the x_j. Let us call

N the size of this set: the procedure must return a sample {EE_i^1,...,EE_i^N} for all i in [1,...,k]. In our case, we chose N=20. The means μ_i of the elementary effects, their standard deviation σ_i and the mean of their absolute values μ_i^* give useful information about the influence of these parameters. When the computation of f is time-consuming, the Morris sampling procedure can be used to limit the number of required computations for a given value of N. In the sampling procedure, a trajectory starts with a random vector of parameters. We successively increase the value of each parameter in a random order by Δ to create a set of k+1 vectors. For each parameter, we can calculate an elementary effect by subtracting the values that the function f takes between two successive points where the value of that parameter is increased. We then repeat the procedure N times in order to have N elementary effects per parameter.

More formally, a trajectory T is initiated by choosing an initial point X_0^T in $\left[0, \frac{1}{2N-1}, \frac{2}{2N-1}, ..., \frac{N-1}{2N-1}\right]^k$ (there are N possible initial values per parameter), and then iteratively increasing each parameter i by $\frac{N}{2N-1}$ in a random order $\{\sigma^T(i)\}_{i\in[1,p]}$ where σ^T is a permutation, to obtain T=$\{X_1^T, X_2^T \dots X_{k+1}^T\}$. Computing the output along this trajectory yields the elementary effects for each parameter *i:*

$d_i^T = f(X^T_{\sigma(i)+1})$- $f\left(X^T_{\sigma(i)}\right) = f(x_1,\dots x_i+\Delta\dots x_k) - f(x_1,\dots x_k)$. We produce *N=20* trajectories.

Initial points are sampled following a Latin Hypercube method, and trajectories are chosen to maximise their dispersion and thus their coverage of the parameters space on which elementary effects are computed, following ref. (Campolongo et al., 2007). However, we do not consider the same dispersion function. In ref. (Campolongo et al., 2007), The dispersion between two trajectories is the sum of the Euclidean distance of all their points taken pairwise:

$$d_{m,l}= \sum_{i}^{k+1}\sum_{j}^{k+1}\sqrt{\sum_{z}^{k}[X_i^m(z)-X_j^l(z)]^2}$$

where $X_j^l(z)$ is the value of parameter number z at step j of trajectory l. This dispersion measure is too computationally expensive for its purpose. We want, for each parameter *i,* to have a representative set {EE_i^1,...,EE_i^N} of its elementary effects. Therefore, it is necessary that for each *i*, the $\{X^t_{\sigma^t\ (i)}\}_{t\in[1,..,N]}$ are well spaced. We therefore propose the following dispersion measure:

$$d_{m,l}= \sum_{i}^{k+1}\sqrt{\sum_{z}^{k}[X_{\sigma^m(i)}^m(z)-X_{\sigma^l(i)}^l(z)]^2}$$

This dispersion measure has the advantage of being less computationally expensive. We want to maximise:

$$ \sum_{m,l} d_{m,l}$$

In our case, we have around k=30 input parameters, hence computing the distance between two trajectories requires around k^2 operations, and computing the dispersion requires $(kN)^2$ operations. If we are to pick the N best trajectories out of the $N^k k!$ existing trajectories, it would require to find the best combination of N trajectories among $N^k k!$, which means a total of $$\binom{N^{k}k!}{N} k^2 N^2 $$ operations (around 10^{768} for N=20 and k =30). This is not computationally feasible if we want to have N sufficiently high. We improve the sampling strategy by using a simulated annealing algorithm instead of a brute force approach, which greatly reduces the computational burden.

Simulated annealing:

initialization

Take N initial points of k parameters with LHS. We sample only over the inferior half-section of each dimension for symmetry reasons. It yields N initial points with coordinates in $$[0,\frac{1}{2(N-1)},...,\frac{N-1}{2(N-1)}]$$, and from each point we will start one trajectory by generating random permutations $\{\sigma^1,...,\sigma^N\}$. Each trajectory is built step by step by adding $$\Delta = \frac{N}{2N-1}$$ to each coordinate in the order $\{\sigma^1(1), \dots \sigma^1(k)\}$. We call $J_p{}^0=\{t^0{}_1 \dots t^0{}_N\}$ this first set of trajectories.

Distance table : compute, for each trajectory $t^0{}_i$ the distance $d^0{}_i = \Sigma d(t_i{}^0 , t_j{}^0)$ (we want to maximise $D = \Sigma d_i$)

T is the "temperature". λ is the cooling factor.

While n < Iterations limits:

step n

- T=λT
- Pick a random integer $i \in [1,...,N]$. Generate a new random permutation. Let us call $t^{\sim}{}_i$ the trajectory built from point i and this permutation. Replacing $t^{n-1}{}_i$ by $t^{\sim}{}_i$ would increase the dispersion by $\Theta = \Sigma d(t_i{}^{\sim} , t_j{}^{n-1}) - d^{n-1}{}_i$.
- If $\Theta \geq 0$
  - Replace $t_j{}^{n-1}$by $t_i{}^{\sim}$ and update the distance table.
- If Θ <0

- With probability $e^{-\frac{\Theta}{T}}$:
  - Replace ${t_j}^{n-1}$by $t_i{}^{\sim}$ and update the distance table.

End

Return the best set of trajectories from all those explored.

6.3 GET-ACC2 model

6.3.1 Overview of the model

The GET-ACC2 model is an integrated climate-energy-economic single-region model with global coverage. It is used for long-term energy system modelling and technology assessment. It describes how the energy system evolves and minimises its costs across the 21st century to meet the energy demand and respect specified constraints, such as a carbon budget or a climate target. GET-ACC2 is composed of two models: the energy system model GET and the reduced complexity climate model ACC2.

The Aggregated Carbon Cycle, Atmospheric Chemistry, and Climate (ACC2) model describes the physical part of the system. K. Tanaka developed the model in 2007. It computes the evolution of physical parameters, such as greenhouse gas concentrations in the atmosphere, the additional radiative forcing that it induces, and the surface mean temperature resulting from a pathway of anthropogenic emissions. The ACC2 model is clearly and comprehensively described in the documentation by Katsumasa Tanaka and Elmar Kriegler (Tanaka et al., 2007)' (Tanaka & O'Neill, 2018).

The global energy transition (GET) model is a simple linear energy system model that was initially developed at Chalmers University by Christian A. Azar and Kristian Lindgren (C. Azar & Lindgren, 2003; C. A. Azar et al., 2000). The current version, GET7.1, is derived from the one used by D.J.A. Johansson and C. Azar in Azar *et al* (2013) and (Johansson et al., 2020)). More information on GET7.0 can be found in ref (Hedenus et al., 2010).

The GET-ACC2 model computes cost-optimal scenarios to balance energy demand with energy supply. It takes as input a set of assumptions about future demand in several subsectors, technology costs and efficiency, and returns a combination of energetic and economic features of the cost-optimal energy mix, such as primary energy needs, marginal and total costs of

production and distribution, etc. The model has 4 kinds of input data: techno-economical parameters, that characterise the costs and efficiencies of the technologies included in the model, climate model parameters, assumptions on future energy demand, and climate policy constraints.

The energy demand comprises four sectors for stationary end-use: industrial process heat, electricity, feed-stock for chemical industry, residential and commercial heating, and eight transport demand subsectors: road (public & private transport), air and rail for passenger transport, and marine, air, rail and road for freight. These energy demand pathways are derived from ENGAGE SSP2 baseline scenarios (Bertram et al., 2021). The GET model computes, at each 10-year timestep, new productive capacity, new vehicles, distribution infrastructure etc. that have to be deployed to meet a given demand, as well as the fluxes of primary and secondary energy, the emission of greenhouse gases that stem from them, and costs incurred by the system. The reference year for dollar value is 2010.

3.1.1 Optimisation procedure The model is solved by a non-linear optimization solver, CONOPT4. There are two options to solve the model: the demand can be either fixed or price-responsive. The solver minimises the objective function: the net present value of future costs (investment costs, O&M costs, fuel costs, carbon tax, etc.), when the demand is fixed, or the net present value of annual surplus, when demand is price-responsive. The discount rate is assumed to be at 5% by default. The solver ensures that the climate constraints are respected - for instance, keeping global warming from pre-industrial level below 1.5°C in 2100. In this study, we use the price-responsive mode.

To allow the demand to decrease when prices grow, price-elasticities are -0.4 for electricity demand (Labandeira et al., 2017), domestic and commercial heating, -0.2 for industry (process heat and feed-stock), and -0.3 for transport demand (Dimitropoulos et al., 2018; Persson et al., 2007).

The model is solved twice:

- A first run with fixed demand and no climate policy ${Q_b}^s$ (b for "baseline", s for "sector") yields baseline end-use prices ${P_b}^s$ at each 10-year timestep, for each sector (the marginal costs of energy supply). Here, the net present value O_{fixed} of future energy system costs C(t) is minimised:

$O_{fixed} = \sum_t C(t)\rho^{-(t-t_0)}$ where $\rho = 1.05$

These prices are considered the reference prices for the demand pathway, and we deduce the reactive demand curve ${Q_r}^s$ (r for "reactive") from the ratio between reference prices and real prices.

$\frac{dlog(Q)}{dlog(P)} = \eta$ hence ${Q_r}^s = {Q_b}^s(\frac{{P_r}^s}{{P_b}^s})^\eta$ where η is the price-elasticity of demand.

- A second run (with elastic demand) computes the consumer surplus of each sector at each 10-year timestep, that is to say the area below the demand curve. The annual social surplus S(t) (figure III.30 and SIII.31) is the consumer surplus minus the production costs, i.e the area below the supply curve:

$$S(t) = \sum_{sectors} [(\frac{{Q_r}^s(t)}{{Q_b}^s(t)})^{\frac{1}{\eta_s}} \frac{{P_b}^s(t)}{\frac{1}{\eta_s}+1} {Q_r}^s(t)] - C(t)$$

The solver maximises the discounted sum $O_{reactive}$ of the annual social surplus between 2020 and 2150.

$O_{elast} = \sum_t S(t)\rho^{-(t-t_0)}$ where $\rho = 1.05$

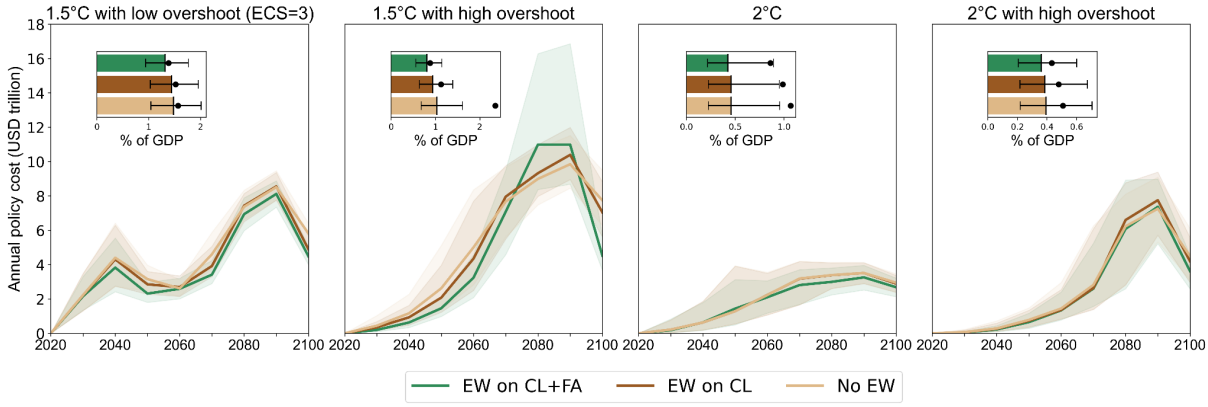

Figure III.30: Annual median mitigation costs in GET-ACC2 (discount rate = 5%). The dotted lines show the 25-75% range.

3.1.2 Model Validation The climate model ACC2 (Kvale et al., 2012; Melnikova et al., 2023; Tanaka & O'Neill, 2018; Tanaka et al., 2007, 2009, 2013, 2018, 2020) is calibrated on historical data (Tanaka et al., 2007), and its temperature response to greenhouse gas emissions has been validated against similar reduced-complexity climate models (Nicholls et al., 2020). The carbon sequestration following an increase in net primary production in ACC2 has been validated against CMIP6 models in the context of an increase in net primary production due to CO2 fertilisation (Melnikova et al., 2023), but not phosphorus fertilisation which is a process (to date) absent from all CMIP6 models.

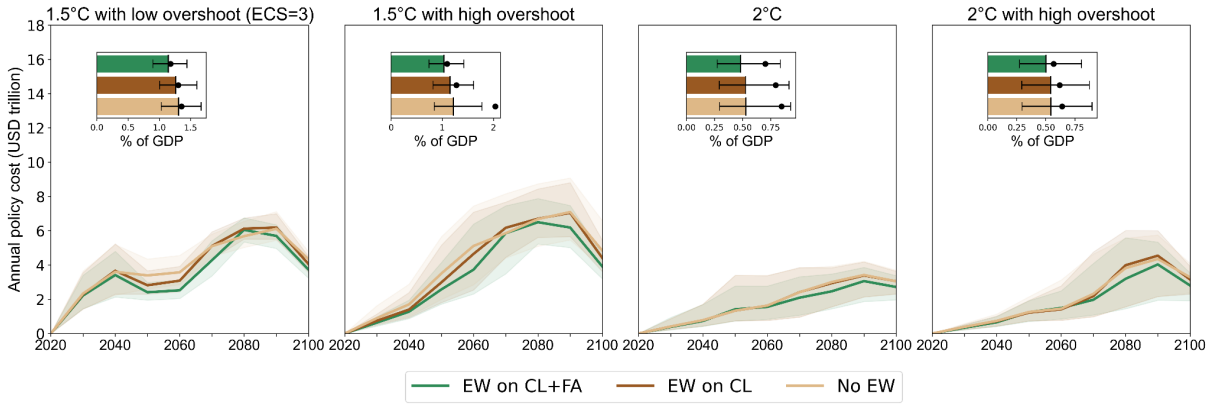

Figure III.31: Annual median mitigation costs in GET-ACC2 (discount rate = 2%). The dotted lines show the 25-75% range.

The land-surface model ORCHIDEE-CNP was well evaluated from site to global scale including nutrient leaching from terrestrial soils and the effects of elevated CO2 on primary productivity and land carbon storage (Friedlingstein et al., 2019; D. Goll et al., 2018; D. S. Goll et al., 2017; Sun et al., 2021). . Further, the response of aboveground productivity to mineral P fertiliser addition was compared with observation-based estimates (D. S. Goll et al., 2021). The emulator that reproduces the NPP response of ORCHIDEE-CNP to basalt addition, relying on a reduced set of assumptions for extrapolating the behaviour of the complex ORCHIDEE-CNP model, is necessarily a simplification of the original model but we checked that it reproduces faithfully the emerging response of the complex model.

The energy system model GET was developed for providing least-cost scenarios of energy transition (C. Azar & Lindgren, 2003; C. Azar et al., 2006, 2013; C. A. Azar et al., 2000; Hedenus et al., 2010; Johansson et al., 2020). The initial state of the energy system is calibrated on IEA data regarding energy flows and production capacities, and technology costs are taken from other energy system models. This kind of forward-looking model is hard to validate (Wilson et al., 2021) because it does not intend to make predictions about the future, but rather to provide quantitatively self-consistent energy scenarios, in an idealised world where a central planner with perfect foresight coordinates the energy transition to achieve climate targets at the lowest cost.

6.3.2 Major updates on GET

The model GET7.0 is described in ref (Hedenus et al., 2010). The model GET7.1, used in this study, was updated on several aspects: supply curves for fossil fuels and bioenergy, marginal abatement costs curves for non-CO_2 gases, the investment costs were updated to account for the rapid decline in wind turbine and solar PV costs as well as batteries.

3.2.1 Fossil fuel supply curves The version GET7.0 assumed a constant cost for fossil fuel extraction. The GET7.1 includes fossil fuels supply curves that represent how costs increase as resources are depleted. These supply curves are derived from the TIAM-UCL model (Welsby et al., 2021).

3.2.2 Biomass supply curve The version GET7.0 assumed a constant cost for bioenergy supply. The GET7.1 model does not model land use, but represents the increasing marginal costs of bioenergy supply. We use an idealised supply curve based on the one computed with the IMAGE3.0 (Daioglou et al., 2019) model (fig. 6 of ref (Daioglou et al., 2019)). We assume that the supply curve follows the equation : $P = P_{max}\ Q^4\ /{Q_{max}}^4 + b$, where b is the initial bioenergy price, P_{max} =15\$2005/GJ, and Q_{max} is the assumed maximum bioenergy supply potential (between 160 and 260 EJ/year). This simple supply curve generally underestimates the biomass supply cost compared to the original data, but it remains an improvement compared to the initial static cost parameterization.

There are two sources of carbon dioxide emissions in the biomass supply process. First, the machinery used for cultivation, management and harvesting of the bioenergy crops can be powered by fossil fuels. In the GET model, the exogenous energy demand pathways are assumed to take account of the use of energy to produce energy (e.g., for the extraction of materials used to produce renewable energy), thus switching from coal to biomass does not increase the energy demand. The low density of the biomass and the additional transport requirements are accounted for through a financial cost but not an energy one. Second, the extension of cultivated lands to increase the biomass supply could affect the vegetation and soil carbon stocks, possibly increasing land-use change emissions (Daioglou et al., 2017; Hanssen et al., 2020). However, the variation in soil carbon stock can be positive or negative depending on the type of land and the type of crops (J. Wang et al., 2023). As a consequence, the governance and regulation of the land-use sector is critical to limit land use change emissions associated with bioenergy production, notably induced direct and indirect land use change (Merfort et al., 2023). Here, consistently with the perfect information, perfect foresight, optimising paradigm of the model, we assume that bioenergy crop areas are chosen wisely in order to minimise land-use change emissions. This corresponds to an emission factor of 5 $kgCO_2$ per GJ of primary energy (12 $kgCO_2$ per GJ of biofuels converted with 41% efficiency from primary energy (Merfort et al., 2023)). Other land use emissions are exogenous.

3.2.3 Methane and Nitrous oxide abatement New abatement cost curves to reduce methane and nitrous oxide emissions are implemented.There are 4 source-dependent abatement cost

curves for methane (for coal, oil, natural gas and non-energy emissions), and one for N_2O.

CH_4 emissions from the energy sector are the product of the quantities of natural gas, oil and coal by the corresponding emission factors (0.275, 0.22, and 0.284 $MtCH_4$ per EJ of gas, oil and coal respectively). These three emission factors can be reduced at the expense of additional costs that are derived from marginal abatement costs curves (Harmsen et al., 2019). Additionally, non-energy methane emissions follow an exogenous baseline based on SSP2. Non-energy methane emissions can also be reduced at the expense of an additional abatement cost (Harmsen et al., 2019).

Bioenergy supply is associated with N_2O emissions (0.01 MtN per EJ). Bioenergy and non-energy (exogenous) N_2O emissions can also be reduced similarly to CH_4 mitigation.

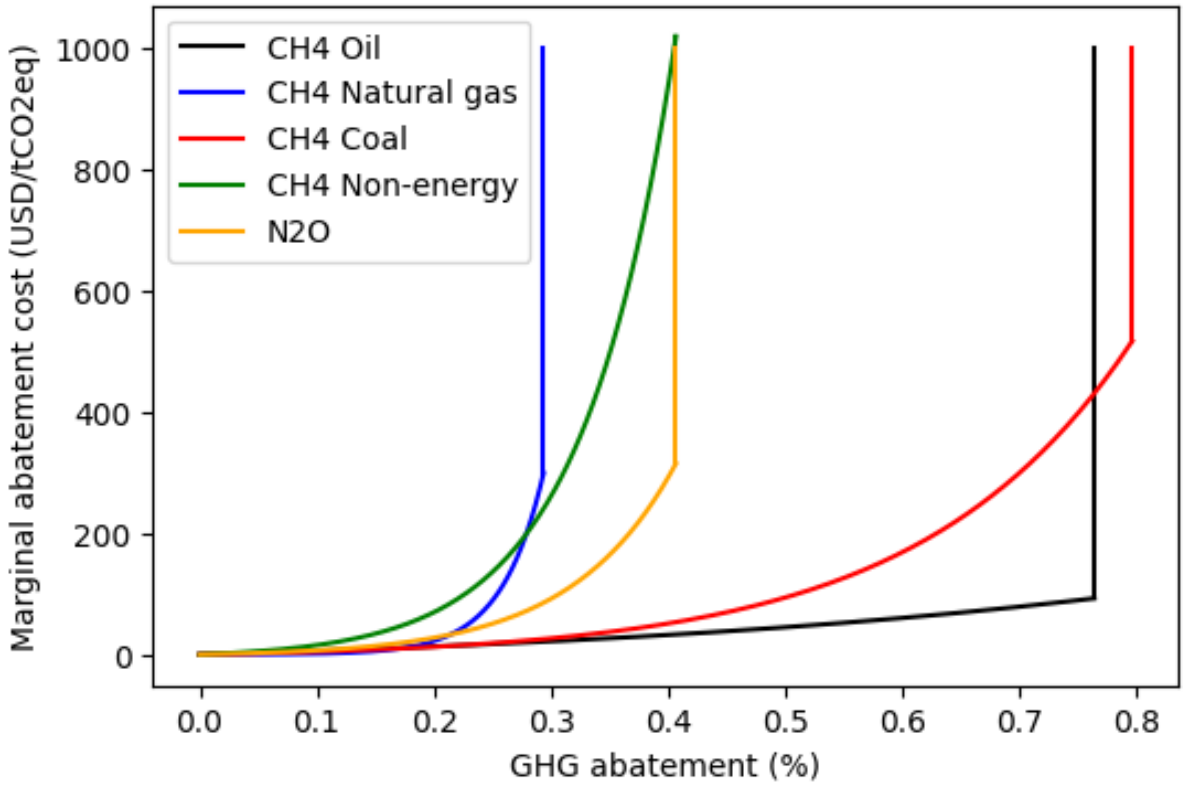

Figure III.32: Marginal abatement cost curves for CH_4, and N_2O

3.2.4 Parameters updates As solar panels, wind turbines and batteries costs have declined, the capital costs in GET7.1 are different from those in GET7.0. Electricity generation costs are based on the data from EIA, NREL, IRENA ("Cost and Performance Characteristics of New Generating Technologies, Annual Energy Outlook 2022", n.d.; IRENA, 2021; NREL, 2021), while H2 and MeOH generation costs are based on the REMIND model (Luderer et al., 2022).

The electric vehicles and plug-in hybrid electric vehicles are also cheaper, as we assume a battery cost of 100$/kWh.

The total CO2 storage reserves were extended to 3000 $GtCO_2$. A maximum annual injection rate of 0.5% of storage reserves was added, following ref. (Strefler et al., 2021) This leads to a maximum annual CO_2 storage of $15GtCO_2$ per year, consistent with annual sequestration rates in the ENGAGE database (Riahi et al., 2021) Furthermore, the extension of annual CCS flows is limited to 150 MtC/year, i.e. 5.5 $GtCO_2$ per decade.

3.2.4 Renewable energy mix The onshore wind power potential is 80EJ/year (Lehtveer et al., 2017). There is no detailed description of wind and solar production in GET, nor of issues related to VRE penetration in power production such as curtailment. The maximum share of variable renewable energy that does not have to be stored is limited to 30%, and the rest can be freely integrated as long as batteries (or cheaper storage with limited potential, such as dams) are purchased. We imposed that the shares of variable renewable energy provided by wind or solar energy cannot exceed given thresholds. Otherwise, since wind power is cheaper than solar, it completely replaces it.

6.3.3 Comparison of mitigation scenarios and baseline

When no climate target nor carbon tax constrains the model, energy supply relies heavily on coal, although the shares of wind, solar and nuclear power also increase (figure S3.3.1). The CO_2 emissions rise steadily across the 21^{st} century and peak around 2100 (figure S3.3.2).

6.3.4 Inverse parameterisation of the climate model ACC2

The spread of uncertainty relating to the climate system is assessed by sampling the equilibrium climate sensitivity (Sherwood et al., 2020) (ECS). In ACC2, several parameters are jointly calibrated on historical values using the inverse mode (Tanaka et al., 2007). Here the value of the ECS is exogenously set, and other parameters are calibrated consistently to this ECS value. The most influential parameters are Q10, by which the rate of terrestrial heterotrophic respiration increases with a temperature increase of 10°C, the factor β, which logarithmically scales the CO_2 fertilisation effect on net primary production with the fractional change of atmospheric CO_2 concentration, and the aerosol forcing. The figure III.35 shows how these parameters vary with the ECS.

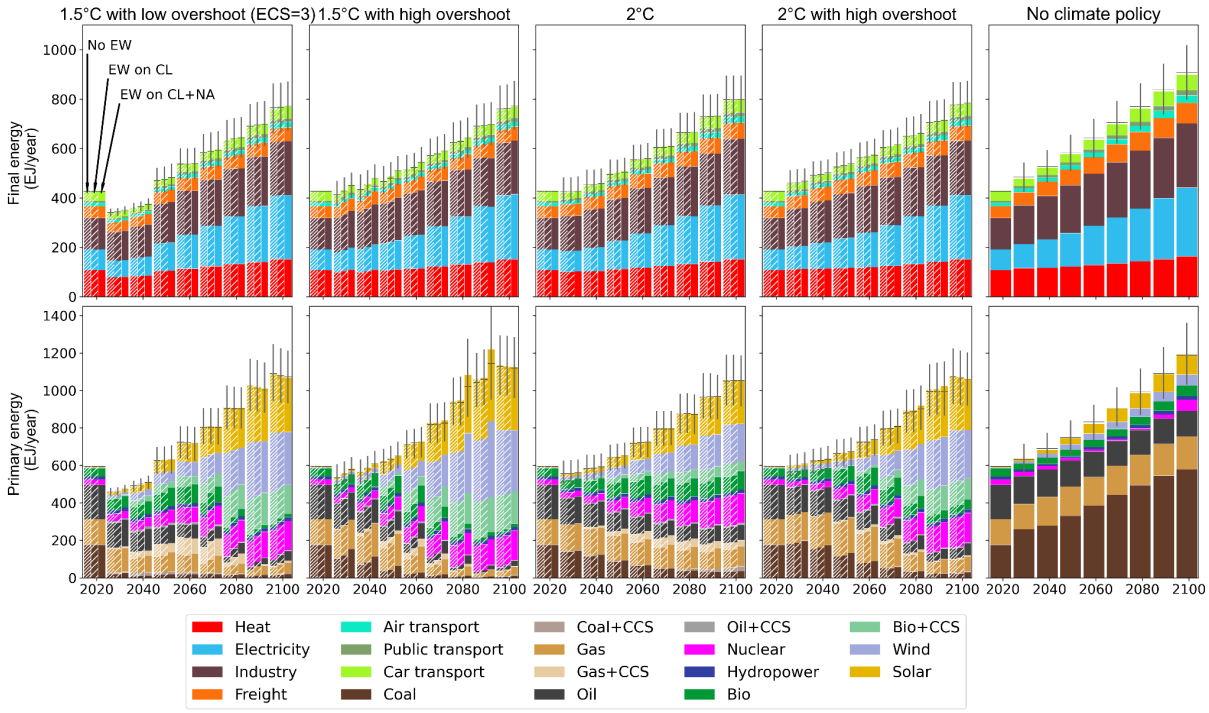

Figure III.33: Energy flows in GET-ACC2. The hatched bars follow the same pattern as in the main text, except for the right panel where no EW is applied. The error bars represent the 25-75% range.

References

Amann, T., Hartmann, J., Struyf, E., de Oliveira Garcia, W., Fischer, E. K., Janssens, I., Meire, P., & Schoelynck, J. (2020). Enhanced Weathering and related element fluxes – a cropland mesocosm approach. *Biogeosciences*, *17*(1), 103–119. https://doi.org/10.5194/bg-17-103-2020

Atima, D., & Suthirat, K. (2016). Estimated Greenhouse Gases Emissions from Mobile and Stationary Sources in the Limestone and Basalt Rock Mining in Thailand. *American Journal of Environmental Sciences*, *12*(5). https://doi.org/10.3844/ajessp.2016.334.340

Azar, C., Johansson, D. J. A., & Mattsson, N. (2013). Meeting global temperature targets—the role of bioenergy with carbon capture and storage. *Environmental Research Letters*, *8*(3), 034004. https://doi.org/10.1088/1748-9326/8/3/034004

Azar, C., & Lindgren, K. (2003). Global energy scenarios meeting stringent CO2 constraints— cost-effective fuel choices in the transportation sector. *Energy Policy*, 16.

Azar, C., Lindgren, K., Larson, E., & Möllersten, K. (2006). Carbon Capture and Storage From Fossil Fuels and Biomass – Costs and Potential Role in Stabilizing the Atmosphere. *Climatic Change*, *74*(1-3), 47–79. https://doi.org/10.1007/s10584-005-3484-7

Azar, C. A., Lindgren, K., & Andersson, B. (2000). Hydrogen Or Methanol in the Transportation Sector?

Beerling, D. J., Epihov, D. Z., Kantola, I. B., Masters, M. D., Reershemius, T., Planavsky, N. J., Reinhard, C. T., Jordan, J. S., Thorne, S. J., Weber, J., Val Martin, M., Freckleton, R. P., Hartley, S. E., James, R. H., Pearce, C. R., DeLucia, E. H., & Banwart, S. A. (2024). Enhanced weathering in the US Corn Belt delivers carbon removal with agronomic benefits. *Proceedings of the National Academy of Sciences*, *121*(9), e2319436121. https://doi.org/10.1073/pnas.2319436121

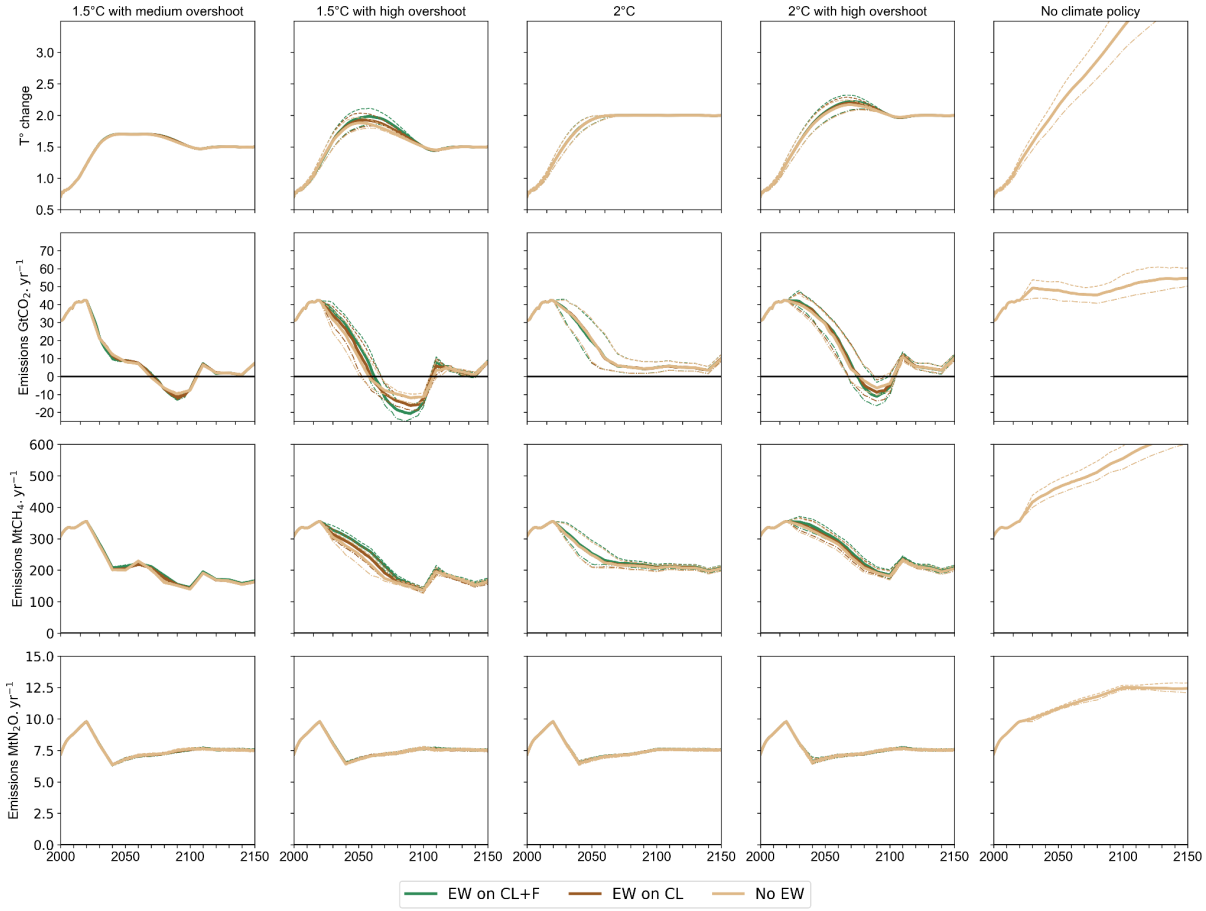

Figure III.34: GHG Emissions and Temperature change in GET-ACC2. The dotted lines show the 25-75% range. When the temperature returns to its target after overshoot, the climate inertia leaves a little space for emissions to bounce back, while keeping the temperature below target. As the calculation is made up to 2150, emissions increase slightly in 2150 because they do not have enough time to affect the climate system: it is a side-effect due to the assumed time horizon.

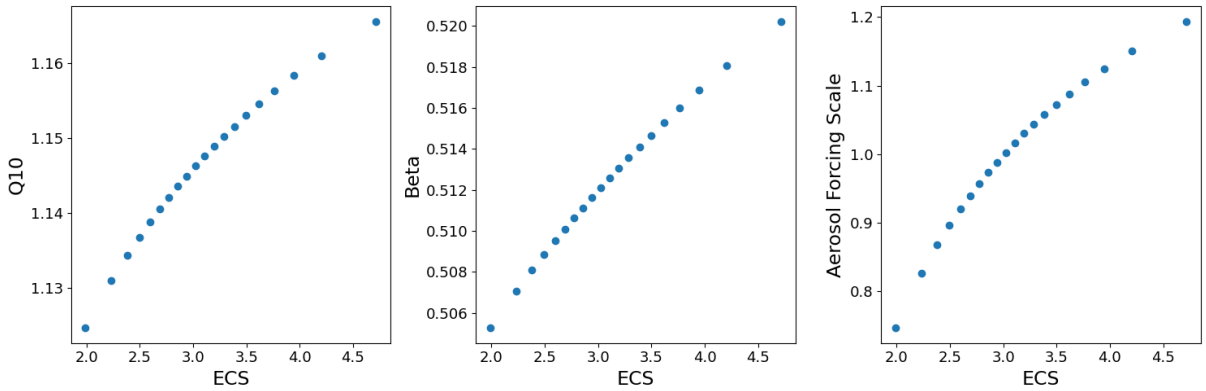

Figure III.35: Correlations between climate parameters Q10, Beta and the Aerosol forcing, as estimated from ACC2 inverse mode.

Beerling, D. J., Kantzas, E. P., Lomas, M. R., Wade, P., Eufrasio, R. M., Renforth, P., Sarkar, B., Andrews, M. G., James, R. H., Pearce, C. R., Mercure, J.-F., Pollitt, H., Holden, P. B., Edwards, N. R., Khanna, M., Koh, L., Quegan, S., Pidgeon, N. F., Janssens, I. A., … Banwart, S. A. (2020). Potential for large-scale CO2 removal via enhanced rock weathering with croplands. *Nature*, *583*(7815), 242–248. https://doi.org/10.1038/s41586-020-2448-9

Berge, H. F. M. ten, Meer, H. G. van der, Steenhuizen, J. W., Goedhart, P. W., Knops, P., & Verhagen, J. (2012). Olivine Weathering in Soil, and Its Effects on Growth and Nutrient Uptake in Ryegrass (Lolium perenne L.): A Pot Experiment. *PLOS ONE*, *7*(8), e42098. https://doi.org/10.1371/journal.pone.0042098

Bertram, C., Riahi, K., Hilaire, J., Bosetti, V., Drouet, L., Fricko, O., Malik, A., Nogueira, L. P., van der Zwaan, B., van Ruijven, B., van Vuuren, D., Weitzel, M., Longa, F. D., de Boer, H.-S., Emmerling, J., Fosse, F., Fragkiadakis, K., Harmsen, M., Keramidas, K., … Luderer, G. (2021). Energy system developments and investments in the decisive decade for the Paris Agreement goals. *Environmental Research Letters*, *16*(7), 074020. https://doi.org/10.1088/1748-9326/ac09ae

Bošeľa, M., & Šebeň, V. (2018). Analysis of the aerial application of fertilizer and dolomitic limestone. *Journal of Forest Science*, *56*, 47–57. https://doi.org/10.17221/29/2009-JFS

Buckingham, F. L., Henderson, G. M., Holdship, P., & Renforth, P. (2022). Soil core study indicates limited CO2 removal by enhanced weathering in dry croplands in the UK. *Applied Geochemistry*, *147*, 105482. https://doi.org/10.1016/j.apgeochem.2022.105482

Buckingham, F. L., Henderson, G. M., & Renforth, P. (2023). Response to Comment from West et al. on, "Soil core study indicates limited CO2 removal by enhanced weathering in dry croplands in the UK". *Applied Geochemistry*, *152*, 105622. https://doi.org/10.1016/j.apgeochem.2023.105622

Campolongo, F., Cariboni, J., & Saltelli, A. (2007). An effective screening design for sensitivity analysis of large models. *Environmental Modelling & Software*, *22*(10), 1509–1518. https://doi.org/10.1016/j.envsoft.2006.10.004

Clair, T. A., & Hindar, A. (2005). Liming for the mitigation of acid rain effects in freshwaters: A review of recent results. *Environmental Reviews*, *13*(3), 91–128. https://doi.org/10.1139/a05-009

Cost and Performance Characteristics of New Generating Technologies, Annual Energy Outlook 2022. (n.d.). 4.

Cox, B., Bauer, C., Mendoza Beltran, A., van Vuuren, D. P., & Mutel, C. L. (2020). Life cycle environmental and cost comparison of current and future passenger cars under different energy scenarios. *Applied Energy*, *269*, 115021. https://doi.org/10.1016/j.apenergy.2020.115021

Daioglou, V., Doelman, J. C., Stehfest, E., Müller, C., Wicke, B., Faaij, A., & van Vuuren, D. P. (2017). Greenhouse gas emission curves for advanced biofuel supply chains. *Nature Climate Change*, *7*(12), 920–924. https://doi.org/10.1038/s41558-017-0006-8

Daioglou, V., Doelman, J. C., Wicke, B., Faaij, A., & van Vuuren, D. P. (2019). Integrated assessment of biomass supply and demand in climate change mitigation scenarios. *Global Environmental Change*, *54*, 88–101. https://doi.org/10.1016/j.gloenvcha.2018.11.012

Dietzen, C., Harrison, R., & Michelsen-Correa, S. (2018). Effectiveness of enhanced mineral weathering as a carbon sequestration tool and alternative to agricultural lime: An incubation experiment. *International Journal of Greenhouse Gas Control*, *74*, 251–258. https://doi.org/10.1016/j.ijggc.2018.05.007

Dimitropoulos, A., Oueslati, W., & Sintek, C. (2018). The rebound effect in road transport: A meta-analysis of empirical studies. *Energy Economics*, *75*, 163–179. https://doi.org/10.1016/j.eneco.2018.07.021

Friedlingstein, P., Jones, M. W., O'Sullivan, M., Andrew, R. M., Hauck, J., Peters, G. P., Peters, W., Pongratz, J., Sitch, S., Le Quéré, C., Bakker, D. C. E., Canadell, J. G., Ciais, P., Jackson, R. B., Anthoni, P., Barbero, L., Bastos, A., Bastrikov, V., Becker, M., … Zaehle, S. (2019). Global Carbon Budget 2019. *Earth System Science Data*, *11*(4), 1783–1838. https://doi.org/10.5194/essd-11-1783-2019

Goll, D., Joetzjer, E., Huang, M., & Ciais, P. (2018). Low Phosphorus Availability Decreases Susceptibility of Tropical Primary Productivity to Droughts. *Geophysical Research Letters*, *45*(16), 8231–8240. https://doi.org/10.1029/2018GL077736

Goll, D. S., Ciais, P., Amann, T., Buermann, W., Chang, J., Eker, S., Hartmann, J., Janssens, I., Li, W., Obersteiner, M., Penuelas, J., Tanaka, K., & Vicca, S. (2021). Potential CO2 removal from enhanced weathering by ecosystem responses to powdered rock. *Nature Geoscience*, *14*(8), 545–549. https://doi.org/10.1038/s41561-021-00798-x

Goll, D. S., Vuichard, N., Maignan, F., Jornet-Puig, A., Sardans, J., Violette, A., Peng, S., Sun, Y., Kvakic, M., Guimberteau, M., Guenet, B., Zaehle, S., Penuelas, J., Janssens, I., & Ciais, P. (2017). A representation of the phosphorus cycle for ORCHIDEE (revision 4520). *Geoscientific Model Development*, *10*(10), 3745–3770. https://doi.org/10.5194/gmd-10-3745-2017

Hanssen, S. V., Daioglou, V., Steinmann, Z. J. N., Doelman, J. C., Van Vuuren, D. P., & Huijbregts, M. A. J. (2020). The climate change mitigation potential of bioenergy with carbon capture and storage. *Nature Climate Change*, *10*(11), 1023–1029. https://doi.org/10.1038/s41558-020-0885-y

Haque, F., Santos, R. M., & Chiang, Y. W. (2020). CO2 sequestration by wollastonite-amended agricultural soils – An Ontario field study. *International Journal of Greenhouse Gas Control*, *97*, 103017. https://doi.org/10.1016/j.ijggc.2020.103017

Harmsen, M. J. H. M., van Vuuren, D. P., Nayak, D. R., Hof, A. F., Höglund-Isaksson, L., Lucas, P. L., Nielsen, J. B., Smith, P., & Stehfest, E. (2019). Data for long-term marginal abatement cost curves of non-CO2 greenhouse gases. *Data in Brief*, *25*, 104334. https://doi.org/10.1016/j.dib.2019.104334

Hartmann, J., & Moosdorf, N. (2012). The new global lithological map database GLiM: A representation of rock properties at the Earth surface. *Geochemistry, Geophysics, Geosystems*, *13*(12). https://doi.org/10.1029/2012GC004370

Hedenus, F., Karlsson, S., Azar, C., & Sprei, F. (2010). Cost-effective energy carriers for transport – The role of the energy supply system in a carbon-constrained world. *International Journal of Hydrogen Energy*, *35*(10), 4638–4651. https://doi.org/10.1016/j.ijhydene.2010.02.064

Ibisch, P. L., Hoffmann, M. T., Kreft, S., Pe'er, G., Kati, V., Biber-Freudenberger, L., DellaSala, D. A., Vale, M. M., Hobson, P. R., & Selva, N. (2016). A global map of roadless areas and their conservation status. *Science*, *354*(6318), 1423–1427. https://doi.org/10.1126/science.aaf7166

IRENA. (2021). *Renewable Power Generation Costs in 2020, International Renewable Energy Agency, Abu Dhabi.*

Johansson, D. J. A., Azar, C., Lehtveer, M., & Peters, G. P. (2020). The role of negative carbon emissions in reaching the Paris climate targets: The impact of target formulation in integrated assessment models. *Environmental Research Letters*, *15*(12), 124024. https://doi.org/10.1088/1748-9326/abc3f0

Kelland, M. E., Wade, P. W., Lewis, A. L., Taylor, L. L., Sarkar, B., Andrews, M. G., Lomas, M. R., Cotton, T. E. A., Kemp, S. J., James, R. H., Pearce, C. R., Hartley, S. E., Hodson, M. E., Leake, J. R., Banwart, S. A., & Beerling, D. J. (2020). Increased yield and CO $_2$ sequestration potential with the C $_4$ cereal *Sorghum bicolor* cultivated in basaltic rock dust-amended agricultural soil. *Global Change Biology*, *26*(6), 3658–3676. https://doi.org/10.1111/gcb.15089

King, D. M., & Perera, B. J. C. (2013). Morris method of sensitivity analysis applied to assess the importance of input variables on urban water supply yield – A case study. *Journal of Hydrology*, *477*, 17–32. https://doi.org/10.1016/j.jhydrol.2012.10.017

Kvale, K., Zickfeld, K., Bruckner, T., Meissner, K. J., Tanaka, K., & Weaver, A. J. (2012). Carbon Dioxide Emission Pathways Avoiding Dangerous Ocean Impacts. *Weather, Climate, and Society*, *4*(3), 212–229. https://doi.org/10.1175/WCAS-D-11-00030.1

Labandeira, X., Labeaga, J. M., & López-Otero, X. (2017). A meta-analysis on the price elasticity of energy demand. *Energy Policy*, *102*, 549–568. https://doi.org/10.1016/j.enpol.2017.01.002

Larkin, C. S., Andrews, M. G., Pearce, C. R., Yeong, K. L., Beerling, D. J., Bellamy, J., Benedick, S., Freckleton, R. P., Goring-Harford, H., Sadekar, S., & James, R. H. (2022). Quantification of CO2 removal in a large-scale enhanced weathering field trial on an oil palm plantation in Sabah, Malaysia. *Frontiers in Climate*, *4*, 959229. https://doi.org/10.3389/fclim.2022.959229

Lehtveer, M., Mattsson, N., & Hedenus, F. (2017). Using resource based slicing to capture the intermittency of variable renewables in energy system models. *Energy Strategy Reviews*, *18*, 73–84. https://doi.org/10.1016/j.esr.2017.09.008

Lewis, A. L., Sarkar, B., Wade, P., Kemp, S. J., Hodson, M. E., Taylor, L. L., Yeong, K. L., Davies, K., Nelson, P. N., Bird, M. I., Kantola, I. B., Masters, M. D., DeLucia, E., Leake, J. R., Banwart, S. A., & Beerling, D. J. (2021). Effects of mineralogy, chemistry and physical properties of basalts on carbon capture potential and plant-nutrient element release via enhanced weathering. *Applied Geochemistry*, *132*, 105023. https://doi.org/10.1016/j.apgeochem.2021.105023

Li, W., Ciais, P., Han, M., Zhao, Q., Chang, J., Goll, D. S., Zhu, L., & Wang, J. (2021). Bioenergy Crops for Low Warming Targets Require Half of the Present Agricultural Fertilizer Use. *Environmental Science & Technology*, *55*(15), 10654–10661. https://doi.org/10.1021/acs.est.1c02238

Luderer, G., Madeddu, S., Merfort, L., Ueckerdt, F., Pehl, M., Pietzcker, R., Rottoli, M., Schreyer, F., Bauer, N., Baumstark, L., Bertram, C., Dirnaichner, A., Humpenöder, F., Levesque, A., Popp, A., Rodrigues, R., Strefler, J., & Kriegler, E. (2022). Impact of declining renewable energy costs on electrification in low-emission scenarios. *Nature Energy*, *7*(1), 32–42. https://doi.org/10.1038/s41560-021-00937-z

M. C. E. Grafton, I. J. Yule, C. E. Davies, R. B. Stewart, & J. R. Jones. (2011). Resolving the Agricultural Crushed Limestone Flow Problem from Fixed-Wing Aircraft. *Transactions of the ASABE*, *54*(3), 769–775. https://doi.org/10.13031/2013.37092

Mankins, J. (1995). Technology Readiness Level – A White Paper.

Melnikova, I., Ciais, P., Boucher, O., & Tanaka, K. (2023). Assessing carbon cycle projections from complex and simple models under SSP scenarios. *Climatic Change*, *176*(12), 168. https://doi.org/10.1007/s10584-023-03639-5

Merfort, L., Bauer, N., Humpenöder, F., Klein, D., Strefler, J., Popp, A., Luderer, G., & Kriegler, E. (2023). Bioenergy-induced land-use-change emissions with sectorally fragmented policies. *Nature Climate Change*. https://doi.org/10.1038/s41558-023-01697-2

Moraes, T. R., Cornago Junior, V. M., Araújo, V. C. R. de, Esperancini, M. S. T., & Antuniassi, U. R. (2021). COST OF AERIAL AND GROUND SPRAYINGS AND TECHNOLOGICAL REPLACEMENT POINT: A CASE STUDY IN THE REGION OF MINEIROS, GO, BRAZIL. *Engenharia Agrícola*, *41*, 359–367. https://doi.org/10.1590/1809-4430-Eng.Agric.v41n3p359-367/2021

Morris, M. D. (1991). Factorial Sampling Plans for Preliminary Computational Experiments. *Technometrics*, *33*(2), 161–174. https://doi.org/10.2307/1269043

Nicholls, Z. R. J., Meinshausen, M., Lewis, J., Gieseke, R., Dommenget, D., Dorheim, K., Fan, C.-S., Fuglestvedt, J. S., Gasser, T., Golüke, U., Goodwin, P., Hartin, C., Hope, A. P., Kriegler, E., Leach, N. J., Marchegiani, D., McBride, L. A., Quilcaille, Y., Rogelj, J., … Xie, Z. (2020). Reduced Complexity Model Intercomparison Project Phase 1: Introduction and evaluation of global-mean

temperature response. *Geoscientific Model Development*, *13*(11), 5175–5190. https://doi.org/10.5194/gmd-13-5175-2020

NREL. (2021). *"2021 Annual Technology Baseline." Golden, CO: National Renewable Energy Laboratory.*

Persson, T. A., Azar, C., Johansson, D., & Lindgren, K. (2007). Major oil exporters may profit rather than lose, in a carbon-constrained world. *Energy Policy*, *35*(12), 6346–6353. https://doi.org/10.1016/j.enpol.2007.06.027

Reershemius, T., Kelland, M. E., Jordan, J. S., Davis, I. R., D'Ascanio, R., Kalderon-Asael, B., Asael, D., Suhrhoff, T. J., Epihov, D. Z., Beerling, D. J., Reinhard, C. T., & Planavsky, N. J. (2023). Initial Validation of a Soil-Based Mass-Balance Approach for Empirical Monitoring of Enhanced Rock Weathering Rates. *Environmental Science & Technology*, *57*(48), 19497–19507. https://doi.org/10.1021/acs.est.3c03609

Renforth, P. (2012). The potential of enhanced weathering in the UK. *International Journal of Greenhouse Gas Control*, *10*, 229–243. https://doi.org/10.1016/j.ijggc.2012.06.011

Riahi, K., Bertram, C., Huppmann, D., Rogelj, J., Bosetti, V., Cabardos, A.-M., Deppermann, A., Drouet, L., Frank, S., Fricko, O., Fujimori, S., Harmsen, M., Hasegawa, T., Krey, V., Luderer, G., Parousos, L., Schaeffer, R., Weitzel, M., van der Zwaan, B., … Zakeri, B. (2021). Cost and attainability of meeting stringent climate targets without overshoot. *Nature Climate Change*, *11*(12), 1063–1069. https://doi.org/10.1038/s41558-021-01215-2

Rinder, T., & von Hagke, C. (2021). The influence of particle size on the potential of enhanced basalt weathering for carbon dioxide removal - Insights from a regional assessment. *Journal of Cleaner Production*, *315*, 128178. https://doi.org/10.1016/j.jclepro.2021.128178

Rogner, H.-H., Aguilera, R. F., Bertani, R., Bhattacharya, S., Dusseault, M. B., Gagnon, L., Haberl, H., Hoogwijk, M., Johnson, A., Rogner, M. L., Wagner, H., & Yakushev, V. (2012). Chapter 7 - Energy Resources and Potentials. In *Global Energy Assessment - Toward a Sustainable Future* (pp. 423–512). www.globalenergyassessment.org

Ryan, P. C., Santis, A., Vanderkloot, E., Bhatti, M., Caddle, S., Ellis, M., Grimes, A., Silverman, S., Soderstrom, E., Stone, C., Takoudes, A., Tulay, P., & Wright, S. (2024). The potential for carbon dioxide removal by enhanced rock weathering in the tropics: An evaluation of Costa Rica. *Science of The Total Environment*, *927*, 172053. https://doi.org/10.1016/j.scitotenv.2024.172053

Sherwood, S. C., Webb, M. J., Annan, J. D., Armour, K. C., Forster, P. M., Hargreaves, J. C., Hegerl, G., Klein, S. A., Marvel, K. D., Rohling, E. J., Watanabe, M., Andrews, T., Braconnot, P., Bretherton, C. S., Foster, G. L., Hausfather, Z., Heydt, A. S., Knutti, R., Mauritsen, T., … Zelinka, M. D. (2020). An Assessment of Earth's Climate Sensitivity Using Multiple Lines of Evidence. *Reviews of Geophysics*, *58*(4). https://doi.org/10.1029/2019RG000678

Strefler, J., Amann, T., Bauer, N., Kriegler, E., & Hartmann, J. (2018). Potential and costs of carbon dioxide removal by enhanced weathering of rocks. *Environmental Research Letters*, *13*(3), 034010. https://doi.org/10.1088/1748-9326/aaa9c4

Strefler, J., Bauer, N., Humpenöder, F., Klein, D., Popp, A., & Kriegler, E. (2021). Carbon dioxide removal technologies are not born equal. *Environmental Research Letters*, *16*(7), 074021. https://doi.org/10.1088/1748-9326/ac0a11

Sun, Y., Goll, D. S., Chang, J., Ciais, P., Guenet, B., Helfenstein, J., Huang, Y., Lauerwald, R., Maignan, F., Naipal, V., Wang, Y., Yang, H., & Zhang, H. (2021). Global evaluation of the nutrient-enabled version of the land surface model ORCHIDEE-CNP v1.2 (r5986). *Geoscientific Model Development*, *14*(4), 1987–2010. https://doi.org/10.5194/gmd-14-1987-2021

Tanaka, K., Boucher, O., Ciais, P., Daniel J. A. Johansson, Johansson, D. J., Daniel J. A. Johansson, Morfeldt, J., & Morfeldt, J. (2020). Cost-effective implementation of the Paris Agreement using flexible greenhouse gas metrics
MAG ID: 3165110065.

Tanaka, K., Johansson, D. J. A., O'Neill, B. C., & Fuglestvedt, J. S. (2013). Emission metrics under the 2 °C climate stabilization target. *Climatic Change*, *117*(4), 933–941. https://doi.org/10.1007/s10584-013-0693-8

Tanaka, K., Kriegler, E., Bruckner, T., Hooss, G., Knorr, W., Raddatz, T., & Tol, R. (2007). Aggregated Carbon cycle, atmospheric chemistry and climate model (ACC2): Description of forward and inverse mode, 14069106. https://doi.org/10.17617/2.994422

Tanaka, K., Lund, M. T., Aamaas, B., & Berntsen, T. (2018). Climate effects of non-compliant Volkswagen diesel cars. *Environmental Research Letters*, *13*(4), 044020. https://doi.org/10.1088/1748-9326/aab18c

Tanaka, K., & O'Neill, B. C. (2018). The Paris Agreement zero-emissions goal is not always consistent with the 1.5 °C and 2 °C temperature targets. *Nature Climate Change*, *8*(4), 319–324. https://doi.org/10.1038/s41558-018-0097-x

Tanaka, K., Raddatz, T., O'Neill, B. C., & Reick, C. H. (2009). Insufficient forcing uncertainty underestimates the risk of high climate sensitivity. *Geophysical Research Letters*, *36*(16), L16709. https://doi.org/10.1029/2009GL039642

Taylor, L. L., Quirk, J., Thorley, R. M. S., Kharecha, P. A., Hansen, J., Ridgwell, A., Lomas, M. R., Banwart, S. A., & Beerling, D. J. (2016). Enhanced weathering strategies for stabilizing climate and averting ocean acidification. *Nature Climate Change*, *6*(4), 402–406. https://doi.org/10.1038/nclimate2882

Thrikawala, S., Weersink, A., Fox, G., & Kachanoski, G. (1999). Economic Feasibility of Variable-Rate Technology for Nitrogen on Corn. *American Journal of Agricultural Economics*, *81*(4), 914–927. https://doi.org/10.2307/1244334

Vanderkloot, E., & Ryan, P. (2023). Quantifying the effect of grain size on weathering of basaltic powders: Implications for negative emission technologies via soil carbon sequestration. *Applied Geochemistry*, *155*, 105728. https://doi.org/10.1016/j.apgeochem.2023.105728

Virtanen, P., Gommers, R., Oliphant, T. E., Haberland, M., Reddy, T., Cournapeau, D., Burovski, E., Peterson, P., Weckesser, W., Bright, J., van der Walt, S. J., Brett, M., Wilson, J., Millman, K. J., Mayorov, N., Nelson, A. R. J., Jones, E., Kern, R., Larson, E., … SciPy 1.0 Contributors. (2020). SciPy 1.0: Fundamental Algorithms for Scientific Computing in Python. *Nature Methods*, *17*, 261–272. https://doi.org/10.1038/s41592-019-0686-2

Wang, F., Zhu, F., Liu, D., Qu, Y., Liu, D., Xie, J., Wang, A., Kang, R., Quan, Z., Li, Y., Chen, X., Li, G., Hobbie, E. A., & Fang, Y. (2024). Wollastonite powder application increases rice yield and CO2 sequestration in a paddy field in Northeast China. *Plant and Soil*. https://doi.org/10.1007/s11104-024-06570-5

Wang, J., Ciais, P., Gasser, T., Chang, J., Tian, H., Zhao, Z., Zhu, L., Li, Z., & Li, W. (2023). Temperature Changes Induced by Biogeochemical and Biophysical Effects of Bioenergy Crop Cultivation. *Environmental Science & Technology*. https://doi.org/10.1021/acs.est.2c05253

Welsby, D., Price, J., Pye, S., & Ekins, P. (2021). Unextractable fossil fuels in a 1.5 °C world. *Nature*, *597*(7875), 230–234. https://doi.org/10.1038/s41586-021-03821-8

West, L. J., Banwart, S. A., Martin, M. V., Kantzas, E., & Beerling, D. J. (2023). Making mistakes in estimating the CO2 sequestration potential of UK croplands with enhanced weathering. *Applied Geochemistry*, *151*, 105591. https://doi.org/10.1016/j.apgeochem.2023.105591

Wilson, C., Guivarch, C., Kriegler, E., van Ruijven, B., van Vuuren, D. P., Krey, V., Schwanitz, V. J., & Thompson, E. L. (2021). Evaluating process-based integrated assessment models of climate change mitigation. *Climatic Change*, *166*(1), 3. https://doi.org/10.1007/s10584-021-03099-9

CHAPTER IV

METHANE REMOVAL

Comparing Methane and Carbon Dioxide Removal for Climate Change Mitigation: Specifications and Impacts

Abstract

Methane is the second most influential anthropogenic greenhouse gas after carbon dioxide, and the potential level of emission reductions are known to be limited due to hard-to-abate sectors such as agriculture. Reducing the contribution of methane to climate change could therefore involve atmospheric methane removal (MR). This potential mitigation option has so far been much less studied than carbon dioxide removal (CDR).Here, we assess the cost and removal potential that MR must meet to ensure equivalent CO_2 emissions and cost savings to CDR in mitigation scenarios, and we compare the effects of MR and CDR on cost-effective mitigation pathways achieving four different climate targets. Using the ACC2-GET integrated carbon cycle, atmospheric chemistry, climate and energy system model, we consider a generic MR technology parameterized with constant unit costs and a maximal removal potential. We show that to replace carbon capture and storage from bioenergy processes, the MR potential have to be at least 180 to 320 $MtCH_4$ per year, which represents between 50% and 90% of current anthropogenic methane emissions, with maximum unit costs between 360 and 1210 $\$/tCO_2eq$, depending on the climate target. Using an intertemporal optimization modelling approach, we found that replacing CDR by MR delays mitigation burdens and reshapes the distribution of intergenerational efforts in climate mitigation. Unlike CDR, MR does not tackle

ocean acidification but can help reduce harmful tropospheric ozone. Finally, we show that the positive temperature feedback to natural methane emissions does not improve the cost-effectiveness of MR relative to CDR, although such feedback is sometimes used as a justification for developing MR techniques.

1 Introduction

1.1 Methane role in climate change

Methane is much less abundant in the atmosphere than carbon dioxide, with a concentration of 1.9 ppm, but the methane concentration has increased by 250% relative to pre-industrial levels (Saunois et al., 2020). Methane plays a significant role in anthropogenic climate change, as its current radiative forcing is equivalent to 60% of the radiative forcing of CO_2 (Myhre et al., 2013). Methane is a short-lived climate forcer: the perturbation lifetime of atmospheric methane is about 12 years (Szopa et al., 2021). This is much shorter than that of carbon dioxide, which follows different dynamics: excess atmospheric carbon is progressively absorbed by the natural sinks, such as the biosphere and the ocean, at a decreasing rate: about half of an emission pulse remains in the atmosphere after 20 years, but still one fourth after thousand years (Joos et al., 2013). Whereas the increase in global temperature is proportional to cumulative carbon dioxide emissions, methane emissions only have a transient effect on temperatures (Allen et al., 2022). However, as methane absorbs infrared radiation more effectively than carbon dioxide, its radiative forcing is higher per unit volume. The time perspective therefore critically influences the comparison between CO_2 and CH_4: the global warming potential of methane is 27.9 over 100 years and 81.2 over 20 years (Forster et al., 2021).

1.2 Methane emissions

Global methane emissions by both natural processes and human activities amounted to about 592 Tg per year in 2017 (Saunois et al., 2020). Methane is naturally emitted by the anoxic degradation of organic matter, in particular in wetlands. Natural sources also include fires and termites, and represent 40% of global methane emissions. Natural methane emissions are involved in positive feedback loops with global warming (Dean et al., 2018). For instance, the anoxic organic matter degradation in wetlands could increase in a warmer climate, due to an increase of wetland area driven by wetter conditions locally, thawing permafrost in the Arctic,

and enhanced methanogenesis due to higher soil temperature and higher atmospheric CO_2 concentration (Kleinen et al., 2021; Zhang et al., 2017).

Agriculture is responsible for around 45% of anthropogenic methane emissions (Saunois et al., 2020), due to enteric fermentation (in ruminants), wetland emissions from rice paddies, and animal waste methane (*Methane Emissions in Livestock and Rice Systems*, 2023). Methane emissions from fossil fuels account for just over a third of anthropogenic emissions, and are due, in roughly equal shares to coal, oil and gas extraction. Coal mining can release coalbed methane due to mine aeration, and methane can leak from oil and gas operations. The remaining anthropogenic emissions originate from waste decomposition.

Methane abatement is sometimes considered a "low-hanging fruit" of climate change mitigation, with cheap mitigation measures in the energy sector bringing additional benefits such as methane recovery, improved safety and air quality (Harmsen et al., 2020). However, agricultural methane emissions are beyond the low-hanging level, and are therefore projected to represent a significant part of residual methane emissions in climate mitigation scenarios (Harmsen et al., 2020). Methane abatement is also gaining political momentum at the international level, as 150 countries recently signed the "Global Methane Pledge", committing to take voluntary actions to reduce global methane emissions by at least 30% from 2020 levels by 2030.

1.3 Methane Removal

Methane removal (MR) consists in eliminating methane from methane point sources or directly from the atmosphere (Boucher & Folberth, 2010). Several methods to remove methane have been proposed, although the literature on their scalability and their possible costs is still sparse (Ming et al., 2022a). However, MR is gaining interest, with the development of a research agenda on atmospheric MR by the National Academies of Sciences, Engineering, and Medicine ("Atmospheric Methane Removal Development of a Research Agenda | National Academies", n.d.).

Several reasons have been raised to justify neglecting MR in comparison to carbon dioxide removal (CDR). Firstly, both reducing CH_4 emissions or implementing removal techniques reduce atmospheric methane concentration due to the ten-year lifetime of atmospheric methane. Unlike CO_2, net negative CH_4 emissions are unnecessary to reduce its temperature impact. Lowering CH_4 emissions decreases temperature, whereas reducing CO_2 emissions to zero only halts temperature increase without reversing it (Lackner, 2020). More broadly, focusing initial mitigation efforts on carbon dioxide is justified given the long perturbation time of CO_2, com-

pared to the transient effect of methane abatement on temperature trends (Abernethy et al., 2021; McKeough, 2022). Secondly, MR poses a number of technical challenges. Methane does not have the chemical properties (weak acidity and strong dipolar momentum) used to capture CO_2. Furthermore, atmospheric methane is 640 times more dilute than CO_2 in terms of mass. Thus, circulating the air in an MR plant alone could require 140 GJ/tCH_4 of electricity (Lackner, 2020).

Arguments for MR exploration have been made despite these drawbacks. MR could help counteract short-term warming and have a rapid impact on climate change, in line with the short-term effect of atmospheric methane (Abernethy et al., 2023; Jackson et al., 2019). Unlike carbon dioxide, methane is not part of the fertilization of the biosphere, so its atmospheric concentration may be reduced below pre-industrial levels (Boucher & Folberth, 2010). Much less MR than CDR is required to achieve a given climate impact due to the higher radiative efficiency of methane (Jackson et al., 2019), and unlike CDR, there is no need for storage since the removed methane can be oxidized to CO_2 without significantly reducing the climate benefits of the process (Boucher & Folberth, 2010). Reaching zero methane emissions is unlikely because methane emissions from food systems are difficult to reduce (Jackson et al., 2021; Nisbet et al., 2020). Furthermore, several studies have pointed out that a positive feedback from rising temperatures on natural methane emissions could occur in the future and may require the removal of atmospheric methane in addition to anthropogenic emission reductions to limit the surge of atmospheric methane concentrations (Boucher & Folberth, 2010; Jackson et al., 2019; Jackson et al., 2021; Ming et al., 2022a).

The technical and economic feasibility of removing atmospheric methane has thus been discussed for a decade, and the plausible costs, scalability and potentials of MR technologies are still very uncertain, not to say unknown. Existing studies exploring MR scenarios have assessed the impact of MR on atmospheric chemistry and temperature by imposing exogenous pathways of methane emission reductions (Abernethy et al., 2021) or methane-oxidizing chlorine emissions (Li et al., 2023). However, how MR could be integrated into the portfolio of existing mitigation options has not been investigated.

This study has two objectives: first, to investigate the relevant removal costs and potentials to enable MR to play a comparable role to BECCS as a key CDR method in climate change mitigation scenarios. Second, to evaluate the effects of MR in mitigation scenarios for emissions and temperature pathways, as well as for the time profile of mitigation efforts, and to contrast them with CDR. Since the increase of natural methane emissions due to global warming has been raised as a rationale for pursuing MR, we examine how accounting for this feedback can change the role of MR in our mitigation scenarios.

1.4 Implementation in a Climate-Energy Model

1.5 Modeling Framework and temperature targets

We use the energy-economy-climate GET-ACC2 described in Chapter 2 (see II and its supplements 6). Since ACC2 (Tanaka et al., 2007) resolves atmospheric chemistry, it is well suited to analyze the joint optimization of different greenhouse-gasses (GHG) emission pathways (Tanaka et al., 2013, 2020). Four climate targets cases are considered, as in Chapter 2: 1.5°C scenarios with low overshoot (up to 0.2°C) and high overshoot (no limit) and 2.0°C scenarios with no overshoot and with high overshoot (no limit). All three overshoot scenarios achieve their respective temperature targets by 2100.

1.6 A Generic GHG Removal Solution

A precise modeling of MR processes is beyond the scope of our study. We refer the interested reader to the existing literature (Abernethy et al., 2023; de_Richter et al., 2017; Li et al., 2023; Ming et al., 2021, 2022a, 2022b; Oeste et al., 2017; Wang et al., 2022; Xiong et al., 2023). Due to the lack of data on MR costs and energy requirements, we consider a generic MR characterized by the following two factors: i) a cost per ton of removed methane c [\$/tCH_4] and ii) a maximum annual removal potential p [tCH_4/year]. We consider only these two factors for two reasons. First, because two dimensions are convenient to represent visually. Second, because costs and potentials are the most typically assessed characteristics of mitigation options including CDR (Fuss et al., 2018). Unlike the energy system model, which typically has a decadal timestep, we optimized the MR characterization factors at a yearly timestep to account for the short atmospheric lifetime of methane. We also constrain the growth rate of MR. We thus add the following equations to the model:

$$MRC(t) = MR(t) \cdot c \tag{E.1}$$

$$MR(t) \leq p \tag{E.2}$$

$$MR(t+1) \leq MR(t) \cdot (1+g) + a \tag{E.3}$$

$$MR(t) = 0 \text{ for } t \ 2030 \tag{E.4}$$

where MRC [\$] is the annual cost of MR, MR [tCH_4] is the annual quantity of methane removed, g is the maximum geometric growth rate, set to 15% which is the standard growth rate for capacity addition in the model, and a is the maximum arithmetic growth rate, set to 10 $MtCH_4$ per year, in order to reach full potential within a decade. We deliberately considered a simplistic model of MR as well as a fast growth rate to facilitate the interpretation of our results. We assume that the methane captured by MR will be fully oxidized and converted to atmospheric CO_2 and subsequently enter into the carbon cycle of the model, although the added CO_2 is almost negligible. In order to compare MR and CDR, we also model a generic CDR based on the same approach to characterizing associated costs and potential (see supplements 6), in addition to the already modeled BECCS (Azar et al., 2013).

2 Willingness to pay for methane removal

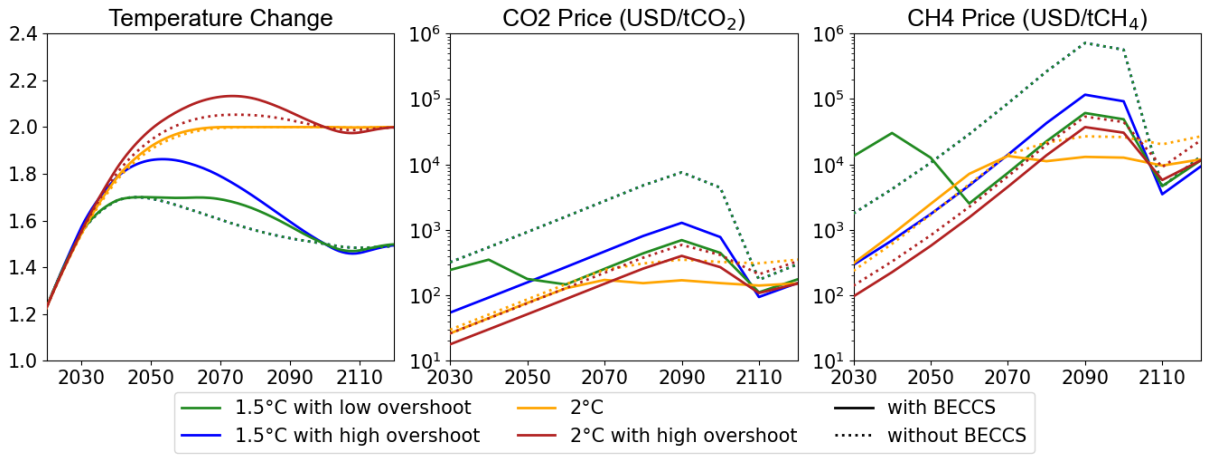

Figure IV.1: Temperature and GHG prices pathways for different climate target cases across the 21st century. **Solid lines:** with BECCS. **Dotted lines:** no BECCS. In that case, 1.5°C with low and high overshoots are identical.

Our model optimizes the GHG abatement costs with perfect foresight. Each solution is associated with a "shadow price" path for each GHG. MR and CDR are used if and only if their marginal costs are exceeded by the shadow price of CH_4 and CO_2, respectively. Understanding the behavior of the GHG prices in relation to climate objectives is thus key to understanding the reliance on MR. The shadow price at time t is the marginal abatement cost, which is equal to the marginal benefit of emitting one more unit of GHG at time t without affecting the climate, or symmetrically the benefit of a free unit GHG removal. Mathematically speaking, it is the dual of the constraint on global temperature at time t expressed in current value terms (Goulder &

Mathai, 2000). When constraints on technology expansion (like E.3) are binding, the shadow price is the sum of the dual of the temperature constraint and the dual of the technology growth rate constraints. The latter expresses that future abatement is constrained by past abatement through technical inertia. As a consequence, there is a benefit of abating more at a given time in order to have more flexibility for future abatement.

GHG prices rise until the temperature constraint becomes binding (Johansson, 2012). The shadow price of carbon grows exponentially with time, with a growth rate equal to the discount rate, and the price of methane grows even faster than the carbon price, increasing by several orders of magnitude over the century (Figure IV.1). The ratio of the two GHG prices increases exponentially at a rate $\frac{1}{\tau}$ where τ is the perturbation lifetime of the temperature associated with a methane emission (Johansson, 2012) (see also Figure IV.7). This phenomenon mirrors the initially lower but increasing importance of methane abatement as the temperature approaches the target level, due to the short atmospheric lifetime of CH_4 (Tanaka et al., 2020). This trend is particularly pronounced in OS cases. Methane abatement can indeed be delayed without affecting the final temperature, yet at the expense of a higher OS (McKeough, 2022). The availability of climate change mitigation options changes the GHG prices in a non-linear way. In the 1.5°C scenario with high OS, the CH_4 prices are almost one order of magnitude higher when BECCS is not available (Figure IV.1), correspondingly increasing the willingness to pay for methane removal. In the 1.5°C scenario with low OS, the maximum temperature of 1.7°C is not reached; as a consequence, the prices are the same as in the high OS scenario. In this case, the near-term methane price is higher in the case with BECCS than in the case without BECCS. It underlines the dependence of the methane price on the temporal proximity of reaching the temperature constraint.

3 Replacing BECCS by MR

3.1 The role of BECCS in mitigation pathways

BECCS were introduced in energy technology portfolios in the early 2000s (Azar & Lindgren, 2003; Azar et al., 2006; van Vuuren et al., 2007), and were the first large-scale CDR option considered in IAMs. BECCS deliver carbon-negative energy in models, which make them attractive for two main reasons. Firstly, their large CDR potential enabled otherwise infeasible unattainable climate targets to be met (Beck & Mahony, 2018; van Vuuren et al., 2007), by compensating for excess emissions in hard-to-abate sectors and for the delay in emission reduc-

tions. Secondly, they greatly reduced costs of stringent mitigation pathways (Azar et al., 2013). These two features made them a ubiquitous component of climate change mitigation scenarios long before the first demonstrators were built (Köberle, 2019), and it is now well-established that CDR is necessary to achieve net zero emissions and the targets of the Paris Agreement (Babiker et al., 2022), although the real-world efficiency of BECCS at the scale projected in mitigation scenarios remains unproven. Note that we compare MR to BECCS and not another CDR such as afforestation or DACCS because they are not represented in the model.

3.2 Equating MR with BECCS

Here, we examine what cost and potential an MR technology should reach in order to have the same crucial role as BECCS. For this purpose, we quantify the equivalence in terms of the induced reduction in policy costs and the cumulative gross CO_2 emissions of the energy system, thereafter the "gross carbon budget". An MR technology should thus reduce policy costs and lead to the same gross carbon budget as BECCS does in our model framework. Alternative metrics may be considered, and this aspect is deferred for future research. Note that we do not consider the net carbon budget, as obtaining without BECCS the same net carbon budget as with BECCS would not be feasible at the same cost and would not require any MR. We then perform simulations without BECCS (bioenergy and fossil CCS remain available) for a wide range of MR potentials and costs, in order to estimate the policy costs and gross carbon budgets for the whole range of MR costs and potentials (Figure IV.2).

The costs of achieving climate objectives, here quantified as the net present value of policy cost (the energy system costs plus the loss of consumer surplus) compared to a baseline without climate policy, can be reduced with MR. Policy costs increase with decreasing MR potential and increasing MR unit cost (Figure IV.2). They are maximal and constant for MR costs higher than the peak shadow price of methane in the no-BECCS case (dotted lines in Figure IV.1)). The gross carbon budget behaves oppositely: the higher the MR potential and the lower its cost, the higher the gross carbon budget.

The costs and potential of the MR technology that would play the same role as BECCS (with regard to policy costs and gross carbon budgets) depend on the temperature target. The required MR potentials range between 178 $MtCH_4$ per year, which is higher than methane emissions from the energy sector, and 320 $MtCH_4$ per year, which is about 90% of total anthropogenic emissions. Costs range from 10\$/$kgCH_4$ (357\$/tCO_2eq, using GWP100 for conversion) to 34\$/$kgCH_4$ (1214 \$/tCO_2eq). These costs are upper limits for MR to be as efficient as BECCS, and are above recent estimates of the social cost of methane (Azar et al., 2023) (4

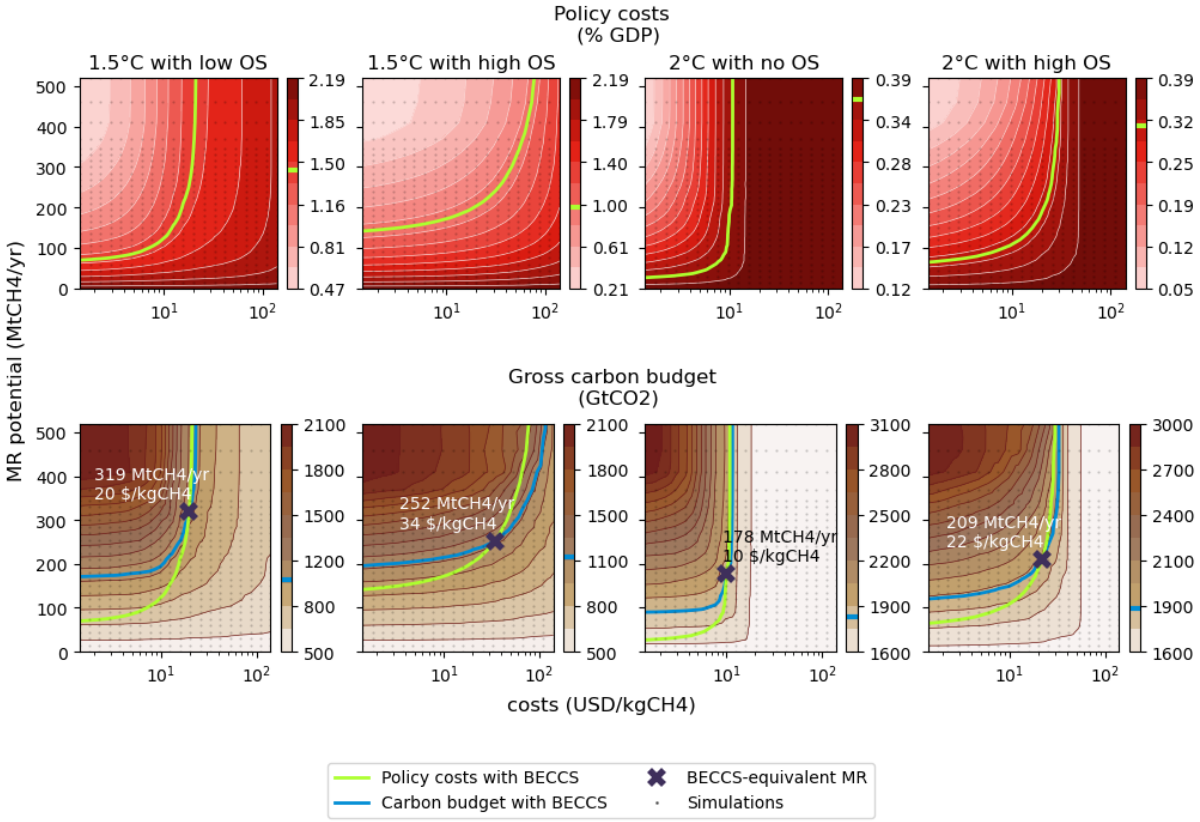

Figure IV.2: Policy costs and gross carbon budgets across the 21st century depending on MR technology for different climate target cases, when no BECCS are available. **X-axis** (log scale): unit cost of methane removal, in USD per $kgCH_4$. **Y-axis**: maximum annual methane removal, in $MtCH_4$ per year. **Top panels:** The color corresponds to policy costs, defined as the net present values of future energy production costs and consumption losses as a percentage of GDP, compared to the no-policy scenario. The green curve is the contour line of the policy costs when BECCS is available. **Bottom panels:** The color corresponds to the gross carbon budgets, defined as the cumulative CO_2 emissions across the 21st century excluding land-use and CDR. The blue curve is the contour line of the gross carbon budgets when BECCS is available. The intersection with the green curve, marked with a **cross**, indicates the cost (in $\$/kgCH_4$) and potential (in $MtCH_4$/year) of an MR technology that becomes equivalent to BECCS when the policy costs and the gross carbon budget are considered together. The **black dots** are the data points between which the policy costs and the carbon budgets are interpolated.

to 9 $\$/kgCH_4$ in 2020 depending on the scenario). It means that the current social cost of methane should not be considered as a threshold to determine future cost-efficiency (Abernethy et al., 2023). Methane Removal (MR) technologies are currently in an early stage of development. However, targeted costs are within a range of approximately 100-1000$/tCO2eq (2.8-28$/kgCH4). For technologies involving the emission of chlorine atoms into the atmosphere, costs could potentially decrease to as low as 2-50$/tCO2eq (0.06-1.4 $/kgCH4) (Ming et al., 2022a). If these targets are met, they will be cheaper than the BECCS-equivalent cost thresholds. However, the likely potentials are still unknown.

3.3 Emissions pathways

Because of the different lifetimes and radiative efficiencies of methane and carbon dioxide, an MR technology allowing the same carbon emissions and cost reductions as BECCS for a given mitigation objective nevertheless has different effects on the scenarios. We explore them by comparing the pathways with BECCS and with MR. To distinguish between what depends on gas properties and what depends on the way BECCS are modeled, we need to introduce a third case of comparison, with a generic CDR method whose cost and potential imply the same role as BECCS. Its cost and potential thus also depend on the climate target case.

The cumulative CDR is much higher than the GWP100-calculated CO_2-equivalent methane eliminated in the MR case (Figure IV.3). MR is used later than CDR, in particular in high overshoot scenarios (Figure IV.3), and net CH_4 emissions reach net-negative levels before 2100 in all MR scenarios except the 2°C without OS case. In this latter case, gross emission pathways of methane and CO_2 are very close for MR and CDR. The gross CO_2 emission pathways differ between MR and CDR in the other cases: in the end of the century, gross CO_2 emissions with MR are much higher in the 1.5°C with low OS case, and lower in the two high OS cases, almost reaching zero residual CO_2 emissions in the 1.5°C with high OS case. Compared with other GHG capture methods, the use of BECCS is projected to grow more gradually throughout the 21st century. Deployment of BECCS is slower due primarily to limited annual growth in geological carbon sequestration capacity and also in energy supply technologies. Once investments in bioenergy supply technologies have been made, operating costs are low enough to justify continued use and subsequent CO_2 sequestration throughout their lifetime, even when carbon prices decline transiently in the 1.5°C with low OS case when the temperature stabilizes and before the temperature decline. As a consequence, the net CO_2 emissions reductions of the generic CDR case are slightly delayed compared to the BECCS case.

3.4 Climate evolution

MR can substitute for CDR to achieve the 1.5°C or 2°C targets, but they affect the climate system and carbon cycle differently. Due to the shorter lifetime of methane, MR induces a faster reduction of the atmospheric methane concentration than what CDR does for the concentration of CO_2. As its radiative efficiency is also higher, the temperature reduction for MR can be more abrupt than for CDR, a feature that is used by the model to postpone MR. As a consequence, the overshoot lasts longer with MR than with CDR (Figure IV.4), increasing the risks of extreme events and crossing tipping points (Ritchie et al., 2021), sea level rise and biodiversity

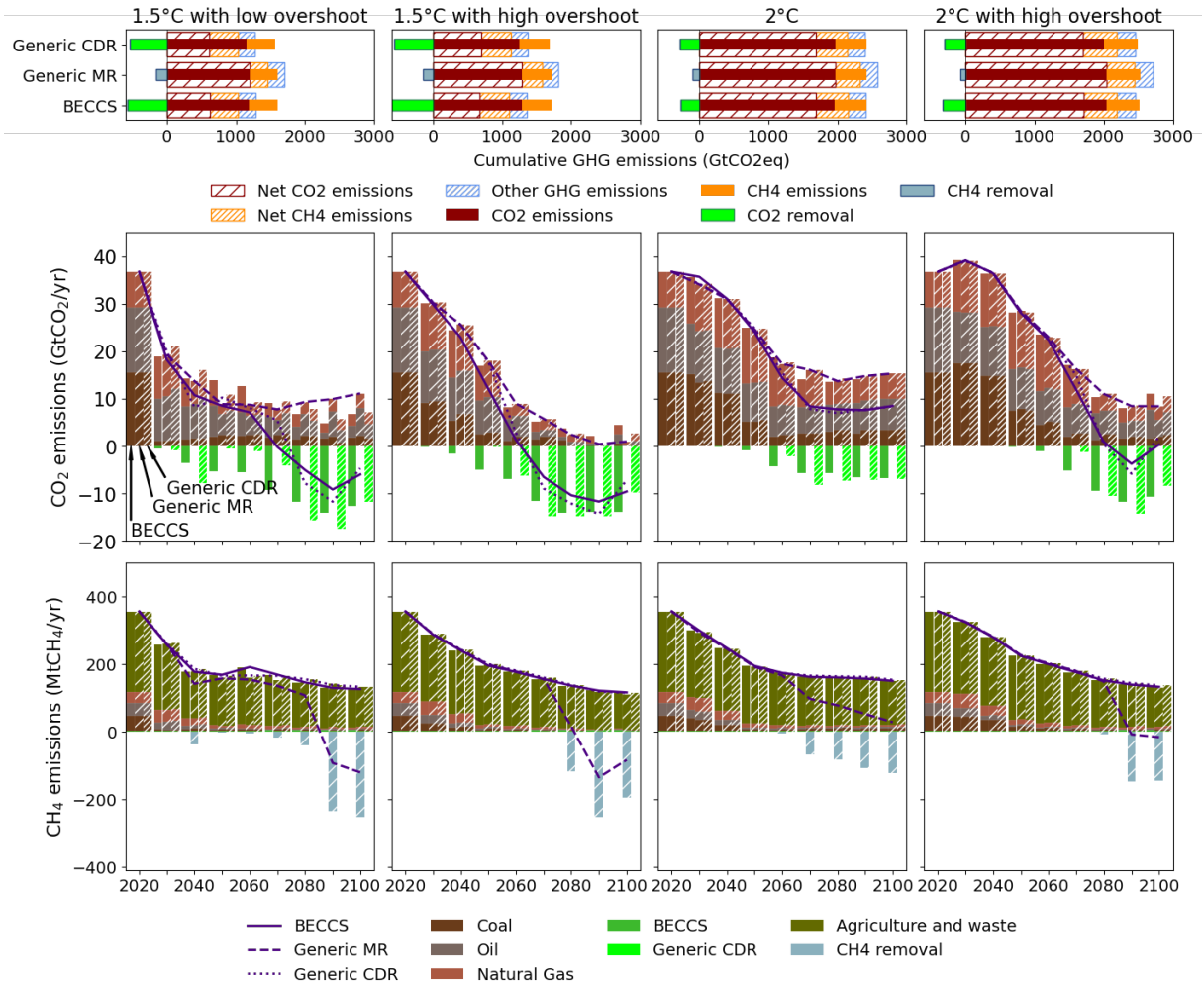

Figure IV.3: Greenhouse gas emissions across the 21st century, for three different GHG removal technologies (a generic CDR, a generic MR, and BECCS) and different climate target cases, in $GtCO_2eq$ based on GWP100. **First row:** Cumulative GHG emissions from 2020 to 2100. **Second row:** CO_2 emissions across the 21st century excluding land-use. Lines represent net emissions. **Third row:** CH_4 emissions across the 21st century. Lines represent net emissions.

loss (Meyer et al., 2022).

The land and ocean sinks capture more carbon in the MR cases because the higher atmospheric CO_2 concentration (Figure IV.4) increases the carbon fertilization of the land sink and the ocean CO_2 uptake. The difference in atmospheric CO_2 increases in the MR and CDR cases is therefore lower than the difference in net CO_2 emissions (Figure IV.4). In the 1.5°C scenarios with CDR, high net negative emissions lead to lower atmospheric CO_2 concentrations than with MR , and the land and ocean sinks absorb less carbon than with MR. However, the proportion of emissions absorbed by natural sinks is higher in the CDR cases: more than 92% in the 1.5°C cases with CDR, and less than 77% with MR. Environmental impacts of GHG removal would also be different depending on the technology used. Reducing atmospheric methane concentrations has a positive impact on air quality by simultaneously reducing tropospheric ozone (Abernethy et al., 2021) (Figure IV.4), although it should be noted that the parameteri-

zation used for the present calculation is valid only around the present day concentration of CH_4 and pollutants, and would require confirmation with a more detailed chemistry transport model. Higher levels of atmospheric CO_2 increases ocean acidification, which is an ongoing threat to marine ecosystems as it affects the organisms producing calcium carbonate shells and skeletons (Heinze et al., 2021). These effects do not only depend on pH, but we use pH as a proxy for ocean acidification (Figure IV.4). The minimum pH value depends on the climate target case and does not vary depending on the GHG removal technology. However, the recovery of pH is strongly reduced when MR is used, as temperatures are stabilized with a higher CO_2 concentration.

3.5 Policy costs and equity

Cumulative policy costs until 2100 are equal by design for the different GHG removal technologies, but their distribution across the 21st century is greatly affected by the technology portfolio in high overshoot cases, but not in low-overshoot scenarios (Figure IV.5), Top panels). Since the use of MR occurs later compared to that of CDR in high overshoot scenarios, the policy costs are proportionately higher at the end of the century. This increases the cost borne by future generations. Consequently, the balance between near-term and long-term efforts is shifted when substituting BECCS with MR, although BECCS already increases the cost borne by future generations in overshoot scenarios (Emmerling et al., 2019). However, determining whether this results in a more or less equitable situation is an ethical issue rather than a purely economic one, as several conflicting factors come into play here: future generations will be richer under the scenario assumptions based on the SSP2 baseline (Bertram et al., 2021), in which per capita GDP grows at around 1.7% per year, thereby easing the effort required, but they will also suffer more from climate change (Thiery et al., n.d.) to which they have not themselves contributed. Furthermore, temperatures would go down later with MR than with CDR, implying higher climate risks.

Intergenerational equity in the effort distribution can nevertheless be assessed from a utilitarian perspective, by explicitly stating the assumptions relating to the utility function. Here we assume that utility takes an "isoelastic" form, usually referred to as a constant relative risk aversion (CRRA) utility function, $u(t) = \frac{c(t)^{1-\gamma}}{1-\gamma}$, where c is the consumption and γ is the elasticity of marginal utility of consumption. This form assumes that the aversion to (intertemporal) inequality and risk is constant in relative terms for different consumption levels. We assume that the consumption loss is proportionate to the policy costs computed by the model (see supplements 6). Following the Ramsey equation (Ramsey, 1928), the discount rate is the sum of

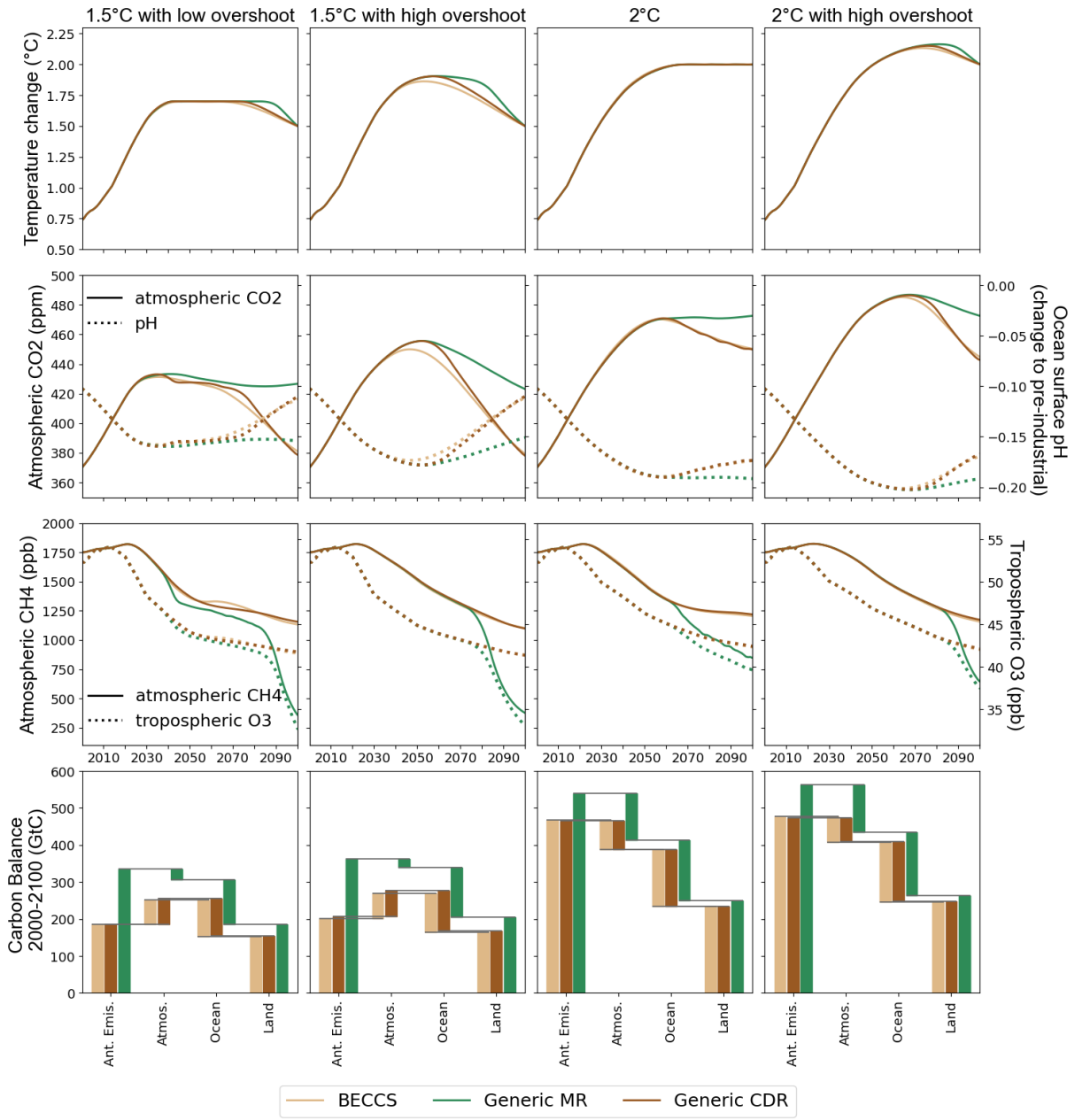

Figure IV.4: Contrasted physical and biogeochemical effects of MR and CDR. First row: Global-annual mean change of surface temperature relative to the preindustrial level. **Second row**: Atmospheric CO_2 concentrations (left y-axis, solid lines) and change of sea surface pH relative to the preindustrial level (right y-axis, dotted lines) across from 2000 to 2100. **Third row:** Atmospheric CH_4 concentrations (left y-axis, solid lines) and tropospheric O_3 concentrations (right y-axis, dotted lines). **Fourth row:** Carbon balance of different pools from 2020 to 2100. The four columns are (i) cumulative net anthropogenic CO_2 emissions (Ant. Emis), (ii) the net change in atmospheric CO_2 burden (Atmos.), (iii) cumulative oceanic CO_2 uptake (Ocean), (iv) cumulative land CO_2 uptake (Land). Red arrows denote the increase of the carbon pools.

two terms: the time preferences rate and the product of the growth rate by γ. The discount rate (5% p.a.) is exogenous in the model, chosen for consistency with the model that produced the base scenario (MESSAGEix). Therefore, the acceptable values for γ range from $\gamma = 0$, corresponding to a linear utility function, neutrality to inequality and strong present preference rate of 5% p.a., and $\gamma = 2.9$ defining a strongly concave utility function, strong aversion to in-

equality and a preference rate of 0% per year. Here, we assess all values consistent with the assumed growth rate and discount rate; however, the ranges of recommendable values for the elasticity of marginal consumption and the time preference rate are slightly narrower ($1 \leq \gamma \leq 2$) (Nesje et al., 2023). This is a post-run analysis, and the 5% discount rate was used for the optimization throughout. In OS cases the annual utility loss strongly increases in the end of the century with MR, for all values of γ, whereas this is only true for γ values below 1.5 with CDR technologies (Figure IV.5, Bottom panels). The effort distribution in the 1.5°C with low overshoot cases is relatively independent of the GHG removal technology. In the 2°C scenarios with low OS and BECCS, the costs and utility losses peak in the 2060s. MR flattens the effort distribution, but this is also the case for generic CDR, implying that the reason is not inherent in MR, but rather in the slower growth of BECCS, which requires earlier deployment and earlier emission reductions.

From the perspective of intertemporal utility, MR therefore appears to be a less equitable strategy than CDR in the high overshoot cases, which could undermine its social acceptability. Intertemporal utility is not the only dimension of equity to consider. Intra-generational equity issues could also be associated with the heterogeneous geographical distribution of CDR potential (Strefler et al., 2021). Both MR and CDR are associated with their own risks for future generations. CDR requires storage, which poses a risk of leakage, in particular for nature-based solutions such as soil carbon sequestration, afforestation and reforestation or biochar (Prado & Mac Dowell, 2023). Similarly, MR must continue, once it has started, in order to maintain a low atmospheric concentration of methane: if it is stopped, the effects of the MR fade away in around ten years and the temperature rises again to the level it would have had without MR. This issue is analogous to the termination issue of solar radiation management which, if terminated unintendedly, say due to a lack of governance, could lead to an abrupt large rebound of temperatures (Boucher et al., 2013; Lee et al., 2021; Parker & Irvine, 2018).

4 Temperature feedback on methane emissions

4.1 Simple implementation in ACC2

Unlike the rise in atmospheric CO_2 which results from anthropogenic emissions (Ciais et al., 2014), the rise in atmospheric CH_4 concentration may be strongly driven by increasing natural emissions: using an earth system model that endogenizes methane emissions from wetlands, fires, termites as well as soil methane uptake, T. Kleinen and his co-authors (Kleinen et al.,

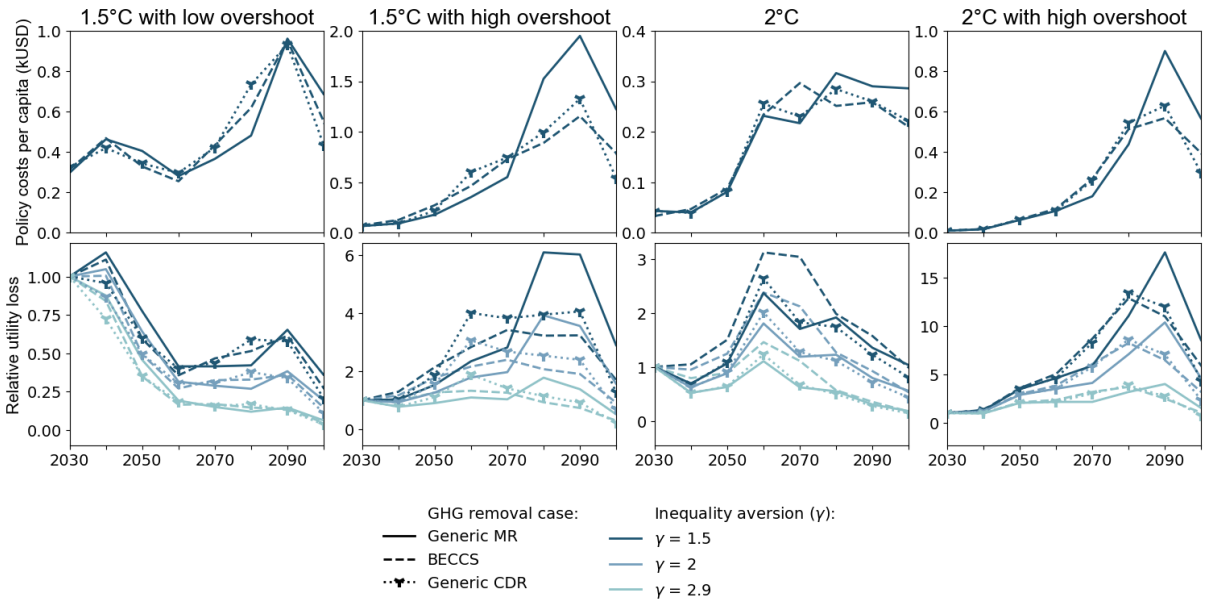

Figure IV.5: Top panels: Per capita annual policy costs across the 21st century. **Policy costs** are the future energy production costs and consumption losses, compared to the no-policy scenario. **Bottom panels:** Utility loss (relative to 2030), for different values of the inequality aversion coefficient γ, assuming that the consumption loss is proportionate to the policy costs. The top panels correspond to the case $\gamma = 0$ without normalization.

2021) find a linear increase of global natural methane emissions with global mean temperature change, with a slope α of 75 [$MtCH_4.year^{-1}.K^{-1}$].

In the original version of ACC2, natural methane emissions are assumed to be a constant N=320 [$MtCH_4.year^{-1}$] based on an inverse calculation. We impose natural methane emissions to be equal to $N + \alpha\,(T(t) - T(2020))$ for $t \geq 2020$ (see supplements 6, where we also discuss the magnitude of the feedback).

4.2 Effects on mitigation pathways

Future natural methane emissions are higher when the temperature feedback is considered. As a result, meeting the same climate targets requires more stringent anthropogenic emission reductions.

Since the maximum temperature reached in our scenarios is 2.15°C, and the temperature in 2020 is 1.23°C, the temperature feedback increases natural methane emissions by up to 69 $MtCH_4$ per year (Figure IV.6)). These additional methane emissions modify the mitigation pathways. We here discuss the BECCS case only. The available gross carbon budgets for the energy sector decrease by 5% in the 1.5°C cases to 7% in the 2°C cases. The effect on mitigation costs is more scenario-dependent: costs increase by 10% in the 1.5°C with high OS, 18% in the

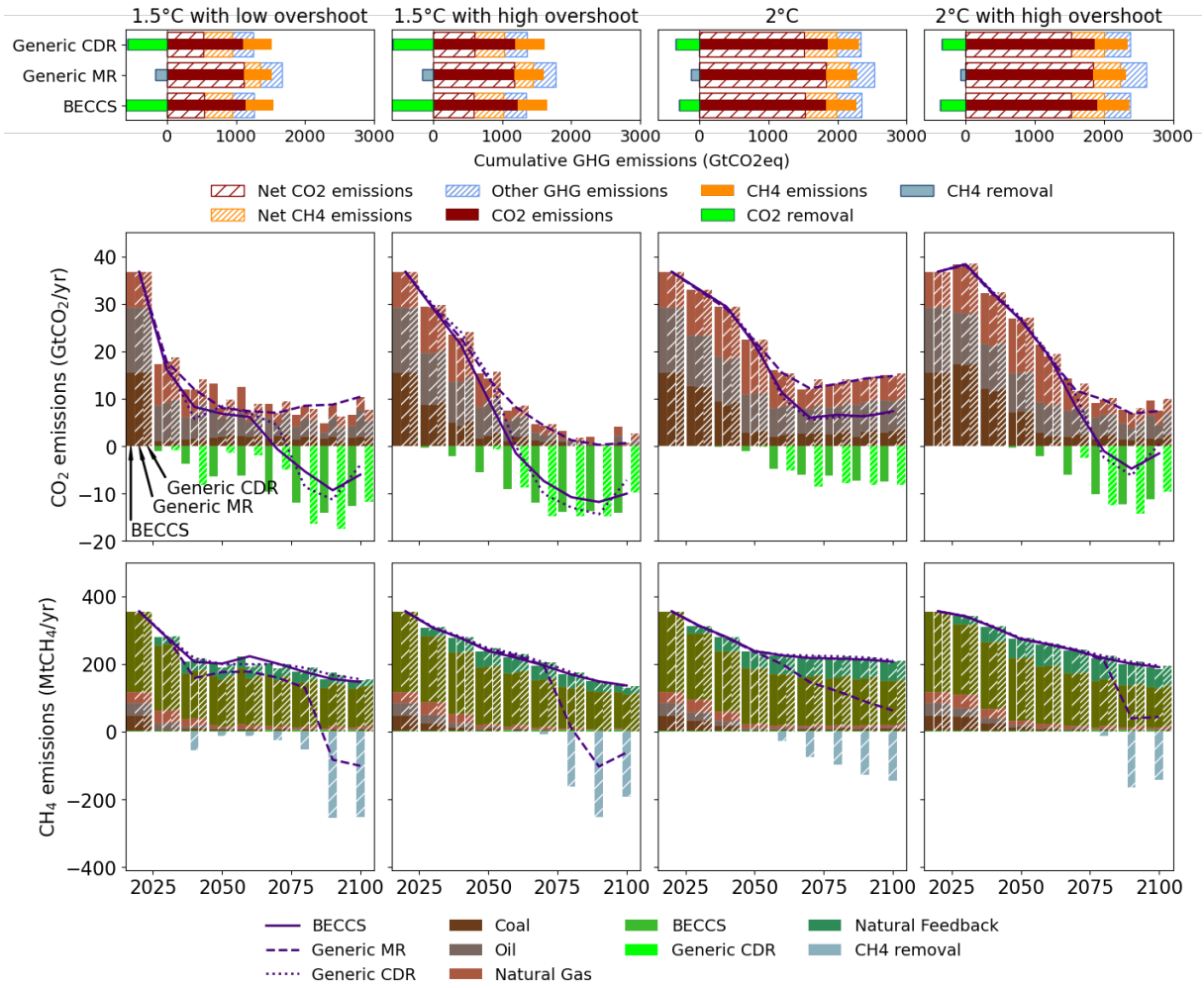

Figure IV.6: Greenhouse gas emissions across the 21st century, for three different GHG removal technologies and different climate target cases, in $GtCO_2eq$ based on GWP100. **First row:** Cumulative GHG emissions from 2020 to 2100. **Second row:** CO_2 emissions across the 21st century excluding land-use. Lines represent net emissions. **Third row:** CH_4 emissions across the 21st century. Lines represent net emissions. The Generic CDR and MR technologies are the same as in the no-feedback case.

1.5°C with low OS, and 22% in the 2°C cases. In the 1.5°C with low OS case, the mitigation efforts are concentrated on the near-term in order to curb the temperature pathway and stay below 1.7°C. Even more stringent near-term CO_2 emission reductions are required if natural methane emissions are higher. The higher relative increase of mitigation costs in the 2°C cases as a consequence of the temperature feedback on methane emissions has two main reasons: firstly, the mitigation costs are lower, and secondly, as higher temperatures make the feedback comparatively more important (i.e. adding more methane in the atmosphere).

4.3 Cost-effectiveness of MR

The need for more stringent mitigation resulting from higher natural methane emissions increases the mitigation costs and the prices of both CO_2 and CH_4, and thereby the willingness to pay for both MR and CDR (Figure IV.7)). This is particularly true in the near-term, because the feedback incentivises earlier mitigation. The ratio of CH_4 price to CO_2 price is slightly higher in the near-term and lower in the long-term when the feedback is implemented.

Including the temperature feedback on natural methane emissions does not make MR more relevant comparatively to BECCS. We show the costs and potentials of MR technologies that would outperform BECCS in terms of carbon budget and total costs, with and without the feedback of temperature on methane emissions (Figure IV.8)). Each MR technology that outperforms BECCS with the feedback also outperforms BECCS without the feedback, but the inverse is not true: there are MR technologies which are associated with lower policy costs and a higher gross carbon budget than BECCS without the feedback, but with higher policy costs and lower gross carbon budgets with the feedback. This is not the case for the generic CDR: the methods associated with the same carbon budget and policy costs as BECCS are the same, whether or not we include the feedback. Consequently, we deduce that MR tends to be made less competitive than CDR by feedback as implemented in the model.

5 Conclusion

To fill the knowledge gap on the deployment of MR technologies in cost-effective mitigation pathways, we looked for the inherent differences and similarities of MR and CDR. As we lacked process-level and economic data on MR technologies, we used a top-down approach to frame the necessary costs and potentials for MR to become competitive with BECCS, based on two metrics: the cumulative gross CO_2 budget and the policy costs. Alternative metrics could consider the maximum rate of emission reductions, or the emission level at temperature stabilization.

We showed that it was theoretically possible for MR to play the same critical role as carbon dioxide removal on mitigation pathways. MR could be cost-effective for unit costs up to 34\$/kgCH_4, but the removal potential needs to reach several hundred Mt CH_4 per year to replace BECCS. Yet it is not known whether such removal levels can be achieved sustainably. The deployment of MR is more delayed than the deployment of CDR, in particular in OS scenarios. As a consequence, a MR technology that delivers the same gross CO_2 budget and cost savings

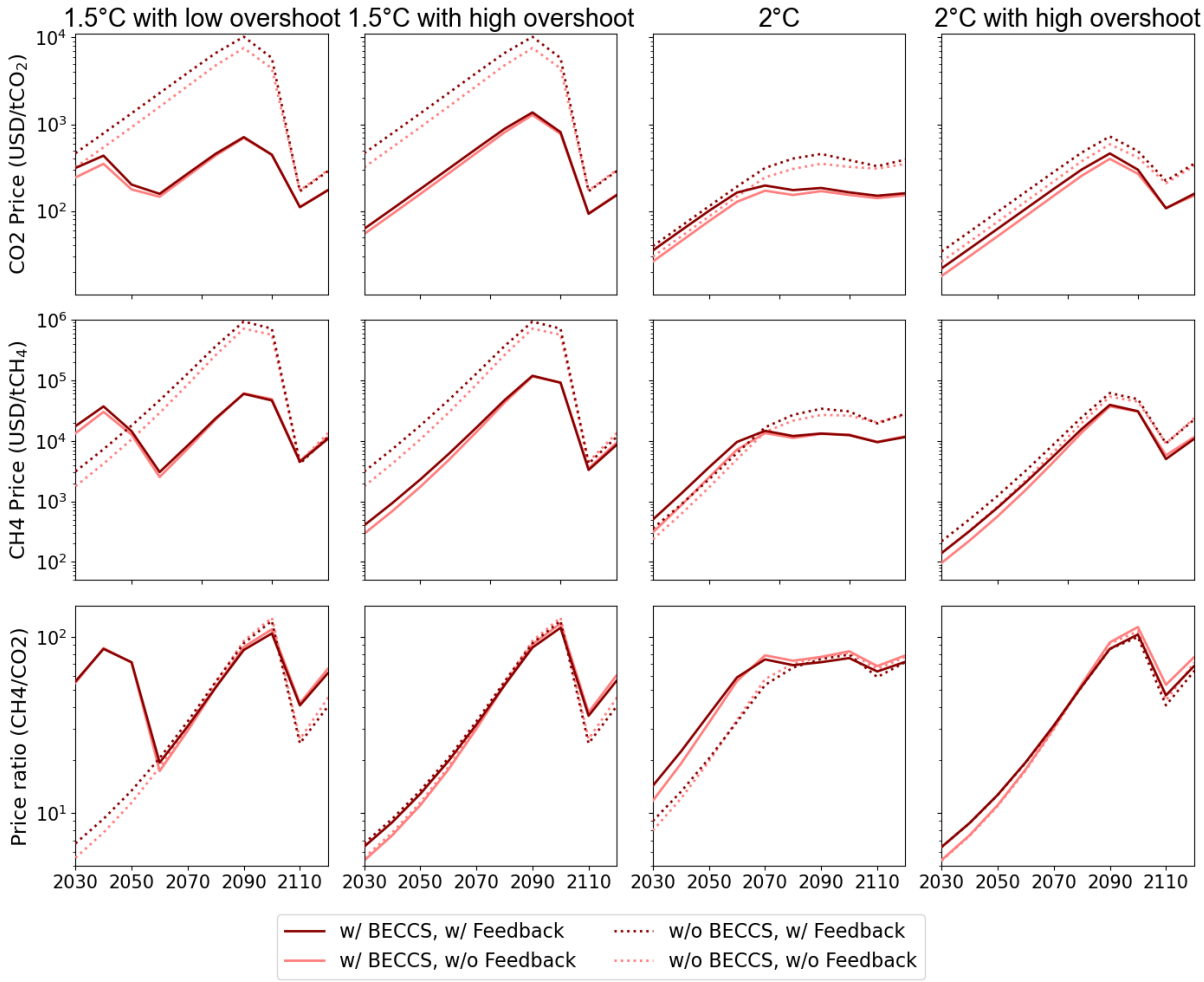

Figure IV.7: CO_2 and CH_4 prices with and without the temperature feedback on natural CH_4 emissions compared to the no-feedback case. **Solid lines:** with BECCS. **Dotted lines:** no BECCS.

than BECCS could make the intergenerational effort distribution less equitable than CDR, and have different earth-system impacts. We also showed that the presence of a positive feedback from climate change on methane emissions did not make MR comparatively more relevant than CDR, because higher natural methane emissions imply that more mitigation is needed for all GHG, not only methane. Assessing other aspects of MR such as possible interactions with the energy system, atmospheric chemistry feedbacks or environmental impacts would require further analyses considering specifically specific processes.

The accuracy of these general results for a specific MR technology depends on how closely it aligns with our simple modeling assumptions, especially those concerning constant MR costs. However, non-linear, concentration-dependent costs are likely. For instance, it was shown that existing active methane oxidation technologies such as thermo-catalysts, photo-catalysts, electro-catalysts and biofilters are not able to oxidize methane at atmospheric concentrations at reasonable energy costs (Abernethy et al., 2023) but that they could be deployed over methane point sources where the concentration is high (Nisbet-Jones et al., 2021). Non-linear costs are

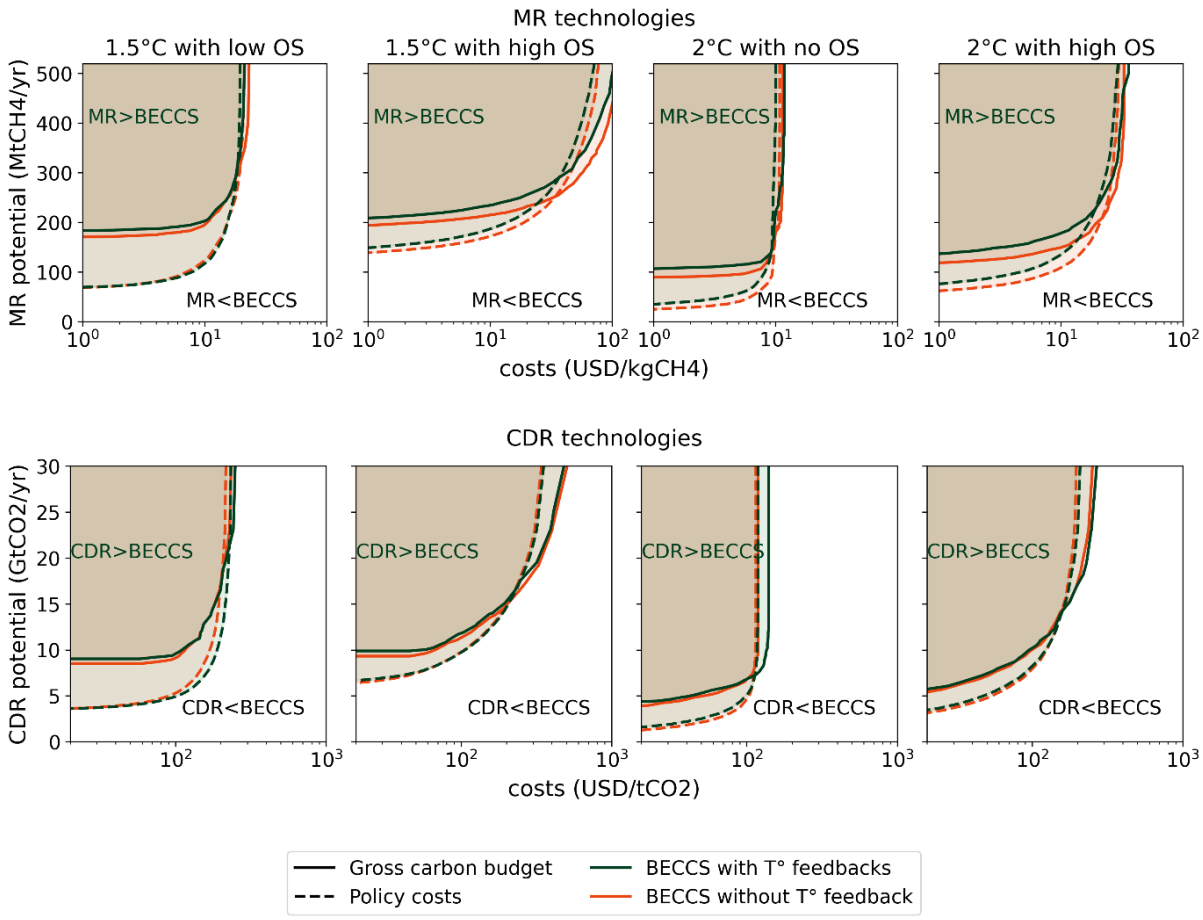

Figure IV.8: Contour lines of BECCS-equivalent MR and CDR with regard to gross carbon budgets (solid line) and policy costs (dotted line) with and without the temperature feedback on natural methane emissions. The shaded area represents the set of MR costs and potentials that allow a higher carbon budget or lower policy costs than BECCS.

also to be expected for methods that enhance atmospheric methane oxidation by increasing OH (Wang et al., 2022) or Cl sinks (Li et al., 2023; Oeste et al., 2017). Recent research (Li et al., 2023) indicates that chlorine emissions could reduce methane concentration only above an emission threshold of 90 Tg/year. Below this threshold, chlorine depletes tropospheric ozone, a critical source of OH which is itself an oxidizing agent of methane, causing the atmospheric lifetime of CH_4 to increase. Achieving the BECCS-equivalent level of hundreds $MtCH_4$ /year could require emitting more than half a Gt chlorine each year, with potentially significant harmful environmental side-effects (Li et al., 2023).

Finally, targeting methane is also a way to mitigate near term warming: methane emission reductions can reduce temperatures while CO_2 emission reductions cannot. MR could strengthen this possibility. In our scenarios, MR is used to quickly reduce temperature after overshoots, but not to mitigate near-term warming. Near-term mitigation could be a more salient feature of MR with alternative scenario assumptions: for instance, assuming fixed energy demand, our model cannot solve the 1.5°C case with low OS with either BECCS or generic

CDR, while it can be solved if MR is available with a potential above 203 $MtCH_4$ per year, highlighting the possible use of MR for shaving the temperature peak. However, methane removal processes are still at a very early stage, their achievable costs, potentials and side-effects are still unknown. It is therefore rather unlikely that they play a significant role in the near-term.

References

Abernethy, S., O'Connor, F. M., Jones, C. D., & Jackson, R. B. (2021). Methane removal and the proportional reductions in surface temperature and ozone. *Philosophical Transactions of the Royal Society A: Mathematical, Physical and Engineering Sciences*, *379*(2210), 20210104. https://doi.org/10.1098/rsta.2021.0104

Abernethy, S., Kessler, M. I., & Jackson, R. (2023). Assessing the potential benefits of methane oxidation technologies using a concentration-based framework. *Environmental Research Letters*. https://doi.org/10.1088/1748-9326/acf603

Allen, M. R., Peters, G. P., Shine, K. P., Azar, C., Balcombe, P., Boucher, O., Cain, M., Ciais, P., Collins, W., Forster, P. M., Frame, D. J., Friedlingstein, P., Fyson, C., Gasser, T., Hare, B., Jenkins, S., Hamburg, S. P., Johansson, D. J. A., Lynch, J., … Tanaka, K. (2022). Indicate separate contributions of long-lived and short-lived greenhouse gases in emission targets. *npj Climate and Atmospheric Science*, *5*(1), 1–4. https://doi.org/10.1038/s41612-021-00226-2

Atmospheric Methane Removal Development of a Research Agenda | National Academies. (n.d.). Retrieved October 31, 2023, from https://www.nationalacademies.org/our-work/atmospheric-methane-removal-development-of-a-research-agenda

Azar, C., Johansson, D. J. A., & Mattsson, N. (2013). Meeting global temperature targets—the role of bioenergy with carbon capture and storage. *Environmental Research Letters*, *8*(3), 034004. https://doi.org/10.1088/1748-9326/8/3/034004

Azar, C., & Lindgren, K. (2003). Global energy scenarios meeting stringent CO2 constraints— cost-effective fuel choices in the transportation sector. *Energy Policy*, 16.

Azar, C., Lindgren, K., Larson, E., & Möllersten, K. (2006). Carbon Capture and Storage From Fossil Fuels and Biomass – Costs and Potential Role in Stabilizing the Atmosphere. *Climatic Change*, *74*(1-3), 47–79. https://doi.org/10.1007/s10584-005-3484-7

Azar, C., Martín, J. G., Johansson, D. J., & Sterner, T. (2023). The social cost of methane. *Climatic Change*, *176*(6), 71. https://doi.org/10.1007/s10584-023-03540-1

Babiker, M., Berndes, G., Blok, K., Cohen, B., Cowie, A., Geden, O., Ginzburg, V., Leip, A., Smith, P., Sugiyama, M., & Yamba, F. (2022). Cross-sectoral perspectives. In P. Shukla, J. Skea, R. Slade, A. A. Khourdajie, R. van Diemen, D. McCollum, M. Pathak, S. Some, P. Vyas, R. Fradera, M. Belkacemi, A. Hasija, G. Lisboa, S. Luz, & J. Malley (Eds.), *Climate Change 2022: Mitigation of Climate Change. Contribution of Working Group III to the Sixth Assessment Report of the Intergovernmental Panel on Climate Change*. Cambridge University Press. https://doi.org/10.1017/9781009157926.005

Beck, S., & Mahony, M. (2018). The politics of anticipation: The IPCC and the negative emissions technologies experience. *Global Sustainability*, *1*, e8. https://doi.org/10.1017/sus.2018.7

Bertram, C., Riahi, K., Hilaire, J., Bosetti, V., Drouet, L., Fricko, O., Malik, A., Nogueira, L. P., van der Zwaan, B., van Ruijven, B., van Vuuren, D., Weitzel, M., Longa, F. D., de Boer, H.-S., Emmerling, J., Fosse, F., Fragkiadakis, K., Harmsen, M., Keramidas, K., … Luderer, G. (2021). Energy system developments and investments in the decisive decade for the Paris Agreement goals. *Environmental Research Letters*, *16*(7), 074020. https://doi.org/10.1088/1748-9326/ac09ae

Boucher, O., Randall, D., Artaxo, P., Bretherton, C., Feingold, G., Forster, P., Kerminen, V.-M., Kondo, Y., Liao, H., Lohmann, U., Rasch, P., Satheesh, S., Sherwood, S., Stevens, B., & Zhang, X. (2013). Clouds and Aerosols. In T. Stocker, D. Qin, G.-K. Plattner, M. Tignor, S. Allen, J. Boschung, A. Nauels, Y. Xia, V. Bex, & P. Midgley (Eds.), *Climate Change 2013: The Physical Science Basis. Contribution of Working Group I to the Fifth Assessment Report of the Intergovernmental Panel on Climate Change* (pp. 571–658). Cambridge University Press. https://doi.org/10.1017/CBO9781107415324.016

Boucher, O., & Folberth, G. A. (2010). New Directions: Atmospheric methane removal as a way to mitigate climate change? *Atmospheric Environment*, *44*(27), 3343–3345. https://doi.org/10.1016/j.atmosenv.2010.04.032

Ciais, P., Sabine, C., Bala, G., Bopp, L., Brovkin, V., al, e., & House, J. I. (2014). Carbon and Other Biogeochemical Cycles. In O. Edenhofer, R. Pichs-Madruga, Y. Sokona, E. Farahani, S. Kadner, K. Seyboth, A. Adler, I. Baum, S. Brunner, P. Eickemeier, B. Kriemann, J. Savolainen, S. Schlömer, C. von Stechow, Z. T, & M. J.C (Eds.), *Climate Change 2013* (pp. 465–570). Cambridge University Press.

Dean, J. F., Middelburg, J. J., Röckmann, T., Aerts, R., Blauw, L. G., Egger, M., Jetten, M. S. M., de Jong, A. E. E., Meisel, O. H., Rasigraf, O., Slomp, C. P., in't Zandt, M. H., & Dolman, A. J. (2018). Methane Feedbacks to the Global Climate System in a Warmer World. *Reviews of Geophysics*, *56*(1), 207–250. https://doi.org/10.1002/2017RG000559

de_Richter, R., Ming, T., Davies, P., Liu, W., & Caillol, S. (2017). Removal of non-CO2 greenhouse gases by large-scale atmospheric solar photocatalysis. *Progress in Energy and Combustion Science*, *60*, 68–96. https://doi.org/10.1016/j.pecs.2017.01.001

Emmerling, J., Drouet, L., Wijst, K.-I. van der, Vuuren, D. van, Bosetti, V., & Tavoni, M. (2019). The role of the discount rate for emission pathways and negative emissions. *Environmental Research Letters*, *14*(10), 104008. https://doi.org/10.1088/1748-9326/ab3cc9

Forster, P., Storelvmo, T., Armour, K., Collins, W., Dufresne, J.-L., Frame, D., Lunt, D., Mauritsen, T., Palmer, M., Watanabe, M., Wild, M., & Zhang, H. (2021). The Earth's Energy Budget, Climate Feedbacks, and Climate Sensitivity. In V. Masson-Delmotte, P. Zhai, A. Pirani, S. L. Connors, C. Péan, S. Berger, N. Caud, Y. Chen, L. Goldfarb, M. I. Gomis, M. Huang, K. Leitzell, E. Lonnoy, J. B. R. Matthews, T. K. Maycock, T. Waterfield, O. Yelekçi, R. Yu, & B. Zhou (Eds.), *Climate Change 2021: The Physical Science Basis. Contribution of Working Group I to the Sixth Assessment Report of the Intergovernmental Panel on Climate Change*. Cambridge University Press. https://doi.org/10.1017/9781009157896.009

Fuss, S., Lamb, W. F., Callaghan, M. W., Hilaire, J., Creutzig, F., Amann, T., Beringer, T., Garcia, W. d. O., Hartmann, J., Khanna, T., Luderer, G., Nemet, G. F., Rogelj, J., Smith, P., Vicente, J. L. V., Wilcox, J., Dominguez, M. d. M. Z., & Minx, J. C. (2018). Negative emissions—Part 2: Costs, potentials and side effects. *Environmental Research Letters*, *13*(6), 063002. https://doi.org/10.1088/1748-9326/aabf9f

Goulder, L. H., & Mathai, K. (2000). Optimal CO2 Abatement in the Presence of Induced Technological Change. *Journal of Environmental Economics and Management*, *39*(1), 1–38. https://EconPapers.repec.org/RePEc:eee:jeeman:v:39:y:2000:i:1:p:1-38

Harmsen, M., van Vuuren, D. P., Bodirsky, B. L., Chateau, J., Durand-Lasserve, O., Drouet, L., Fricko, O., Fujimori, S., Gernaat, D. E. H. J., Hanaoka, T., Hilaire, J., Keramidas, K., Luderer, G., Moura, M. C. P., Sano, F., Smith, S. J., & Wada, K. (2020). The role of methane in future climate strategies: Mitigation potentials and climate impacts. *Climatic Change*, *163*(3), 1409–1425. https://doi.org/10.1007/s10584-019-02437-2

Heinze, C., Blenckner, T., Martins, H., Rusiecka, D., Döscher, R., Gehlen, M., Gruber, N., Holland, E., Hov, Ø., Joos, F., Matthews, J. B. R., Rødven, R., & Wilson, S. (2021). The quiet crossing of ocean tipping points. *Proceedings of the National Academy of Sciences*, *118*(9), e2008478118. https://doi.org/10.1073/pnas.2008478118

Jackson, R. B., Solomon, E. I., Canadell, J. G., Cargnello, M., & Field, C. B. (2019). Methane removal and atmospheric restoration. *Nature Sustainability*, *2*(6), 436–438. https://doi.org/10.1038/s41893-019-0299-x

Jackson, R. B., Abernethy, S., Canadell, J. G., Cargnello, M., Davis, S. J., Féron, S., Fuss, S., Heyer, A. J., Hong, C., Jones, C. D., Damon Matthews, H., O'Connor, F. M., Pisciotta, M., Rhoda, H. M., De Richter, R., Solomon, E. I., Wilcox, J. L., & Zickfeld, K. (2021). Atmospheric methane removal: A research agenda. *Philosophical Transactions of the Royal Society A: Mathematical, Physical and Engineering Sciences*, *379*(2210), 20200454. https://doi.org/10.1098/rsta.2020.0454

Johansson, D. J. A. (2012). Economics- and physical-based metrics for comparing greenhouse gases. *Climatic Change*, *110*(1-2), 123–141. https://doi.org/10.1007/s10584-011-0072-2

Joos, F., Roth, R., Fuglestvedt, J. S., Peters, G. P., Enting, I. G., von Bloh, W., Brovkin, V., Burke, E. J., Eby, M., Edwards, N. R., Friedrich, T., Frölicher, T. L., Halloran, P. R., Holden, P. B., Jones, C., Kleinen, T., Mackenzie, F. T., Matsumoto, K., Meinshausen, M., … Weaver, A. J. (2013). Carbon dioxide and climate impulse response functions for the computation of greenhouse gas metrics: A multi-model analysis. *Atmospheric Chemistry and Physics*, *13*(5), 2793–2825. https://doi.org/10.5194/acp-13-2793-2013

Kleinen, T., Gromov, S., Steil, B., & Brovkin, V. (2021). Atmospheric methane underestimated in future climate projections. *Environmental Research Letters*, *16*(9), 094006. https://doi.org/10.1088/1748-9326/ac1814

Köberle, A. C. (2019). The Value of BECCS in IAMs: A Review. *Current Sustainable/Renewable Energy Reports*, *6*(4), 107–115. https://doi.org/10.1007/s40518-019-00142-3

Lackner, K. S. (2020). Practical constraints on atmospheric methane removal. *Nature Sustainability*, *3*(5), 357–357. https://doi.org/10.1038/s41893-020-0496-7

Lee, J.-Y., Marotzke, J., Bala, G., Cao, L., Corti, S., Dunne, J., Engelbrecht, F., Fischer, E., Fyfe, J., Jones, C., Maycock, A., Mutemi, J., Ndiaye, O., Panickal, S., & Zhou, T. (2021). Future Global Climate: Scenario-Based Projections and Near-Term Information. In V. Masson-Delmotte, P. Zhai, A. Pirani, S. L. Connors, C. Péan, S. Berger, N. Caud, Y. Chen, L. Goldfarb, M. I. Gomis, M. Huang, K. Leitzell, E. Lonnoy, J. B. R. Matthews, T. K. Maycock, T. Waterfield, O. Yelekçi, R. Yu, & B. Zhou (Eds.), *Climate Change 2021: The Physical Science Basis. Contribution of Working Group I to the Sixth Assessment Report of the Intergovernmental Panel on Climate Change*. Cambridge University Press. https://doi.org/10.1017/9781009157896.006

Li, Q., Meidan, D., Hess, P., Añel, J. A., Cuevas, C. A., Doney, S., Fernandez, R. P., Van Herpen, M., Höglund-Isaksson, L., Johnson, M. S., Kinnison, D. E., Lamarque, J.-F., Röckmann, T., Mahowald,

N. M., & Saiz-Lopez, A. (2023). Global environmental implications of atmospheric methane removal through chlorine-mediated chemistry-climate interactions. *Nature Communications*, *14*(1), 4045. https://doi.org/10.1038/s41467-023-39794-7

McKeough, P. (2022). A case for ensuring reductions in CO2 emissions are given priority over reductions in CH4 emissions in the near term. *Climatic Change*, *174*(1-2), 4. https://doi.org/10.1007/s10584-022-03428-6

Methane emissions in livestock and rice systems. (2023, September 25). FAO. https://doi.org/10.4060/cc7607en

Meyer, A. L. S., Bentley, J., Odoulami, R. C., Pigot, A. L., & Trisos, C. H. (2022). Risks to biodiversity from temperature overshoot pathways. *Philosophical Transactions of the Royal Society B: Biological Sciences*, *377*(1857), 20210394. https://doi.org/10.1098/rstb.2021.0394

Ming, T., Gui, H., Shi, T., Xiong, H., Wu, Y., Shao, Y., Li, W., Lu, X., & De Richter, R. (2021). Solar chimney power plant integrated with a photocatalytic reactor to remove atmospheric methane: A numerical analysis. *Solar Energy*, *226*, 101–111. https://doi.org/10.1016/j.solener.2021.08.024

Ming, T., Li, W., Yuan, Q., Davies, P., de Richter, R., Peng, C., Deng, Q., Yuan, Y., Caillol, S., & Zhou, N. (2022a). Perspectives on removal of atmospheric methane. *Advances in Applied Energy*, *5*, 100085. https://doi.org/10.1016/j.adapen.2022.100085

Ming, T., Xiong, H., Shi, T., Wu, Y., Wang, C., Wen, Y., Li, W., De Richter, R., & Zhou, N. (2022b). A novel green technology: Reducing carbon dioxide and eliminating methane from the atmosphere. *International Journal of Energy Research*, *46*(14), 20107–20120. https://doi.org/10.1002/er.8675

Myhre, G., Shindell, D., Bréon, F.-M., Collins, W., Fuglestvedt, J., Huang, J., Koch, D., Lamarque, J.-F., Lee, D., Mendoza, B., Nakajima, T., Robock, A., Stephens, G., Takemura, T., & Zhang, H. (2013). Anthropogenic and natural radiative forcing. In T. F. Stocker, D. Qin, G.-K. Plattner, M. Tignor, S. K. Allen, J. Doschung, A. Nauels, Y. Xia, V. Bex, & P. M. Midgley (Eds.), *Climate Change 2013: The Physical Science Basis. Contribution of Working Group I to the Fifth Assessment Report of the Intergovernmental Panel on Climate Change* (pp. 659–740). Cambridge University Press. https://doi.org/10.1017/CBO9781107415324.018

Nesje, F., Drupp, M. A., Freeman, M. C., & Groom, B. (2023). Philosophers and economists agree on climate policy paths but for different reasons. *Nature Climate Change*, *13*(6), 515–522. https://doi.org/10.1038/s41558-023-01681-w

Nisbet, E. G., Fisher, R. E., Lowry, D., France, J. L., Allen, G., Bakkaloglu, S., Broderick, T. J., Cain, M., Coleman, M., Fernandez, J., Forster, G., Griffiths, P. T., Iverach, C. P., Kelly, B. F. J., Manning, M. R., Nisbet-Jones, P. B. R., Pyle, J. A., Townsend-Small, A., al-Shalaan, A., … Zazzeri, G. (2020). Methane Mitigation: Methods to Reduce Emissions, on the Path to the Paris Agreement. *Reviews of Geophysics*, *58*(1), e2019RG000675. https://doi.org/10.1029/2019RG000675

Nisbet-Jones, P. B. R., Fernandez, J. M., Fisher, R. E., France, J. L., Lowry, D., Waltham, D. A., Woolley Maisch, C. A., & Nisbet, E. G. (2021). Is the destruction or removal of atmospheric methane a worthwhile option? *Philosophical Transactions of the Royal Society A: Mathematical, Physical and Engineering Sciences*, *380*(2215), 20210108. https://doi.org/10.1098/rsta.2021.0108

Oeste, F. D., de Richter, R., Ming, T., & Caillol, S. (2017). Climate engineering by mimicking natural dust climate control: The iron salt aerosol method. *Earth System Dynamics*, *8*(1), 1–54. https://doi.org/10.5194/esd-8-1-2017

Parker, A., & Irvine, P. J. (2018). The Risk of Termination Shock From Solar Geoengineering. *Earth's Future*, *6*(3), 456–467. https://doi.org/10.1002/2017EF000735

Prado, A., & Mac Dowell, N. (2023). The cost of permanent carbon dioxide removal. *Joule*, *7*(4), 700–712. https://doi.org/10.1016/j.joule.2023.03.006

Ramsey, F. P. (1928). A Mathematical Theory of Saving. *The Economic Journal*, *38*(152), 543–559. https://doi.org/10.2307/2224098

Ritchie, P. D. L., Clarke, J. J., Cox, P. M., & Huntingford, C. (2021). Overshooting tipping point thresholds in a changing climate. *Nature*, *592*(7855), 517–523. https://doi.org/10.1038/s41586-021-03263-2

Saunois, M., Stavert, A. R., Poulter, B., Bousquet, P., Canadell, J. G., Jackson, R. B., Raymond, P. A., Dlugokencky, E. J., Houweling, S., Patra, P. K., Ciais, P., Arora, V. K., Bastviken, D., Bergamaschi, P., Blake, D. R., Brailsford, G., Bruhwiler, L., Carlson, K. M., Carrol, M., … Zhuang, Q. (2020). The Global Methane Budget 2000–2017. *Earth System Science Data*, *12*(3), 1561–1623. https://doi.org/10.5194/essd-12-1561-2020

Strefler, J., Bauer, N., Humpenöder, F., Klein, D., Popp, A., & Kriegler, E. (2021). Carbon dioxide removal technologies are not born equal. *Environmental Research Letters*, *16*(7), 074021. https://doi.org/10.1088/1748-9326/ac0a11

Szopa, S., Naik, V., Adhikary, B., Artaxo, P., Berntsen, T., Collins, W., Fuzzi, S., Gallardo, L., Kiendler-Scharr, A., Klimont, Z., Liao, H., Unger, N., & Zanis, P. (2021). Short-Lived Climate Forcers. In V. Masson-Delmotte, P. Zhai, A. Pirani, S. L. Connors, C. Péan, S. Berger, N. Caud, Y. Chen, L. Goldfarb, M. I. Gomis, M. Huang, K. Leitzell, E. Lonnoy, J. B. R. Matthews, T. K. Maycock, T. Waterfield, O. Yelekçi, R. Yu, & B. Zhou (Eds.), *Climate Change 2021: The Physical Science Basis. Contribution of Working Group I to the Sixth Assessment Report of the Intergovernmental Panel on Climate Change*. Cambridge University Press. https://doi.org/10.1017/9781009157896.008

Tanaka, K., Boucher, O., Ciais, P., Daniel J. A. Johansson, Johansson, D. J., Daniel J. A. Johansson, Morfeldt, J., & Morfeldt, J. (2020). Cost-effective implementation of the Paris Agreement using flexible greenhouse gas metrics
MAG ID: 3165110065.

Tanaka, K., Johansson, D. J. A., O'Neill, B. C., & Fuglestvedt, J. S. (2013). Emission metrics under the 2 °C climate stabilization target. *Climatic Change*, *117*(4), 933–941. https://doi.org/10.1007/s10584-013-0693-8

Tanaka, K., Kriegler, E., Bruckner, T., Hooss, G., Knorr, W., Raddatz, T., & Tol, R. (2007). Aggregated Carbon cycle, atmospheric chemistry and climate model (ACC2): Description of forward and inverse mode, 14069106. https://doi.org/10.17617/2.994422

Thiery, W., Lange, S., Rogelj, J., Schleussner, C.-F., Gudmundsson, L., Seneviratne, S. I., Frieler, K., Emanuel, K., Geiger, T., Bresch, D. N., Zhao, F., Willner, S. N., Buchner, M., Volkholz, J., Bauer, N., Chang, J., Dury, M., Francois, L., Grillakis, M., … Wada, Y. (n.d.). Age-dependent extreme event exposure.

van Vuuren, D. P., den Elzen, M. G. J., Lucas, P. L., Eickhout, B., Strengers, B. J., van Ruijven, B., Wonink, S., & van Houdt, R. (2007). Stabilizing greenhouse gas concentrations at low levels: An assessment of reduction strategies and costs. *Climatic Change*, *81*(2), 119–159. https://doi.org/10.1007/s10584-006-9172-9

Wang, Y., Ming, T., Li, W., Yuan, Q., De Richter, R., Davies, P., & Caillol, S. (2022). Atmospheric removal of methane by enhancing the natural hydroxyl radical sink. *Greenhouse Gases: Science and Technology*, *12*(6), 784–795. https://doi.org/10.1002/ghg.2191

Xiong, H., Ming, T., Wu, Y., Li, W., Mu, L., de Richter, R., Yan, S., Yuan, Y., & Peng, C. (2023). Numerical analysis of a negative emission technology of methane to mitigate climate change. *Solar Energy*, *255*, 416–424. https://doi.org/10.1016/j.solener.2023.02.048

Zhang, Z., Zimmermann, N. E., Stenke, A., Li, X., Hodson, E. L., Zhu, G., Huang, C., & Poulter, B. (2017). Emerging role of wetland methane emissions in driving 21st century climate change. *Proceedings of the National Academy of Sciences*, *114*(36), 9647–9652. https://doi.org/10.1073/pnas.1618765114

6 Supplements

6.1 Generic CDR

6.1.1 Implementation in GET-ACC2

As for the generic MR, we model a generic CDR with constant unit costs c [\$/tCO$_2$], total costs CRC[\$], annual potential p. g is the maximum geometric growth rate, set to 15% which is the standard growth rate in the model, and a is the maximum arithmetic growth rate, set to 370 MtCO$_2$ per year, in order to reach full potential (typically around 10 GtCO$_2$/year, depending on the scenario) within a decade. For comparison, the growth of the CCS capacity in GET-ACC2 is constrained to reproduce the rate of CCS deployment is the ENGAGE scenario database (Bertram et al., 2021), with an annual arithmetic growth rate of 550 MtCO$_2$/year, yielding a much slower deployment of CCS (including BECCS) than of the generic CDR.

$$CRC(t) = CR(t) \cdot c \quad \text{(E.1)}$$

$$CR(t) \leq p \quad \text{(E.2)}$$

$$CR(t+1) \leq CR(t) \cdot (1+g) + a \quad \text{(E.3)}$$

$$CR(t) = 0 \text{ for t <2030} \quad \text{(E.4)}$$

6.1.2 Generic CDR equivalent to BECCS

As for the generic MR, we estimate the potential and costs of the generic CDR to play the same role as BECCS with regard to cumulative gross CO$_2$ emissions and policy costs (Figure IV.9).

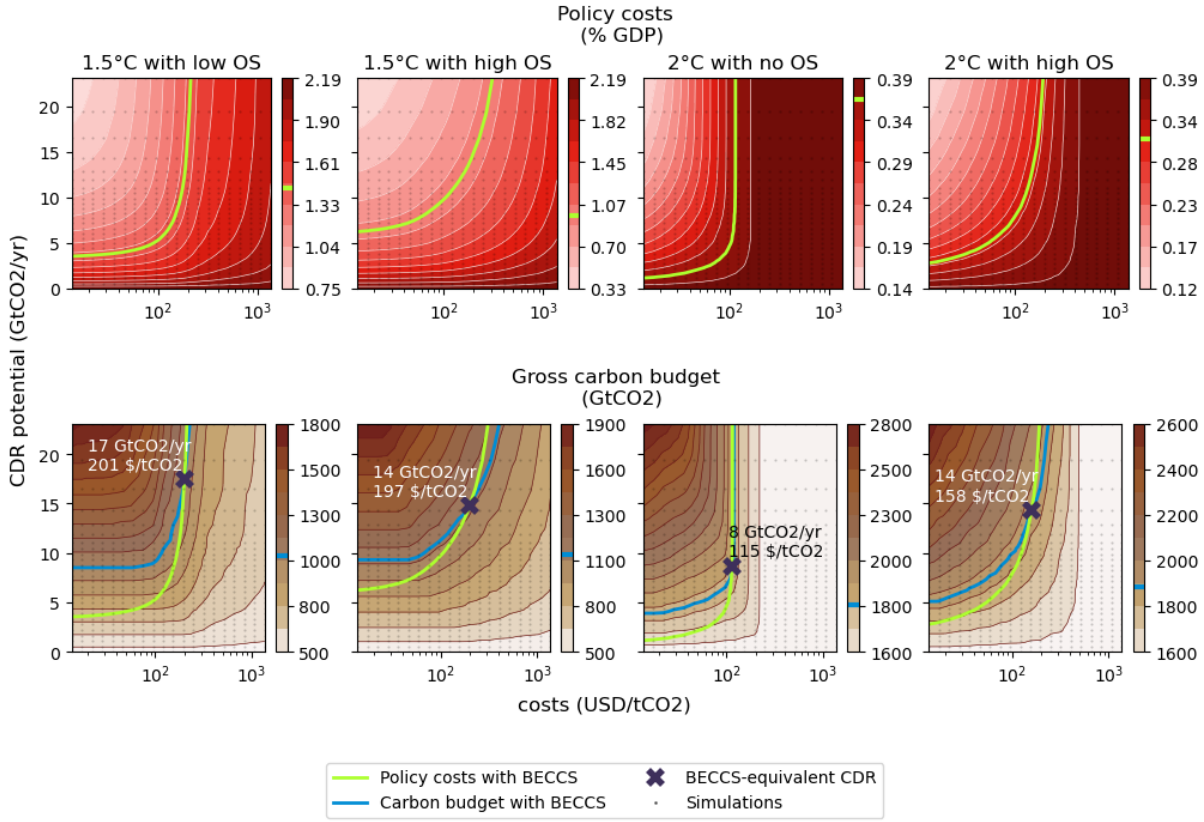

Figure IV.9: Policy costs and gross carbon budgets across the 21st century depending on generic CDR technology for different climate target cases, when no BECCS are available. **X-axis** (log scale): unit cost of carbon dioxide removal, in USD per tCO_2. **Y-axis**: maximum annual carbon dioxide removal, in $GtCO_2$ per year. **Top panels:** The color corresponds to policy costs, defined as the net present values of future energy production costs and consumption losses as a percentage of GDP, compared to the no-policy scenario. The green curve is the contour line of the policy costs when BECCS is available. **Bottom panels:** The color corresponds to the gross carbon budgets, defined as the cumulative CO_2 emissions across the 21st century excluding land-use and CDR. The blue curve is the contour line of the gross carbon budgets when BECCS is available. The intersection with the green curve, marked with a **cross**, defines the cost (in $\$/tCO_2$) and potential (in $GtCO_2$/year) of a CDR technology that could replace BECCS when the two metrics are considered together. The **black dots** are the data points between which the policy costs and the carbon budgets are interpolated.

6.2 Temperature feedback on natural methane emissions

6.2.1 Natural methane emissions in ACC2

In the original version of ACC2, natural methane emissions are assumed to be a constant N [$MtCH_4.year^{-1}$]. The ACC2 model parameters are estimated with a model inversion following Tarantola's inverse estimation theory. The inverse mode uses prior values of data and parameters, as well as uncertainty ranges, to estimate the posterior (most likely) set of values for both data and parameters given the model equations. The data used are global-annual-mean time series of GHG concentrations, ocean and land CO_2 uptakes and surface air temperature until 2000. As a consequence, after changing the equations of the model, the most likely values of

parameters must be recalculated using the inverse mode of the model.

Here, we want natural methane emissions to be equal to $N + \alpha\delta T(t)$, where α is the linear increase coefficient of global natural methane emissions with global mean temperature change found by T. Kleinen and his co-authors (Kleinen et al., 2021), thereafter called the α-feedback. The value of N should then be estimated using the inverse mode (Tanaka et al., 2007, 2009). However, we did not apply this step for this study. Although this limits the internal consistency of the model, parameter estimation using the inverse mode was not compatible with data from the 2000-2020 period, which is not yet included in the calibration stage.

6.2.2 Attempt using ACC2 inverse mode

When running the inverse mode with the implementation of the temperature feedback, the only modified parameters are the posterior value of N and the posterior value of preindustrial atmospheric lifetime of methane with respect to OH depletion.

N increases by 12%, from 320 to 358 $MtCH_4.year^{-1}$, moving further away from the uncertainty range estimated for natural emissions estimated from top-down assessments (Saunois et al., 2020), 194-267 $MtCH_4.year^{-1}$. Adding the α-feedback to the model equations does not improve the consistency between data and equations, as it increases the cost function which describes the mismatch between data, parameters and equations. This new parameterisation strongly affects the historical 2000-2020 period, since ACC2 is only calibrated until 2000. Because of the α-feedback, total natural CH4 emissions amount to $N + \alpha\delta T(t)$. With this new parameterization, in 2020, the temperature change approaches 1.2°C. Thus, total natural CH4 emissions are worth 450 Tg in 2020. This is 40% more than the 319Tg that we had when not considering the feedback, and this value contradicts the literature range (Saunois et al., 2020). In the future, for all mitigation scenarios that we assessed, the temperature change is typically below 2.15°C. Thus, the maximum effect of the α-feedback on future emissions is an increase of 161 $TgCH_4$/year compared to the preindustrial era, or 71.3 Tg compared to 2020. Therefore, future temperatures increase natural methane emissions by at most 15% above the 450 Tg of natural CH4 emissions in 2020. Thus, with the α-feedback, natural emissions of methane become too high, and the future temperature scenario does not have a strong influence.

The methane lifetime with regard to OH depletion decreases from 8.54 years to 7.54 years, thus a 12% decline. The decline of the methane lifetime is therefore roughly compensating the maximum impact of future α-feedback on methane emissions (15%). To sum up, this setting has more important effects on the 2000-2020 period than on the future, which prevents us from

isolating the effect of the α-feedback, and is not suited to our analysis.

Alternatively, one can consider the α-feedback from 2000 onwards only. With this setting, global warming reaches more than 1.34°C compared to preindustrial levels in 2021, which is inconsistent with historical records, and makes the 1.5°C target with low overshoot virtually impossible to achieve.

This is why, until the future extension of the model calibration period to the previous two decades, we limit ourselves to a simple feedback model starting from 2020 onwards, without changing the posterior parameters values compared to the no α-feedback case.

6.2.3 Discussion of the feedback magnitude

Comparison with the methane-climate feedback estimates in IPCC As explained by T. Kleinen and his coauthors (Kleinen et al., 2021), the α-feedback magnitude of 75 $TgCH_4.K^{-1}.year^{-1}$ is in the higher range of the literature and is notably higher than the CMIP6 estimates (Meinshausen et al., 2020).

It can be compared with the range of wetland methane-feedback and permafrost-feedback estimates reported by the IPCC (Canadell et al., 2021): 0.03 ± 0.01 $W.m^{-2}.K^{-1}$ for wetlands (up to 0.01-0.16 $W.m^{-2}.K^{-1}$ if the increased CO_2 concentration is considered), and 0.01 [0.003 to 0.04, 5-95% range] $W.m^{-2}.K^{-1}$ for permafrost.

The climate feedback is defined as $\frac{\delta N}{\delta x}\frac{dx}{dT}$ where $\frac{\delta N}{\delta x}$ is the top-of-atmosphere energy balance in response to a change in x induced by a change in surface temperature T.

We can find an approximation of the climate feedback corresponding to the α-feedback using the ACC2 model formulation of the radiative forcing RF, which corresponds to the net heat flux at the top of the atmosphere after the stratosphere has returned to equilibrium (Kriegler, 2005; Tanaka et al., 2007).

We have $\frac{\delta RF}{\delta c_{CH4}} = \mu_{CH4}\frac{1}{2\sqrt{c_{CH4}}}$ where c_{CH4} is the atmospheric methane concentration, μ_{CH4} is a constant equal to 0.036 $W.m^{-2}.ppb^{0.5}$ (neglecting the overlap with N_2O absorption band).

The atmospheric methane concentration follows an exponential decay law, $\frac{dc_{CH4}}{dt} = \frac{e}{\nu} - \frac{c_{CH4}}{\tau}$, where e is the total methane emissions (Tg/year), τ is the methane atmospheric lifetime (9 years) and ν is the mass to concentration conversion factor for methane, equal to 2.746 Tg/ppb. At equilibrium, we thus have $c_{CH4} = \tau.\frac{e}{\nu}$. We thus write:

$\frac{dc_{CH4}}{dT} = \frac{\tau}{\nu}\frac{de}{dT} = \tau\frac{\alpha}{\nu}$.

Finally, it yields: $\frac{\delta RF}{\delta c_{CH4}}\frac{dc_{CH4}}{dt} = \mu_{CH4}\frac{1}{2\sqrt{c_{CH4}}}\tau\frac{\alpha}{\nu} = 0.1$ W.m^{-2}.K^{-1}. The α-feedback magnitude estimated by Kleinen et al. is thus above IPCC range. Here, we implement their simple linear feedback in the model for convenience and to assess the effect on methane removal.

Comparison with the carbon cycle feedbacks The increase of temperature and atmospheric CO_2 concentration due to anthropogenic emissions disturb the global carbon cycle. Although the mechanisms involved are complex and non-linear, the modeled response of land and ocean carbon sinks to anthropogenic perturbations from earth system models can be described using linear feedbacks parameters β and γ (Canadell et al., 2021), with subscripts L for land and O for ocean:

$$\Delta C_L = \beta_L \Delta CO_2 + \gamma_L \Delta T$$

$$\Delta C_O = \beta_O \Delta CO_2 + \gamma_O \Delta T$$

The $\beta - f$eedback parameter describe the increased ocean or land carbon uptake following the increase in atmospheric concentration, and is positive for all CMIP6 models. The γ-feedback parameter describes the temperature effect on land or ocean carbon uptake, and is likely to be negative for both although there are large variations across CMIP6 models, in particular for the land sink. The IPCC reports a mean value for the total temperature-feedback $\gamma_O + \gamma_L$ of -50.25 [± 34.5] PgC.K^{-1} across models (Canadell et al., 2021).

There is no straightforward way of comparing the α-feedback magnitude with the γ-feedback as the first one describes an increase of a flux of methane emissions whereas the second one describes the change of a carbon stock. Still, since the carbon-cycle feedbacks are estimated in a quasi-equilibrium framework, we suggest to compare them with the equilibrium increase of atmospheric methane burden at equilibrium: $\frac{dq_{CH4}}{dT} = \tau\frac{de}{dT} = \tau\alpha = 675$ TgCH$_4$.K^{-1} where q is the atmospheric methane burden (see *supra*). Hence, a warming of 1°C increases the atmospheric methane burden by 675 TgCH$_4$ and the CO_2 burden by 50 PgC, thus a ratio of 272 gCO$_2$/gCH$_4$ which is lower than the atmospheric mass ratio between CO_2 and CH_4, equal to 640. This analysis therefore suggests that these climate feedbacks increase CH_4 concentration more than CO_2 concentration in relative terms.

6.3 Surplus loss as a proxy for consumption losses

We assume that the surplus loss, computed as the sum of energy system costs and energy consumption losses (at each time step), is proportional to the general consumption loss of the economy. Figure IV.11 shows that energy system costs are proportional to consumption losses for the WITCH model but not for the REMIND-MAgPIE model. Then, Figure IV.10 shows that varying the value of the proportionality coefficient from 1 to 5 has little influence on the shape of the utility loss.

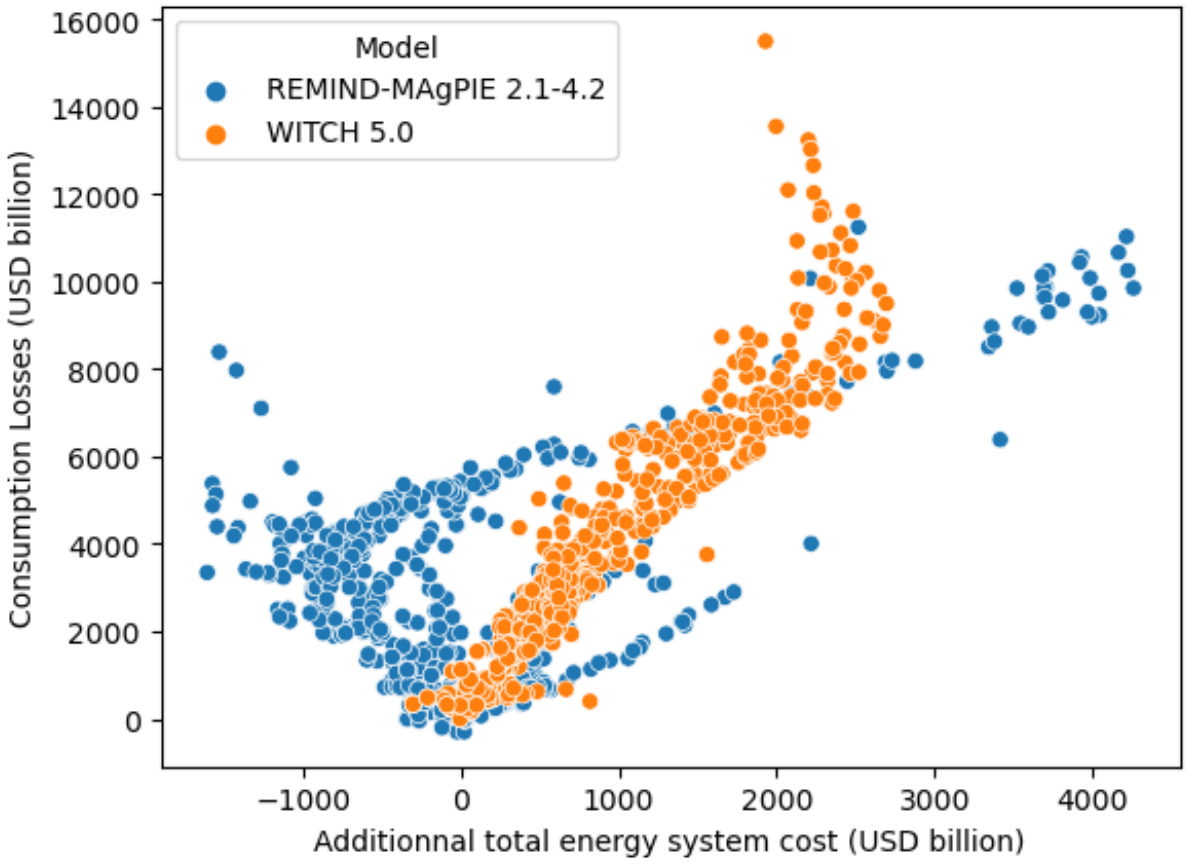

Figure IV.10: Global additional total energy system costs and consumer losses in the engage database. There is one point per timestep, for all scenarios from the ENGAGE database (Bertram et al., 2021), from the two models for which these values are available.

References

Bertram, C., Riahi, K., Hilaire, J., Bosetti, V., Drouet, L., Fricko, O., Malik, A., Nogueira, L. P., van der Zwaan, B., van Ruijven, B., van Vuuren, D., Weitzel, M., Longa, F. D., de Boer, H.-S., Emmerling, J., Fosse, F., Fragkiadakis, K., Harmsen, M., Keramidas, K., … Luderer, G. (2021). Energy

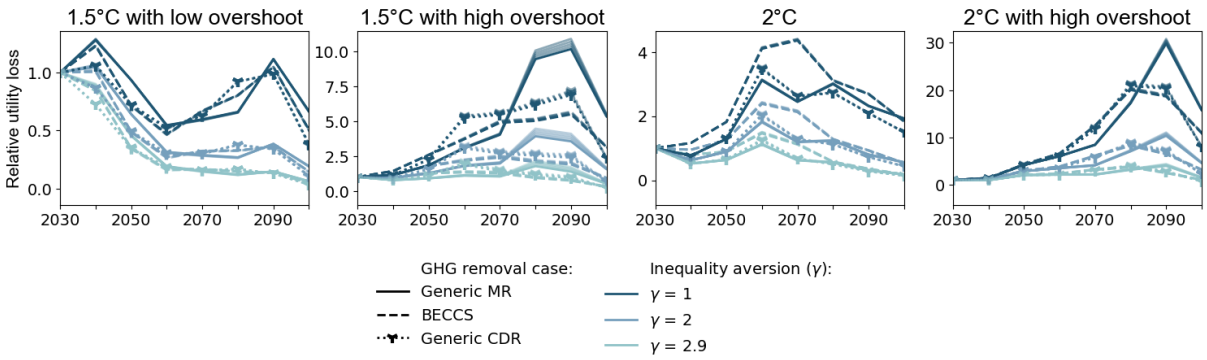

Figure IV.11: Utility loss (relative to 2030), for different values of the inequality aversion coefficient γ, assuming that the consumption loss is proportionate to the policy costs with a proportionality coefficient that takes the values 1 (dark line) and 2,3,4,5 (lighter lines).

system developments and investments in the decisive decade for the Paris Agreement goals. *Environmental Research Letters*, *16*(7), 074020. https://doi.org/10.1088/1748-9326/ac09ae

Canadell, J., Monteiro, P., Costa, M., Cotrim da Cunha, L., Cox, P., Eliseev, A., Henson, S., Ishii, M., Jaccard, S., Koven, C., Lohila, A., Patra, P., Piao, S., Rogelj, J., Syampungani, S., Zaehle, S., & Zickfeld, K. (2021). Global Carbon and other Biogeochemical Cycles and Feedbacks. In V. Masson-Delmotte, P. Zhai, A. Pirani, S. L. Connors, C. Péan, S. Berger, N. Caud, Y. Chen, L. Goldfarb, M. I. Gomis, M. Huang, K. Leitzell, E. Lonnoy, J. B. R. Matthews, T. K. Maycock, T. Waterfield, O. Yelekçi, R. Yu, & B. Zhou (Eds.), *Climate Change 2021: The Physical Science Basis. Contribution of Working Group I to the Sixth Assessment Report of the Intergovernmental Panel on Climate Change*. Cambridge University Press. https://doi.org/10.1017/9781009157896.007

Kleinen, T., Gromov, S., Steil, B., & Brovkin, V. (2021). Atmospheric methane underestimated in future climate projections. *Environmental Research Letters*, *16*(9), 094006. https://doi.org/10.1088/1748-9326/ac1814

Kriegler, E. (2005). *Imprecise probability analysis for integrated assessment of climate change* [doctoralthesis]. Universität Potsdam.

Meinshausen, M., Nicholls, Z. R. J., Lewis, J., Gidden, M. J., Vogel, E., Freund, M., Beyerle, U., Gessner, C., Nauels, A., Bauer, N., Canadell, J. G., Daniel, J. S., John, A., Krummel, P. B., Luderer, G., Meinshausen, N., Montzka, S. A., Rayner, P. J., Reimann, S., … Wang, R. H. J. (2020). The shared socio-economic pathway (SSP) greenhouse gas concentrations and their extensions to 2500. *Geoscientific Model Development*, *13*(8), 3571–3605. https://doi.org/10.5194/gmd-13-3571-2020

Saunois, M., Stavert, A. R., Poulter, B., Bousquet, P., Canadell, J. G., Jackson, R. B., Raymond, P. A., Dlugokencky, E. J., Houweling, S., Patra, P. K., Ciais, P., Arora, V. K., Bastviken, D., Bergamaschi, P., Blake, D. R., Brailsford, G., Bruhwiler, L., Carlson, K. M., Carrol, M., … Zhuang, Q. (2020). The Global Methane Budget 2000–2017. *Earth System Science Data*, *12*(3), 1561–1623. https://doi.org/10.5194/essd-12-1561-2020

Tanaka, K., Kriegler, E., Bruckner, T., Hooss, G., Knorr, W., Raddatz, T., & Tol, R. (2007). Aggregated Carbon cycle, atmospheric chemistry and climate model (ACC2): Description of forward and inverse mode, 14069106. https://doi.org/10.17617/2.994422

Tanaka, K., Raddatz, T., O'Neill, B. C., & Reick, C. H. (2009). Insufficient forcing uncertainty underestimates the risk of high climate sensitivity. *Geophysical Research Letters*, *36*(16), L16709. https://doi.org/10.1029/2009GL039642

CHAPTER V

GENERAL CONCLUSION

In this thesis, I have explored three different aspects of climate change mitigation strategies in three successive chapters. I started by discussing the possible effects of recovery packages on future emission pathways. I then examined deployment scenarios for two global warming mitigation technologies: CO_2 removal from terrestrial enhanced weathering of basalt, and methane removal. The common thread running through the three chapters is the use of forward-looking models that quantify the evolution of the energy system required to reduce greenhouse gas emissions.

1 Green recovery

The first chapter hinges on an ex-post analysis of mitigation scenarios from IAMs, which I compared with an inventory of low-carbon investment packages contained in post-COVID-19 recovery plans. The question at hand was whether the scale of stimulus investments is sufficient to effectively initiate the energy transition. My comparison between investments projected in the modelled decarbonization scenarios and those outlined in the stimulus plans suggested that we were significantly far from the mark, representing less than 6-24% (depending on the model) of the required emission reduction in 2030. The chapter also explained that our focus on low-carbon investments in existing IAM scenarios is not entirely satisfactory, because emission reductions in IAMs are driven by carbon prices. These carbon prices incentivize low-carbon investments, but also disincentivize carbon-intensive energy supply and reduce energy demand. Therefore, emission reductions are only partly caused by low-carbon investments in IAMs. To overcome this issue, we considered that the result of our calculation is an upper bound of the

emission reduction that could be caused by low-carbon investments, overestimating the actual emission reduction. However, it could also be theoretically possible to have a greater emissions reduction for a given level of investments than assumed with this method. Despite these caveats, a comparison with two other studies confirmed our diagnosis that recovery investments were likely to have a limited impact on post-COVID-19 emissions.

The results would have been strengthened by completing the ex-post analysis of IAM results with investment-driven scenarios, explicitly simulating public investment policies and the relevant interactions with private finance. Analyses of the climate effects of post-COVID-19 recovery plans have adopted different perspectives, either comparing the possible effects of different policies, or analyzing the policies actually implemented. The first group of studies advocated combining economic recovery and energy transition, and proposed instruments to promote this synergy (Andrijevic et al., 2020; Gawel & Lehmann, 2020; Hepburn et al., 2020; Hourcade et al., 2021; Kuzemko et al., 2020). Another group of studies simulated recovery scenarios corresponding to different hypothetical stimulus measures (Dafnomilis et al., 2022; P. M. Forster et al., 2020; Lahcen et al., 2020; Pollitt et al., 2021), following the orders of magnitude of the announced plans (Rochedo et al., 2021; Shan et al., 2021; Van De Ven et al., 2022), to assess their possible outcomes in terms of growth, emissions and employment. Yet, none of these modeling studies have simulated actual stimulus packages, except for the study by Rochedo et al. (Rochedo et al., 2021), which was based on the amount of low-carbon investments actually announced. The Rochedo study did not represent their true sectoral distribution and instead used the distribution recommended by the IEA (IEA, 2021). Later studies were published after our article was written. The study of Van de Ven et al. (Van De Ven et al., 2022) was based on amounts actually committed, but studied different sectoral breakdowns. Finally, a recent OECD publication investigates the future impact of recovery measures supporting low-carbon technologies, implemented within a large-scale model with a high level of technological disaggregation (Aulie et al., 2023) Their inventory of recovery policies is more up to date than that of my analysis. Their inventory identified $1.29 trillion targeted to low-carbon technologies worldwide, while my inventory includes $0.511 trillion. Their simulations only include OECD and EU countries, which have invested $1.22 trillion. They suggest a reduction of CO_2 emissions by 1.15 $GtCO_2$/year in 2030 compared to the baseline, in OECD and EU countries. For comparison, using the linear relationships between investments and emission reductions from the first chapter, since the GDP forecast in 2030 is $62 trillion, my estimate of the emission reduction for the OECD and EU in 2030 corresponding to their estimate of the recovery packages is 1.0-5.2 $GtCO_2$/year, depending on the underlying model. Although the two estimates are relatively comparable, the underlying methods are fundamentally different, let alone the different cut-off dates of stimulus packages. Indeed, the OECD report stresses the contrasted

long-term and short-term impacts of different types of investment and subsidies on learning effects and technological spillovers to reduce emissions. For instance, research and development subsidies are assumed to be six times more efficient to reduce cumulative emissions until 2050 than direct investment to support technology adoption, underlining the added value of a dedicated modeling to quantitatively assess recovery policies.

2 Enhanced weathering

The second chapter focuses on assessing mitigation scenarios involving the application of basalt dust on natural areas, a carbon dioxide removal technology known as enhanced weathering (EW) that has not been studied extensively. In order to do this, I coupled a simple climate model with an energy system model. Subsequently, I developed a new enhanced weathering module, drawing from existing literature and integrating results from previous modeling research (Goll et al., 2021). The coupled model (GET-ACC2) was then employed to examine how the addition of the biotic CDR effect could alter the deployment of enhanced weathering in cost-optimal scenarios. We observe that the biotic effect makes a significant contribution. Furthermore, more basalt is applied when forest areas are included, which also increases the abiotic CDR. Adding forest application reduces the total policy costs and the marginal abatement costs of emissions. The need for bioenergy is also reduced, resulting in a lower bioenergy use and biomass price. The formulation of the climate objective plays an important role in these effects, which are more important when a temporary overshoot of the end-of-century target is allowed, and when this target is 1.5°C rather than 2°C. The increased profitability of EW in overshoot scenarios is due to the delay in mitigation efforts and comes at the expense of a higher temperature overshoot. The sensitivity of the model to parameters was assessed with a Morris sampling procedure. This procedure was useful in checking and improving the numerical validity of the model, which had been rendered unstable by certain nonlinear equations of the phosphorus cycle modulus. The model includes several notable simplifying assumptions that have facilitated its development but limit its realism: no spatial disaggregation to accurately represent the progressive application of basalt to areas with more difficult access, simplified weathering processes (**cipollaEffectsPrecipitationSeasonality2022**; Calabrese et al., 2022; Vicca et al., 2022), and no limitation considered on basalt supply, allowing very high extraction levels in the model. Besides, potentially harmful environmental side-effects of enhanced weathering have been reported and are discussed in the research led by Daniel Goll (Goll et al., 2021) which formed the basis for our study. These side-effects include the release of toxic heavy metals (Haque et al., 2020; Vienne et al., 2022), changes in soils and river pH, eutrophication of aquatic systems and health risks due to fine basalt particles (Santos et al.,

2023). They were not further assessed in this study but deserves attention particularly if the aerial application of basalt dust over forests were to be experimented.

The new model developed in this chapter has a certain room for improvement. In particular, improving the geographic disaggregation of the enhanced weathering emulator would be useful for two reasons. Firstly, it would enable a more realistic representation of the spreading logistic. Secondly, the interactions of EW with bioenergy crops and forests could then be explored at the local level. In our aggregated model, EW and bioenergy with carbon capture and storage (BECCS) are competing as concurrent methods of removing carbon dioxide. However, the use of EW to improve soil productivity could also make other CDR options such as BECCS or afforestation and reforestation (AR) more efficient and less land-intensive. The lack of land-use module in GET-ACC2 makes it unsuitable for a spatially-explicit description of enhanced weathering. Therefore, these synergies between EW, BECCS and AR remain to be further explored with a more appropriate model.

3 Methane removal

In the third chapter, I used the GET-ACC2 model to study methane removal by making use of the model's feature that the energy system is hard-linked with the climate system. This feature allows analyzing the role of methane removal technologies, in comparison with the roles of CDRs, under the mitigation pathways for the Paris temperature targets by directly considering the distinct short-lived nature of methane, which would not be properly investigated by most other IAMs relying on the commonly used conversion into CO2-equivalent emissions. Since the methane removal technologies are still at an embryonic stage, I have explored the costs and potential that a methane removal technology would need to become a major climate mitigation option. To quantify a significant methane removal option, I relied on a comparison with carbon dioxide removal, which is now considered an essential and unavoidable tool to achieve the Paris agreement targets. Considering that carbon dioxide removal are valuable in models due to their ability to enable stringent climate targets to be met by compensating for excess emissions in hard-to-abate sectors at greatly reduced costs, I hypothesized that the role of a given greenhouse gas removal technology to achieve a given climate target could be measured with two metrics: the reduction of the total costs, and the cumulative gross carbon dioxide emissions from the energy sector. Following these assumptions, it is theoretically possible to identify necessary characteristics of methane removal that can replace large-scale carbon dioxide removal solutions such as BECCS under each of the four different climate mitigation pathways.

The mitigation pathways with "equivalent" methane removal or carbon dioxide removal are however different in the following two respects. Firstly, methane removal is used later than carbon dioxide removal, as it rapidly affects temperature pathways. As a consequence, the costs borne by future generations are higher with methane removal than with CDR. Secondly, earth-system impacts are different. The use of equivalent methane removal, instead of the BECCS, leads to a more sustained overshoot period. Furthermore, I added a simple model that describes increasing natural methane emissions due to global warming, and it shows that this temperature feedback on methane emissions cannot be justified as an argument in favor of methane removal. Using alternative metrics for GHG comparison, such as the average residual gross CO_2 emissions after temperature stabilization or the decline rate of gross CO_2 emission reduction, might change the results. The aim of the "generic" methane removal technology, modeled with constant costs, fast scale-up and fixed potential, is to represent a simple benchmark against which individual methane removal technology could be compared in the future when more data become available. However, it does not cover all possible methane removal techniques, and this approach could be further developed by modeling techniques with the same average cost and the same potential, but obeying different dynamics, for instance depending on other variables such as the atmospheric concentration of methane, or with non-linear costs.

This study can be complemented by a longer-term analysis, as we observe that by 2100, the atmospheric methane concentration is on a downward trajectory. Theoretically, it would have to continue to decrease to compensate for residual CO_2 emissions, meaning that methane removal would have to continue with ever lower atmospheric concentrations. This poses two problems: firstly, the radiative forcing of methane, as well as the atmospheric chemistry module used in this study are not calibrated for concentration levels that would be lower than pre-industrial levels, and secondly, it is possible that the atmospheric methane concentration level becomes so low that it affects the technical or financial feasibility of methane removal. It then follows that gross CO_2 emissions would instead have to reach zero to stabilize temperature after the potential of methane removal is exhausted. However, this could take place only after the first half of the 22^{nd} century if this scenario were to occur.

4 General Discussion

The chapters on enhanced weathering and methane removal rely on energy transition scenarios until 2100, based on a stylized model of the energy system. The energy system model, starting with a fossil fuel-dominated scenario, responds to climate constraints by replacing

unabated fossil fuels with less carbon-intensive energy sources and adding greenhouse gas removal technologies, adhering to constraints on technological market shares and expansion rates, ultimately selecting the scenario minimizing the net present value of costs, including technology costs and consumption loss. The scenarios are therefore determined exclusively by considerations of technical feasibility and economic optimality (J. Forster et al., 2020). These elements explain the specific features of the scenarios, such as the tendency to postpone the mitigation efforts whenever possible, and to widely implement the most economically viable methods, such as GHG removal techniques, up to admittedly unrealistic levels and rates. These patterns are a common issue of cost-effective models like GET-ACC2, and must be taken into account to interpret the results accurately.

The two-way coupling between the energy system model and a climate model is another feature of the model. It enables temperature targets to be imposed directly, without having to rely on "proxies" such as carbon budgets. This also makes it possible to simultaneously optimize emission reductions for the various GHGs without having to use fixed metrics that imply economically sub-optimal pathways. This is an advantage over many other cost-effective IAMs and a useful feature for studying mitigation measures involving short-lived climate forcers such as methane, but it implies extending to the climate system the perfect knowledge and foresight already assumed for the future of the energy system through intertemporal optimization. As a consequence, our treatment of uncertainties differs from the one used by the IPCC for the climate assessment of emission scenarios (“Annex III”, 2023). The IPCC calculates ex-post the probability distribution of the temperature rise associated with a given emissions scenario. In our case, uncertainties about costs are treated in the same way as uncertainties on the response of the climate system to anthropogenic emissions, which is parameterized here by the equilibrium climate sensitivity (see supplements 6). There is an apparent paradox in the treatment of uncertainty in the context of perfect foresight models. The resolution of the model based on intertemporal optimization assumes an omniscient global planner. During the Monte-Carlo procedure, each realization corresponds to an optimal trajectory for a given set of parameters that are assumed to be perfectly known by this planner, but not by us. In this way, uncertainty about climate sensitivity does not make the temperature reached in 2100 uncertain, but it does affect the costs of achieving it, the underlying climate policies and the technical choices calculated by the model. The range of results therefore corresponds to the operating range of the model over a plausible space of parameters, and not to the distribution probability of the outcomes resulting from a given course of climate policies.

The reliance on CDR in mitigation scenarios has raised concerns, CDR being considered as an indispensable instrument for climate mitigation but also as a possibly dangerous distraction impeding imperative emissions mitigation efforts (Anderson, 2015; Anderson & Peters,

2016; Anderson et al., 2023; Fuss et al., 2014; IPCC, 2022; Obersteiner et al., 2001; Warszawski et al., 2021). The uncertainties surrounding the discussed Greenhouse Gas (GHG) removal techniques in this thesis could therefore also be considered in the assessment of their efficacy and respective merits or drawbacks. The aggregated model we employ is inherently bound to maintain a certain level of abstraction, and as such it is not well-suited for exploring all kinds of risks or adverse effects. However, it could be used to explore the consequences of delaying drastic and immediate emissions reductions by relying on the future availability of CDR or another back-up technology with a possible carbon lock-in towards high-temperature pathways if these technologies turn out to be less efficient than expected. The assessment of the additional costs of GHG removal technologies falling short of expectations could also provide an additional metric to compare MR and CDR.

5 Policy relevance

The work described in this thesis was presented in the introduction as a contribution to the study of climate change mitigation strategies. The objective is therefore scientific, and could be pursued for the sole purpose of knowledge. However, climate science, and the study of mitigation strategies even more so do not take place in an ivory tower free from social, historical and political contingency. On the contrary, science and policy influence each other in a process of co-production (Jasanoff, 2004). Scientific results irrigate the political debate and policy-making: in that respect, parties to the Paris agreement committed to "undertake rapid reductions [...] in accordance with best available science". Conversely, researchers are actively seeking policy-relevance, which in turn guides scientific production. For this purpose, IPCC aims at being "policy-relevant, but not policy-prescriptive" (Hermansen et al., 2021), and scientific production cannot be totally indifferent to the concerns of policymakers. The active search for policy-relevance is thus a key factor to explain the establishment of the IAM modeling community and its current preeminence in the third working group of IPCC (van Beek et al., 2020) as well as the ongoing developments of models and scenarios (Keppo et al., 2021; van Beek et al., 2022). Reciprocally, building mitigation scenarios contributes to shaping possible futures and delineating the political choices to achieve them, as illustrated by the emergence of CDR (Beck & Mahony, 2018). Consequently, translating modeling results into mitigation policy considerations is an important but thorny process, with the risk that a share of the information is lost in translation. To effectively contribute to the development of mitigation policies, the modelling results, the underlying assumptions and the associated limitations must therefore be accounted together, while uncertainties should not be used to delay action.

References

Anderson, K. (2015). Duality in climate science. *Nature Geoscience*, *8*(12), 898–900. https://doi.org/10.1038/ngeo2559

Anderson, K., Buck, H. J., Fuhr, L., Geden, O., Peters, G. P., & Tamme, E. (2023). Controversies of carbon dioxide removal. *Nature Reviews Earth & Environment*, 1–7. https://doi.org/10.1038/s43017-023-00493-y

Anderson, K., & Peters, G. (2016). The trouble with negative emissions. *Science*, *354*(6309), 182–183. https://doi.org/10.1126/science.aah4567

Andrijevic, M., Schleussner, C.-F., Gidden, M. J., McCollum, D. L., & Rogelj, J. (2020). COVID-19 recovery funds dwarf clean energy investment needs. *Science*, *370*(6514), 298–300. https://doi.org/10.1126/science.abc9697

Annex III: Scenarios and Modelling Methods. (2023, August 17). In IPCC (Ed.), *Climate Change 2022 - Mitigation of Climate Change* (1st ed., pp. 1841–1908). Cambridge University Press. https://doi.org/10.1017/9781009157926.022

Aulie, F., Dechezleprêtre, A., Galindo-Rueda, F., Kögel, C., Pitavy, I., & Vitkova, A. (2023). Did COVID-19 accelerate the green transition? https://www.oecd-ilibrary.org/content/paper/5b486c18-en

Beck, S., & Mahony, M. (2018). The politics of anticipation: The IPCC and the negative emissions technologies experience. *Global Sustainability*, *1*, e8. https://doi.org/10.1017/sus.2018.7

Calabrese, S., Wild, B., Bertagni, M. B., Bourg, I. C., White, C., Aburto, F., Cipolla, G., Noto, L. V., & Porporato, A. (2022). Nano- to Global-Scale Uncertainties in Terrestrial Enhanced Weathering. *Environmental Science & Technology*, *56*(22), 15261–15272. https://doi.org/10.1021/acs.est.2c03163

Dafnomilis, I., Chen, H.-H., den Elzen, M., Fragkos, P., Chewpreecha, U., van Soest, H., Fragkiadakis, K., Karkatsoulis, P., Paroussos, L., de Boer, H.-S., Daioglou, V., Edelenbosch, O., Kiss-Dobronyi, B., & van Vuuren, D. P. (2022). Targeted Green Recovery Measures in a Post-COVID-19 World Enable the Energy Transition. *Frontiers in Climate*, *4*. Retrieved August 30, 2023, from https://www.frontiersin.org/articles/10.3389/fclim.2022.840933

Forster, J., Vaughan, N. E., Gough, C., Lorenzoni, I., & Chilvers, J. (2020). Mapping feasibilities of greenhouse gas removal: Key issues, gaps and opening up assessments. *Global Environmental Change*, *63*, 102073. https://doi.org/10.1016/j.gloenvcha.2020.102073

Forster, P. M., Forster, H. I., Evans, M. J., Gidden, M. J., Jones, C. D., Keller, C. A., Lamboll, R. D., Quéré, C. L., Rogelj, J., Rosen, D., Schleussner, C.-F., Richardson, T. B., Smith, C. J., & Turnock, S. T. (2020). Current and future global climate impacts resulting from COVID-19. *Nature Climate Change*, *10*(10), 913–919. https://doi.org/10.1038/s41558-020-0883-0

Fuss, S., Canadell, J. G., Peters, G. P., Tavoni, M., Andrew, R. M., Ciais, P., Jackson, R. B., Jones, C. D., Kraxner, F., Nakicenovic, N., Le Quéré, C., Raupach, M. R., Sharifi, A., Smith, P., & Yamagata, Y. (2014). Betting on negative emissions. *Nature Climate Change*, *4*(10), 850–853. https://doi.org/10.1038/nclimate2392

Gawel, E., & Lehmann, P. (2020). Killing Two Birds with One Stone? Green Dead Ends and Ways Out of the COVID-19 Crisis. *Environmental & Resource Economics*, 1–5. https://doi.org/10.1007/s10640-020-00443-y

Goll, D. S., Ciais, P., Amann, T., Buermann, W., Chang, J., Eker, S., Hartmann, J., Janssens, I., Li, W., Obersteiner, M., Penuelas, J., Tanaka, K., & Vicca, S. (2021). Potential CO2 removal from en-

hanced weathering by ecosystem responses to powdered rock. *Nature Geoscience*, *14*(8), 545–549. https://doi.org/10.1038/s41561-021-00798-x

Haque, F., Chiang, Y. W., & Santos, R. M. (2020). Risk assessment of Ni, Cr, and Si release from alkaline minerals during enhanced weathering. *Open Agriculture*, *5*(1), 166–175. https://doi.org/10.1515/opag-2020-0016

Hepburn, C., O'Callaghan, B., Stern, N., Stiglitz, J., & Zenghelis, D. (2020). Will COVID-19 fiscal recovery packages accelerate or retard progress on climate change? *Oxford Review of Economic Policy*, *36*, S359–S381. https://doi.org/10.1093/oxrep/graa015

Hermansen, E. A. T., Lahn, B., Sundqvist, G., & Øye, E. (2021). Post-Paris policy relevance: Lessons from the IPCC SR15 process. *Climatic Change*, *169*(1), 7. https://doi.org/10.1007/s10584-021-03210-0

Hourcade, J.-C., Dasgupta, D., & Ghersi, F. (2021). Accelerating the speed and scale of climate finance in the post-pandemic context. *Climate Policy*, *21*(10), 1383–1397. https://doi.org/10.1080/14693062.2021.1977599

IEA. (2021). *World Energy Outlook 2021*. https://www.oecd-ilibrary.org/content/publication/14fcb638-en

IPCC. (2022). *Climate Change 2022: Mitigation of Climate Change. Contribution of Working Group III to the Sixth Assessment Report of the Intergovernmental Panel on Climate Change*. IPCC.

Jasanoff, S. (2004). Ordering knowledge, ordering society. *States of knowledge: The co-production of science and social order*, *2044*.

Keppo, I., Butnar, I., Bauer, N., Caspani, M., Edelenbosch, O., Emmerling, J., Fragkos, P., Guivarch, C., Harmsen, M., Lefèvre, J., Le Gallic, T., Leimbach, M., McDowall, W., Mercure, J.-F., Schaeffer, R., Trutnevyte, E., & Wagner, F. (2021). Exploring the possibility space: Taking stock of the diverse capabilities and gaps in integrated assessment models. *Environmental Research Letters*, *16*(5), 053006. https://doi.org/10.1088/1748-9326/abe5d8

Kuzemko, C., Bradshaw, M., Bridge, G., Goldthau, A., Jewell, J., Overland, I., Scholten, D., Van de Graaf, T., & Westphal, K. (2020). Covid-19 and the politics of sustainable energy transitions. *Energy Research & Social Science*, *68*, 101685. https://doi.org/10.1016/j.erss.2020.101685

Lahcen, B., Brusselaers, J., Vrancken, K., Dams, Y., Da Silva Paes, C., Eyckmans, J., & Rousseau, S. (2020). Green Recovery Policies for the COVID-19 Crisis: Modelling the Impact on the Economy and Greenhouse Gas Emissions. *Environmental and Resource Economics*, *76*(4), 731–750. https://doi.org/10.1007/s10640-020-00454-9

Obersteiner, M., Azar, Ch., Kauppi, P., Möllersten, K., Moreira, J., Nilsson, S., Read, P., Riahi, K., Schlamadinger, B., Yamagata, Y., Yan, J., & van Ypersele, J.-P. (2001). Managing Climate Risk. *Science*, *294*(5543), 786–787. https://doi.org/10.1126/science.294.5543.786b

Pollitt, H., Lewney, R., Kiss-Dobronyi, B., & Lin, X. (2021). Modelling the economic effects of COVID-19 and possible green recovery plans: A post-Keynesian approach. *Climate Policy*, *21*(10), 1257–1271. https://doi.org/10.1080/14693062.2021.1965525

Rochedo, P. R. R., Fragkos, P., Garaffa, R., Couto, L. C., Baptista, L. B., Cunha, B. S. L., Schaeffer, R., & Szklo, A. (2021). Is Green Recovery Enough? Analysing the Impacts of Post-COVID-19 Economic Packages. *Energies*, *14*(17), 5567. https://doi.org/10.3390/en14175567

Santos, R. M., Araujo, F., Jariwala, H., Khalidy, R., Haque, F., & Chiang, Y. W. (2023). Pathways, roundabouts, roadblocks, and shortcuts to safe and sustainable deployment of enhanced rock weathering in agriculture. *Frontiers in Earth Science*, *11*, 1215930. https://doi.org/10.3389/feart.2023.1215930

Shan, Y., Ou, J., Wang, D., Zeng, Z., Zhang, S., Guan, D., & Hubacek, K. (2021). Impacts of COVID-19 and fiscal stimuli on global emissions and the Paris Agreement. *Nature Climate Change*, *11*(3), 200–206. https://doi.org/10.1038/s41558-020-00977-5

Van De Ven, D.-J., Nikas, A., Koasidis, K., Forouli, A., Cassetti, G., Chiodi, A., Gargiulo, M., Giarola, S., Köberle, A. C., Koutsellis, T., Mittal, S., Perdana, S., Vielle, M., Xexakis, G., Doukas, H., & Gambhir, A. (2022). COVID-19 recovery packages can benefit climate targets and clean energy jobs, but scale of impacts and optimal investment portfolios differ among major economies. *One Earth*, *5*(9), 1042–1054. https://doi.org/10.1016/j.oneear.2022.08.008

van Beek, L., Hajer, M., Pelzer, P., van Vuuren, D., & Cassen, C. (2020). Anticipating futures through models: The rise of Integrated Assessment Modelling in the climate science-policy interface since 1970. *Global Environmental Change*, *65*, 102191. https://doi.org/10.1016/j.gloenvcha.2020.102191

van Beek, L., Oomen, J., Hajer, M., Pelzer, P., & van Vuuren, D. (2022). Navigating the political: An analysis of political calibration of integrated assessment modelling in light of the 1.5 °C goal. *Environmental Science & Policy*, *133*, 193–202. https://doi.org/10.1016/j.envsci.2022.03.024

Vicca, S., Goll, D. S., Hagens, M., Hartmann, J., Janssens, I. A., Neubeck, A., Peñuelas, J., Poblador, S., Rijnders, J., Sardans, J., Struyf, E., Swoboda, P., van Groenigen, J. W., Vienne, A., & Verbruggen, E. (2022). Is the climate change mitigation effect of enhanced silicate weathering governed by biological processes? *Global Change Biology*, *28*(3), 711–726. https://doi.org/10.1111/gcb.15993

Vienne, A., Poblador, S., Portillo-Estrada, M., Hartmann, J., Ijiehon, S., Wade, P., & Vicca, S. (2022). Enhanced Weathering Using Basalt Rock Powder: Carbon Sequestration, Co-benefits and Risks in a Mesocosm Study With Solanum tuberosum. *Frontiers in Climate*, *4*. Retrieved November 22, 2023, from https://www.frontiersin.org/articles/10.3389/fclim.2022.869456

Warszawski, L., Kriegler, E., Lenton, T. M., Gaffney, O., Jacob, D., Klingenfeld, D., Koide, R., Costa, M. M., Messner, D., Nakicenovic, N., Schellnhuber, H. J., Schlosser, P., Takeuchi, K., Leeuw, S. V. D., Whiteman, G., & Rockström, J. (2021). All options, not silver bullets, needed to limit global warming to 1.5 °C: A scenario appraisal. *Environmental Research Letters*, *16*(6), 064037. https://doi.org/10.1088/1748-9326/abfeec